The University Of Sheffield.

Detention Performance of Green Roof Systems: Experimental Characterisation and Numerical Modelling

Zhangjie Peng

Supervised by:

Prof Virginia Stovin

Dr Colin Smith

A thesis submitted in part fulfilment of the requirements

for the degree of Doctor of Philosophy in Civil Engineering

Department of Civil & Structural Engineering

The University of Sheffield

April 2021

Declaration

I declare that no portion of the work contained in this thesis has been submitted in support of an application for another degree or qualification of this or any university or other institutes of learning. The work is my own except where indicated. All quotations have been distinguished by quotation marks and the sources acknowledged.

Acknowledgements

First of all, I would like to thank Prof Virginia Stovin for providing encouragement, guidance, and support at every stage of my PhD. I would also like to express my thanks to Dr Colin Smith, who provided support during the course of this research.

This project would not have been completed without the hard work and dedication of Dr Gianni Vesuviano, who conducted the drainage layer experiments prior to this PhD programme. My special appreciation is also given to Dr Simon De-Ville and Dr Christian Berretta, who pre-processed and collected the field green roof monitoring data.

This PhD work would not have been possible without the contributions of the technicians (Mr Martin Taylor, Mark Foster and Paul Osborne, in the Department of Civil and Structural Engineering, The University of Sheffield) in establishing the experimental apparatus.

I would like to thank the University of Sheffield, Faculty of Engineering, who provided financial support throughout my PhD research.

I also like to acknowledge the valuable input from various people outside of the University of Sheffield. Firstly, to Brad Garner of Green Roof Diagnostics for the experimental design and data collection from an innovative green roof system. Secondly, to Dr Scott Jeffers and Derek Hidalgo at Green Roof Diagnostics, for their contributions in obtaining and analysing the experimental data from the innovative green roof system.

Finally, I would like to thank my family and friends for their support throughout the course of this work.

Abstract

Green roofs, as an example of Sustainable Drainage Systems (SuDS), can benefit stormwater management through retention and detention processes. Retention in a green roof refers to the rainwater that is retained in the system, and detention is the process that leads to lag and attenuation effects in the system runoff hydrograph. The understanding of retention in green roof systems has been well-established. However, the understanding and modelling of green roof detention processes are less developed. The physical properties of green roof substrates that contribute to detention performance have not been fully characterised to date. Current research in detention modelling lacks a generic physically-based model capable of modelling the detention processes in a complete green roof system. In this study, the physical properties of green roof substrates were characterised, and a physically-based detention model capable of representing the detention processes in a complete green roof system was developed.

The Soil Water Release Curves (SWRC) for four representative green roof substrates were determined using the hanging column method, and the Hydraulic Conductivity Function (HCF) for the substrates was characterised in an infiltration column using steady-state and transient techniques. The conventional natural soil-derived HCF model — Durner-Mualem model, for which the model parameters were from the measured SWRC data, was shown to provide a poor fit to the measured HCF data. A new three-segment HCF curve was, therefore, proposed to fit measured HCF data for the green roof substrates. Detention tests were carried out on 100 mm and 200 mm deep substrates using four simulated design storms. The runoff and moisture content data collected during the detention tests were used to validate the HCFs using the Richards Equation. The results showed that the new HCF provides a better estimation of the runoff and moisture content profiles than the Durner-Mualem model.

A two-stage physically-based detention model was developed for complete green roof systems in this study. In the model, the vertical flow in the substrate is represented by the Richards Equation, and the horizontal flow in the underlying drainage layer is modelled by the Saint Venant equation. This two-stage physically-based model, together with the green roof model in SWMM (Storm Water Management Model) were validated using measured runoff profiles from two contrasting green roof systems: a conventional green roof system; and an innovative system. Both models showed a reasonable estimation of the runoff profiles from the green roof systems. However, due to the limitation that the models are not capable of representing the flow conditions in the innovative green roof system's detention layer, the model results were less accurate than for the conventional green roof system.

Contents

Declaration I

Acknowledgements II

Abstract III

List of Figures XI

List of Tables XXI

List of Abbreviations XXII

List of Symbols XXIII

1 Introduction, aim and objectives 1

1.1 Background 1

1.2 Aim and objectives 3

1.3 Thesis structure and content 5

1.4 Publications 7

2 Literature Review 9

2.1 Chapter overview 9

2.2 Sustainable Drainage Systems (SuDS) 9

2.2.1 Drivers for SuDS design and applications 10

2.3 Green roofs 11

2.3.1 Vegetation layer 12

2.3.2 Substrate 13

2.3.3 Drainage layer 13

2.4 Green roof hydrological performance 14

2.4.1 Retention 14

2.4.2 Detention 15

2.4.3 Variations in green roof performance 16

2.5 Green roof substrate physical properties 19

2.5.1 Basic physical properties 19

2.5.2 Hydraulic Properties 20
2.6 Green roof hydrological modelling 30
2.6.1 Retention modelling 30
2.6.2 Detention modelling 32
2.7 Chapter summary 40
3 Experimental Methods 43
3.1 Chapter overview 43
3.2 FLL tests 43
3.3 Soil Water Release Curve (SWRC) characterisation 44
3.3.1 Hanging column method 44
3.3.2 Pressure extractor method 45
3.4 Hydraulic Conductivity Function (HCF) measurement 45
3.4.1 Steady-state method 47
3.4.2 Transient method 48
3.5 Detention tests 49
3.5.1 Substrate detention tests 49
3.5.2 Drainage layer detention tests 50
3.5.3 Complete green roof system detention tests 51
3.5.4 Innovative green roof system detention tests 51
3.5.5 Field green roof test beds 52
3.6 Chapter summary 53
4 Internal Fluctuations in Green Roof Substrate Moisture Content During Storm Events: Monitored Data and Model Simulations 56
4.1 Chapter overview 56
4.2 Experimental set-up 56
4.2.1 The test beds 56
4.2.2 Substrate characteristics 58
4.3 Data analysis 58

4.4 Detention modelling 59
4.5 Substrate detention models 60
4.5.1 The Reservoir Routing model 60
4.5.2 The Richards Equation 60
4.5.3 The drainage layer model 61
4.6 Model Implementation 61
4.6.1 Retention 61
4.6.2 Reservoir Routing parameters for the drainage layer 61
4.6.3 Reservoir Routing parameters for the substrates 63
4.6.4 Richards Equation 64
4.7 Results 65
4.7.1 Moisture content behaviour during storms 65
4.7.2 Substrate characteristics 67
4.7.3 Model validation 68
4.8 Discussion 72
4.8.1 Soil water release curve 72
4.8.2 Hydraulic conductivity function 73
4.8.3 Lower boundary condition 74
4.9 Conclusions 76
5 Characterisation of Green Roof Substrate Physical Properties 78
5.1 Chapter overview 78
5.2 The trial green roof substrates 78
5.3 Basic properties 79
5.4 Soil water release curve (SWRC) 79
5.5 Hydraulic conductivity function (HCF) 80
5.6 Detention tests with the substrates 80
5.7 Model evaluation 80
5.8 Results and discussion 81

5.8.1 Basic properties 81
5.8.2 Soil water release curve (SWRC) 82
5.8.3 Hydraulic conductivity function (HCF) 84
5.8.4 Detention tests with the substrates 88
5.9 Conclusions 96
6 Modelling of Green Roof Substrate Detention Using the Richards Equation 97
6.1 Chapter overview 97
6.2 Green roof substrates and measured data 97
6.3 Model implementation 97
6.3.1 Substrate parameters 97
6.3.2 Boundary and initial conditions 98
6.4 Model evaluation 98
6.5 Results and discussion 98
6.5.1 Modelled runoff profiles 98
6.5.2 Modelled moisture content profiles 108
6.6 Conclusions 114
7 A Two-Stage Physically-Based Green Roof Detention Model 115
7.1 Chapter overview 115
7.2 Green roof drainage layer model 115
7.2.1 A physically-based model for the drainage layer 115
7.2.2 Parametric study 118
7.2.3 Results and Discussion 119
7.3 Modelling of green roof drainage layers 120
7.3.1 Drainage layer detention tests 120
7.3.2 Derivation of Manning's n 121
7.3.3 Results and discussion 121
7.3.4 Conclusions 128
7.4 A two-stage green roof detention model 128

7.5 Validation of the two-stage physically-based model using laboratory data 129
7.5.1 Laboratory green roof test bed 129
7.5.2 Model implementation 130
7.5.3 Results 131
7.5.4 Discussion 133
7.5.5 Conclusions 139
7.6 Validation of the two-stage physically-based model using field data 139
7.6.1 The field green roof test bed and rainfall events 139
7.6.2 Model implementation 139
7.6.3 Results 140
7.6.4 Further investigations on the two-stage physically-based detention model 141
7.6.5 Conclusions 149
8 Validation of the Physically-based Green Roof Detention Model with an Innovative Green Roof System 150
8.1 Chapter overview 150
8.2 The innovative green roof system 150
8.3 Experimental set-up and test programme 151
8.4 Model implementation 151
8.4.1 Model representation 151
8.4.2 Model parameters 153
8.5 Model validation and calibration 154
8.6 Results 154
8.6.1 Detention performance 154
8.6.2 Model validation 159
8.6.3 Model calibration 165
8.7 Discussion 169
8.8 Conclusions 170
9 Modelling of Two Green Roof Detention Using SWMM 171

9.1 Chapter overview 171
9.2 The SWMM green roof model 171
9.2.1 Introduction 171
9.2.2 Green roof detention processes representation 172
9.2.3 Comparison between the SWMM and the physically-based models 174
9.2.4 Validation of the MATLAB SWMM green roof model 175
9.2.5 Sensitivity analysis 177
9.3 Validation of the SWMM green roof model 178
9.3.1 Green roof systems 178
9.3.2 Laboratory detention tests 179
9.3.3 Substrate parameters 179
9.3.4 Drainage layer parameters 179
9.3.5 Model validation and calibration 181
9.3.6 Results 181
9.4 Discussion 191
9.4.1 Comparison of models 191
9.4.2 Infiltration model 195
9.4.3 Percolation model 195
9.4.4 Drainage layer model 196
9.5 Conclusions 197
10 Discussion 199
10.1 Chapter overview 199
10.2 Field capacity 199
10.3 Pore size distribution 203
10.4 Influence of compaction 205
10.5 Instrument accuracy and limitations 206
10.6 SWRC and HCF measurements 211
10.7 Model initial and boundary conditions 213

10.8 Model accuracy and substrate heterogeneity 216
11 Conclusions and Future Work 218
11.1 Chapter overview 218
11.2 Summary of findings 218
11.3 Future work 220
11.4 Key findings 222
References 224
Appendix A. Instrument Calibration 232
A.1 Instrument calibration 232
A.1.1 Moisture probes 232
A.1.2 Pressure transducers 233
A.2 Characterisation of the relationship between pumping rate and rainfall rate 234
A.3 Results 234
Appendix B. Solving the Richards Equation in MATLAB: Model Development and Validation 239
B.1 Introduction 239
B.2 Method 239
B.3 Model implementation 240
B.4 Model validation 242
B.4.1 van Genuchten-Mualem model 243
B.4.2 Durner-Mualem model 243
B.4.3 Sensitivity analysis 244
B.4.4 Spatial discretisation sensitivity analysis 245
B.5 Conclusions 246
Appendix C. Supplementary Materials for Green Roof Substrate Detention Tests (Chapter 5 and Chapter 6). 248
Appendix D. Example of MATLAB Code 250

List of Figures

Figure 2.1. Four pillars of SuDS design (Woods Ballard et al., 2015)..... 10
Figure 2.2. Conceptual SuDS management train (Woods Ballard et al., 2015). 10
Figure 2.3. Typical structure of a green roof system (Vesuviano et al., 2014). 12
Figure 2.4. Typical green roof substrates (Stovin et al., 2015). 13
Figure 2.5. Typical green roof drainage layers (Vesuviano 2014). 14
Figure 2.6. Detention metrics (Stovin et al., 2017). 15
Figure 2.7. Particle size distribution recommendations for extensive green roof substrates (FLL, 2008). 20
Figure 2.8. Water desorption curve of a green roof substrate..... 24
Figure 2.9. Moisture content in the substrate pore space at different conditions; (a). Below field capacity; (b). Between field capacity and saturation; (c). at saturation (Hillel et al., 1998). 25
Figure 2.10. An example of deriving the pore size distribution from the SWRC (Liu and Fassman-Beck. 2018)..... 25
Figure 2.11. Examples of HCFs, a function of the suction head (left) and a function of moisture content (Right) (curves were generated based on the Mualem model and the SWRC presented in **Figure 2.8**). 27
Figure 2.12. Conceptual water balance model of green roof (Kasmin et al., 2010). 30
Figure 2.13. Hydrological processes in a green roof system (Stovin, 2010). 32
Figure 3.1. Hanging column apparatus for Soil Water Release Curve measurement. 45
Figure 3.2. Infiltration column apparatus for HCF determinations (all dimensions in mm). 47
Figure 3.3. Rainfall simulator used for detention tests (Vesuviano and Stovin, 2013). 51
Figure 3.4. Experimental set-up for the detention tests with the detention layer and the innovative green roof system. 52
Figure 4.1. The experimental site at the University of Sheffield, UK and section view of the green roof test bed with the water content reflectometers (WCR, moisture probes) location (dimensions in mm) within the substrate (Berretta et al., 2014)..... 57
Figure 4.2. Conceptual green roof hydrological model: left – vertical profile through a typical green roof system indicating the layers associated with retention and detention processes; right – components of a two-stage detention model, indicating the two alternative options for representing substrate detention considered in this chapter. 60
Figure 4.3. Distribution of the calibrated Reservoir Routing model parameters for the drainage layer using the net rainfall and runoff data from TB7. 62

Figure 4.4. Distribution of the calibrated Reservoir Routing model parameter for the substrate of TB1. 63
Figure 4.5. Monitored rainfall, runoff and moisture content profiles for the five selected storm events (vertical dashed line indicates the time significant runoff was firstly observed, vertical dotted line represents the time rainfall stops, the solid vertical line is the time two hours after rainfall stops and the corresponding moisture content is assumed to indicate local field capacity). 66
Figure 4.6. Water release curves and hydraulic conductivity functions. (a) SWRC A is fitted to the van-Genuchten model, SWRC B is fitted to the Durner model, both models were fitted using hanging column and pressure plate extractor data; (b) plots of the new HCF and the HCFs derived from the two SWRC in (a) via the Mualem model. 68
Figure 4.7. Monitored and modelled runoff using the Reservoir Routing model and the Richards Equation (Richards Equation was implemented in MATLAB using SWRC B-Mualem model and constant suction head lower boundary condition). 70
Figure 4.8. Validation of temporarily stored moisture (Richards Equation was implemented in MATLAB using SWRC B-Mualem model and constant suction head lower boundary condition). (a) Depth-averaged temporary storage; (b) scatter plot comparison of moisture content for all storm events (depth-averaged); (c) comparison of vertical moisture content profiles. 71
Figure 4.9. Validation of runoff and temporarily stored moisture. (a) Monitored and modelled runoff; (b) monitored and modelled vertical moisture content profiles using the SWRC A-Mualem model. 73
Figure 4.10. Validation of runoff and temporarily stored moisture. (a) monitored and modelled runoff; (b) monitored and modelled vertical moisture content profiles using the SWRC B-Equation 4.4 model. 74
Figure 4.11. Validation of runoff and temporarily stored moisture. (a) Monitored and modelled runoff; (b) monitored and modelled vertical moisture content profiles using the SWRC B-Mualem model and free drainage boundary condition. 75
Figure 4.12. Validation of runoff and temporarily stored moisture. (a) Monitored and modelled runoff; (b) monitored and modelled vertical moisture content profiles using the SWRC B-Mualem model and the seepage boundary condition. 76
Figure 5.1. Photographs of the four trial substrates. 79
Figure 5.2. Particle Size Distribution (PSD) for the four green roof substrates (the graph is plotted with the errors to the average values of the three tests to show the variation between test samples). 82

Figure 5.3. Soil Water Release Curve (SWRC) for the four green roof substrates (the graph is plotted with the errors to the average values of the three tests to show the variation between test samples, and the data for HLS is the same data presented in Chapter 4)..... 83
Figure 5.4. Measured unsaturated hydraulic conductivity, estimated (Durner-Mualem model) and fitted (three-segment curve and simplified laboratory curve) hydraulic conductivity functions (HCFs) for the four substrates (the two vertical lines indicate the intercepts: the moisture content corresponding to 6 cm (right line) and 100 cm (left line) suction head; the horizontal line indicates the hydraulic conductivity of 0.1 cm/min). Note: New measurements replace the preliminary data points for HLS reported in **Figure 4.4(b)**. 85
Figure 5.5. Measured runoff profiles for the substrate detention tests (the vertical line indicates the end of the rainfall event). 89
Figure 5.6. Measured runoff and moisture content profiles during the detention tests for MCS. 92
Figure 5.7. Measured runoff and moisture content profiles during the detention tests for HLS. 93
Figure 5.8. Measured runoff and moisture content profiles during the detention tests for SCS. 94
Figure 5.9. Measured runoff and moisture content profiles during the detention tests for NSM. 95
Figure 6.1. Measured and modelled runoff profiles for the 100 mm MCS using the Durner-Mualem model and three-segment curve. 99
Figure 6.2. Measured and modelled runoff profiles for the 200 mm MSC using the Durner-Mualem model and three-segment curve. 100
Figure 6.3. Measured and modelled runoff profiles for the 100 mm HLS using the Durner-Mualem model and three-segment curve. 101
Figure 6.4. Measured and modelled runoff profiles for the 200 mm HLS using the Durner-Mualem model and three-segment curve. 101
Figure 6.5. Measured and modelled runoff profiles for the 100 mm SCS using the Durner-Mualem model and three-segment curve. 102
Figure 6.6. Measured and modelled runoff profiles for the 200 mm SCS using the Durner-Mualem model and three-segment curve. 103
Figure 6.7. Measured and modelled runoff profiles for the 100 mm NSM using the Durner-Mualem model and three-segment curve. 104
Figure 6.8. Measured and modelled runoff profiles for the 200 mm NSM using the Durner-Mualem model and three-segment curve. 104

Figure 6.9. Measured and modelled runoff profiles using the simplified laboratory curve (MCS). 105
Figure 6.10. Measured and modelled runoff profiles using the simplified laboratory curve (HLS). 106
Figure 6.11. Measured and modelled runoff profiles using the simplified laboratory curve (SCS). 106
Figure 6.12. Measured and modelled runoff profiles using the simplified laboratory curve (NSM). 107
Figure 6.13. R_t^2 distributions for the modelled runoff profiles using the Durner-Mualem model, the three-segment curve and the simplified laboratory curve. 107
Figure 6.14. Measured and modelled moisture content profiles for the 100 mm MCS using the Durner-Mualem model and three-segment curve. 109
Figure 6.15. Measured and modelled moisture content profiles for the 100 mm HLS using the Durner-Mualem model and three-segment curve. 110
Figure 6.16. Measured and modelled moisture content profiles for the 100 mm SCS using the Durner-Mualem model and three-segment curve. 110
Figure 6.17. Measured and modelled moisture content profiles for the 100 mm NSM using the Durner-Mualem model and three-segment curve. 111
Figure 6.18. Measured and modelled moisture content profiles for the 200 mm MCS using the Durner-Mualem model and three-segment curve. 112
Figure 6.19. Measured and modelled moisture content profiles for the 200 mm HLS using the Durner-Mualem model and three-segment curve. 112
Figure 6.20. Measured and modelled moisture content profiles for the 200 mm SCS using the Durner-Mualem model and three-segment curve. 113
Figure 6.21. Measured and modelled moisture content profiles for the 200 mm NSM using the Durner-Mualem model and three-segment curve. 113
Figure 7.1. Schematic diagram for the horizontal flow in a green roof drainage layer. 117
Figure 7.2. Modelled runoff profiles for simulations 1 to 4 using the physically-based drainage layer model. 119
Figure 7.3. Modelled runoff profiles for simulations 5 and 6 using the physically-based drainage layer model. 120
Figure 7.4. Drainage layers used for investigation in this study; (a) ZinCo Floradrain FD 25; (b) ZinCo Floradrain FD 40; (c) ZinCo Floraset FS 75 (Vesuviano, 2014). 121

Figure 7.5. The relationship between Manning's n and the averaged R_t^2 for each drainage layer. 122

Figure 7.6. R_t^2 for all the model results using the best-estimated Manning's n in different categories; (a) in drainage layer types; (b) in rainfall intensities; (c) in drainage lengths; (d) in slopes. 123

Figure 7.7. R_t^2 for all the modelled tests using the best-estimated Manning's n grouped in different configurations (the drainage layer are labelled as drainage layer type, slope and drainage length). 124

Figure 7.8. Cases where the physically-based drainage layer model achieves the best and the worst fit for the FD 25 drainage layer (with Manning's n = 0.0017); left column: the best fit; right column: the worst fit..... 125

Figure 7.9. Cases where the physically-based drainage layer model achieves the best and the worst fit for the FD 40 drainage layer (with Manning's n = 0.002); left column: the best fit; right column: the worst fit..... 126

Figure 7.10. Cases where the physically-based drainage layer model achieves the best and the worst fit for the FS 75 drainage layer (with Manning's n = 0.0017); left column: the best fit; right column: the worst fit..... 127

Figure 7.11. Examples of cases where the physically-based drainage layer model provides unstable solutions. 128

Figure 7.12. The concept of the two-stage physically-based green roof detention model. 129

Figure 7.13. Configuration of the laboratory green roof system (dimensions in mm). 130

Figure 7.14. Modelled and measured runoff profiles and cumulative depths using the two-stage physically-based model with the parameter identified from drainage layer isolated tests (i.e. Manning's n = 0.0017). 132

Figure 7.15. Hysteretic SWRCs for the MCS substrate (the wetting curve is a constructed curve). 134

Figure 7.16. Measured and modelled runoff profiles and cumulative depths that considers substrate hysteresis effects. 135

Figure 7.17. Measured and modelled runoff profiles and cumulative depths that excluded the retention capacity of the filter sheet and moisture mat. 136

Figure 7.18. The relationship between Manning's n and the mean R_t^2 of the 15 tests. 137

Figure 7.19. Measured and modelled runoff profiles and cumulative depths using the physically-based model and calibrated Manning's n (i.e. n = 0.006)..... 138

Figure 7.20. Modelled and measured runoff profiles for the five selected rainfall events (**Table 4.3**) using the physically-based model and model parameters determined in isolated component experiments in the laboratory. 141
Figure 7.21. The sensitivity of the model results (two-stage physically-based model) to Manning's n. 143
Figure 7.22. The relationship between Manning's n and the mean R_t^2 of the five selected rainfall events. 144
Figure 7.23. Example of a sedum vegetated green roof system that roots system reached drainage layer (Source: https://www.gtspecifier.co.uk/green-roofs-living-walls/green-roof-garden-vegetation/sedum-green-roof-trays). 144
Figure 7.24. Modelled and measured runoff profiles for the five selected rainfall events using the physically-based model and different values of Manning's n. 145
Figure 7.25. Model results of the 12 models (**Table 7.2**) in response to two design storms (the measured runoff profiles for these two events can be found in **Figure 7.14**). 148
Figure 7.26. R_t^2 distribution of the modelled runoff profiles in the five selected rainfall events (**Table 4.3**) using the 12 models in **Table 7.2**. 149
Figure 8.1. The configurations of the innovative green roof system (dimensions in mm) (source: https://www.purple-roof.com/). 151
Figure 8.2. The physically-based detention model for the innovative green roof system. 152
Figure 8.3. Measured SWRC and fitted Durner model for the MMS. 153
Figure 8.4. Measured runoff from the detention layer in response to the low rainfall intensity (0.17 mm/min). 155
Figure 8.5. Measured runoff from the detention layer in response to the medium rainfall intensity (0.78 mm/min). 155
Figure 8.6. Measured runoff from the detention layer in response to the high rainfall intensity (1.9 mm/min). 155
Figure 8.7. Temporary storage in the detention layer in response to the storms. 156
Figure 8.8. Measured runoff from the complete innovative green roof system in response to the low rainfall intensity (0.17 mm/min). 157
Figure 8.9. Measured runoff from the complete innovative green roof system in response to the medium rainfall intensity (0.78 mm/min). 157
Figure 8.10. Measured runoff from the complete innovative green roof system in response to the high rainfall intensity (1.9 mm/min). 158
Figure 8.11. Temporary storage in the complete innovative green roof system in the storms. 158

Figure 8.12. The relationship between Manning's n and mean R_t^2 of the modelled runoff from the detention layer in response to the six tests. 159
Figure 8.13. Measured and modelled runoff from the detention layer using the physically-based model (Manning's n = 0.017, at the low rainfall intensity, 0.17 mm/min). 160
Figure 8.14. Measured and modelled runoff from the detention layer using the physically-based model (Manning's n = 0.017, at the medium rainfall intensity, 0.78 mm/min). 160
Figure 8.15. Measured and modelled runoff from the detention layer using the physically-based model (Manning's n = 0.017, at the high rainfall intensity, 1.9 mm/min). 160
Figure 8.16. Optimised Manning's n for the detention layer in response to different rainfall intensities. 161
Figure 8.17. Modelled water level distribution within the detention layer in response to the low rainfall intensity (0.17 mm/min) using the physically-based model (Manning's n = 0.017). 161
Figure 8.18. Modelled water level distribution within the detention layer in response to the low rainfall intensity (0.78 mm/min) using the physically-based model (Manning's n = 0.017). 162
Figure 8.19. Modelled water level distribution within the detention layer in response to the low rainfall intensity (1.9 mm/min) using the physically-based model (Manning's n = 0.017). 162
Figure 8.20. Measured and modelled runoff from the complete system using the physically-based model (Manning's n = 0.017, at the low rainfall intensity, 0.17 mm/min). 163
Figure 8.21. Measured and modelled runoff from the complete system using the physically-based model (Manning's n = 0.017, at the medium rainfall intensity, 0.78 mm/min). 163
Figure 8.22. Measured and modelled runoff from the complete system using the physically-based model (Manning's n = 0.017, at the high rainfall intensity, 1.9 mm/min). 163
Figure 8.23. Modelled water level distribution within the detention layer in the complete system in response to the low rainfall intensity (0.17 mm/min) using the physically-based model (Manning's n = 0.017). 164
Figure 8.24. Modelled water level distribution within the detention layer in the complete system in response to the low rainfall intensity (0.78 mm/min) using the physically-based model (Manning's n = 0.017). 165
Figure 8.25. Modelled water level distribution within the detention layer in the complete system in response to the low rainfall intensity (1.9 mm/min) using the physically-based model (Manning's n = 0.017). 165
Figure 8.26. The relationship between Manning's n and mean R_t^2 of the modelled runoff from the complete green roof system in response to the nine tests. 166

Figure 8.27. Measured and modelled runoff from the complete system using the physically-based model (Manning's n=0.028, at the low rainfall intensity, 0.17 mm/min). 167
Figure 8.28. Measured and modelled runoff from the complete system using the physically-based model (Manning's n=0.028, at the medium rainfall intensity, 0.78 mm/min)..... 167
Figure 8.29. Measured and modelled runoff from the complete system using the physically-based model (Manning's n=0.028, at the high rainfall intensity, 1.9 mm/min). 167
Figure 8.30. Modelled water level distribution within the detention layer in the complete system in response to the low rainfall intensity (0.17 mm/min) using the physically-based model (Manning's n = 0.028). 168
Figure 8.31. Modelled water level distribution within the detention layer in the complete system in response to the low rainfall intensity (0.78 mm/min) using the physically-based model (Manning's n = 0.028). 168
Figure 8.32. Modelled water level distribution within the detention layer in the complete system in response to the low rainfall intensity (1.9 mm/min) using the physically-based model (Manning's n = 0.028). 169
Figure 9.1. Representation of green roof detention processes in SWMM. 172
Figure 9.2. Model results generated by the SWMM software and the MATLAB code; (a) water flux; (b) temporary storage in the drainage layer; (c) moisture content in the substrate..... 177
Figure 9.3. Modelled runoff profiles from a green roof system using different values of drainage layer roughness and the void fraction using the SWMM green roof model; (a) drainage layer roughness coefficient; (b) drainage layer void fraction. 178
Figure 9.4. Measured and modelled runoff profiles from the conventional green roof drainage layer using the SWMM green roof model (with a roughness coefficient of n_3=0.0578). 182
Figure 9.5. Measured and modelled runoff profiles from the innovative green roof detention layer using the SWMM green roof model (with a roughness coefficient of n_3=0.952, rainfall intensity of 0.17 mm/min). 183
Figure 9.6. Measured and modelled runoff profiles from the innovative green roof detention layer using the SWMM green roof model (with a roughness coefficient of n_3=0.952, rainfall intensity of 0.78 mm/min). 183
Figure 9.7. Measured and modelled runoff profiles from the innovative green roof detention layer using the SWMM green roof model (with a roughness coefficient of n_3=0.952, rainfall intensity of 1.9 mm/min). 184
Figure 9.8. Relationship between optimised drainage layer roughness coefficient and rainfall intensity for the detention layer in the innovative green roof system. 184

Figure 9.9. Measured and modelled runoff profiles from the conventional green roof system using the SWMM green roof model (n_3=0.0578). 185
Figure 9.10. Measured and modelled runoff profiles for the innovative green roof system using the SWMM green roof model (with a roughness coefficient of n_3=0.952, rainfall intensity of 0.17 mm/min). 186
Figure 9.11. Measured and modelled runoff profiles for the innovative green roof system using the SWMM green roof model (with a roughness coefficient of n_3=0.952, rainfall intensity of 0.78 mm/min). 187
Figure 9.12. Measured and modelled runoff profiles for the innovative green roof system using the SWMM green roof model (with a roughness coefficient of n_3=0.952, rainfall intensity of 1.9 mm/min). 187
Figure 9.13. Measured and modelled runoff profiles from the conventional green roof system using the SWMM green roof model and calibrated roughness coefficient (n_3=0.502). 189
Figure 9.14. Measured and modelled runoff profiles for the innovative green roof system using the SWMM green roof model (with a calibrated roughness coefficient of n_3=1.416, rainfall intensity of 0.17 mm/min). 190
Figure 9.15. Measured and modelled runoff profiles for the innovative green roof system using the SWMM green roof model (with a calibrated roughness coefficient of n_3=1.416, rainfall intensity of 0.78 mm/min). 190
Figure 9.16. Measured and modelled runoff profiles for the innovative green roof system using the SWMM green roof model (with a calibrated roughness coefficient of n_3=1.416, rainfall intensity of 1.9 mm/min). 191
Figure 9.17. Measured and modelled runoff from the complete conventional green roof system using the identified parameters from the drainage layer isolated detention tests (2SPB: the two-stage physically-based model developed in Chapter 7 and the results have been presented in **Figure 7.14**; SWMM-GR: SWMM green roof model presented in this chapter and the results have been presented in **Figure 9.9**)..... 192
Figure 9.18. Measured and modelled runoff from the complete innovative green roof system using the identified parameters from the detention layer isolated detention tests; (2SPB: the two-stage physically-based model explored in Chapter 8 and the results have been presented in **Figure 8.20**, **Figure 8.21** and **Figure 8.22**; SWMM-GR: SWMM green roof model introduced in this chapter and the results have been presented in **Figure 9.10**, **Figure 9.11** and **Figure 9.12**). 194

Figure 9.19. Measured and modelled substrate and bottom runoff from a conventional and an innovative green roof systems using the calibrated parameters; (a) conventional green roof system; (b) innovative green roof system. 196
Figure 9.20. Measured and modelled runoff from the FD 25 drainage layer using the tow-stage physically-based model (2SPB) and the SWMM green roof model (SWMM-GR) (the model results for the SWMM-GR model have been presented in **Figure 9.4**). 197
Figure 10.1. The FLL field capacity and the measured moisture content for four field green roof test beds 2 hours after rainfall events (adopted based on the moisture content data in De-Ville et al., 2018). 201
Figure 10.2. Substrate moisture content measured by the moisture probe 2 hours after storm events for the substrate detetnion tests in Section 3.5.1 (the shaded area indicates the range of FLL field capacity). 203
Figure 10.3. Pore size distribution for the four green roof substrates derived from the fitted Durner equation presented in **Table 5.2**. 204
Figure 10.4. The maximum water holding capacity and permeability (FLL method) for four green roof substrates with and without compaction. 206
Figure 10.5. Calibration equations determined for the moisture probes using different dataset (the horizontal lines indicate typical lower and upper boundaries for the moisture content measured in the detention tests). 208
Figure 10.6. The measured moisture content in the substrate in response to the design storms using the calibration equations in **Figure 10.5**. 209
Figure 10.7. A conceptual representation of the stratification effect in green roof substrates. 214
Figure 10.8. Moisture content distribution with the depth of the substrate at initial conditions for a field green roof test bed (TB1). 215
Figure 10.9. Moisture content distribution with the depth of the substrate at initial conditions (substrate columns for the detention tests described in Section 3.5.1). 216

List of Tables

Table 2.1. Classification of green roof detention modelling approaches..... 32

Table 3.1. Summary of experimental methods/data used in this study. 54

Table 4.1. Hydrological characteristics of the five selected storm events and TB1 hydrological performance. 59

Table 4.2. Value of parameters used in the Reservoir Routing Model. 63

Table 4.3. Local field capacity determined for each storm event. 65

Table 4.4. HLS Substrate characteristics according to FLL (2008) test methods. 67

Table 4.5. Fitted parameters for the SWRCs for the HLS substrate. 67

Table 5.1. Substrate physical characteristics according to FLL (2008) test methods. 81

Table 5.2. Fitted Soil Water Release Curve (SWRC) parameters for the substrates. 84

Table 5.3. RMSE for the Durner-Mualem model and the three-segment curve. 86

Table 5.4. Parameters for the three-segment curves. 87

Table 5.5. Value of parameters for the simplified laboratory curve. 88

Table 6.1. R_t^2 for the modelled runoff profiles using the Durner-Mualem model, the three-segment curve and the simplified laboratory curve. 108

Table 7.1 Value of parameters set for the models 118

Table 7.2. Model parameters for the 12 models. 147

Table 8.1 Value of parameters for the MMS substrate. 153

Table 9.1. Comparison of the SWMM and the physically-based models. 175

Table 9.2. Values of parameters put into the model for the MATLAB code validation. 176

Table 9.3. Value of parameters for the SWMM green roof model. 180

List of Abbreviations

1D	One Dimensional
ADWP	Antecedent Dry Weather Period
ASTM	American Society for Testing and Materials
BMPs	Best Management Practices
CSO	Combined Sewer Overflow
ET	Evapotranspiration
FLL	Forschungsgesellschaft Landschaftsentwicklung Landschaftsbau
HCF	Hydraulic Conductivity Function
HLS	Heather and Lavender Substrate
LID	Low Impact Development
MCS	Marie Curie Substrate
MMS	Moerings Mix Substrate
MWHC	Maximum Water Holding Capacity
NSM	New Substrate Mix
PSD	Particle Size Distribution
RMSE	Root of the Mean Square Error
RPM	Revolutions Per Minute
SCS	Sedum Carpet Substrate
SMEF	Soil Moisture Extraction Function
SuDS	Sustainable Drainage System
SWMM	Storm Water Management Model
SWRC	Soil Water Release Curve
TB	Test bed
WCR	Water Content Reflectometer (moisture content probe)
WSUD	Water Sensitive Urban Design
XMT	X-ray Microtomography

List of Symbols

a, b	Empirical parameters in the new and the simplified HCFs
A_1	Green roof surface area
d_1	Depth of water stored on the surface layer
d_3	Depth of water stored in storage layer
d_{50}	50% pass particle size
D_1	Surface depression storage depth
D_2	Thickness of soil layer
D_3	Thickness of drainage layer
ET	Evapotranspiration
ET_t	Actual evapotranspiration rate at time step t
f	Infiltration rate
f_1	Infiltration rate of surface water into soil layer
f_2	Percolation rate of water through the soil layer into storage layer
F	Cumulative infiltration
$g(r)$	Frequency of pore size r
h	Suction head
h_s	Water level above base bed
h_{t1}	Temporary water storage in the substrate at time t
h_{t2}	Temporary water storage in the drainage layer at time t
H	Total hydraulic head
HCO	Soil hydraulic slope
H_P	The elevation of the lowest moisture probe
i	Precipitation rate falling directly on the surface layer
k_D, n_D	Empirical parameters in the drainage layer Reservoir Routing model
k_G, n_G	Empirical parameters in the substrate Reservoir Routing model
k_s, n_s	Empirical parameters in the complete green roof Reservoir Routing model
$K(h)$	Unsaturated hydraulic conductivity at suction head h
K_m	Measured data
K_p	Predicted data
K_S	Saturated hydraulic conductivity
$K(S_e)$	Unsaturated hydraulic conductivity at S_e
K_r	Relative hydraulic conductivity

L	Length of the drainage layer
N	Number of measured data points
n_s	Surface roughness coefficient
n_3	Drainage layer roughness coefficient
n_f	Manning's roughness coefficient (Manning's n)
P	Precipitation
PET_t	Potential evapotranspiration rate at time step t
q	Flow rate through a unit area of soil
q_1	Surface layer runoff or overflow rate
q_3	Drainage layer outflow rate
q_m	Measured runoff/moisture content data
q_{mean}	Mean value of the observed data
q_o	Observed runoff/moisture content data
Qin	Inflow rate to the substrate
$Qout$	Outflow from the substrates
r	Radius of pore size
R	Rainfall/recharge
s_f	Bed friction slope
S	Temporary storage in the green roof system
S_1	Green roof test bed slope
S_e	Relative saturation
S_{max}	Maximum substrate storage capacity
S_t	Substrate moisture content at time step t
t	Discretised time step
U_s	Cross-sectional flow velocity
$v(x,t)$	Velocity at distance x and time t
w	Empirical parameters in the Durner model
W_1	Total length along edge of the roof where runoff is collected
x	Distance coordinate
z	Depth of the soil
Z	Elevation of discretised spatial step
α, n	Empirical parameters in van-Genuchten model
α_1, n_1, m_1	Empirical parameters in the Durner model
α_2, n_2, m_2	Empirical parameters in Durner model

$\beta_1, \gamma_1, \beta_2, \gamma_2, \beta_3, \gamma_3$	Empirical parameters for the three-segment HCF curve
Δt	Discretised time step
θ	Substrate moisture content
θ_1, θ_2	The two intercepts on the measured HCF
θ_3	Moisture content at the top of the soil layer
θ_{FC}	Moisture content at field capacity
θ_p	Porosity
θ_r	Residual moisture content
θ_s	Saturated moisture content
ρ_b	Dry bulk density
ρ_s	Particle density
ρ_w	Density of the water
σ	Surface tension between the water and the air
τ	Tortuosity parameter
ϕ	Porosity
$\emptyset_1$	Void fraction of any surface volume
$\emptyset_2$	Soil porosity
$\emptyset_3$	Void fraction of the drainage layer
φ_2	Suction head at the infiltration wetting front formed in the soil

1 Introduction, aim and objectives

1.1 Background

Conventional stormwater management techniques are reliant on buried pipes or tanks to provide effective drainage for urban surfaces. However, urbanisation has resulted in previous urban green space and permeable landscapes being replaced by impervious surfaces such that more rainfall becomes surface runoff, and the conventional practices cannot manage the heavy load effectively anymore. When under pressure, the combined sewer systems discharge stormwater and diluted effluent into open watercourses via Combined Storm Overflows (CSOs). These discharges may have potential health and environmental issues, as well as causing aesthetic pollution. In this context, alternative stormwater management approaches, described as Sustainable Drainage System (SuDS) in the UK or Best Management Practices (BMPs), Low Impact Development (LID), Water Sensitive Urban Design (WSUD) worldwide, that focus on reducing runoff volume, improving runoff quality and providing amenity and biodiversity benefits, have been developed (Woods Ballard et al., 2015).

Green roofs are one example of SuDS devices that control the rainfall at source. A green roof system typically consists of three layers — vegetation, substrate and drainage layer. Vegetation in a green roof system provides runoff reduction through interception and evapotranspiration; the substrate layer provides an appropriate balance of water, air and nutrients to support vegetation and provide retention and detention benefits; and the function of the drainage layer is to drain excess water from the substrate effectively. One of the advantages that green roofs have over other SuDS devices is that they are capable of restoring green spaces without requiring extra land space. Like most SuDS techniques, green roofs replicate pre-development hydrology processes via retention and detention. With a good understanding of the moisture behaviour within the green roof substrate during the dry weather period, the actual evapotranspiration rate from the green roof can be accurately estimated using existing models. Hence, green roof retention or initial losses may be estimated confidently. However, the physical processes occurring within the green roof substrate leading to the detention of runoff during the rainfall are poorly understood. The focus of this project is on the physical mechanisms that determine the green roof substrate detention performance during rainfall events.

Green roof substrates are engineered media that comprise lightweight materials (e.g. crushed brick and pumice) and organic matter. A wide range of particle sizes (from < 0.063 mm to >10 mm) can be seen in a green roof substrate. Compared to natural soil, green roof substrates are coarser

and more heterogeneous. The physical characteristics of the porous substrate affect its suitability to support plant growth and its effectiveness at retaining rainfall and detaining runoff. Understanding the physical properties of green roof substrates is essential for predicting and evaluating the hydrological performance of a green roof system. However, the study of hydraulic properties of green roof substrates is in its infancy. Most studies only reported basic properties that are not sufficient to describe the dynamic changes that occur within the substrates during and between storm events.

The key physical properties that control the dynamic hydraulic response are the water retention characteristics and unsaturated hydraulic conductivity. During a rainfall event, once the retention capacity of the substrate is filled by the rainfall at the start of the rainfall, the moisture content in a green roof substrate usually ranges between field capacity and saturation. The physical properties within this range are of critical importance for detention modelling. However, to date, very few studies have focused on measuring the substrates' physical properties in this range. Without experimental measurements of unsaturated hydraulic conductivity for green roof substrates, the Mualem equation, a soil-derived hydraulic conductivity function, is frequently used to estimate the unsaturated hydraulic conductivity for green roof substrate. To date, no study has validated the Mualem equation for green roof substrates, although it is frequently used in studies that use the Richards Equation to model green roof runoff. Therefore, further experimental characterisation of green roof substrate unsaturated hydraulic conductivity would be beneficial to understand the physical processes of unsaturated flows within green roof substrates.

In a modelling framework, the hydrological performance of a green roof system is modelled through retention and detention processes. Retention is rainwater that is retained in the system does not leave the system; retention can be accurately estimated using a green roof specific evapotranspiration model during the dry weather period. Detention is the process that leads to lag and attenuation effects in the system runoff hydrograph. Compared to retention modelling, there are more options for detention models. It can either be a semi-empirical model (e.g. the Reservoir Routing model with only two model coefficients) or a physically-based model (e.g. Richards Equation with more input parameters). Many of the existing green roof detention models are empirical models, which means the reported parameter values are specific to individual green roof systems. A generic model to describe the hydrological performance of any green roof in response to any storm must be process-based (physically-based). To date, some physically-based modelling tools (i.e. HYDRUS and SWMM) have been validated and calibrated

for green roof substrates. However, these models rely on the input parameters (i.e. hydraulic properties), and rigorous validation of these models have not been presented.

Both the substrate layer and the drainage layer in a green roof system provide detention, but some of the current physically-based models only account for the detention effect in the substrate and neglect the effect of the drainage layer. A simple reservoir routing model has been shown to be able to model the detention processes in the green roof drainage layer (Vesuviano and Stovin, 2013). However, the model parameters are configuration specific. Recently, an innovative material has been proposed to enhance the detention performance of conventional green roof systems. However, to date, no physically-based model has been proposed to model the detention processes in this innovative green roof system. The issues highlighted above imply that a new modelling framework is needed to combine a physically-based substrate model with a physically-based drainage layer-specific model.

1.2 Aim and objectives

The overall aim of this project is to understand how unsaturated hydraulic conductivity varies with the degree of saturation in green roof substrates and to develop a physically-based green roof detention model. The aim is to be achieved through the completion of the following objectives.

Objective One: Experimental characterisations of green roof substrate physical properties and detention performance

A series of laboratory tests are conducted to determine the basic physical properties of green roof substrates. The Soil Water Release Curves of green roof substrates are determined using the hanging column and pressure extractor methods, and the measured data is used to evaluate existing Soil Water Release Curve models. Whilst there are standard methods for the Hydraulic Conductivity Function measurement, these will require some refinement and adaption to make them suitable for application to green roof substrates. The unsaturated hydraulic conductivity, which determines how fast water flows through the substrate, is measured using the infiltration column method. The steady-state technique is adopted to give accurate measurements of the hydraulic conductivity at high moisture contents, and the transient technique is used to measure the data at low moisture contents. The capability of existing Hydraulic Conductivity Functions to represent green roof substrate's unsaturated hydraulic conductivity is evaluated based on the measured data points, and new green roof substrates Hydraulic Conductivity Functions are formulated based on the measured data. A series of detention tests are conducted with green

roof substrates to understand the moisture content variations during storms. The measured rainfall-runoff and moisture content data during the detention tests provide opportunities for further validation of detention models.

Objective Two: Modelling of green roof substrate detention using the Richards Equation

The Richards Equation is implemented in MATLAB to be capable of taking an arbitrary Hydraulic Conductivity Function as input to obtain a numerical solution. The measured moisture content data is used to investigate the best model boundary conditions for the Richards Equation. The Soil Water Release Curve and the Hydraulic Conductivity Function determined from Objective 1 are used within the Richards Equation to regenerate the runoff and moisture content profiles within the substrates during the detention tests. The model results are compared with the measured runoff and moisture content profiles to evaluate the model performance with different combinations of Soil Water Release Curves and Hydraulic Conductivity Functions.

Objective Three: Development of a physically-based model for green roof drainage layers

A physically-based model is developed for green roof drainage layers. The investigated drainage layers include the conventional plastic board drainage layers that have been used in green roof systems for decades and an innovative green roof drainage layer that has emerged recently in the green roof industry. The data from the drainage layer detention tests are used to identify model parameters, and the performance of the model is assessed based on the model's ability to regenerate the runoff profiles from the layers.

Objective Four: Validation of physically-based green roof detention models using two green roof systems

The substrate Richards Equation and the physically-based drainage layer model developed from Objective 3 are combined to form a two-stage green roof detention model, and this model is used to predict the detention in two complete green roof systems. The model is validated using the measured runoff profiles from a conventional green roof system under laboratory and field conditions, as well as an innovative green roof system tested in the laboratory. The industry-standard model — Storm Water Management Model (SWMM) — is evaluated using the measured runoff profiles from the same green roof systems. SWMM predictions are compared with the two-stage physically-based model, and the advantages and limitations of both models are discussed based on the comparison of results.

1.3 Thesis structure and content

This thesis comprises 11 chapters.

Chapter 1 provides a short introduction to the background and highlights the lack of both experimental characterisations of green roof substrates hydraulic properties and a physically-based green roof detention model. It also presents objectives to achieve the overall aim of the research.

Chapter 2 presents a review of relevant recent literature. Urban drainage practices are outlined before a more in-depth introduction to the SuDS philosophy and to green roofs specifically. A detailed review of green roof substrate properties and experimental methods for characterising those properties is then provided. The experimental and modelling approaches for green roof drainage layers are also reviewed in this chapter. The current state of knowledge surrounding green roof hydrological performance and modelling is outlined before the implications of developing a physically-based green roof detention model are explored.

Chapter 3 details the experimental methods employed in this study. The approaches to experimentally determine the basic physical properties, Soil Water Release Curve and Hydraulic Conductivity Function of green roof substrates are outlined in this chapter. The detention test with green roof substrates, green roof drainage layers and complete green roof systems are detailed in this chapter. The experiments described in this chapter provide the data for detention models development and validation in later chapters.

Chapter 4 presents the preliminary investigation on the Richards Equation. The runoff data collected from a field green roof test bed is used to investigate the Richards Equation's capability of modelling the runoff profiles. The runoff data is also used to investigate the influence of the Soil Water Release Curve and Hydraulic Conductivity Function on the model results. The collected moisture content data during storms is used to understand moisture content variations in the substrate. The moisture content data is also used to investigate the best boundary conditions to represent the substrate moisture content behaviour using the Richards Equation.

Chapter 5 presents the results of characterised Soil Water Release Curve, Hydraulic Conductivity Function and detention performance of four representative green roof substrates. The parameters for existing Soil Water Release Curve models are calibrated to fit the measured data points. The capability of an existing Hydraulic Conductivity Functions to represent green roof substrate unsaturated Hydraulic Conductivity is assessed based on the measured data. A three-

segment Hydraulic Conductivity Function and a simplified Hydraulic Conductivity Function are proposed based on the measured data.

Chapter 6 validates the Richards Equation using the measured data during the detention tests. The physical properties required by the Richards Equation are as determined in Chapter 5, and the modelling approaches developed in Chapter 4 are used to regenerate the runoff and moisture content profiles from green roof substrates recorded during the detention tests conducted in Chapter 3. The model results using an existing Hydraulic Conductivity Function and the new Hydraulic Conductivity Functions proposed in Chapter 5 are compared with the measured results, and the suitability of the Hydraulic Conductivity Functions modelling the substrate detention effects is assessed based on the comparisons.

Chapter 7 develops a two-stage physically-based green roof detention model. Firstly, a physically-based model is developed for green roof drainage layers, and then the drainage layer model is combined with the substrate Richards Equation model (Chapter 6) to form the two-stage detention model. The model's performance is assessed based on the modelled runoff profiles from a laboratory and a field conventional green roof system. Calibration is conducted to improve the model results further, and more in-depth investigation on the limitations and uncertainties of the model in representing the detention processes in this convention green roof system are also explored.

Chapter 8 considers the two-stage physically-based green roof detention model's (Chapter 7) performance in modelling the runoff profiles from an innovative green roof system. The parameters required by the model are identified from independent tests, and the identified parameters are used in the model to regenerate the runoff profiles from the complete system during the detention tests. The performance of the model is evaluated based on the modelled and measured runoff profiles. Further calibration is conducted to improve the model results.

Chapter 9 utilises the SWMM green roof model to model the runoff profiles from the conventional green roof system and the innovative green roof system considered in Chapter 7 and Chapter 8. The methods to identify the required model parameters are described in this chapter. The model performance is assessed based on its ability to regenerate the measured runoff profiles. The model results of the SWMM green roof model are also compared with the results of the physically-based model presented in Chapter 7 and Chapter 8. The advantages and limitations of both models are discussed.

Chapter 10 is the synthesis and discussion. It discusses some of the limitations and uncertainties associated with this study. Suggested modifications to the methods used in this study are provided, together with the implications for future research.

Chapter 11 concludes the thesis, relating summarised findings to the initial primary objectives and overall study aim. Future work highlighted by this study is also discussed in this chapter.

1.4 Publications

As of April 2021, two published journal papers, a conference paper and a further submitted journal paper, have resulted from work presented in, or related to, this thesis.

Journal papers

Chapter 3

Peng, Z., Smith, C., Stovin, V., 2019. Internal fluctuations in green roof substrate moisture content during storm events: Monitored data and model simulations. *J. Hydrol.* 573, 872–884. https://doi.org/10.1016/j.jhydrol.2019.04.008

Peng, Z., Smith, C., Stovin, V., 2020. The importance of unsaturated hydraulic conductivity measurements for green roof detention modelling. *J. Hydrol.* 590, 125273. https://doi.org/10.1016/j.jhydrol.2020.125273

Peng, Z., Garner, B., Stovin, V., 2021. Two green roof detention models applied in two green roof systems. *J. Hydrol. Eng.* (under review).

Chapter 4

Peng, Z., Smith, C., Stovin, V., 2019. Internal fluctuations in green roof substrate moisture content during storm events: Monitored data and model simulations. *J. Hydrol.* 573, 872–884. https://doi.org/10.1016/j.jhydrol.2019.04.008

Chapter 5 & Chapter 6

Peng, Z., Smith, C., Stovin, V., 2020. The importance of unsaturated hydraulic conductivity measurements for green roof detention modelling. *J. Hydrol.* 590, 125273. https://doi.org/10.1016/j.jhydrol.2020.125273

Chapters 7, 8 & 9

Peng, Z., Garner, B., Stovin, V., 2021. Two green roof detention models applied in two green roof systems. *J. Hydrol. Eng.* (under review).

Conference paper

Peng, Z. & Stovin, V., 2018. Internal fluctuations in green roof substrate moisture content during a storm event. 11th International Conference on Urban Drainage Modelling (UDM2018). Palermo, Italy, 23 September 2018 - 26 September 2018.

2 Literature Review

2.1 Chapter overview

This chapter comprises a comprehensive review of relevant green roof research in the literature. The benefits of Sustainable Drainage Systems (SuDS) are discussed in a wider context, and the role of green roofs in SuDS is explored in particular. Despite the multiple benefits of green roof systems, only the hydrological performance of extensive green roof systems is addressed in this review. The system compositions and the role of them in the overall hydrological performance are evaluated based on existing studies. The physical properties of green roof substrates and the methods of determining such properties are reviewed explicitly in this chapter. The application of the measured physical properties within various modelling frameworks is discussed. Current modelling approaches to predict green roof hydrological performance are also considered in this chapter. The approach of using the Richards equation, the physically-based unsaturated flow equation, to simulate detention in green roof substrates is presented. This chapter concludes by highlighting current knowledge gaps and the opportunities for further research that this thesis builds upon.

2.2 Sustainable Drainage Systems (SuDS)

Sustainable Drainage Systems (SuDS) are stormwater management strategies that are developed to meet four objectives: a reduction in surface water quantity, an increase in surface water quality, and an increase in amenity and biodiversity (**Figure 2.1**) (Woods Ballard et al., 2015). The terminology SuDS is widely used in the UK; other terminologies such as Low Impact Development (LID), Water Sensitive Urban Design (WSUD), and Best Management Practices (BMPs) are used internationally to describe the approaches that minimise the hydrological impacts of urbanisations (Fletcher et al., 2015). The overall philosophy of SuDS is to replicate the natural hydrological cycle in developed urban areas and manage the water at the source. Besides the benefits listed in the four pillars, SuDS also provide various environmental, ecological and economic benefits. Unlike conventional drainage systems, in which large hard engineering storage tanks or attenuation control structures are built to slow down the surface runoff, SuDS are intended to be small, discrete units, controlling the surface water at source. Most SuDS devices infiltrate the rainfall directly to the natural soil and provide a storage element to allow stormwater to be temporarily stored. Typical infiltration SuDS devices include soakaways, rain gardens, bio-retention cells, infiltration trenches, permeable pavements and infiltration basins (Woods Ballard et al., 2015). The connection of various SuDS devices (SuDS management train

design) is intended to maximise the benefits of each SuDS device (**Figure 2.2**). The train design usually starts at the upstream end of the catchment to prevent runoff from being generated, thus decreasing the overall drainage demands, and a series of additional devices will be used to convey the stormwater. Small scale infiltration devices are used alongside conveyance channels to provide additional volume reductions, and large schemes such as retention ponds or wetlands are capable of dealing with the excess flows from the site control. The SuDS Manual (Woods Ballard et al., 2015) provides several case studies for specific SuDS applications.

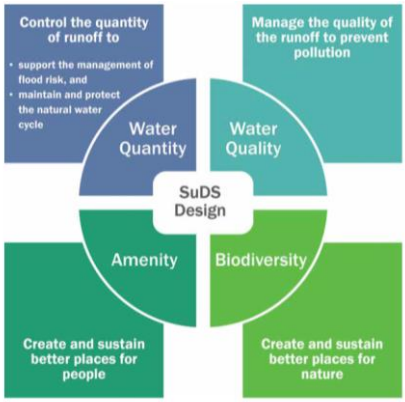

Figure 2.1. Four pillars of SuDS design (Woods Ballard et al., 2015).

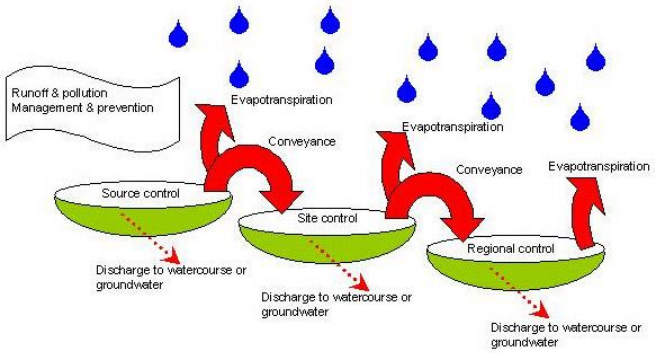

Figure 2.2. Conceptual SuDS management train (Woods Ballard et al., 2015).

2.2.1 Drivers for SuDS design and applications

Within England and Wales, 81% of the population lives in an urban area; this has increased 7% compared to the survey in 2001 (ONS, 2013). With urbanisation, naturally draining ground areas are replaced by impermeable roads, roofs and other paved areas. This development increases the drainage demand and the flow rate of runoff in the urban area. Undeveloped natural areas have the ability to retain and detain surface runoff. Plants and vegetation in natural areas can intercept rainfall; the permeable surface of natural areas helps water to infiltrate to the ground and return the water into the atmosphere through evapotranspiration. Conventional drainage systems rely

on the capacity of buried pipes to convey excess stormwater from the site to the receiving watercourses (separate sewer system) or water treatment works (combined sewer system). In a combined sewer network, to prevent excess flows from overwhelming the water treatment works during heavy or persistent rainfall events, combined sewer overflows (CSO) have been incorporated into the upstream network. A CSO is designed to spill excess stormwater flows to natural receiving watercourses. This is an effective way of dealing with excess flows, but frequent spillages cause water quality issues in the receiving watercourses.

The 'UK Climate Projections' predict that by 2080s, there is a 90% probability that the UK will experience wetter winters with up to 30% of more rainfall and more intense summer rainfall compared to baseline climate values from 1961 to 1990 (Murphy et al., 2020). The increasing precipitation in winter will challenge the existing sewer network and add pressure on UK's treatment plants. Large scale flooding in the UK is not a rare phenomenon. In 2007, southern Britain experienced serious flooding as a result of continuous rainfall from late spring to early summer. In Sheffield, many areas were affected by the event in 2007; in those most affected areas, flooding was more extreme than the 1947 benchmark event (Marsh and Hannaford, 2007).

Urbanisation, climate change projections and historical flooding indicate that more efficient drainage and water management strategies are needed to cope with increasing surface water. CIRIA provides guidance on the applications of SuDS devices for new developments (Woods Ballard et al., 2015) or retrofit of SuDS to existing developments (Digman et al., 2012). Both resources provide information on SuDS design. However, more research is still needed to fully understand the behaviour of each SuDS device in response to complicated real natural conditions and to predict the response of these devices to different design scenarios (Stovin, 2010).

2.3 Green roofs

A green roof is a form of SuDS that provides various benefits, including reducing runoff quantity, improving runoff quality, increasing biodiversity, providing amenity and ecological benefits. Amongst all the benefits, the benefits of green roofs in managing stormwater are of the most interest to urban drainage engineers. A green roof is a roof covered with vegetation and growing medium over the building, which provides a degree of retention, attenuation and water treatment (Woods Ballard et al., 2015). The concept of planting vegetation on roof space has been in existence for millennia. However, it was only in recent years that it was considered as a technique to mitigate urban flood risk and adopted in stormwater management. Green roof systems can take various forms. They can be either as an intensive green roof which is more like a garden with a deep substrate and more attractive plants, or an engineered extensive green roof

that has a very shallow substrate and does not require too much maintenance. Typically, a green roof system consists of three main layers: vegetation layer, substrate and drainage layer. A fabric filter is added to isolate the substrate layer from the drainage layer, and a root barrier is installed beneath the drainage layer to prevent roots from damaging building structures (**Figure 2.3**).

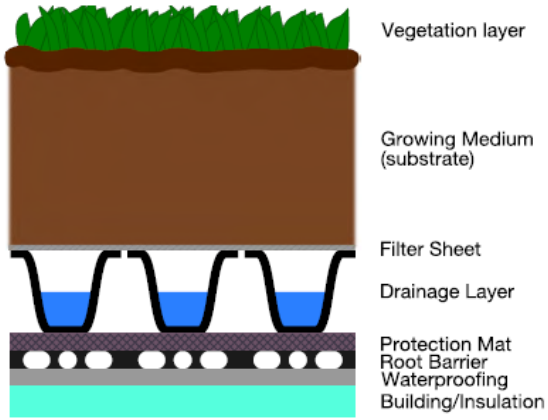

Figure 2.3. Typical structure of a green roof system (Vesuviano et al., 2014).

2.3.1 Vegetation layer

Vegetation in a green roof system provides runoff reduction through interception and evapotranspiration. Potentially any type of vegetation can be used in a green roof system, but considering the shallow substrate and the requirement for low maintenance and no irrigation, vegetation used in an extensive green roof system is usually highly drought-tolerant plants like sedum (Dvorak and Volder, 2010). However, some native plants, wildflowers and grass are also seen in green roofs (Abdef, 2012; Fassman-Beck et al., 2013; Razzaghmanesh and Beecham, 2014).

20% to 40% of the total moisture lost from the green roof to the atmosphere is due to plant evapotranspiration (Voyde et al., 2010). Different plant species have different evapotranspiration rates. Many studies have been conducted to identify the effect of different vegetation treatments on green roof hydrological performance. Fassman-Beck and Simcock (2008) compared the ET rates from sedum green roof test beds and New Zealand local species green roof test beds; it was found that the sedum supports higher evapotranspiration rates, resulting in lower runoff volumes. Poë et al. (2015) found that the green roof test beds installed with sedum reduced runoff significantly more than equivalent systems with meadow flower vegetation. However, they also found that introducing vegetation to a green roof system can reduce its ability to return water to the atmosphere, as greater levels of evaporation from a bare dark substrate were

observed compared to the green planted coverage; this is particularly significant during the initial 4 to 12 days after a rainfall event.

2.3.2 Substrate

Unlike conventional natural soil, green roof substrates are highly engineered, lightweight materials, typically with high mineral content and low fine particles (**Figure 2.4**). Green roof substrate is the most important component of the whole system; it provides an appropriate balance of water, air and nutrients to support vegetation and provides the most hydrological benefits. For an extensive green roof system, the typical substrate depth is around 50 mm to 150 mm (FLL, 2008). A green roof substrate can be a mixture of inorganic component (e.g. crushed bricks, light expanded clay, gravel and sand) and organic matter (e.g. compost, bark, coir) (Yio et al., 2013). Inorganic aggregates create the pore spaces for air, water and gas exchange and facilitate good drainage. Organic matter acts as an amendment to support key functions of plant growth (VanWoert et al., 2005). The most common aggregate material used in the green roof substrate in the UK is crushed recycled bricks, and elsewhere such as New Zealand, pumice, zeolite, topsoil, and sand are also used (Fassman and Simcock, 2012). The FLL guideline (a German green roof standard) restricts the size and percentages of various particles used in the green roof substrate in order to provide sufficient drainage (FLL, 2008).

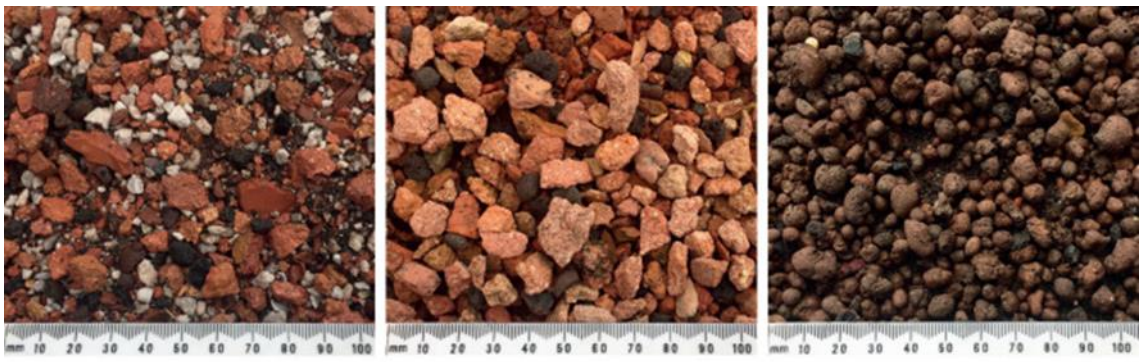

Figure 2.4. Typical green roof substrates (Stovin et al., 2015).

2.3.3 Drainage layer

The function of a green roof drainage layer is to drain excess water from the substrate effectively. Two classes of drainage layers are widely used in modern green roof systems: one is a granular drainage layer, which consists of large particles such as gravel or pumice with large voids to allow rapid drainage; the other is a synthetic drainage layer formed in hard plastic or expanded polystyrene modules (Vesuviano, 2014). Compared to the granular drainage layer, a synthetic drainage layer provides additional functions to the green roof substrate and vegetation. Runoff

could be stored in the drainage layer that has a profiled surface on the upper side, and the stored water could be transferred upwards to the substrate and be taken by the vegetation during the dry weather period (Vesuviano, 2014). **Figure 2.5** presents some of the synthetic drainage layers for green roofs. Most recently, some green roof systems have also utilised vertically oriented polyester thread fabric for the drainage layer to limit outflow and consequently enhance detention (https://www.purple-roof.com/).

Figure 2.5. Typical green roof drainage layers (Vesuviano 2014).

2.4 Green roof hydrological performance

2.4.1 Retention

Retention refers to the rainwater that is retained in the green roof and does not leave the system as runoff (Stovin et al., 2015). Retention typically occurs at the beginning of a rainfall event. Vegetation firstly intercepts a portion of the rain on its leaves. Then, rain infiltrates the substrate and fills up the small pore space in the substrate up to field capacity. Lastly, the excess rain will enter the drainage layer and become runoff (sometimes, the drainage layer also provides a specific storage capacity).

Evapotranspiration is a critical process that recovers the substrate retention capacity during the dry weather period. Many field-monitoring studies have been conducted on green roof retention performance under various climate conditions worldwide (Li and Babcock, 2014). Although small event depths with high levels of retention performance could skew reported metrics to higher levels of retention performance (De-Ville, 2017), retention performance is commonly reported as either total volumetric retention, which is a percentage of total retained water over total rainfall depth over the study period, or as a mean per event retention (VanWoert et al., 2005).

Annual retention of a green roof system typically varies from 50% to 75% of total rainfall depth, depending on the climate and configuration. During a rainfall event, the initial moisture content and the substrate depth determine the retention performance of a green roof. In a single rainfall event, the average retention of green roofs ranges from 30% to 86%, but it can be close to zero

and as high as 100% depending on the rainfall depth and initial moisture content (Fassman-Beck et al., 2013; Li and Babcock, 2014; Stovin et al., 2012; Voyde et al., 2010). The study duration is essential for retention monitoring as longer duration studies may represent more typical local climate conditions and the retention performance is representative of the system's long-term performance; while short-duration studies are influenced by abnormal weather conditions, which could result in an extremely low percentage of retention. These empirical retention monitoring studies provide limited information on understanding the physical processes that drive retention performance.

2.4.2 Detention

Detention is the processes that lead to lag and attenuation effects in the runoff hydrograph. Detention in green roof systems is highly linked with the large pore spaces in the substrate that cannot retain water but provide resistance to vertical water flow (Vesuviano et al., 2014). As **Figure 2.6** shows detention effects can be described as peak runoff delay, time to start of runoff delay, centroid delay and peak flow reduction (Stovin et al., 2015), but most studies tend to report the performance as peak attenuation and peak delay. In general, green roofs can provide more than 50% peak reduction compared to conventional roofs, and the reduction increases with the depth of the substrate (Fassman-Beck et al., 2013; Stovin et al., 2012; Voyde et al., 2010). Field monitoring studies also reported green roof detention performance in response to single rainfall events. Based on studies of a green roof system at the University of Sheffield, Sheffield, UK., the peak runoff delay can be as long as 283 minutes, whilst for the worst case, the green roof system cannot provide any peak delay effect (Stovin et al., 2012) for intensive long rainfall events.

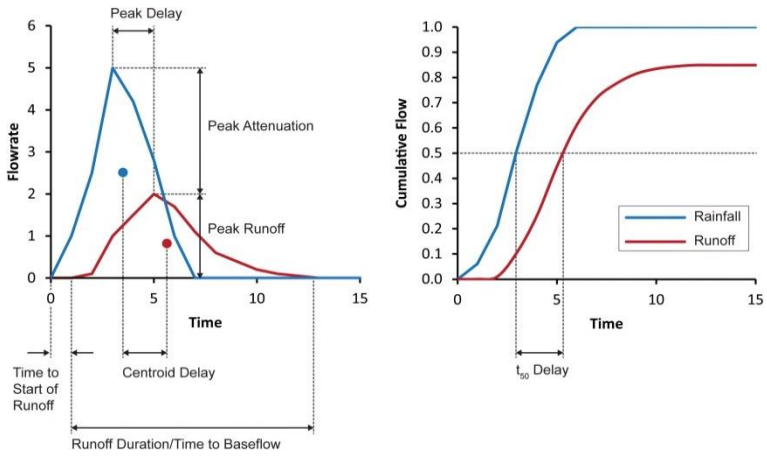

Figure 2.6. Detention metrics (Stovin et al., 2017).

2.4.3 Variations in green roof performance

Green roof performance can be influenced by roof configuration (i.e. slope, drainage layer, substrate depth and type, and vegetation), rainfall characteristics (i.e. duration, intensity and total depth), and antecedent dry period (i.e. initial moisture content) (Czemiel Berndtsson, 2010) etc. Studies have been undertaken worldwide to explore the influence of these factors.

Vegetation

VanWoert et al. (2005) found that vegetated configurations could provide greater retention performance than the unvegetated system, although moisture losses from vegetated systems are only greater than unvegetated systems when moisture available for evapotranspiration starts to be restricted (Poë et al., 2015; Stovin et al., 2015).

Vegetation treatment also has a significant influence on green roof detention performance. The above-ground vegetation could introduce delays to runoff, and the development of root systems in the substrate is expected to change the pore size distribution and pore space connectivity, and consequently the substrate permeability (De-Ville et al., 2017; Stovin et al., 2015). A long–term monitoring study on vegetated and unvegetated green roof test beds revealed that the vegetated configurations exhibited greater peak attenuation than the unvegetated configurations (Stovin et al., 2015).

Substrate characteristics

The Maximum Water Holding Capacity (MWHC), also referred to as field capacity, was found to be associated with green roof retention performance in Fassman-Beck and Simcock (2012) and Poë et al. (2015). An elevated field capacity could improve a green roof's overall retention performance.

Substrate composition was found to affect green roof detention performance (Stovin et al., 2015). A substrate with a high permeability showed low peak attenuation and poor detention performance (Stovin et al., 2015). The particle size distribution can also influence green roof detention performance. The substrate with a high portion of large, uniformly-sized and round particles has a high porosity and permeability, which decreases the detention performance (Stovin et al., 2015) .

Climate

Based on the monitoring studies worldwide, green roof retention performance under different climate conditions seems to be different. However, it is hard to establish exactly the same green

roof systems in different climate locations. With a good understanding of the physical drivers of green roof retention (i.e. evapotranspiration), Stovin et al. (2013) conducted a modelling study of long-term green roof retention performance across the UK, which provided an insight into the influence of climate. They found that greater retention occurs in drier and hotter climates with reduced rainfall and longer antecedent dry period, where water loss through evapotranspiration is high; in wetter and cooler climates, total retention volumes are higher, but a high total rainfall leads to a lower proportion of retention.

Although rainfall characteristics and antecedent conditions influence the green roof detention performance (i.e. time to start of runoff, peak delay, peak attenuation and runoff duration), the detention processes within the green roof are dependent only on the roof's physical configuration (i.e. roof's slope, substrate type and depth, drainage layer composition etc.) (Stovin et al., 2017). Therefore, detention processes are not influenced by climate.

Ageing

A green roof system is a live system, the interaction between vegetation and substrate may change the physical properties of the substrate over time and, as a consequence, affect the hydrological performance. De-Ville et al. (2017) found that although some of the substrate's physical properties changed over time (i.e. maximum water holding capacity, pore size distribution, porosity and saturated hydraulic conductivity), the influence of substrate ageing on the hydrological performance (retention and detention) is minor.

Seasonal variation

Seasonal variation in green roof performance is expected due to the change in temperature and rainfall characteristics with the season (Fassman-Beck et al., 2013). Long-term monitoring data is critical for understanding the seasonal variation in green roof performance. For example, Voyde et al. (2010) did not find any seasonal variation in performance based on 1 year of monitoring data from a green roof system in New Zealand. However, the same green roof showed a reduction in per-event retention for winter when 2 years' data were analysed (Fassman-Beck et al., 2013). The reduction in retention performance in winter is believed to be caused by the low evapotranspiration rates that did not allow the green roof to dry out between storms. Whilst many studies have confirmed that green roof retention capabilities are reduced in winter and increased in summer (Fassman-Beck et al., 2013; Stovin et al., 2012), Stovin et al. (2012) found that the green roof system in Sheffield, UK, had a higher retention capacity in spring than in summer. The higher rainfall depths of the summer storms contribute to the lack of retention in

summer. Whilst these monitoring studies have highlighted seasonal trends in green roof retention performance, it is hard to identify whether these variations are wholly due to climate or due to changes that also occur in the substrate that affect the system's retention characteristics (De-Ville et al., 2018; Stovin et al., 2012).

In the study of De-Ville et al. (2018), 6 years of substrate moisture and rainfall-runoff data were used to investigate the seasonal variations of green roof retention and detention performance. It was found that, although the configurations of the green roof test beds are different, all the green roof test beds showed a seasonal trend in potential retention and detention performance. Although long-term evolution in retention and detention performance is also evident, the sub-annual changes observed in their study are an order of magnitude higher than long-term evolution. The seasonal vegetation behaviour and the seasonal variation in the substrate's wetting and drying response are believed to cause the seasonal variation in retention performance; the vegetation growth phases and the sub-annual variation in substrate water repellency were hypothesised to influence the detention performance (De-Ville et al., 2018).

Effect of composition and depth

Substrate composition has been found to affect the green roof substrates' field capacity and consequently the retention performance. A high proportion of small voids results in a high field capacity and, therefore, potentially better retention performance (Stovin et al., 2015). Retention is dependent on the system's ability to lose moisture via evapotranspiration. Therefore, substrate depth does not have much impact on retention. However, a deeper substrate may provide more moisture for evapotranspiration and increase the evapotranspiration rate.

Yio et al. (2013) investigated the effect of organic matter and substrate depth on green roof substrate detention performance. They conducted a series of detention tests with a brick-based green roof substrate of different depths and proportions of organic matter. They concluded that detention in green roof substrates increases as a function of substrate depth and the proportion of organic matter.

Stratification

Limited published literature has explored the effect of stratification on green roof hydrological performance. However, there is evidence that stratification would occur in green roof substrate and alters the substrate physical properties and the hydrological performance (De-Ville, 2017). Stratification is believed to be caused by the 'wash through' processes in the substrate. Rainfall takes away the fines in the substrate through the runoff and causes the accumulations of fine

particles at the bottom. Bouzouidja et al. (2018) identified a fall in organic matter content in green roof substrates over a four year study period and reported a reduction in the mass of particles smaller than 2 mm. From a long-term monitored moisture content data of different depths of green roof test beds, the highest moisture content is always at the bottom of the substrate, which also indicates a vertical gradient in the substrates' physical characteristics (Berretta et al., 2014; De-Ville et al., 2018). Fassman-Beck et al. (2010) conducted a series of experiments to investigate the effect of compaction and stratification. They reported that fine particles were washed from the substrate within the first 5 minutes but that there were no further losses after 6 hours. The particle size distribution analysis of the substrate at different depths suggested that fine sand-sized (0.5–0.25 mm) particles were the most mobile fraction of the substrate. There were 10% w/w more of these fine particles in the lower 10 mm than the upper 30 mm.

Many of the effects and trends highlighted above can be understood with reference to the substrate's physical properties, which will be addressed in the following sections.

2.5 Green roof substrate physical properties

The moisture balance of a green roof is an important control upon its hydrological performance, and a significant portion of a green roof's moisture storage is provided within the substrate. Therefore, the hydrological response to a rainfall event is strongly influenced by the substrate's physical characteristics (Carbone et al., 2014). From a hydrological point of view, the physical properties that influence the substrate's response to rainfall include porosity, particle size distribution, maximum water holding capacity (field capacity), permeability (saturated hydraulic conductivity), water release characteristics and unsaturated hydraulic conductivity.

2.5.1 Basic physical properties

Porosity dictates a substrate's capacity for air and water. A balance of 35% to 65% maximum water holding capacity and 10% air content at maximum water capacity is suggested by the FLL (2008). Substrates need to be configured with particles that facilitate the appropriate proportions of different pore size to serve specific functions to obtain this balance.

Laboratory determination of porosity involves direct measurements of bulk density and particle density. The dry bulk density is determined based on the dry weight of a sample of known volume, and particle density can be determined by the pycnometer method (Hillel 2004; FLL 2008; Liu and Fassman-Beck 2016). Porosity can then be calculated from the following equation:

$$\theta_p = 1 - \frac{\rho_b}{\rho_s} \qquad \text{Equation 2.1}$$

where θ_p is the porosity, ρ_b is the dry bulk density (kg/m^3) and ρ_s the particle density (kg/m^3).

Particle size distribution (PSD) analysis is a conventional soil physics analysis; it consists of isolating various particle sizes and quantifying each size's relative abundance. The purpose of specifying particle size distribution for green roof substrates is to achieve suitable drainage requirements based on the dependency that exists between the particle size distribution and the pore size distribution. For extensive green roof substrates, the FLL suggests a range of particle size distributions should be used (**Figure 2.7**); any green roof substrate's particle size distribution curve ideally should be between the left and right curve limits to achieve suitable water conducting capacity. Some other reference values, such as Rationale and Target Value and New Zealand Agronomic Equivalent, are also seen in the literature (Fassman and Simcock, 2012) to define the suitable particle size distribution for a green roof substrate.

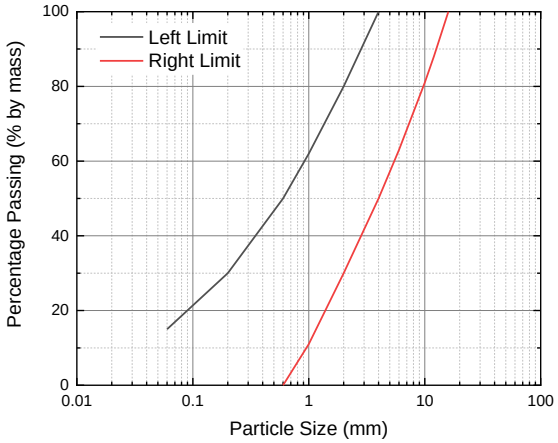

Figure 2.7. Particle size distribution recommendations for extensive green roof substrates (FLL, 2008).

d_{50} is the value of the particle size at 50% in the cumulative particle size distribution curve. d_{50} is usually used to represent the medium particle size of a substrate.

2.5.2 Hydraulic Properties

From a hydrological perspective, the hydraulic properties of green roof substrates are of more interest than those basic physical properties described in Section 2.5.1. Almost every study on green roof hydrology quantifies at least some of the substrate's hydraulic properties and correlates these properties with hydrological performance (Berretta et al., 2014; De-Ville et al., 2017; Fassman and Simcock, 2012; Liu and Fassman-Beck, 2018, 2017, 2016; Stovin et al., 2015). The most frequently measured hydraulic properties, which are also recommended by the FLL (2008), are maximum water holding capacity (field capacity) and water permeability (saturated hydraulic conductivity).

2.5.2.1 Maximum water holding capacity (MWHC)

Maximum water holding capacity (MWHC) or field capacity is the maximum moisture content that the substrate holds against gravity. Field capacity in soil science is defined as the amount of water that a well-drained soil holds against gravitational force and when downward drainage is markedly decreased (Veihmeyer and Hendrickson, 1931). The concept of field capacity is also commonly used in the green roof field. It is believed that the green roof substrate does not generate any runoff if the moisture content in the substrate is below field capacity. In practice, two methods are typically applied to determine green roof substrates' field capacity: the FLL method and the Soil Water Release Curve (SWRC) method. The FLL method is a time-based method. The field capacity is determined by measuring the moisture content of an approximately 12 cm deep substrate after 2 hours of drainage from saturation (FLL, 2008). The SWRC method is a pressure-based method that involves the measurement of the Soil Water Release Curve. The moisture content corresponding to 100 cm suction head is defined as field capacity (Fassman and Simcock, 2012; Liu and Fassman-Beck, 2018). However, a suction head of 330 cm has also been adopted in literature to define the green roof substrate field capacity (Berretta et al., 2014). A wider suction head range between 60 cm to 330 cm has been used in natural soil to define field capacity (de Oliveira et al., 2015). Many researchers have suggested benchmark capillary pressures (suction) in soils when field capacity is attained. However, this approximation is inconsistent because there is no assurance that the drainage from the soil would become negligible at these benchmark pressures (Twarakavi et al., 2009).

It is argued that the static approximation of field capacity is inappropriate due to the highly dynamic characteristics of the soil. To solve this problem, several researchers developed techniques for estimating field capacity using dynamic approaches. Nachabe (1998) proposed that the field capacity of soil should correspond to the soil moisture content when the drainage flux from the soil is equal to the daily evapotranspiration rate. A drainage flux from the soil bottom of 0.005 cm/d was proposed by Hillel et al. (1998), while Meyer and Gee (1999) suggested that the drainage flux should be a value between 0.001 cm/d and 0.1 cm/d. Twarakavi et al. (2009) studied a wide range of natural soils and derived a generic equation for field capacity estimation based on a 0.01 cm/d bottom flux. Assouline and Or (2014) proposed a method associated with hydraulic continuity loss due to field capacity attainment. However, different field capacity values will be obtained if the depth of interest is different even for the same type of soil, which could limit the application of this method for green roof substrates.

Whilst the FLL method is a standard method to estimate field capacity for a green roof substrate, the methods of determining field capacity adopted from soil science have also been used to

define green roof substrate field capacity. However, those natural soil-based methods may not be suitable for green roof substrate, as significant differences exist between natural soil and green roof substrates (e.g. texture, particle and pore sizes and hydraulic properties). There is some evidence that inconsistencies arise when using different methods to determine field capacity for green roof substrates (Conn et al., 2020). For example, field capacity determined by the FLL method is 64% higher than the value determined by the SWRC method using the 330 cm suction head criterion for Heather and Lavender green roof substrate (HLS) (Berretta et al., 2014). Using 100 cm or 330 cm suction head criterion makes little difference to the determination of field capacity (0.28 v/v versus 0.25 v/v) for the HLS.

Retention dominates the water losses from the substrate when the substrate moisture content is below the MWHC, and detention processes are at substrate moisture content higher than MWHC. Therefore, MWHC represents the boundary between retention and detention processes in green roof substrates, and the value of MWHC determines the intercept point where a detention model should be used to represent the processes. However, the method to determine the field capacity for a green roof substrate is inconsistent. Therefore, there is a need for a metric that makes the field capacity determined by different methods consistent and representative of the field capacity for a field green roof system.

2.5.2.2 Permeability

Permeability in FLL (2008) is equivalent to saturated hydraulic conductivity, and it is defined as the ability of the substrate to conduct water when it is fully saturated. It should be noted that in this thesis, to be consistent with the FLL standard, the term 'permeability' is the same as saturated hydraulic conductivity. In Soil Science, permeability is a property specific to the soil characteristics and has a unit of m^2, whilst, the saturated hydraulic conductivity is also influenced by the properties of the fluid flowing through the soil and has a unit of m/s (Hillel et al., 1998). Saturated hydraulic conductivity dictates how fast the runoff will be generated when the substrate is saturated. However, in engineered green roof substrates, saturation rarely happens in storms. To achieve good drainage conditions, the FLL suggests that the saturated hydraulic conductivity of extensive green roof substrate should be between 0.6 to 70 mm/min, and most reported values of green roof substrate saturated hydraulic conductivity are all within this range (De-Ville et al., 2017; Liu and Fassman-Beck, 2018; Poë et al., 2015; Stovin et al., 2015).

The falling head method suggested in FLL (2008) is routinely used to determine the saturated hydraulic conductivity for green roof substrates. The constant head method (ASTM, 2006), a conventional method to determine the saturated hydraulic conductivity of natural soil, could be

used to determine green roof substrate saturated hydraulic conductivity. However, no literature has ever reported this testing method with green roof substrates. Non-invasive X-ray microtomography (XMT) combined with the Lattice Boltzmann Method (LBM) techniques have also been used on green roof substrates to determine saturated hydraulic conductivity (De-Ville et al., 2017).

The FLL method of determining green roof substrate saturated hydraulic conductivity measures the time it takes for 10 mm of ponded water to flow through the substrate. However, it is argued that as ponding is not expected to occur in operation, the measurement is less meaningful (Fassman and Simcock, 2012). The XMT method estimates the substrate saturated hydraulic conductivity based on the substrate internal pore size distribution. This method is more complicated than the FLL method, as it involves X-ray scanning and fluid flow simulation.

The flow rate from the substrate could decrease rapidly as the substrate becomes unsaturated (i.e. moisture content reduces from saturation to field capacity).; The flow rate estimated based on the saturated hydraulic conductivity may be orders of magnitude higher than the actual runoff rates associated with green roof systems responding to storm events. Therefore, the saturated hydraulic conductivity is not appropriate to represent the water flow rate within green roof substrates during storms.

The physical properties discussed above are all static properties; they cannot reflect the dynamic characters of green roof substrate interacting with water during rainfall events. Physical properties such as water retention characteristic curve and unsaturated hydraulic conductivity are more relevant to represent the dynamic change in the substrates.

2.5.2.3 Soil Water Release Curve (SWRC)

The Soil Water Release Curve (SWRC) represents the relationship between moisture content and suction potential, and it describes the ability of the substrate to retain water. The SWRC can either be a water desorption (drying) curve, which refers to the decrease in moisture content due to an increased pore water suction head, or an imbibition (wetting) curve, referring to the increase in moisture content with decreasing suction head. **Figure 2.8** presents an example of the desorption curve of a green roof substrate. The curve in **Figure 2.8** was generated based on the Durner model, and the model parameters were calibrated based on the measured SWRC data, which will present in Chapter 5. The SWRC of a green roof substrate always decreases in moisture content with increased suction head. However, the shape and the slope of the curve depends on the substrate texture and pore size distribution. Based on the SWRC method of determining field capacity (highlighted in Section 2.5.2.1), depending on the shape of the SWRC of the substrate,

the moisture content corresponding to the suction head of field capacity (from 60 to 330 cm) can cover a broad range.

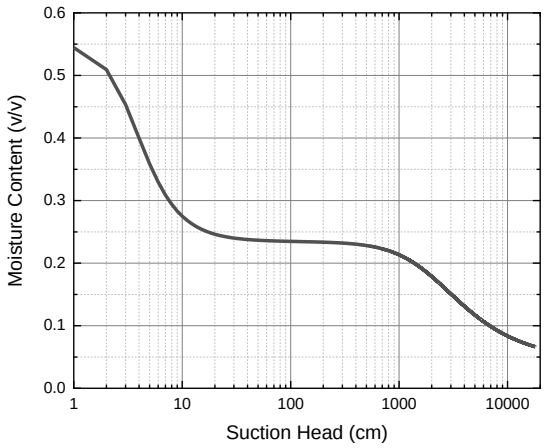

Figure 2.8. Water desorption curve of a green roof substrate.

The SWRC can dictate the substrate's ability to retain water and the amount of water available for plants. The wilting point is defined as the volume of water retained in the substrate with a suction pressure that is so high that the force of plant roots is insufficient to extract any moisture from the substrate. The volume of water between field capacity and the wilting point represents the amount of water available for plants. The volume of water between field capacity and saturation is the temporary storage that the substrate can provide during storms. **Figure 2.9** shows the moisture distribution in the substrate pore space at different conditions. At low moisture content, water is only present in the smallest pores, and due to the lack of connection between water-filled pores, the water flow in the substrate is not substantial (**Figure 2.9(a)**). When moisture content increases to above field capacity, the connections between water-filled pores are established. At this condition, water flow could be observed in the substrate, and runoff will be collected at the bottom of the substrate (**Figure 2.9(b)**). Continued wetting can bring the substrate to saturation, where all the pores in the substrate are occupied by water (**Figure 2.9(c)**). At this condition, water flows through the substrate at its fastest transmission rate.

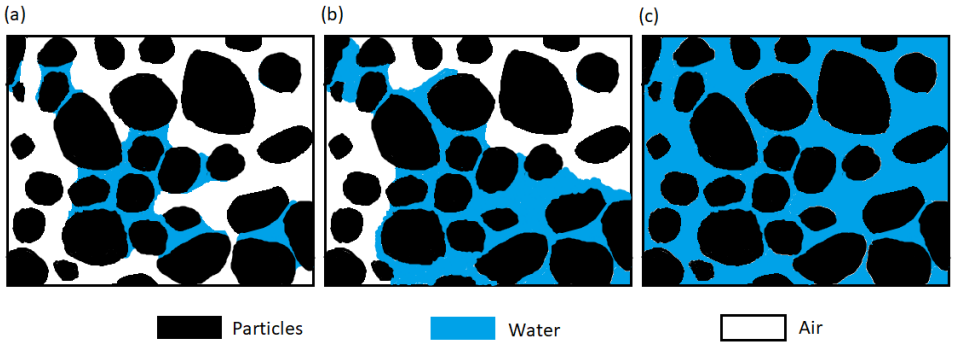

Figure 2.9. Moisture content in the substrate pore space at different conditions; (a). Below field capacity; (b). Between field capacity and saturation; (c). at saturation (Hillel et al., 1998).

The SWRC is related to the size and interconnectivity of substrate pores. Based on the capillary rise equations (Equations 2.2 and 2.3), the SWRC can be used to derive the pore size distribution in the substrate (Liu and Fassman-Beck, 2018). **Figure 2.10** gives an example of a pore size distribution derived from a SWRC. As the flow rate and moisture detention through a substrate tend to be controlled by the volume of macropores (>50 µm) (Conn et al., 2020; Menon et al., 2015), knowing the pore size distribution of the substrate also informs the ability of the substrate to conduct water and therefore its detention performance.

$$r = \frac{2\sigma}{\rho_w g|h|} \qquad \text{Equation 2.2}$$

$$g(r) = \frac{d\theta}{dr} \qquad \text{Equation 2.3}$$

where σ is the surface tension between the water and the air, r is the radius of pore size (cm), ρ_w is the density of the water (g/cm^3), h is the suction head (cm), $g(r)$ is the frequency of pore size r and θ is the moisture content.

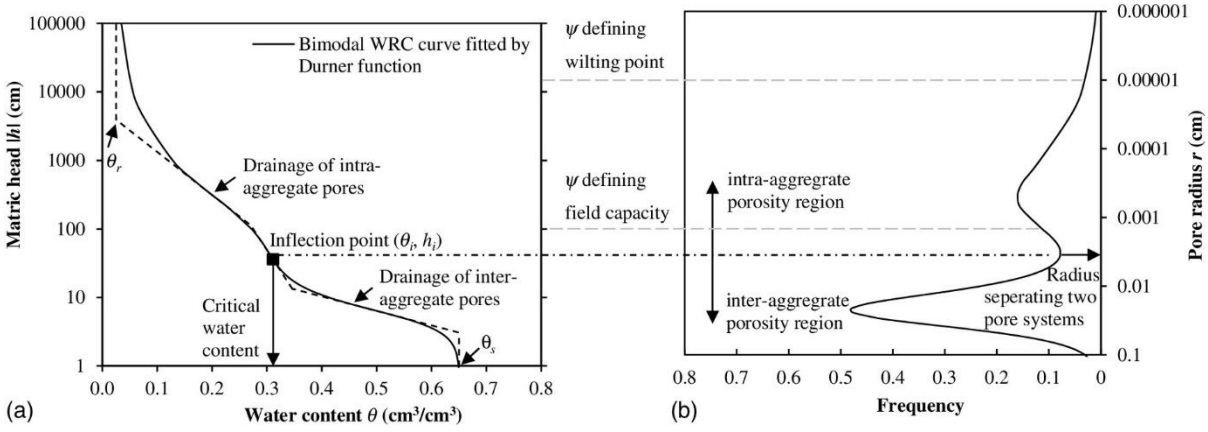

Figure 2.10. An example of deriving the pore size distribution from the SWRC (Liu and Fassman-Beck. 2018).

Experimental measurement of SWRC

There is no standard method for deriving the SWRC specific to green roof substrates. Methods of measuring SWRC for green roof substrates have emanated from the soil science community. The two most adopted methods of determining SWRC are the hanging column method and pressure extractor. According to ASTM (2016), the hanging column method is most suitable for low suction heads between 0 cm to 800 cm, and the pressure extractor method is for higher suction heads (i.e. >1000 cm). The hanging column method involves establishing a continuous hydraulic connection between the substrate samples and a ceramic tension plate at different suction heads. The pressure extractor applies gas pressure to the sample rather than water tension.

SWRC models

Several empirical equations that describe the relationship between moisture content and suction head for natural soil have been applied to represent the SWRC for green roof substrates. These models range from very simple forms such as the Brooks and Corey equation (Equation 2.4) (Brooks and Corey, 1964) to more complicated forms, such as the Durner equation (Equation 2.5) (Durner, 1994). The most frequently used SWRC model is the van Genuchten equation (Equation 2.6) (van Genuchten, 1980). However, it should be noted that, as these functions are derived from natural soil, they may not be valid for the engineered green roof substrate.

$$S_e = \frac{\theta - \theta_r}{\theta_s - \theta_r} = |\alpha h|^{-n} \qquad \text{Equation 2.4}$$

$$S_e = \frac{\theta - \theta_r}{\theta_s - \theta_r} = w[1 + (\alpha_1 h)^{n_1}]^{-m_1} + (1 - w)[1 + (\alpha_2 h)^{n_2}]^{-m_2} \qquad \text{Equation 2.5}$$

$$S_e = \frac{\theta - \theta_r}{\theta_s - \theta_r} = [1 + (\alpha h)^{n}]^{-m} \qquad \text{Equation 2.6}$$

where S_e is the relative saturation, $S_e = 1$ represents full saturation and $S_e = 0$ corresponds to the residual water content, θ_r is the residual moisture content, θ_s is the saturated moisture content, θ is the moisture content, h is the suction head (cm), α, n, w, α_1, n_1, m_1, α_2, n_2, m_2 are empirical parameters, α is the inverse of air-entry value, n is a pore size distribution index and $m = 1 - \frac{1}{n}$.

The SWRC for seven green roof substrates were measured using the hanging column method and the pressure extractor method in Liu and Fassman-Beck (2016). The hanging column method was adopted to determine the water retention curve from 1 to 100 cm suction head, and the pressure extractor method was used to measure the curve from 100 cm to 15000 cm suction head. Ten data points in the water retention curve were measured for each green roof substrate, and the

Durner model (Equation 2.5) was then fitted to the measured points. It was concluded that a green roof substrate is a dual pore system that the SWRC of the substrate can be divided into overlapping regions, and the Durner model is capable of representing the substrate's SWRC.

As the moisture content in a green roof substrate during a storm is typically between field capacity and saturation (equivalent to 0 cm to 100 cm suction head), the data within this range is particularly critical to be measured accurately. Whilst Liu and Fassman-Beck (2016) represents the first attempt to characterise green roof substrates SWRC comprehensively; it should be noted that their data typically only included five points in the <100 cm suction head range, and they did not explicitly confirm the goodness of fit of the Durner model within this critical range. There is, therefore, a need for more focused laboratory characterisation in this specific range.

2.5.2.4 Unsaturated hydraulic conductivity

Unsaturated Hydraulic Conductivity is the hydraulic conductivity when the substrate is partially saturated. The **Hydraulic Conductivity Function (HCF)** is the function that represents the relationship between unsaturated hydraulic conductivity and moisture content or suction head (**Figure 2.11**). Understanding HCF within a green roof substrate is critical to predicting how much water can be temporarily stored in the substrate (to increase moisture content) and how much water flows through the substrate and becomes runoff.

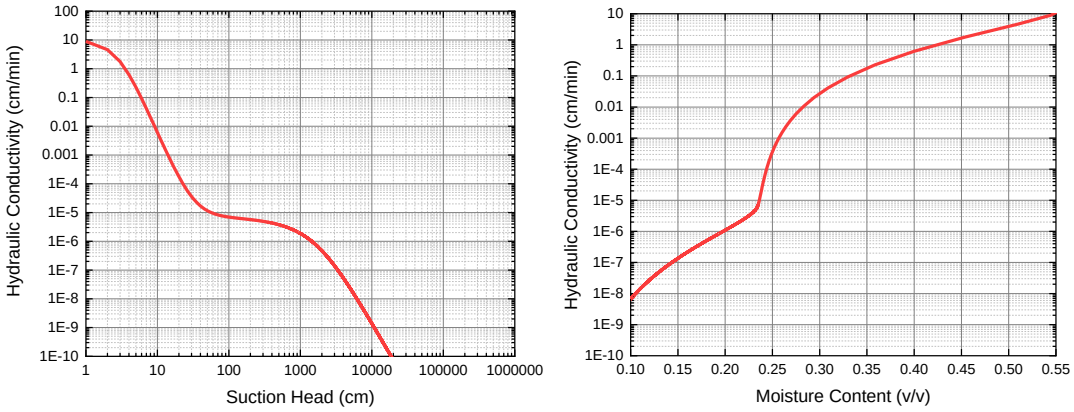

Figure 2.11. Examples of HCFs, a function of the suction head (left) and a function of moisture content (Right) (curves were generated based on the Mualem model and the SWRC presented in **Figure 2.8**).

Experimental Measurement of Unsaturated Hydraulic Conductivity

The measurement of unsaturated hydraulic conductivity involves producing unsaturated conditions in the soil and measuring the corresponding moisture content/suction head and water flux.

ASTM

ASTM (2010) provides seven methods for measuring soil unsaturated hydraulic conductivity, which potentially could be adopted to measure green roof substrate unsaturated hydraulic conductivity. The differences between the methods relate to the forces driving the water flow. The infiltration column method uses the elevation and suction head gradient to drive the flow; water flows from the top of a soil column to the bottom, unsaturated hydraulic conductivity is measured during the wetting processes. The imbibition column method is a reverse process to the infiltration column method. Soil absorbs water from the lower reservoir, and flows are from the bottom of the column to the top. The drainage column method involves a drying process with an initially saturated soil sample, and the unsaturated hydraulic conductivity is measured during the drying processes. The evaporation column method also starts with an initially saturated soil sample, but solar radiation drives the flow within the soil column. Other methods, such as the axis translation and centrifuge methods, are also relevant to the unsaturated hydraulic conductivity measurement. However, these methods have high requirements for equipment and only suitable for small scale samples.

In the ASTM infiltration column tests, the soil sample is placed in a column with a honeycomb pattern of holes at the bottom, tensiometers and soil moisture probes are inserted into the soil at different depths within the column. An infiltration flow control system is required to impose different infiltration rates on the soil column. The required flow rates are typically smaller than the saturated hydraulic conductivity. An outflow measurement system is placed at the bottom of the column to collect and measure outflow rates. To interpret measured moisture content and suction head data to unsaturated hydraulic conductivity, steady-state and transient techniques may be adopted. Steady-state refers to the condition where there is no suction head gradient present in the soil column, and the flow is driven by gravity only. The transient technique refers to the state before the soil reaches a steady-state condition, and the flow is driven by the hydraulic gradient (gravitational gradient and suction head gradient).

The unsaturated hydraulic conductivity of seven green roof substrates has been successfully measured by the ASTM infiltration method in Liu and Fassman-Beck (2018). Both the steady-state and transient techniques were used to interpret the results for the unsaturated hydraulic conductivity. Limited by the experimental set-up, only a few data points between saturation and field capacity (the range of data points that are critical to detention modelling) were obtained. Therefore, improvement is certainly needed to be able to obtain more unsaturated hydraulic conductivity data in this range.

Infiltrometer

Under the assumption that the infiltration rate of soil under a certain suction head relates to its unsaturated hydraulic conductivity, a small portable device mini-disk infiltrometer has been introduced to measure the on-site soil unsaturated hydraulic conductivity (Dohnal et al., 2010; Zhang 1997). This device comprises a mariotte chamber, a stainless steel disk and a water reservoir. The Mariotte chamber is used to apply suction to the soil sample in contact with the steel disk. Limitations of this device are 1) it can only apply suction heads between 0.5 cm and 7 cm to the soil so that the measurements are only slightly below saturation; 2) it cannot measure the unsaturated hydraulic conductivity directly; the measured infiltration rates have to be interpreted to unsaturated hydraulic conductivity using SWRC parameters; 3) this device only has a small contact area with the soil surface, it cannot be used for a large scale measurement of unsaturated hydraulic conductivity. No applications of the mini-disk infiltrometer on green roof substrate have been found in the literature.

Hydraulic Conductivity Function (HCF)

Unlike SWRC models, very few existing models can be used to estimate unsaturated hydraulic conductivity. The most commonly used model is the Mualem equation (Mualem, 1976):

$$K_r(S_e) = \frac{K(S_e)}{K_s} = S_e^{0.5}\left[\int_0^{S_e} \frac{dS_e}{h(S_e)}\right]^2 \Big/ \left[\int_0^1 \frac{dS_e}{h(S_e)}\right]^2 \qquad \text{Equation 2.7}$$

where $K_r(S_e)$ is the relative unsaturated hydraulic conductivity (cm/min) at relative saturation S_e, K_S is the saturated hydraulic conductivity(cm/min), $K(S_e)$ is the unsaturated hydraulic conductivity (cm/min) at S_e and all other symbols are as defined before.

When integrated with the Brooks and Corey equation (Equation 2.4), the Mualem equation can be rewritten as:

$$K(S_e) = K_s S_e^{2.5+2/n} \qquad \text{Equation 2.8}$$

When integrated with the Durner equation (Equation 2.5), the Mualem equation can be rewritten as:

$$K(S_e) = K_s\left(wS_{e_1} + (1-w)S_{e_2}\right)^{\tau} \times \frac{\left\{w\alpha_1\left[1-\left(1-S_{e_1}^{1/m_1}\right)^{m_1}\right]+(1-w)\alpha_2\left[1-\left(1-S_{e_2}^{1/m_2}\right)^{m_2}\right]\right\}^2}{(w\alpha_1+(1-w)\alpha_2)^2} \qquad \text{Equation 2.9}$$

where $S_{e_1} = [1+(\alpha_1 h)^{n_1}]^{-m_1}$, $S_{e_2} = [1+(\alpha_2 h)^{n_2}]^{-m_2}$ and τ is the tortuosity parameter usually assumed to be 0.5.

And when integrated with the van Genuchten equation (Equation 2.6), the Mualem equation can be rewritten as:

$$K(S_e) = K_s S_e^{0.5} \left[1 - (1 - S_e^{1/m})^m\right]^2 \qquad \text{Equation 2.10}$$

However, the Mualem equation is derived from soil-based data. As differences in texture and composition exist between natural soil and green roof substrate, this function's validity for green roof substrate is unknown.

Liu and Fassman-Beck (2018) compared the measured green roof substrate's unsaturated hydraulic conductivity data points with the predicted curve based on the Durner-Mualem model (Equation 2.9), and they found that the estimated curves did not fit the measured points well. The Durner-Mualem approach tended to underestimate the unsaturated hydraulic conductivity for most of their green roof substrates, demonstrating the need for a new HCF suitable for green roof substrates.

2.6 Green roof hydrological modelling

As monitoring studies only reflect the hydrological performance of a specific type of green roof, and cannot be used for predictions, more generic approaches (e.g. conceptual models and physically-based models) that permit the modelling of green roof hydrological performance have been explored. Green roof hydrological modelling can be split into retention and detention modelling. Retention modelling refers to the estimation of rainfall losses (**Figure 2.12**), and detention modelling refers to routing the transient storage (**Figure 2.12**).

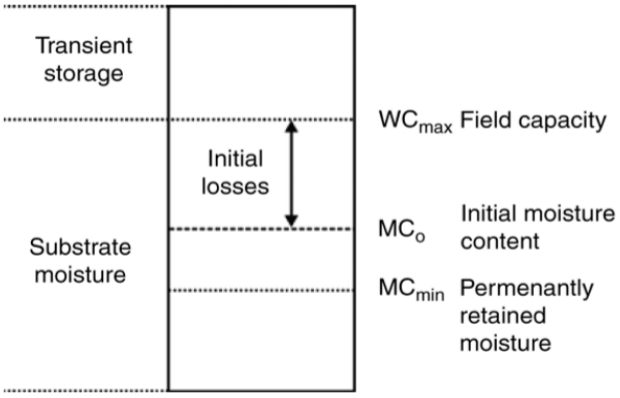

Figure 2.12. Conceptual water balance model of green roof (Kasmin et al., 2010).

2.6.1 Retention modelling

Retention is commonly modelled via the following equations (Stovin et al., 2013):

$$\mathrm{Runoff_t} = \begin{cases} 0, & \text{if } \mathrm{S_{t-1}} + \mathrm{P_t} - \mathrm{ET_t} \le \mathrm{S_{max}} \\ \mathrm{P_t} - (\mathrm{S_{max}} - \mathrm{S_{t-1}}) - \mathrm{ET_t}, & \text{if } \mathrm{S_{t-1}} + \mathrm{P_t} - \mathrm{ET_t} > \mathrm{S_{max}} \end{cases} \quad \text{Equation 2.11}$$

where t is the discretised time step, S is the temporary storage in the green roof system (mm), P is precipitation (mm), ET is evapotranspiration (mm), and $\mathrm{S_{max}}$ is the maximum substrate storage capacity (i.e. field capacity of the substrate) (mm). Substrate moisture content is then updated:

$$\mathrm{S_t} = \begin{cases} \mathrm{S_{t-1}} + \mathrm{P_t} - \mathrm{ET_t}, & \text{if } \mathrm{S_{t-1}} + \mathrm{P_t} - \mathrm{ET_t} \le \mathrm{S_{max}} \\ \mathrm{S_{max}}, & \text{if } \mathrm{S_{t-1}} + \mathrm{P_t} - \mathrm{ET_t} > \mathrm{S_{max}} \end{cases} \quad \text{Equation 2.12}$$

It has been highlighted in Stovin et al. (2013) that accurately estimating the evapotranspiration (ET) rate is critical to predicting green roof hydrological performance. Many evapotranspiration models have been adopted to predict the ET rate from green roof systems. These models include the **Thornthwaite equations** (Wilson, 1990), which predicts ET as a function of temperature (Kasmin et al., 2010; Peng and Stovin, 2017); **Hargreaves equation** (Hargreaves and Samani, 1985), which requires only a few weather parameter inputs (Cipolla et al., 2016; Hilten et al., 2008); and the most sophisticated **Penman-Monteith approach** (Allen et al., 1998; Berretta et al., 2014). As these ET models were initially developed to estimate the ET from crops, considering the influence of vegetation species, crop factors were introduced and calibrated using the monitored ET data from green roofs to model the ET from green roofs (Berretta et al., 2014; Kasmin et al., 2010).

The ET rate estimated from the standard ET models highlighted above is the potential ET rate (the ET rate with well-watered condition). However, as green roof system is normally a non-irrigated system, substrate moisture available for ET becomes restricted with time, so the actual ET rate tends to decay with time or moisture content. Using the potential ET rate for the actual ET rate would overestimate the ET rate (Poë et al., 2015; Stovin et al., 2013) and over predict the retention performance for green roof systems. As a consequence, a Soil Moisture Extraction Function (SMEF) model (Equation 2.13), which estimates the actual ET rate as a fraction of potential ET rate and moisture content, was suggested for green roofs (Stovin et al., 2013). The fraction in this model is the ratio of temporal water content to maximum water content. Green roof ET has been well understood (Poë et al., 2015), and existing models can accurately predict the actual ET rate from a green roof system (Berretta et al., 2014).

$$\mathrm{ET_t} = \mathrm{PET_t} \times \frac{\mathrm{S_t}}{\mathrm{S_{max}}} \quad \text{Equation 2.13}$$

where $\mathrm{PET_t}$ is the potential ET rate, and $\mathrm{S_t}$ is substrate moisture content.

2.6.2 Detention modelling

2.6.2.1 Introduction

Processes that lead to the detention (or delay) of runoff are generally assumed to be associated with the green roof's substrate and drainage layers. Detention processes associated with the vegetation layer are considered to be negligible. Detention occurs in the substrate layer as runoff moves vertically downwards towards the underlying drainage layer. The flow of runoff in the drainage layer is parallel to the roof surface, and further detention may occur depending on the drainage layer configuration and roof length (**Figure 2.13**).

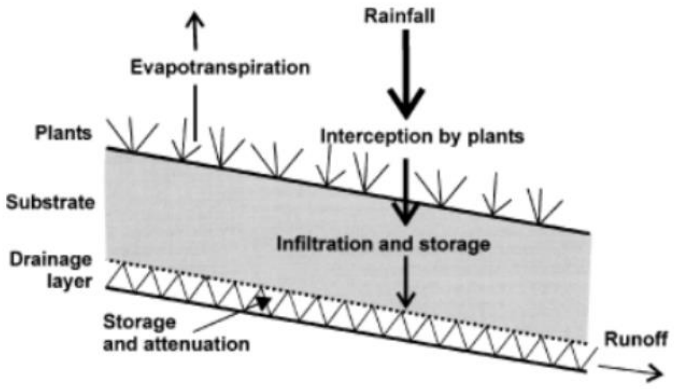

Figure 2.13. Hydrological processes in a green roof system (Stovin, 2010).

Detention modelling approaches can be broadly divided into two categories: lumped (or whole-system) models and multi-layered models. This classification is shown in **Table 2.1**, and further discussion of each approach is provided in Sections 2.6.2.2 to 2.6.2.3.

Table 2.1. Classification of green roof detention modelling approaches

Model Type	**Approach**	**Comments**
Lumped		
Empirical	Unit Hydrograph	Lacks transferability/generalisation
Conceptual	Reservoir Routing	Lacks transferability/generalisation
Multi-layered		
Substrate		
Conceptual	Reservoir routing	Lacks transferability/generalisation
Physically-based	Darcy's Law, Green-Ampt	• Generic approaches; • Computationally complex;

	Model, Richards Equation	• Significant demands for parameterisation; • Uncertainties around validity for green roof substrates.
Simplified physically-based	SWMM	• Reduced complexity of computation and parametrisation; • Uncertainties around validity for green roof substrates.
Drainage layer		
Conceptual	Reservoir Routing	Lacks transferability/generalisation
Physically-based	Saint Venant equation	• Generic approach; • Computationally complex; • Significant demands for parameterisation; • Uncertainties around validity for green roof drainage layers.
Simplified physically-based	SWMM	• Reduced complexity of computation and parametrisation; • Uncertainties around validity for green roof drainage layers.

In lumped models, all detention processes are combined into a single, empirical relationship. Reservoir routing and unit hydrograph-based approaches have both been used to capture observed green roof detention effects when suitably parameterised. The main limitation of these approaches, however, is the lack of transferability/generalisation; they may only be applied to the specific systems from which the model parameters were derived.

In multi-layered modelling approaches, different models are used to represent the key detention processes associated with the substrate and drainage layer. These approaches can be broadly classified into physically-based models, simplified physically-based models, and conceptual models.

Physically-based modelling approaches have the potential to explicitly account for the key detention processes occurring in the green roof substrate and drainage layers. However, these approaches can be computationally intensive and are typically dependent on the detailed physical characterisation of the green roof components. Whilst there are examples of these methods being employed to model green roof detention, few convincing validation cases have been

presented. The limitations and uncertainties of the work done to date will be highlighted in the following sections.

2.6.2.2 Lumped models

Lumped models combine detention processes in a green roof system into a single, empirical relationship. Lumped models are usually derived from field observations, and they are specific to a certain type and configuration of green roof systems.

2.6.2.2.1 Empirical model

The Unit-hydrograph is an empirical approach used for natural catchments to estimate the surface runoff in response to rainfall events from a characterised hydrograph. As the runoff profile from a green roof system shares the same shape as the natural catchment surface runoff profile, this approach was also used to derive the runoff from green roofs. Villarreal and Bengtsson (2005) derived a 1 mm and 1-minute unit-hydrograph for a green roof test bed using three pairs of rainfall and runoff profiles in response to uniform rainfall inputs. The prediction of runoff made using a unit hydrograph approach may be less accurate if the storm is not spatially or temporally uniform. Berryman and Stovin (2010) explored three alternative time area diagram approaches (cumulative area discharging profile, instantaneous profile, exponential profile) derived from monitoring data within MicroDrainage to simulate the runoff from a green roof system. One limitation of these models is that they can only estimate the runoff response from a green roof with the same characteristics and vegetation as the one employed in the experiments.

2.6.2.2.2 Conceptual model

The most commonly used conceptual model for green roof detention modelling is the Reservoir Routing model (Equations 2.14-2.15), in which a Reservoir Routing equation simulates the detention processes (Kasmin et al., 2010; Stovin et al., 2013):

$$\mathrm{S_t} = \mathrm{S_{t-1}} + \mathrm{Qin_t}\Delta\mathrm{t} - \mathrm{Qout_t}\Delta\mathrm{t} \qquad \text{Equation 2.14}$$

$$\mathrm{Qout_t} = \mathrm{k_s}\mathrm{S_{t-1}^{n_s}} \qquad \text{Equation 2.15}$$

where Qin is the inflow rate to the substrate (mm/min), Qout is the outflow from the substrate (mm/min), $\Delta\mathrm{t}$ is the discretised time step, h is the temporarily stored water (mm), and k_s and $\mathrm{n_s}$ are the routing parameters.

The Reservoir Routing model has been used in many studies to simulate the runoff from green roof systems, and the model has shown a good ability to regenerate the runoff profiles (Kasmin et al., 2010; Stovin et al., 2013). However, like the empirical model, the parameters in the model

rely on calibration with measured rainfall and runoff data, and the calibrated parameters are only valid for a specific configuration.

2.6.2.3 Multi-layered modelling approaches

As a green roof system consists of multiple layers (**Figure 2.3**), the detention processes in each independent component can be modelled separately. As discussed in the previous section (Section 2.3), the substrate and the drainage layer in a green roof system provide the key detention processes. Multi-layered models use different models to represent the detention processes associated with the substrate and the drainage layer. These models can be broadly classified into conceptual models, physically-based models and simplified physically-based models.

2.6.2.3.1 Substrate

Conceptual model

The Reservoir Routing model (Equations 2.14 and 2.15) was first proposed to model the detention effects in a complete green roof system (Kasmin et al., 2010). However, the Reservoir Routing model was also employed to characterise the relationships between water depth and runoff rate from brick-based green roof substrates (Vesuviano et al., 2014; Yio et al., 2013). As this model was proposed to represent the detention processes in the green roof substrate only, the model parameters can be determined from independent substrate tests. However, the model parameters are not independent of substrate depth; therefore, intensive characterisation experiments are still needed to calibrate the relevant parameters.

Physically-based model

The physically-based models for green roof substrate include Darcy's Law, the Green-Ampt model and the Richards Equation (Bursztа-Adamiak and Mrowiec, 2013; Cipolla et al., 2016; Hilten et al., 2008; Liu and Fassman-Beck, 2017; Palla et al., 2012; Peng and Stovin, 2017; She and Pang, 2009). As these models are physically based, calibration with measured rainfall-runoff is not typically required to determine the model parameters. The model parameters in these models are only dependent on detailed physical characterisations of the green roof components. However, these approaches can be computationally intensive or only suitable for a specific flow condition.

Darcy's law (Darcy, 1856) is an expression of the conservation of momentum that describes the flow through a porous medium (Equation 2.16). Darcy's law assumes that hydraulic conductivity is constant during the wetting process, and the hydraulic head gradient drives the water flow. Darcy's Law is only applicable to saturated media. She and Pang (2010) used Darcy's Equation to

simulate the flows in the substrate under saturated conditions. However, saturation is a rare condition for green roof substrates, and it is questionable whether it is useful to employ Darcy's law in a model framework. The assumptions made for Darcy's law mean that it is poorly suited to model the hydrological processes within the substrate during storms.

$$q = K_s(\frac{h+z}{z}) \quad \text{Equation 2.16}$$

where q is the flow rate through a unit area of soil (cm/min), K_s is the soil saturated hydraulic conductivity (cm/min), h is the suction head (cm), and z is the depth of the soil (cm).

The **Green-Ampt** model (Green and Ampt, 1991) describes the water infiltration processes into deep soil from an initial ponding condition. The Green-Ampt model assumes a sharp horizontal wetting front, which divides a saturated zone at the top and an unsaturated zone below. The governing equations of the Green-Ampt model are given in Equation 2.17 and Equation 2.18.

$$f = K_s[1 + \frac{(\phi-\theta)h}{F}] \quad \text{Equation 2.17}$$

$$K_s t = F - (\phi - \theta)h\ln[1 + \frac{F}{(\phi-\theta)h}] \quad \text{Equation 2.18}$$

where f is infiltration rate (cm/min), K_s is saturated hydraulic conductivity (cm/min), ϕ is porosity, θ is moisture content, h is suction head at the wetting front (cm), F is cumulative infiltration (cm) (from time 0 to time t).

The parameters in the Green-Ampt model can be determined from independent substrate characterisation tests. She and Pang (2010) utilised the Green-Ampt model to simulate the unsaturated flows within the substrate. However, instead of characterising the physical properties of the substrate, they calibrated the model parameters based on the measured rainfall and runoff data.

The Green-Ampt model is also integrated into the Storm Water Management Model (SWMM) green roof module to simulate the water infiltration from the substrate surface to the deep substrate (Rossman and Huber, 2016). A few studies have utilised this model within SWMM to simulate the runoff from green roof substrate (Burszta-Adamiak and Mrowiec, 2013; Johannessen et al., 2019; Palla and Gnecco, 2015; Peng and Stovin, 2017). However, none of these studies has fully characterised the green roof substrate physical properties, and the model parameters have either been calibrated or assumed. Besides, as the Green-Ampt model assumes a ponding zone upon the substrate surface (this rarely occurs in a green roof system), this model cannot provide

any detention effects due to the surface infiltration for a green roof substrate with a high saturated hydraulic conductivity.

The **Richards Equation** is an unsaturated flow equation derived from the continuity equation with Darcy's Law substituted. The Richards Equation in 1D (vertical) form can be written as follows (Equation 2.19) (it should be noted that Richards Equation can be in water content form or mixed form of suction head and water content) (Richards, 1931).

$$\frac{\partial \theta}{\partial t} = \frac{\partial}{\partial Z}\left[K(h)\left(\frac{\partial h}{\partial Z} - 1\right)\right] \qquad \text{Equation 2.19}$$

where θ is the moisture content, t is the discretised time step (min), Z is the elevation of discretised spatial step (cm) and $K(h)$ is the unsaturated hydraulic conductivity at suction head h (cm/min).

The Richards Equation is a non-linear partial differential equation. The SWRC and the HCF are needed to obtain an approximate solution for the Richards Equation. The Richards Equation is thought to be the most robust physically-based model for green roof substrate. It describes the wetting (infiltration) processes within the substrate during the rainfall using physical parameters, which generalises the application of the model. However, as a partial differential equation, it is computationally expensive.

HYDRUS-1D is a free commercial software to simulate water, heat and solute movement in porous media (Šimůnek et al., 2008). Many of the published literature using the Richards Equation to model green roof substrate has been implemented in HYDRUS-1D. As significant demands for experimental parameterisation of SWRC and HCF are needed to use the Richards Equation, those properties have not always been characterised for green roof substrates. The model parameters used in the Richards Equation in literature are typically estimated based on natural soils or reference to literature for a similar texture (Castiglia Feitosa and Wilkinson, 2016; Hilten et al., 2008; Liu and Fassman-Beck, 2018, 2017; Palla et al., 2012; Soulis et al., 2017). Uncertainties around the validity of these parameter values/relationships for green roof substrates exist in these studies.

Hilten et al. (2008) employed the Richards Equation in HYDRUS-1D to regenerate the runoff profiles from a 100 mm green roof substrate. Instead of characterising the physical properties for the substrate, the parameters for sand were used for the substrate. Although the modelled runoff showed good consistency with the measured runoff, the validation was conducted with the total daily runoff volume rather than instantaneous runoff profiles. The model's ability to reproduce the green roof's runoff profiles was therefore not evaluated.

Palla et al. (2012) modelled the detention performance of a 200 mm substrate in HYDRUS-1D. The hydraulic parameters required by the model were either estimated from a similar soil texture or calibrated from five selected events. Palla et al. (2009) modelled the green roof detention in HYDRUS-2D. The SWRC for the substrate were determined and measured through the pressure extractor method. However, instead of measuring the substrate HCF, the Mualem model was used to estimate the HCF.

Liu and Fassman-Beck (2017) employed HYDRUS-1D to regenerate the runoff profiles from 100 mm green roof substrates in response to constant rainfall inputs. The Durner model was used to estimate the SWRC, and the Mualem equation was adopted to estimate the unsaturated hydraulic conductivity. The model tended to delay the time to start runoff and overestimate the substrate's peak flow rate. The unsatisfactory model behaviour was believed to be caused by the occurrence of preferential flow in the substrate, and the model results were improved when a preferential flow model was utilised. However, comparing the measured and estimated HCF for the substrates, it is evident that the Mualem model underestimated the HCF. The poor model performance could potentially also be attributed to the unrealistic estimation of the substrate unsaturated hydraulic conductivity.

One of the limitations of using HYDRUS is that the functions used in the model are not user-defined. For example, only the Mualem equation can be selected to estimate the HCF. Based on an existing study on measuring the HCFs for green roof substrates (Liu and Fassman-Beck, 2018), the Maulem equation was shown to underestimate the unsaturated hydraulic conductivity of green roof substrates. Therefore, another modelling framework is needed to allow alternative HCFs to be utilised in conjunction with the Richards Equation.

Simplified physically-based model

The **Percolation model in SWMM** (Equation 2.20) is a simplified form of the Richard Equation under the assumption of steady-state flow. Under a steady-state flow condition, as no vertical gradient is presented in the substrate, the flow is driven only by gravity. The flow from the substrate at this condition is a function of moisture content and saturated hydraulic conductivity. The percolation model in SWMM provides an estimate of the flow rate based on the moisture content when the moisture content is above field capacity. The parameters in this model can be determined by characterising the substrate physical properties. However, the hydraulic slope has to be determined through the measurement of HCF or estimated through a soil texture-based model (Equation 2.21). This model has been integrated into the SWMM green roof model, and many studies have used this model to simulate the runoff from green roof substrates (Burszta-

Adamiak and Mrowiec, 2013; Palla and Gnecco, 2015; Peng and Stovin, 2017). However, the validity of this model and the model used to estimate the HCF have not been independently validated for green roof substrates.

$$f_2 = \begin{cases} 0, & \theta_2 \leq \theta_{FC} \\ K_s \exp\left(-HCO(\emptyset_2 - \theta_s)\right), & \theta_2 \geq \theta_{FC} \end{cases} \quad \text{Equation 2.20}$$

$$HCO = 0.48 \times \%\text{sand} + 0.85 \times \%\text{clay} \quad \text{Equation 2.21}$$

where f_2 is the percolation rate (cm/min), $\emptyset_2$ is the porosity, θ_s is the moisture content, θ_{FC} is the field capacity, and HCO is the hydraulic slope.

2.6.2.3.2 Drainage layer

Conceptual model

The Reservoir Routing model (Equations 2.14 and 2.15) has been applied to model the runoff from green roof drainage layers in a few studies (Vesuviano et al., 2014; Vesuviano and Stovin, 2013), and the parameters for the model were parameterised from the independent drainage layer tests.

Physically-based model

For the green roof system where the drainage layer is a soil-based material (e.g. gravel), the Richards Equation has been utilised to model the detention processes (Palla et al., 2012, 2009). However, the Richards Equation is not capable of modelling the detention processes in a plastic-board based drainage layer.

The **Saint Venant equation** (Equation 2.22) is a physically-based model for 1D gradually varied unsteady flow in an open channel (Chow et al., 1988). This model estimates the water level profile along the length of the drainage layer; the runoff from the layer can be calculated from a mass balance equation. A good estimation of the depth-averaged flow velocity (U_s) is critical for utilising this model. This velocity term can be estimated from Manning's Equation (Equation 2.23), in which the material-specific Manning's n needs to be characterised from independent drainage layer tests. The Saint Venant equation is thought to be capable of representing the flow condition in green roof drainage layers during storms. However, the validity of this model in representing the detention in green roof drainage layers has not been validated in the literature. The computational cost of this model can also be high.

$$\frac{\partial h_s}{\partial t} + \frac{\partial h_s U_s}{\partial x} = R(x,t) \quad \text{Equation 2.22}$$

$$U_s = \frac{{h_s}^{2/3}}{n_f}\sqrt{S_f} \qquad \text{Equation 2.23}$$

where h_s is the unit storage of water (cm), U_s is the depth-averaged flow velocity (cm/min), t is time (min), x is the distance coordinate (cm) and R(x,t) is the rate of recharge (cm/min), s_f is the fraction slope and n_f is the Manning's roughness coefficient or Manning's n.

Simplified physically-based model

Manning's Equation in SWMM is a simplified physically-based model (Equation 2.24) under the assumptions of uniform and steady flow.

$$q_3 = \frac{1.49}{n_3}\sqrt{S_1}(W_1/A_1)\emptyset_3(d_3)^{\frac{5}{3}} \qquad \text{Equation 2.24}$$

where q_3 is the drainage layer outflow rate (cm/min), $\emptyset_3$ is the void fraction of the drainage layer, D_3 is the drainage layer thickness (cm), n_3 is the drainage layer roughness coefficient, S_1 is the system slope, W_1 is the total length along the edge of the roof where runoff is collected (cm), A_1 is the roof surface area (cm^2), d_3 is the depth of water in the storage layer (cm).

This model has been proposed and used for a green roof drainage layer, and the prediction of the runoff profiles relies on the correct characterisation of drainage layer roughness. Without any characterisation for the specific drainage layer, a roughness of 0.05 was used in She and Pang. (2010) to simulate the runoff from the layer.

Few studies have independently validated Manning's Equation for green roof drainage layers. Vesuviano (2014) calibrated the roughness coefficient for a few types of plastic board-based green roof drainage layers using the measured rainfall-runoff data. It found that Manning's Equation does not have a significant advantage over the Reservoir Routing model. Given the fact that the model parameters in Manning's Equation are independent of drainage layer slope and length, it has a wider application than the Reservoir Routing model. However, further detailed investigation into the validity of this model for modelling the runoff from green roof drainage layers is still needed.

2.7 Chapter summary

Through a broad literature review of previous works, the following knowledge gaps are identified:

Retention and detention are the two main hydrological processes in a green roof system. Retention dominates the water losses from the substrate in dry weather periods, and detention determines the magnitude and timing of the runoff profiles from the system. The maximum water

holding capacity or field capacity represents the boundary between retention and detention processes. However, the method to determine maximum water holding capacity or field capacity for a green roof substrate is inconsistent in the literature. Therefore, a metric that generalises the maximum water holding capacity or field capacity determined by different methods and represents the condition of a field green roof system is needed.

In the context of representing physical processes within green roof substrates, the Richards Equation has been employed to represent the dynamic processes within the substrate during storms. However, to use the Richards Equation, the SWRC and HCF need to be characterised for the substrate. Some experimental characterisation studies focusing on these two relationships have been conducted in the literature. However, limited by the apparatus and time, a limited understanding has been developed from current studies, especially regarding the unsaturated hydraulic conductivity of green roof substrate. With little knowledge on the unsaturated hydraulic conductivity of green roof substrates, it is hypothesised that current approaches that use a soil-based equation to estimate the unsaturated hydraulic conductivity for green roof substrates introduce uncertainties and errors to the model results. New HCF functions derived from measured laboratory data for green roof substrates can provide a more accurate estimation of the substrate unsaturated hydraulic conductivity than the exiting HCF models and improve the model results.

Exiting models that solve the Richards Equation only accept the Durner type of model to estimate the unsaturated hydraulic conductivity. However, based on previous studies, it is evident that this type of model does not provide accurate estimations of the hydraulic conductivity for green roof substrate. Therefore, a new model that is capable of solving the Richards Equation using new HCF equations would overcome the limitation of existing models.

Empirical models based on the Reservoir Routing model have been proposed to characterise the runoff from different plastic-based green roof drainage layers. However, the model parameters are configuration-dependent; intensive characterisation experiments are needed to identify the relevant parameters. A physically-based model, of which model parameters can be identified from component isolated characterisation experiments, is believed to be capable of providing a good representation of the detention performance of green roof drainage layers with a more general application than the empirical models.

SWMM is a widely used model for practitioners to estimate or test the hydrological response of green infrastructure designs. The capability of the SWMM model modelling green roof detention performance has not been rigorously validated and evaluated in previous studies. Especially the

capability of the SWMM model modelling a recently emerged innovative green roof that utilises a polyester fabric as the drainage layer. In addition, the physically-based model of modelling the detention of a complete green roof system also needs validation with measured data.

Given the gap in current knowledge, there is a novel opportunity to explore how the hydraulic conductivity varies with moisture content for green roof substrates. Coupled measurements of green roof substrates' Soil Water Release Curve and Hydraulic Conductivity Function will provide the new knowledge required for the development of physically-based detention models for green roof substrates. The review of green roof drainage layer models revealed the need for a generic physically-based model. The drainage layer model development in this study will inform the modelling of detention processes in complete green roof systems.

3 Experimental Methods

3.1 Chapter overview

This chapter introduces the experimental methods employed in this study. Firstly, the experiments that were designed, developed and conducted by the author at the University of Sheffield are introduced. These experiments include: the FLL tests to determine PSD, d_{50}, bulk density, porosity, MWHC and water permeability (saturated hydraulic conductivity); the SWRC characterisation for green roof substrates using hanging column and pressure extractor methods; the HCF measurement using the steady-state and transient techniques; and the substrate detention tests.

The experiments conducted by previous researchers or a third party are then outlined. These experiments include the detention tests with drainage layers, a complete conventional green roof system, an innovative detention layer and an innovative green roof system that contains multiple layers.

This chapter contributes to the following publications:

Peng, Z., Smith, C., Stovin, V., 2019. Internal fluctuations in green roof substrate moisture content during storm events: Monitored data and model simulations. *J. Hydrol.* 573, 872–884. https://doi.org/10.1016/j.jhydrol.2019.04.008

Peng, Z., Smith, C., Stovin, V., 2020. The importance of unsaturated hydraulic conductivity measurements for green roof detention modelling. *J. Hydrol.* 590, 125273. https://doi.org/10.1016/j.jhydrol.2020.125273

Peng, Z., Garner, B., Stovin, V., 2021. Two green roof detention models applied in two green roof systems. *J. Hydrol. Eng.* (under review).

3.2 FLL tests

The Forschungsgesellschaft Landschaftsentwicklung Landschaftsbau (FLL) (FLL, 2008) is a standard guidance for determining selected green roof substrate physical properties. The FLL outlines laboratory test methods, apparatus, and standard target values for substrates to achieve their design functions. In this study, properties determined for the substrates using the FLL methods included particle size distribution (PSD), d_{50}, bulk density, porosity, maximum water holding capacity (MWHC) and water permeability (saturated hydraulic conductivity), and the tests were conducted with three replicated of three samples from the same batch.

3.3 Soil Water Release Curve (SWRC) characterisation

The Soil Water Release Curve (SWRC) is determined by measuring paired values of suction head and moisture content. In this study, similar to the methods adopted in Liu and Fassman-Beck (2018), the hanging column (Carter and Gregorich, 2007) method was used to characterise the SWRC at low suction heads, and the pressure extractor (Carter and Gregorich, 2007) method was used to determine the curve at high suction heads.

3.3.1 Hanging column method

The hanging column method yields SWRCs in terms of matric suction. This method involves establishing a continuous hydraulic connection between the sample and the tension plate. Various suction heads are applied to the specimen by elevating the sample relative to the drainage point. The corresponding volumetric water contents are measured by weighing the samples after removal from the apparatus. This method is typically suitable for low suction heads (i.e. suction head <5 m).

Figure 3.1 illustrates the hanging column apparatus used in this study. The system consists of a water-saturated porous plate connected to a water column attached to a bottle full of water open to the atmosphere. The substrate specimens were placed in contact with a saturated porous plate, and the water flows from the specimens until the equilibrium water content corresponding to the applied suction was reached. A 100 mm (diameter) × 100 mm (height) plastic ring was used to hold the substrate. Considering the specific characteristics of green roof substrates, a wet strengthened filter sheet was attached to the base of the ring to avoid sample residues on the ceramic plate at the end of the test.

The characterisations started with saturated samples, and 11 successive suction heads (6 cm to 100 cm) were applied to the substrate samples to construct the SWRC. An equilibrium state was judged to have been attained when the water stopped leaving the substrate for four hours, and the water in the reservoir started to move backwards to the substrate samples. The samples were weighed after they reached the equilibrium state, and then the suction head was increased. When samples reached equilibrium at the final suction head, they were transferred to steel trays and dried in the oven at 105°C for 24 hours to determine the sample dry weights and to calculate moisture content at each suction head. Three replications were conducted with each substrate of three samples from the same batch to minimise the uncertainties associated with subsampling.

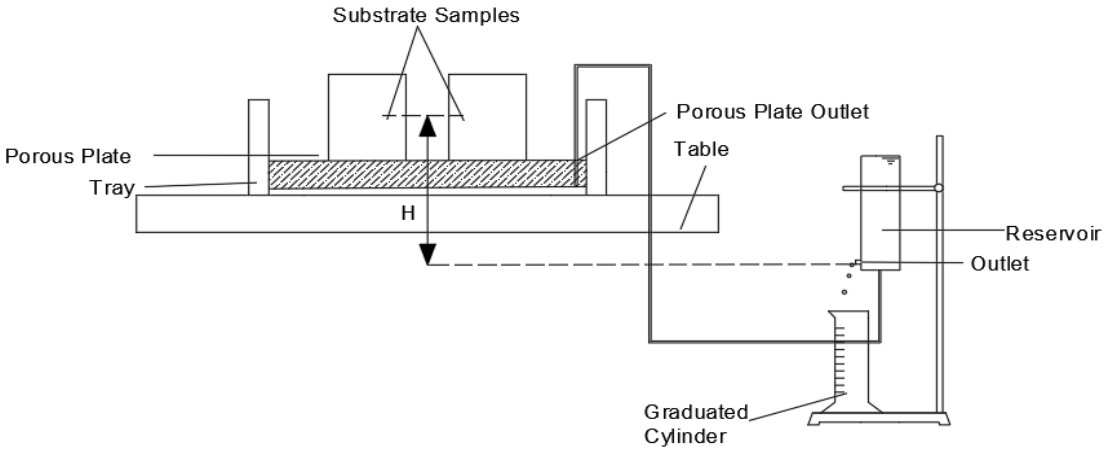

Figure 3.1. Hanging column apparatus for Soil Water Release Curve measurement.

3.3.2 Pressure extractor method

The pressure extractor method refers to the method that applies gas pressure to force water release from the samples (Carter and Gregorich, 2007); this method is most commonly used in the range of suction heads from 33 kPa (approx. 3.3 m) to 1500 kPa (approx. 150 m). Pressure extractor data collected by previous researchers are considered within this study; however, no new data were collected.

3.4 Hydraulic Conductivity Function (HCF) measurement

A hydraulic conductivity function determines how fast water flows through the substrate and how fast runoff to be generated. The hydraulic conductivity function (HCF) is defined as the relationship between unsaturated hydraulic conductivity and moisture content or matric head. The HCF has to be defined when using the Richards Equation to model green roof detention performance. However, quantitative measurement of the HCF is not easy; hydraulic conductivity can vary over many orders of magnitude within the same soil as a function of moisture content (Hillel et al., 1998). There are several laboratory methods to determine the HCF (ASTM, 2010), but all methods are based on Darcy's law, which states that the hydraulic conductivity is equal to the coefficient of proportionality between the flow rate and the hydraulic gradient. Limited by test durations and apparatus, there is no single test that can be applied to the substrate to measure the HCF over the whole range of moisture content (i.e. both below field capacity and above field capacity) (ASTM, 2010). ASTM D7664-10 (ASTM, 2010) outlines a range of test methods that may be used to measure unsaturated hydraulic conductivity. The infiltration column method was judged to be the most suitable method in this context, considering the physical characteristics of green roof substrates and the flexibility of the apparatus. Liu and

Fassman-Beck (2018) have previously demonstrated the potential value of this method in the context of green roof substrates and bio-retention media.

The infiltration column method was employed in this study to characterise the vertical hydraulic conductivities of green roof substrates. For relatively high hydraulic conductivities (in this case, $K(\theta)$ > 0.014 cm/min), the steady-state method is appropriate, whilst the transient method permits characterisation at lower hydraulic conductivities. The measured runoff rate and moisture content under steady-state conditions were related to determine the HCF at high hydraulic conductivity, and the paired moisture content and suction head measurements under transient conditions were used to characterise the HCF at low hydraulic conductivities.

Figure 3.2 illustrates the apparatus used for HCF determinations. Instruments used in the test were calibrated prior to the test (Appendix A). Two set-ups of the same configurations were used in the experiments at the same time to measure the HCF of the two samples of the same substrate. The apparatus comprises an infiltration flow control system, sample column, moisture content measurement devices, suction head measurement devices and an outflow measurement system. Inspired by the experimental set-up of Yio et al. (2013), the infiltration rate was controlled by a peristaltic pump (Watson Marlow, 503U) and an 8 mm (inner diameter) tube. In this study, 11 steady infiltration rates, ranging from 0.014 cm/min to 1.41 cm/min, were applied to the substrates. Hypodermic needles (BD, Microlance 3 26G and 21G) were used to distribute the water evenly to the substrate surface. The small needles (26G) are capable of distributing a low flow rate (≤0.14 cm/min), and the large needles (21G) are suitable for high flowrates (≥0.14 cm/min). The water distribution panel consists of 37 needles; they are arranged in a regular octagon with three needles along each side, seven needles across the longest axes and five needles across the shortest axes. The distance between adjacent needles is 40 mm, so the octagon has sides of 120 mm, and is 240 mm long across its longest axes. The sample column is 540 mm high and has a diameter of 300 mm. The height was chosen to ensure that there is a volume of the substrate that is not influenced by the boundary conditions, and the diameter was chosen to minimise wall effects. A perforated base covered by a layer of mesh and filter sheet (Zinco, Systemfilter SF) was placed above a funnel. A runoff collecting barrel with a pressure transducer (Druck Inc. PDCR 1830) was used to measure water depth in a straight-sided collection barrel, which was subsequently used to determine the outflow from the substrate. Five moisture probes (P1 to P5, Meter, 5TM) and three tensiometers (T1 to T3, Meter, T5x) were placed at different depths to measure the change in moisture content and suction head, respectively. The moisture probes were put into place while the column was being filled with substrates, and the substrate around the probes was gently pressed in place to obtain a good hydraulic connection.

The substrate was placed gently within the column using a trowel. No compaction was applied to the substrate considering the strength of the apparatus. The tensiometers were inserted into the substrate once the substrate had reached a steady-state under the lowest flowrate to avoid water losses from the tensiometer reservoir in the dry substrate. The moisture probes were connected to a Meter Em50 data logger, whilst the tensiometers and pressure transducers were connected to a Campbell Scientific CR1000 data logger. Continuous readings from the sensors were recorded at 1-minute time intervals.

Calculation of unsaturated hydraulic conductivities was based on the Richards Equation (Equation 2.19). Two techniques, steady-state and transient, were used to interpret measured data to hydraulic conductivities. In a given time step, the flow through a Z cm of the substrate can be calculated by Equation 3.1.

$$q = \int_0^z \frac{\partial \theta}{\partial t} dz = K(\theta)\left(\frac{\partial h}{\partial z} - 1\right) \qquad \text{Equation 3.1}$$

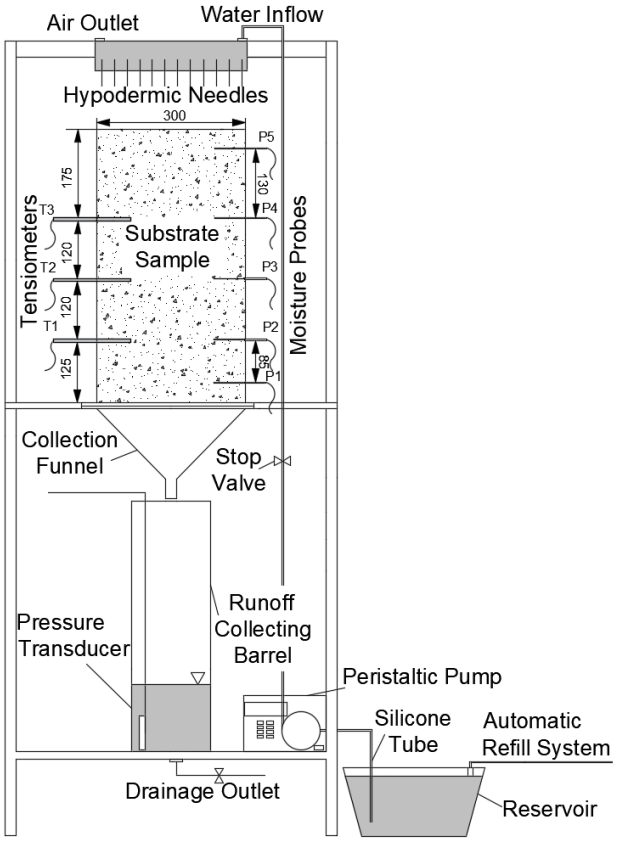

Figure 3.2. Infiltration column apparatus for HCF determinations (all dimensions in mm).

3.4.1 Steady-state method

The steady-state condition applies when moisture content does not change with depth, and water flow is driven only by gravity. In this state, as no suction head gradient is present with depth, the

hydraulic conductivity is equal to the imposed infiltration rate or the outflow rate. However, due to the heterogeneous nature of green roof substrates, variations between probe readings at specific positions in the substrate are always present; in this study, steady-state was judged to be attained when the change in moisture content over an hour at all five depths was less than 0.0008 v/v. 0.0008 v/v is the resolution of the moisture probes. Outflow measurements were conducted once a steady-state had been attained. Limited by the capacity of the collecting barrel, the duration for the outflow measurement was between 5 minutes and 1 hour, depending on the infiltration rate imposed on the substrate. To exclude the influence of boundary conditions, the moisture contents measured by the topmost and bottommost probes were excluded from the analysis. The measured moisture contents from the remaining three probes at steady state were averaged to provide the mean moisture content corresponding to each outflow rate. The applied flowrate started from the lowest rate, and when a steady-state was judged to be achieved, the flowrate was then increased, and the same procedures were repeated for the next flowrate. 11 data points on the HCF were determined using the steady-state technique.

3.4.2 Transient method

The transient method, which is also referred to as the instantaneous profile method, allows unsaturated hydraulic conductivity to be calculated using transient measurements of moisture content and matric head. The transient measurements were conducted under conditions of no inflow after all the steady-state measurements were finished. The sample column used to hold the substrate has a perforated base, so when inflow stops, drainage dominates initially, followed by evaporation later on. The total hydraulic head at two adjacent vertical positions (the points where the tensiometers and moisture probes are) was calculated from measured suction heads to determine the direction of flow, and then the measured data was used to calculate the hydraulic conductivity using Equations 3.1 to 3.4. The calculated hydraulic conductivity was then correlated with the averaged moisture content over the two adjacent positions.

The hydraulic gradient between each of the depths in the substrate column where moisture content is measured can be calculated by the following equation (Equation 3.2).

$$\left(\frac{\mathrm{dH}}{\mathrm{dz}}\right)_{\mathrm{m}} = -1 - \left(\frac{\mathrm{h_m} - \mathrm{h_{m-1}}}{\mathrm{z_{m-1}} - \mathrm{z_m}}\right) \qquad \text{Equation 3.2}$$

where H is the total hydraulic head (cm), m is an integer assigned to each of the measurement point/moisture probes (the upper moisture probe shall be assigned $\mathrm{m}=1$ with increasing values assigned to each probe with the depth of the substrate column), h is the matric suction (cm), and z is the elevation of each probe (cm).

During a given time interval Δt and depth interval $z_{m+1} - z_m$, the unit flow rate downstream from a point m is given as follows:

$$q^j = \sum_{m=1}^{n} \left(\theta_m^j - \theta_m^{j-1}\right)(z_{m+1} - z_m) \qquad \text{Equation 3.3}$$

Where q is the unit flow rate (cm/min), j is the current time step, θ is the measured moisture content, and n is the total number of measurement points used in the calculation, other symbols are as defined before.

The hydraulic conductivity K_j can be calculated using the following equation:

$$K_j = -\frac{q^j}{\Delta t(\frac{dH}{dz})_m} \qquad \text{Equation 3.4}$$

As the drying process starts from the top of the substrate, the decrease in moisture content and suction head in the bottom layer of the substrate occurs slowly. Due to the instrument failure of the lower tensiometer and moisture probe 2 in some cases, to maintain consistency, the measured data from the top two tensiometers and moisture probe 3 and 4 were used for analysis. The responses of the tensiometers are slower than the moisture probes, and they failed to capture the dynamics in the substrate at the very beginning of the drainage process. The measured moisture content and suction were therefore recorded after the tensiometers started to give reasonable measurements (reasonable measurements refers to readings from tensiometers below 0 cm). The recorded data was used to calculate hydraulic conductivity using Equations 3.1 to 3.4. The change in moisture content and suction head during drainage is fast, so a 10-minute time-step was used for the calculation. In contrast, as relatively slow changes occur due to evaporation, a 180-minute time-step was used for the evaporation-phase hydraulic conductivity calculations.

3.5 Detention tests

3.5.1 Substrate detention tests

The apparatus used for HCF characterisations (**Figure 3.2**) was also used for the substrate detention tests. To represent typical green roof system build-ups, substrate detention tests were conducted on 100 mm and 200 mm deep substrates. To evaluate substrate detention performance in response to various rainfall intensities and rainfall profiles, four design storms were applied to the substrates. In Design Storms 1, 2 & 3, 0.1, 0.37 and 0.51 mm/min constant rainfall was applied to the substrates for 30 minutes. These intensities are equivalent to the intensities associated with one-hour 1 in 1, 10 and 30 years Sheffield (UK) rainfall (NERC, 1999). As the response at the start and the end of the event is of interest, the design storms were applied

for a reduced duration of 30 minutes. Design storm 4 is a storm profile with 9.2 mm of total rainfall distributed over five 6-minute time-steps according to the UK 75% summer profile (NERC, 1975). Before each test, the substrate was placed in the column and levelled off without compaction. The substrate was initially wetted with 1.2 mm/min of rainfall for 2 hours, and it was then left to drain for 2 hours to ensure that it was at field capacity (FLL, 2008; Yio et al., 2013). The moisture content measured by the lowest moisture probe at field capacity was recorded, then a design storm was applied to the substrate for 30 minutes. Three replications were conducted. Without changing the layout of the column, the lowest moisture probe was used to record the moisture change in the 100 mm substrates during the detention tests. The moisture content measurements recorded by the two lowest moisture probes in the 200 mm substrates make it possible to investigate the vertical moisture content gradients within the substrates during the storms. Runoff from the bottom of the substrate was recorded by the pressure transducer in the collecting barrel. Control tests were conducted without a substrate component.

3.5.2 Drainage layer detention tests

The detention tests with green roof drainage layers were conducted by Dr Vesuviano as part of his PhD programme (Vesuviano, 2014). A large scale rainfall simulator consisting of a rainfall supply system, rainfall distribution system and runoff collection system was developed to test the detention performance of the drainage layers in response to different rainfall intensities (**Figure 3.3**). The rainfall simulator has a length of 5 m and a width of 1 m with an adjustable slope and drainage length. Rainfall was supplied and distributed by a pressurised dripper network from the top. The actual flow rate supplied to a dripper network during a test was measured by a nutating disk volumetric flow meter (Badger Meter Europa GmbH, Neuffen, Germany) with a volume resolution of 0.1 litres and a time resolution of 15 seconds. Runoff leaves the simulator through a full width opening at its downstream end and ends up in a collection barrel. The depth of water in the barrel was recorded at 1-second intervals by a Druck PTX 1730 pressure transducer (GE Sensing, Groby, UK). The time-series runoff profiles were calculated based on the differential increase in volume over each time step. A full description of the experimental setup can be found in Vesuviano (2014) and Vesuviano and Stovin (2013).

With each drainage layer, two drainage lengths (2 m and 5 m), two slopes (2% and 17.6%) and five constant rainfall intensities (0.1 mm/min, 0.3 mm/min, 0.6 mm/min, 1.2 mm/min and 2.0 mm/min) were considered.

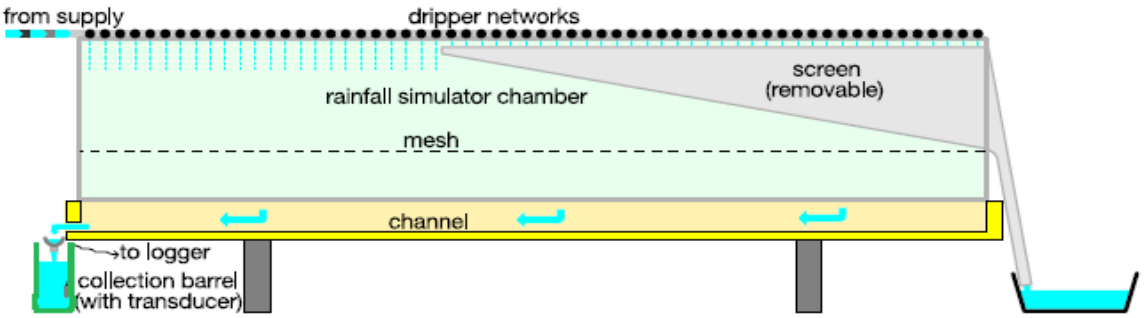

Figure 3.3. Rainfall simulator used for detention tests (Vesuviano and Stovin, 2013).

3.5.3 Complete green roof system detention tests

The apparatus in **Figure 3.3** was also used to conduct the detention tests with a complete conventional green roof system. The detention tests were conducted by Dr Fred Sonnenwald at ZinCo GmbH international headquarters in 2012. Five 60-minute design storms were tested with three replications. Three of the design storms are constant rainfall events at 0.3 mm/minute, 0.6 mm/minute, and 1.2 mm/minute. The other two design storms are time-varying storms equivalent to 1-in-10 year and 1-in-100 year 75% summer storm for Sheffield, UK. The total rainfall depths of 21.94 mm and 44.81 mm rainfall were discretised into 15 4-minute steps (NERC, 1975) to generate the two time-varying rainfall profiles. Sixteen hours of detention time was allowed after each rainfall test to allow all the runoff resulting from one test to be sufficiently captured and without allowing significant evaporation to take place. Prior to the test, a constant 1.2 mm/minute rainfall was applied for 60 minutes to the system, and subsequently, it was set to drain for 16 hours to allow the system to return to field capacity at the beginning of the test. Runoff data was collected at 1-minute time steps throughout the tests. A full description of the test programme can be found in Vesuviano et al. (2014).

3.5.4 Innovative green roof system detention tests

Two types of detention test were undertaken in the laboratory with an innovative green roof system. Firstly, tests were undertaken on the detention layer component in isolation. Secondly, tests were undertaken with the complete systems to provide validation data for the complete model. Detention tests with the detention layer and the complete innovative green roof system were conducted by Green Roof Diagnostics, LLC (Culpeper, Virginia, USA).

Figure 3.4 shows the set-up for the detention tests. The water supply reservoir was placed on a scale (with a sensitivity of 0.2 kg) above the test bed to monitor the volume of water applied. The applied water was distributed evenly from the top by a pressurised spray network. Two reservoirs downstream of the test bed were each placed on scales (0.2 kg sensitivity) to collect the surface

runoff (if any) and the bottom runoff. As there is a possibility that the sprayed water could land on the ground, the weight of the test bed was continuously recorded to determine the actual rainfall landed on the surface of the test bed. The rollers beneath the test bed were used to pull the test bed into place. The detention tests were conducted at three constant rainfall intensities (approximately 0.17 mm/min, 0.78 mm/min and 1.9 mm/min) for 15 minutes. The rainfall intensities are representative of local low, medium and high rainfall intensities. All tests were conducted over the full length and width of the test bed (6.1 m × 1.1 m) at a 2% slope. Three replications were conducted for each rainfall intensity, and data were recorded at a 1-minute time step.

In all cases, the tests were run with systems that could be considered to be at field capacity, such that no initial losses (retention) would occur, and the data collected reflects detention processes only. In practice, this was achieved by wetting and then draining the systems until drainage substantially ceased prior to commencing the detention tests, such that the volume of rainfall applied during testing would result in approximately the same volume of runoff.

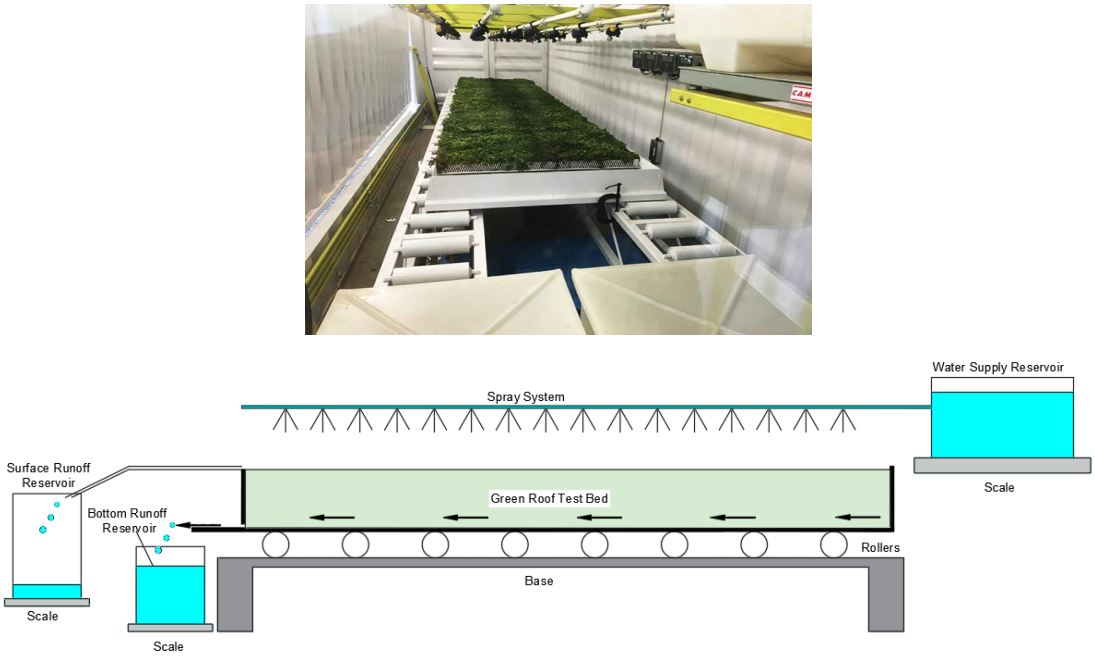

Figure 3.4. Experimental set-up for the detention tests with the detention layer and the innovative green roof system.

3.5.5 Field green roof test beds

The monitored data from field green roof test beds was used in this study to evaluate the capability of the models to regenerate runoff profiles for field green roofs. This monitoring programme was established in 2009 and lasted about nine years. The test site consists of nine

green roof test beds (TBs) that vary in substrate composition and vegetation treatment. On-site climate data and rainfall data, runoff from each test bed and moisture content at three depths in the green roof test bed were recorded throughout the test period. Further descriptions of the field test beds can be found in Section 4.2.1, and a full description of the field monitoring programme can be found in Berretta et al. (2014), De-Ville et al. (2018) and Stovin et al. (2015).

3.6 Chapter summary

This chapter introduced the experimental methods used in this study and provides a summary of these experimental methods and data collected from the experiments.

Table 3.1. Summary of experimental methods/data used in this study.

Experiment/Method/Data Name	Experiment Component	Replication	Type of Rainfall	Results will present/measured data will use in	Comment
FLL tests	Green roof substrates for conventional green roof systems (MCS, HLS, SCS and NSM)	Three replications with three samples	-	Chapters 4 and 5	New experiments conducted by the author
Hanging column method (SWRC)	Green roof substrates for conventional and innovative green roof systems (MCS, HLS, SCS, NSM and MMS)	Three replications with three samples	-	Chapters 5 and 8	New experiments conducted by the author
Pressure extractor method (SWRC)	Green roof substrates for conventional green roof systems (MCS, HLS, SCS and NSM)	Three replications with three samples	-	Chapter 5	Experiments were conducted by previous researchers (Berretta et al., 2014)
Steady-state and Transient methods (HCF)	Green roof substrates for conventional green roof systems (MCS, HLS, SCS and NSM)	Two replications with two samples	-	Chapter 5	New experiments conducted by the author
Substrate detention tests	Green roof substrates for conventional green roof systems (MCS, HLS, SCS and NSM)	Three replications with the same sample	Design Storms	Chapters 5 and 6	New experiments conducted by the author

Drainage layer detention tests	Drainage layers of conventional green roof systems	Three replications with the same sample	Design Storms	Chapter 7	Experiments were conducted by previous researchers (Vesuviano and Stovin, 2013)
Conventional green roof system detention tests	A complete conventional green roof system	Three replications with the same build-up	Design Storms	Chapters 7 and 9	Experiments were conducted by previous researchers (Vesuviano et al., 2014)
Innovative green roof system detention tests	The detention layer in an innovative green roof system and a complete innovative green roof system	Three replications with the same build-up	Design Storms	Chapters 8 and 9	Experiments were conducted by Green Roof Diagnostics
Field green roof test beds	Conventional green roof systems	-	Real Rainfall	Chapters 4 and 7	Data was collected by previous researchers (Berretta et al., 2014; Stovin et al., 2015)

4 Internal Fluctuations in Green Roof Substrate Moisture Content During Storm Events: Monitored Data and Model Simulations

4.1 Chapter overview

This chapter considers the implementation of the Richards Equation in modelling detention effects in green roof substrates. The focus of this preliminary modelling study was to understand the influence of model parameters and boundary conditions on the modelled runoff and internal moisture content profiles. The work was supported by previously collected rainfall, runoff and moisture content data from field green roof test beds, together with a limited set of new laboratory characterisations of substrate physical properties.

The Reservoir Routing model provides an alternative, less computationally intensive, approach to modelling detention; this chapter therefore also includes comparisons between the performance of the Richards Equation model and the empirical Reservoir Routing model. The modelled runoff profiles from a field green roof test bed using the Richards Equation and the empirical Reservoir Routing model are compared to the measured data to evaluate the model performance. The internal moisture content profiles measured at three vertical locations in the green roof test bed are used to investigate the boundary conditions for the Richards Equation to represent the measured data.

This chapter forms the following publication:

Peng, Z., Smith, C., Stovin, V., 2019. Internal fluctuations in green roof substrate moisture content during storm events: Monitored data and model simulations. *J. Hydrol.* 573, 872–884. https://doi.org/10.1016/j.jhydrol.2019.04.008

4.2 Experimental set-up

4.2.1 The test beds

The field monitored data from the field green roof test beds involves the work of several researchers (Dr Simon Poë, Dr Christian Berretta and Dr Simon De-Villie). The test site, located on a fifth-floor terrace of the Sir Robert Hadfield building (53.3816, -1.4773), The University of Sheffield, UK, consists of nine green roof test beds (TBs) which vary systematically in substrate composition and vegetation treatment (**Figure 4.1**). Each test bed is 3 m long × 1 m wide with a 1.5° slope. The test beds consist of an impermeable hard plastic tray base, a drainage layer (Zinco Floradrain FD 25), a filter sheet (Zinco Systemfilter SF) and one of nine substrates (80 mm deep) and vegetation combinations. On-site climate data, including temperature, solar radiation, wind

speed and relative humidity, were recorded by a Campbell Scientific weather station at 1-hour intervals. 0.2 mm resolution AGR-100 tipping bucket rain gauges manufactured by Environmental Measures Ltd. were used to record the on-site rainfall. A collection tank equipped with a Druck Inc. PDCR 1830 pressure transducer under each test bed was used for runoff measurement at 1 min intervals. The pressure transducers were calibrated against volumes on site. A full description of the test beds can be found in Berretta et al. (2014), De-Ville et al. (2018), and Stovin et al. (2015).

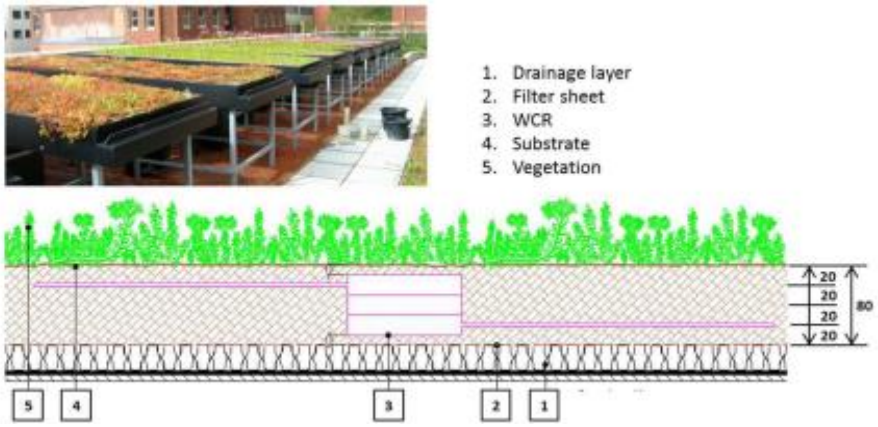

Figure 4.1. The experimental site at the University of Sheffield, UK and section view of the green roof test bed with the water content reflectometers (WCR, moisture probes) location (dimensions in mm) within the substrate (Berretta et al., 2014).

Test bed 1 (TB1) is a sedum vegetated green roof with heather and lavender substrate (HLS), and TB7 is an unvegetated bed with HLS substrate. Both test beds were equipped with moisture content sensors. The other seven TBs are not relevant to the present study.

Substrate moisture content data was collected from March 2011. Three moisture content reflectometers (Campbell Scientific CS616), inserted at 20 mm (Top), 40 mm (Mid) and 60 mm (Bottom) below the surface of the green roof, provided continuous moisture content measurement at 5-minute intervals. The rods of the mid and top probes were installed 90° and 180° respectively from the lower one in order to avoid interference of the measurement reading taken by the probes. A diagram showing the location of the moisture probes can be found in **Figure 4.1**. The moisture content reflectometers were calibrated at 20°C in a laboratory environment from 0.05 to 0.40 v/v, and an appropriate temperature correction was applied. The moisture content in the substrate could exceed 0.4 v/v during storms. However, it is not straightforward to calibrate the moisture probes above 0.4 v/v with our substrates due to the rapid drainage of water that occurs once the moisture content exceeds field capacity.

4.2.2 Substrate characteristics

HLS is a brick-based substrate comprising crushed bricks, pumice and organic matter, including compost with fibre and clay materials. Basic physical properties (bulk density, porosity, maximum water holding capacity, water permeability and particle size distribution) were determined for the HLS substrate following the FLL guidance (FLL, 2008) (Section 3.2). To minimise the uncertainties associated with subsampling, each test was conducted with three replications.

The Soil Water Release Curve (SWRC) for the HLS substrate was determined by the pressure plate extraction and hanging column methods described in Section 3.3. The data points measured by the pressure extractor method were previously reported by Berretta et al. (2014), whilst the data points for low suction heads, using the hanging column method, were newly determined and added to the dataset for model fitting. At high suction heads, the SWRC reflects the difficulty of water extraction from the substrate the during dry weather period; therefore, the SWRC at low suction heads is more relevant to detention processes during storm events.

4.3 Data analysis

The monitored moisture content data spans the period from March 2011 to February 2016. It was found that 92 out of the 444 identified events had complete and reliable rainfall and runoff records for TB1 and TB7; these events are referred to as 'valid' events. The rainfall-runoff data collected from 2010 was used to calibrate Reservoir Routing model parameters, and five representative storm events were selected for model validation. **Table 4.1** lists the characteristics of the five selected storm events, the performance of TB1 in response to the storms and the observed initial moisture content. The purpose of selecting TB1 for analysis is that TB1 is a representative commercial extensive green roof configuration that has demonstrated a good performance in retention and detention (Stovin et al., 2015). The return period for each event was estimated based on the Sheffield (UK) rainfall (NERC, 1999). The five selected storms include events in all four seasons. Individual storm events were defined as being separated by at least 6 hours' continuous dry period (Stovin et al., 2012). All events had > 8 mm rainfall and generated at least 5 mm runoff. The 21/Oct/2013 event is the heaviest storm with a return period of greater than one year. No rainfall was retained in the test bed during this storm, which suggests that the test bed was already at field capacity. In contrast, the 26/Aug/2015 event had a relatively long antecedent dry weather period (ADWP), and the return period for this event is less than one year. In this storm event, 61% of the rainfall was retained by the green roof test bed. The monitored rainfall-runoff data for TB7 was selected to derive Reservoir Routing model parameters for the drainage layer, as the detention effects in this test bed are only controlled by the substrate and

the drainage layer. The rainfall-runoff and moisture content data for TB1 was used to validate the substrate models and investigate the moisture content behaviour during storms.

Table 4.1. Hydrological characteristics of the five selected storm events and TB1 hydrological performance.

Event No.	Date	Rainfall Duration (h)	Rainfall depth (mm)	ADWP (h)	Peak rainfall intensity (mm/5 min)	Return Period (yr)	Retention (%)	Initial moisture content			
								Top	Mid	Bot	Mean
228	06/Dec/2012	14.02	12.20	70.43	0.60	<1	29.97	0.37	0.393	0.453	0.406
292	21/Oct/2013	27.35	31.80	10.90	1.00	>1	0	0.356	0.36	0.414	0.377
361	24/May/2014	28.22	24.13	16.63	1.73	<1	8.73	0.351	0.366	0.408	0.375
396	08/Nov/2014	4.43	8.40	15.52	0.36	<1	6.21	0.344	0.37	0.419	0.377
458	26/Aug/2015	11.63	13.00	57.23	2.67	<1	60.81	0.298	0.316	0.339	0.318

4.4 Detention modelling

During a storm event, the substrate moisture content temporarily rises above field capacity, leading to the generation of runoff. To account for detention in the substrate and the drainage layer, a two-stage green roof detention model, as proposed by Vesuviano et al. (2014) and Palla et al. (2012), was used in this study (**Figure 4.2**). Two approaches were taken to model the detention effect in the substrate: a lumped (black box) approach based on Reservoir Routing; or a physically-based finite element approach based on unsaturated flow hydraulics and the Richards Equation (**Figure 4.2**). A second Reservoir Routing equation was used to represent the detention effect in the drainage layer. The modelled runoff and the temporary storage in the substrates were compared with the monitored data to evaluate the performance of the models. Sonnenwald et al. (2014) demonstrated that the R_t^2 (Young et al., 1980) (Equation 4.1) provided a robust and generically applicable indicator of model performance for temporally-varying data. Therefore, R_t^2 was used to describe the goodness of fit between modelled and monitored runoff.

$$R_t^2 = 1 - \frac{\sum_{i=1}^{T}(q_o - q_m)^2}{\sum_{i=1}^{T}(q_o)^2} \qquad \text{Equation 4.1}$$

where T is the total number of observed data, q_o is the observed data and q_m is the modelled data. A value of R_t^2 equal to one corresponds to a perfect match of modelled data to the observed data.

It should be noted that R_t^2 is only one aspect to assess the performance of a model; it is critical to evaluate the performance of the model from the perspective of the generated runoff profiles, as a model can achieve a high value of R_t^2 but fails to correctly capture the rising and falling limbs of the runoff profiles.

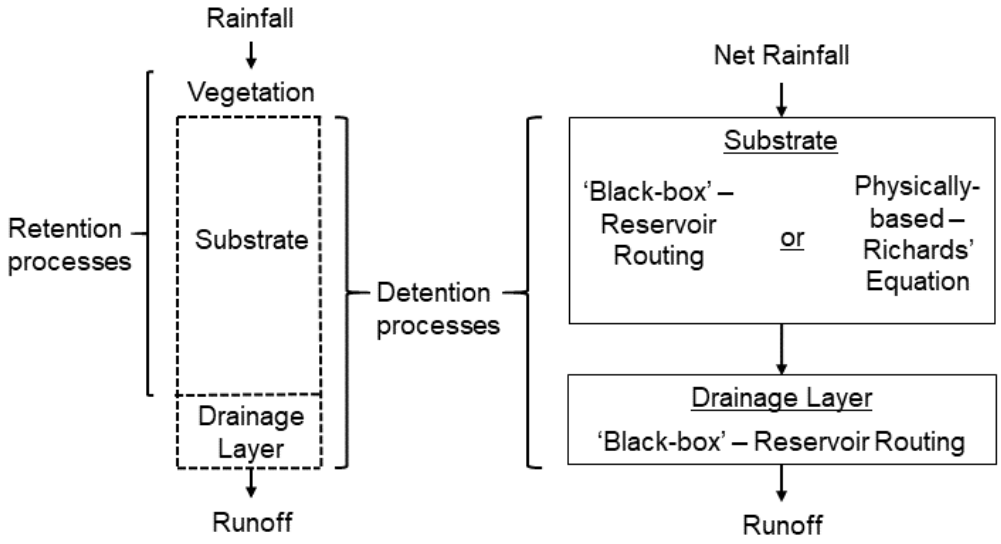

Figure 4.2. Conceptual green roof hydrological model: left – vertical profile through a typical green roof system indicating the layers associated with retention and detention processes; right – components of a two-stage detention model, indicating the two alternative options for representing substrate detention considered in this chapter.

4.5 Substrate detention models

4.5.1 The Reservoir Routing model

The lumped Reservoir Routing model is given by the following equations:

$$\mathrm{Qout_t} = \mathrm{k}_G \mathrm{h}_{\mathrm{t}-1}^{n_G} \qquad \text{Equation 4.2}$$

$$\mathrm{h_t} = \mathrm{h_{t-1}} + \mathrm{Qin_t}\Delta\mathrm{t} - \mathrm{Qout_t}\Delta\mathrm{t} \qquad \text{Equation 4.3}$$

where Qin is the inflow due to rainfall in mm/min, Qout is the runoff from the green roof substrate in mm/min, h is the stored water, in mm, $\Delta\mathrm{t}$ is the discretisation time step and k_G ($\mathrm{mm}^{(1-\mathrm{n_G})}/\mathrm{min}$) and $\mathrm{n_G}$ (dimensionless) are routing parameters.

4.5.2 The Richards Equation

The 1-D vertical Richards Equation is given in Equation 2.19. To solve the Richards Equation, functions describing the relationship between moisture content and suction head (Soil Water Release Curve, SWRC) and the relationship between unsaturated hydraulic conductivity and moisture content or suction head (Hydraulic Conductivity Function, HCF) are needed. For initial investigation, the Durner equation (Durner, 1994) (Equation 2.5) was used for SWRC, and the Durner-Mualem equation (Equation 2.9) was used to estimate unsaturated hydraulic conductivity as a function of the suction head. Further investigation was conducted using the van-Genuchten model (van Genuchten, 1980) (Equation 2.6) for SWRC and the van-Genuchten-Mualem equation

(Mualem, 1976) (Equation 2.5) for HCF. The Durner equation and a new HCF equation based on the equation proposed by Marshall et al. (1996) (Equation 4.4) were also used to investigate the influence of the HCF.

$$k(\theta) = a\theta^{b} \qquad \text{Equation 4.4}$$

where a, b are empirical parameters.

4.5.3 The drainage layer model

For a green roof with a drainage layer, it is expected that detention occurs as the runoff drains through the drainage layer, and the delay depends on the roof length and drainage layer configuration (Stovin et al., 2015; Vesuviano et al., 2014; Vesuviano and Stovin, 2013). Previous studies have confirmed that different types and dimensions of drainage layers may have different detention characteristics, and a simple nonlinear storage routing model, for which the parameters only depend on the drainage layer physical characteristics, is capable of modelling this effect (Vesuviano et al., 2014; Vesuviano and Stovin, 2013; Palla et al., 2012). In the present study, a nonlinear Reservoir Routing equation (Equations 4.2 and 4.3, where Qin is the inflow to the drainage layer from the substrate and $Qout$ is the runoff from the drainage layer) was applied to model the drainage layer detention.

4.6 Model Implementation

Figure 4.2 shows the hydrological processes in a green roof system, the rainfall-runoff model is characterised by three processes: initial losses (retention), detention due to the substrate, and detention due to the drainage layer. As the focus of this thesis is on the second process, substrate detention, it was necessary to eliminate the effects of retention and drainage layer detention from the monitored rainfall and runoff data.

4.6.1 Retention

To model the detention for each selected event, the retention, which was calculated as the difference between the monitored rainfall and runoff depths, was removed from the start of the rainfall profile such that only net rainfall (**Figure 4.2**) was routed to runoff.

4.6.2 Reservoir Routing parameters for the drainage layer

The drainage layer is consistent between all test beds. Reservoir Routing parameters for the drainage layer were identified by eliminating the effects of substrate detention from monitored runoff responses from TB7. TB7 data is used here for two reasons: firstly, because its substrate is comparable to one that has been assessed in independent laboratory detention tests; and

secondly, because it is an unvegetated system, so no additional detention effects that might be associated with vegetation or roots are expected.

A substrate-specific study (Yio et al., 2013) showed that the parameter for the substrate Reservoir Routing model (k_G, subscript G refers to growing media/substrate) relates to the depth and the water permeability of the substrate. The k_G value is transferable between substrates if they have similar components, depth and physical properties. The HLS substrate in TB7 has the same properties as the substrate studied in Yio et al. (2013). Therefore, the TB7 substrate Reservoir Routing coefficients k_G and n_G were assumed to correspond to the values presented there (0.212 $mm^{(1-n)}$/min and 2.0 respectively).

The k_D and n_D values for the drainage layer were then calibrated from the net rainfall and runoff data from TB7 by fixing the substrate parameters to 0.212 $mm^{(1-n_G)}/min$ and 2.0, respectively.

shows the distribution of calibrated model parameters. The median calibrated values of k_D and n_D were found to be 0.026 $mm^{(1-n_G)}/min$and 1.196, respectively, using the TB7 data from the 92 valid storm events. These parameter values were applied to represent the drainage layer detention in subsequent analyses. The Reservoir Routing models were all run at 5-minute time steps to match the time interval of measured data.

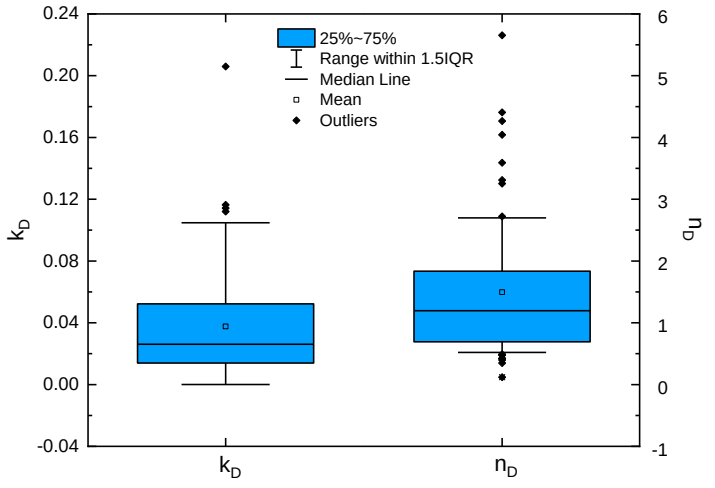

	N total	Mean	Standard Deviation	Sum	Minimum	Median	Maximum
kD	92.000	0.038	0.035	3.463	0.000	0.026	0.206
nD	92.000	1.497	1.110	137.702	0.120	1.196	6.239

Figure 4.3. Distribution of the calibrated Reservoir Routing model parameters for the drainage layer using the net rainfall and runoff data from TB7.

4.6.3 Reservoir Routing parameters for the substrates

As TB1 is a vegetated green roof, even though it shares the same substrate with TB7, the presence of vegetation could provide extra detention effects, so the substrate Reservoir Routing parameter (k_G) for this test bed needs to be calibrated from monitored rainfall-runoff data. Calibration was conducted with the net rainfall-runoff data from the 92 valid events by fixing k_D to 0.026 $mm^{(1-n)}/min$, n_D to 1.196 (the calibrated values from TB7) and n_G was fixed at a value of 2.0 based on the finding of Yio et al. (2013), who demonstrated that model performance was insensitive to changes in n_G value. **Figure 4.4** shows the distribution of calibrated parameter, and the calibrated median value of 0.175 $mm^{(1-n_G)}/min$ was used for the k_G of TB1 substrate (**Table 4.2**).

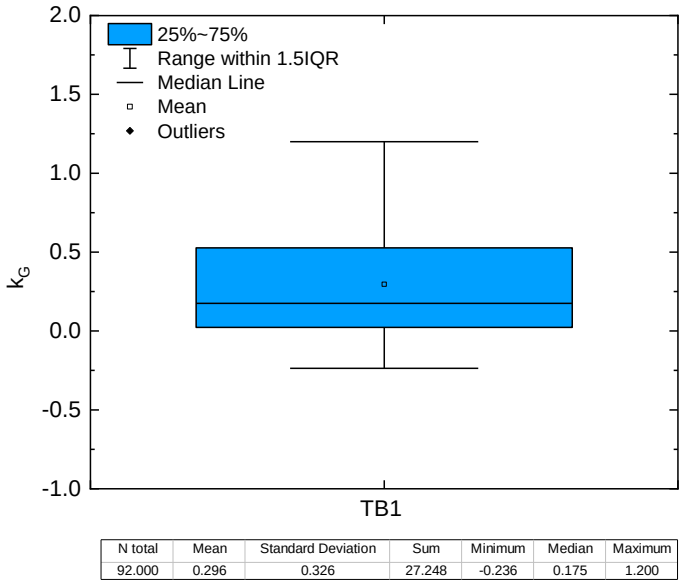

Figure 4.4. Distribution of the calibrated Reservoir Routing model parameter for the substrate of TB1.

Table 4.2. Value of parameters used in the Reservoir Routing Model.

	Value	
Parameter	TB7	TB1
k_G	0.212	0.175
n_G	2.000	2.000
k_D	0.026	0.026
n_D	1.196	1.196

4.6.4 Richards Equation

4.6.4.1 SWRC and HCF parameters

Both the van-Genuchten model (Equation 2.6) and the Durner Equation (Equation 2.5) were fitted to the data points on the SWRC measured by the hanging column and pressure extractor methods (Section 3.3). The fitting and parameter determination was performed using the SWRC Fit software (Seki, 2010). Initial simulations were conducted with the Durner Equation and Durner-Mualem Equation (Equation 2.9). The saturated hydraulic conductivity used within the Mualem Equation was determined by the FLL tests (K_s = 25 mm/min). For further investigation, the van-Genuchten-Mualem Equation (Equation 2.10) and a different HCF (Equation 4.4) were also applied to investigate the influence of SWRC and HCF on the model results.

4.6.4.2 Boundary and initial conditions

For each rainfall event, the upper boundary was set as a Neumann condition in which the surface flux equals the net rainfall input R (Equation 4.5); the lower boundary was set to be a constant suction head. The relevant suction head was calculated from the vertically averaged monitored moisture content two hours after the rainfall stopped. This value is taken to represent field capacity (De-Ville et al., 2018; FLL, 2008). The initial condition was set to be a constant hydraulic head. The moisture content at mid-depth of the substrate was set to the value of field capacity (the mean value of the moisture content at the three depths), and the suction head of this middle point was calculated from the SWRC. The suction heads for the rest of the vertical profile were calculated according to Equation 4.6.

$$K(h)\left(\frac{\partial h}{\partial Z} - 1\right) = R \qquad \text{Equation 4.5}$$

where R is the net rainfall (cm/min), and all the symbols are as defined before.

$$h_i = h_{i+1} - Z_i + 4 \qquad \text{Equation 4.6}$$

where h_i (cm) is the suction head at point i, and Z_i (cm) is the elevation of point i. The upper layer of the substrate was assigned a value of $i = 1$. The reference level of elevation (i.e. Z = 0.0 cm) is at the bottom of the substrate, and the value of 4 in Equation 4.6 represents the elevation of the middle depth of the substrate.

The Richards Equation was solved in MATLAB using the *pdepe* function by discretising the 80 mm of the substrate into 101 node points. The purpose of building the model in MATLAB is to allow a flexible selection of HCFs. The validation of the MATLAB code for solving the Richards Equation against the standard method of HYDRUS-1D can be found in Appendix B. The Richards Equation model was run at 5-minute time steps to match the time interval of measured data. The drainage

layer Reservoir Routing model was adopted to model the lateral flows in the drainage layer and generate the runoff from TB1. The parameters for the drainage layer were the calibrated values as determined before.

4.7 Results

4.7.1 Moisture content behaviour during storms

Figure 4.5 presents the rainfall, runoff and moisture content data from TB1 for the five selected rainfall events. Temporary increases in moisture content may be seen to occur in response to rainfall, after which the monitored moisture content returns to a constant value (assumed equal to field capacity). The vertical dashed line indicates the time when the first significant runoff was observed, and the vertical dotted line is the time when rainfall stopped, the vertical solid line is two hours after rainfall stopped, and the corresponding measured moisture content is interpreted as the local field capacity (**Table 4.3**). Any further reduction below field capacity is expected to be due to evapotranspiration. During the events for which the substrate initial moisture content was below local field capacity (6/Dec/2012 24/May/2014 and 26/Aug/2015), a significant increase in moisture content was witnessed in the substrate at the beginning of the storm prior to the onset of runoff. In the event where the substrate was relatively dry (26/Aug/2015), a wetting front (i.e. a delay in the rise of moisture content at the bottom of the substrate compared with the top) was evident. Once the substrate moisture content reached local field capacity, it tended to increase simultaneously with rainfall. The maximum temporary storage in the substrate during the selected storms was generally less than 0.06 v/v, equivalent to 4.8 mm in an 80 mm deep substrate. In general, the runoff was generated after the substrate reached local field capacity, but runoff was generated before the lower substrate reached its local field capacity in the event on 6/Dec/2012, which may indicate preferential flow.

Table 4.3. Local field capacity determined for each storm event.

		Local field capacity			
		TB1			
Event No.	Date	Top	Mid	Bot	Mean
228	06/Dec/2012	0.391	0.414	0.485	0.430
292	21/Oct/2013	0.355	0.360	0.410	0.375
361	24/May/2014	0.360	0.375	0.416	0.384
396	08/Nov/2014	0.344	0.396	0.419	0.387
458	26/Aug/2015	0.319	0.343	0.374	0.345
Overall mean					0.384

Table 4.3 lists the local field capacity determined for each event. The three moisture content probes indicate slightly different moisture content levels at field capacity. Differences in the

absolute values are to be expected in coarse-grained heterogeneous green roof substrates that may have consolidated over time. The lowest field capacity was found for the event on 25/Aug/2015, and the highest field capacity was associated with the event on 8/Nov/2014, which is believed to be caused by the seasonal variation of substrate physical characteristics (De-Ville et al., 2018).

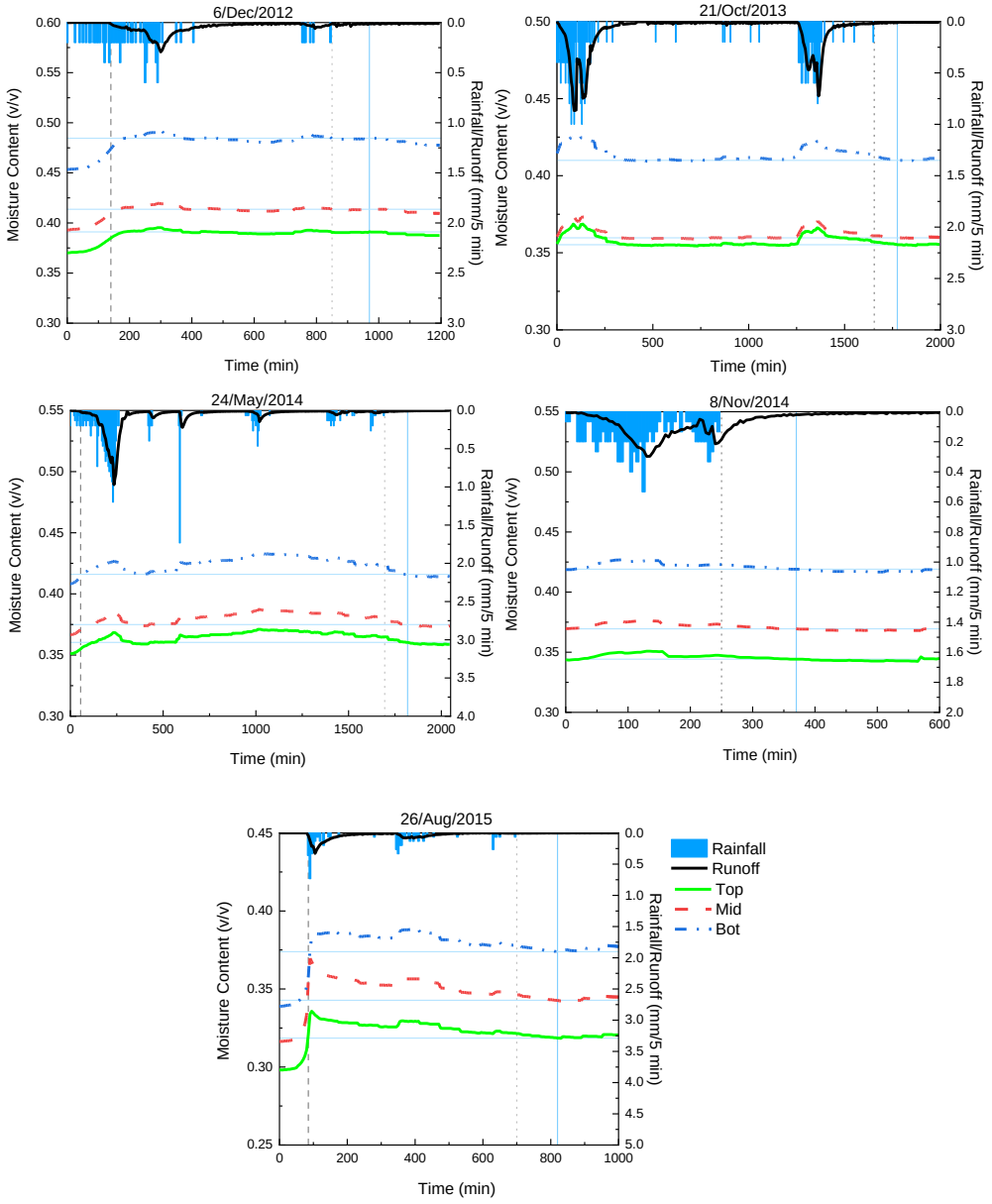

Figure 4.5. Monitored rainfall, runoff and moisture content profiles for the five selected storm events (vertical dashed line indicates the time significant runoff was firstly observed, vertical dotted line represents the time rainfall stops, the solid vertical line is the time two hours after rainfall stops and the corresponding moisture content is assumed to indicate local field capacity).

4.7.2 Substrate characteristics

Table 4.4 lists the results of FLL tests for the HLS green roof substrates. The maximum water holding capacity determined by the FLL tests is close to the average local field capacity (0.385 vs 0.384), indicating that the FLL tests do provide reasonable estimations of on-site field capacity.

Table 4.4. HLS Substrate characteristics according to FLL (2008) test methods.

Properties	Unit	Mean	St.Dev
Particle size <0.063 mm	%	2.72	0.25
d_{50}	mm	5.05	0.07
Bulk density	g/cm^3	0.81	0.05
Porosity	%	55.6	0.85
Maximum water holding capacity	%	38.53	0.60
Permeability	mm/min	25	7.16

Figure 4.6 presents the measured points and fitted SWRCs for the HLS substrate. SWRC A is the fitted van-Genuchten model, and SWRC B is the fitted Durner model. Both models were fitted using the full experimental dataset, determined by the hanging column and pressure plate extractor methods. As **Figure 4.6(a)** shows, only minor differences were present between the two models. However, the Durner model has a slightly higher R^2 value (**Table 4.5**), which indicates a better fit for the measured data. This may indicate that the green roof substrate is more likely to be a dual-porosity system (Liu and Fassman-Beck, 2017). **Table 4.5** lists the calibrated parameters for the van-Genuchten (SWRC A) and Durner (SWRC B) models. The fitted Durner parameters (SWRC B) were used in the Richards Equation to generate runoff and vertical moisture content profiles, but further investigation was conducted with the van-Genuchten model in Section 4.8.

Table 4.5. Fitted parameters for the SWRCs for the HLS substrate.

Van-Genuchten (SWRC A)		Durner (SWRC B)	
Parameter	Value	Parameter	Value
Θ_s	0.556	Θ_s	0.556
Θ_r	0	Θ_r	0
α	0.807	α_1	0.306
n	1.157	n_1	2.255
		α_2	0.02
		n_2	1.194
		w_1	0.378
R^2	0.988	R^2	0.995

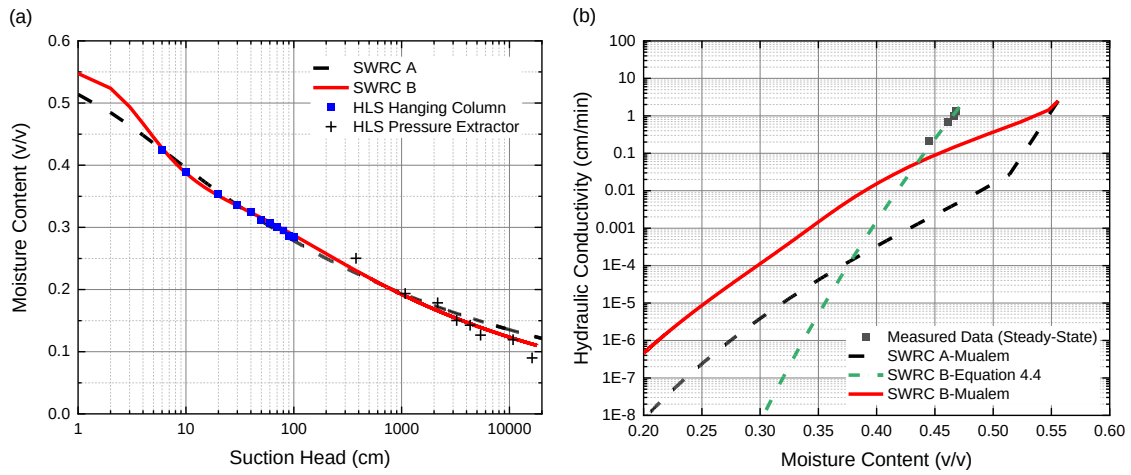

Figure 4.6. Water release curves and hydraulic conductivity functions. (a) SWRC A is fitted to the van-Genuchten model, SWRC B is fitted to the Durner model, both models were fitted using hanging column and pressure plate extractor data; (b) plots of the new HCF and the HCFs derived from the two SWRC in (a) via the Mualem model.

Application of the Richards Equation requires data on the substrate's unsaturated hydraulic conductivity in the form of a Hydraulic Conductivity Function (HCF). Typically, the HCF is derived from the SWRC via the Mualem model. **Figure 4.6(b)** shows the Durner-Mualem (SWRC B) and van-Genuchten-Mualem (SWRC A) derived HCFs for the HLS substrate. However, previous authors have questioned the applicability of these derived HCFs to coarse-grained heterogeneous green roof substrates (e.g. Liu and Fassman-Beck, 2018). **Figure 4.6(b),** therefore, includes a third HCF, which has been derived from preliminary laboratory tests (based on the ASTM steady-state infiltration column test method (ASTM, 2010)) undertaken on the HLS substrate. Given the sparse nature of this preliminary data set, the basic HCF model presented in Equation 4.4 has been fitted to the data. Substantial differences may be observed between the Mualem-based HCF functions and the new function derived from laboratory measurements. Whilst further work required to refine the testing procedures and to extend the laboratory data coverage, it is nonetheless interesting to investigate how the alternative HCF would affect the model's prediction of substrate runoff detention. The influence of HCF on model predictions, therefore, is considered in Section 4.8.

4.7.3 Model validation

Figure 4.7 compares modelled and monitored runoff from the test bed in response to the five selected storm events. Note that for both substrate detention models, the detention due to the drainage layer was modelled using the calibrated Reservoir Routing model described in Section 4.5.3. With most R_t^2 values higher than 0.8, it is confirmed that both the Reservoir Routing model

and the Richards Equation can achieve satisfactory results for runoff prediction. Both models provided more accurate predictions of runoff in response to heavy rainfall events. The 21/Oct/2013 (return period >1 year) and the 8/Nov/2014 events (return period nearly one year) have the highest R_t^2 value. Both models tended to underestimate the peak runoff rate and delay the time to peak slightly for the event on 26/Aug/2015. This may reflect an overestimation of detention in the drainage layer. Alternatively, the slight difference between the substrates used in TB7 and Yio et al. (2013) and the introduction of a filter sheet in the field test bed could result in an overestimation of substrate detention. During the heaviest 21/Oct/2013 event, the difference between the two models is minor. The Richards Equation had better performance than the Reservoir Routing model in the 24/May/2014 and 26/Aug/2015 events when the local field capacity was relatively low compared with the rest of the events. However, the Richards Equation had worse performance in the 6/Dec/2012 event, when the local field capacity was high. Except for the fact that the Richards Equation requires several input parameters, there is no apparent advantage of the Reservoir Routing model over the Richards Equation. The fact that the Reservoir Routing model relies on calibrated parameters that do not necessarily have physical meaning limits its generic application.

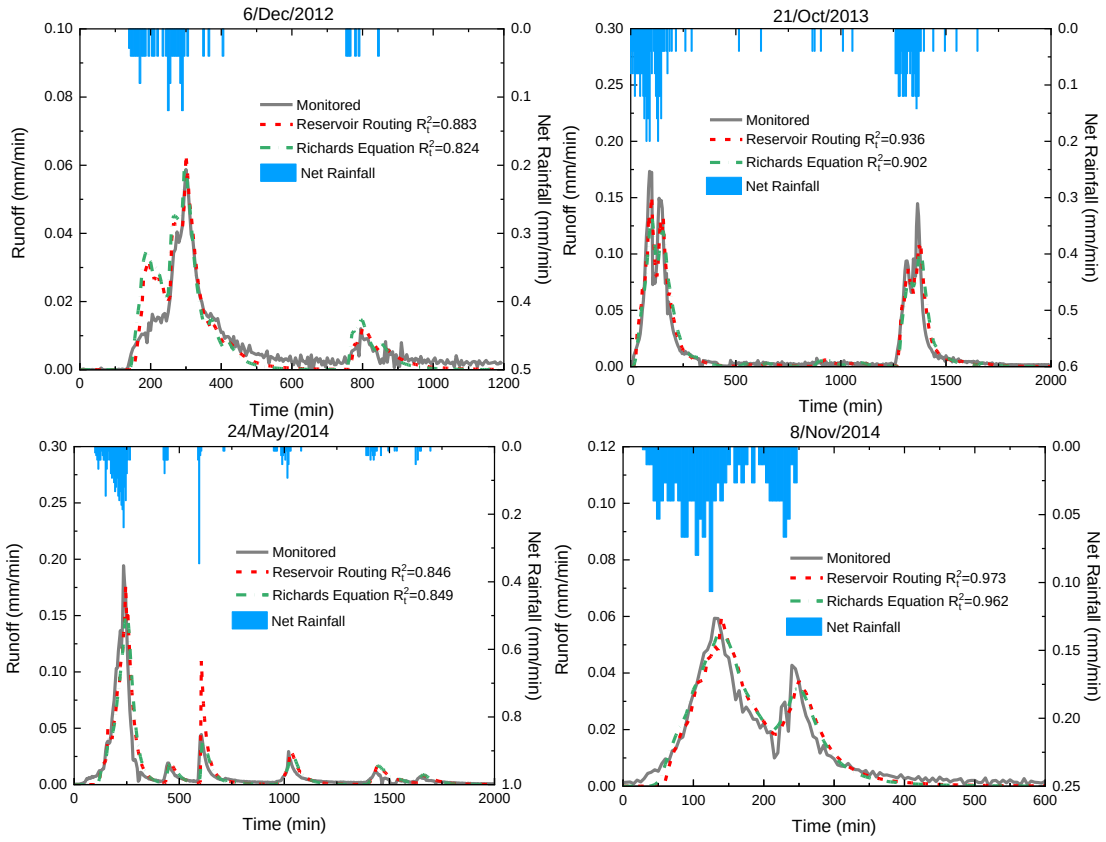

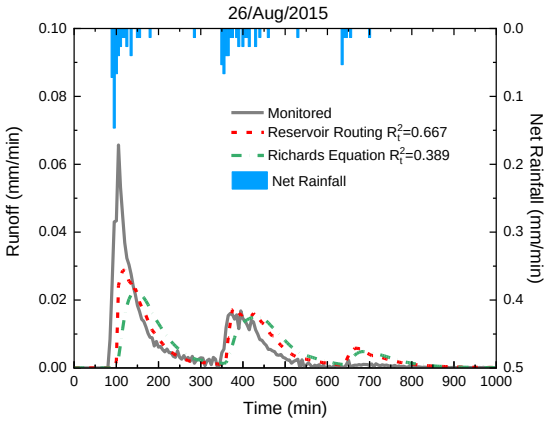

Figure 4.7. Monitored and modelled runoff using the Reservoir Routing model and the Richards Equation (Richards Equation was implemented in MATLAB using SWRC B-Mualem model and constant suction head lower boundary condition).

This type of model validation (based on runoff) has been presented in previous research (Kasmin et al., 2010; Peng and Stovin, 2017; Stovin et al., 2013; Vesuviano et al., 2014). However, further independent validation is provided by the monitored moisture content data. **Figure 4.8(a)** shows the dynamic responses of modelled and measured temporary storage in TB1 during the heaviest 21/Oct/2013 event. The modelled temporary storage curves were smoothed by performing 4 adjacent points regression. The modelled temporary storage is more dynamic compared with the measured, which may reflect the response rate of the moisture probes. However, the overall timing of the temporary storage is modelled well by both models, even though more water is predicted by the Richards Equation to be stored in the substrate. Whilst, in this case, the Richards Equation appears to overestimate the temporarily stored moisture, this is not always the case.

The temporarily stored runoff, modelled by the Reservoir Routing model, was converted to moisture content using Equation 4.7.

$$\theta_t = \frac{h_t}{80} + \theta_{FC} \qquad \text{Equation 4.7}$$

where θ_t is the moisture content at time t, h_t is the modelled temporary storage by the Reservoir Routing model (mm), 80 is the depth of the substrate (mm), θ_{FC} is the depth-averaged local field capacity for each event.

Figure 4.8(b) compares observed versus modelled moisture content for all five selected storm events. Both the observed and modelled moisture data were recorded every 5 minutes, starting from the time when significant runoff was first observed to the end of the storm. The dotted lines represent ±5% deviation. The predictions of both models are consistent, but the Richards Equation tends to overestimate the moisture content, while the Reservoir Routing model is more

likely to underestimate the moisture content. Overall, the moisture content using both models is within ±5% error.

As the Richards Equation is solved over a depth profile, validation of the vertical moisture content profile is possible. **Figure 4.8(c)** compares the modelled and observed moisture content fluctuations at three depths for the 21/Oct/2013 event. This comparison reveals stronger vertical gradients in the modelled responses compared with the observed data. Potential reasons for this are explored within Section 4.8.

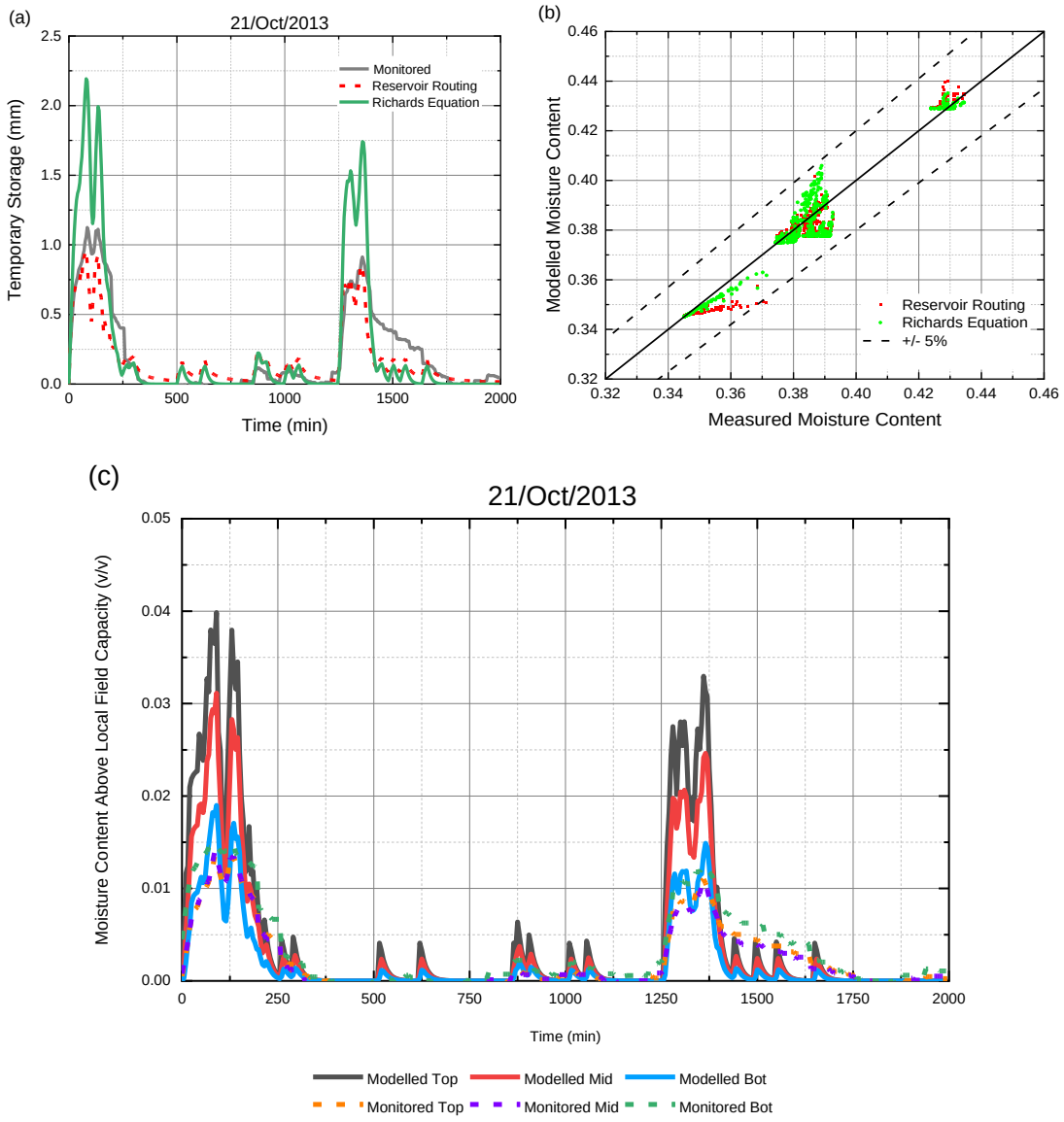

Figure 4.8. Validation of temporarily stored moisture (Richards Equation was implemented in MATLAB using SWRC B-Mualem model and constant suction head lower boundary condition). (a) Depth-averaged temporary storage; (b) scatter plot comparison of moisture content for all storm events (depth-averaged); (c) comparison of vertical moisture content profiles.

4.8 Discussion

Modelling green roof substrate detention using the Richards Equation requires several input parameters. Conventionally, these parameters are derived from natural soil-based empirical equations. This section aims to investigate the influence of SWRC, HCF and lower boundary conditions on the model prediction. The event on 21/Oct/2013 was used to undertake the analysis, and different SWRC, HCF and lower boundary conditions were considered.

4.8.1 Soil water release curve

The modelling with Richards Equation reported earlier (**Figure 4.7** and **Figure 4.8**) was based on SWRC B (**Figure 4.6(a)**), in which a Durner model was fitted to the data points determined by the hanging column and pressure plate extractor methods. In terms of fitting to measured SWRC data, the differences between SWRC B (Durner) and SWRC A (van-Genuchten) are minor. The question raised here is whether this minor difference in SWRC could influence the overall modelling results. SWRC A (**Figure 4.6(a)**) was used with the Mualem model to regenerate the runoff and vertical moisture content profile for the event on 21/Oct/2013.

Figure 4.9(a) shows the monitored and modelled runoff using SWRC A-Mualem and SWRC B-Mualem model. Some noticeable differences are evident between the two models. More significant detention effects in the substrate were modelled by the SWRC A-Mualem model. The time to start of runoff was delayed by about an hour, and the model underestimated the peak runoff by nearly 60%. **Figure 4.9(b)** presents the modelled vertical moisture content profile using the SWRC A-Mualem model. Compared with **Figure 4.8(a)**, in which the vertical moisture content profile was modelled using the SWRC B-Mualem model, significantly more water is modelled to be temporarily stored in the substrate.

In terms of SWRC, the two models both have good fits to the measured data, and no notable difference was evident; however, significant differences were observed in the modelled runoff and vertical moisture content profile. This appears to be caused by the differences in SWRC derived HCF. As shown in **Figure 4.6(b)**, the HCFs associated with the two models show considerable differences. The SWRC A HCF gives lower values of unsaturated hydraulic conductivity than SWRC B, and as a consequence, more water is predicted to be stored in the substrate. More discussion on the influence of HCF is provided in Section 4.8.2.

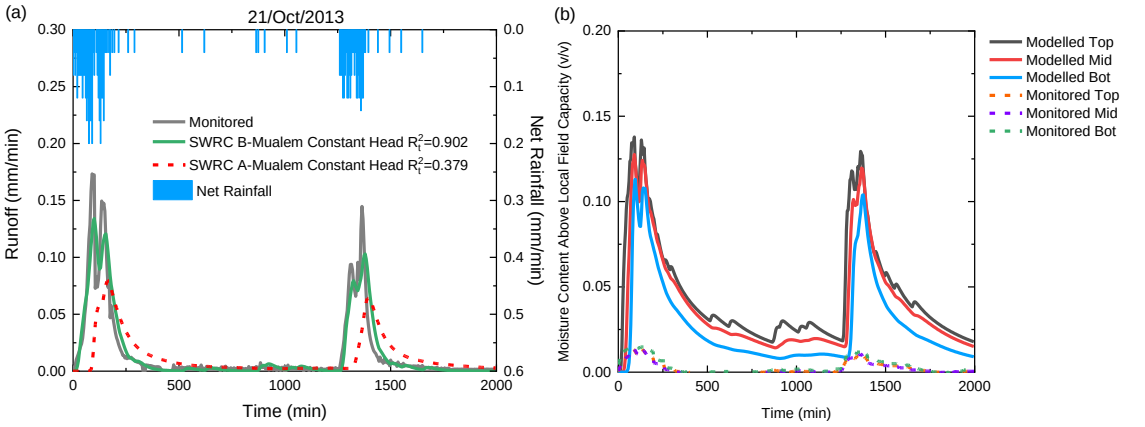

Figure 4.9. Validation of runoff and temporarily stored moisture. (a) Monitored and modelled runoff; (b) monitored and modelled vertical moisture content profiles using the SWRC A-Mualem model.

4.8.2 Hydraulic conductivity function

The Mualem equation is not independent of the SWRC; changing the SWRC also changes the HCF. As shown in **Figure 4.6(b)**, SWRC A and SWRC B lead to different estimates of the HCF. As a consequence, it is difficult to distinguish whether it is the minor difference in SWRC or the HCF that influenced the prediction. In addition, as suggested in previous studies, the Mualem equation may not provide the best fit for the measured unsaturated hydraulic conductivity (Liu and Fassman-Beck, 2018). The investigation here aims to assess the influence of HCF on the predictions. The work reported earlier utilised SWRC B in combination with the Mualem HCF formulation (**Figure 4.7** and **Figure 4.8**). Here one additional option is considered: SWRC B-Equation 4.4.

Figure 4.10(a) shows the modelled runoff using the SWRC B-Equation 4.4 formula. Compared with the runoff modelled by the SWRC B-Mualem model, the peak runoff was reduced by about 70%. **Figure 4.10(b)** presents the modelled vertical moisture content profile using Equation 4.4 HCF. The maximum moisture content nearly doubled the quantity shown in **Figure 4.8(c)**. In terms of the runoff prediction and the vertical moisture content profile, the model results of the Richards Equation is clearly significantly influenced by the HCF, which indicates that a suitable HCF is needed to correctly characterise the dynamics of moisture content variation in the substrate. This observation may be even more relevant when deeper systems (e.g. intensive green roofs or bio-retention cells) are to be modelled. In this case, despite the fact that Equation 4.4 appears to fit the preliminary laboratory data better than the two other options, SWRC B-Mualem appears to result in the most representative model prediction. However, it should be noted that Equation

4.4 was calibrated based on three measurement points; this new HCF could be not a good representation of the green roof substrate HCF.

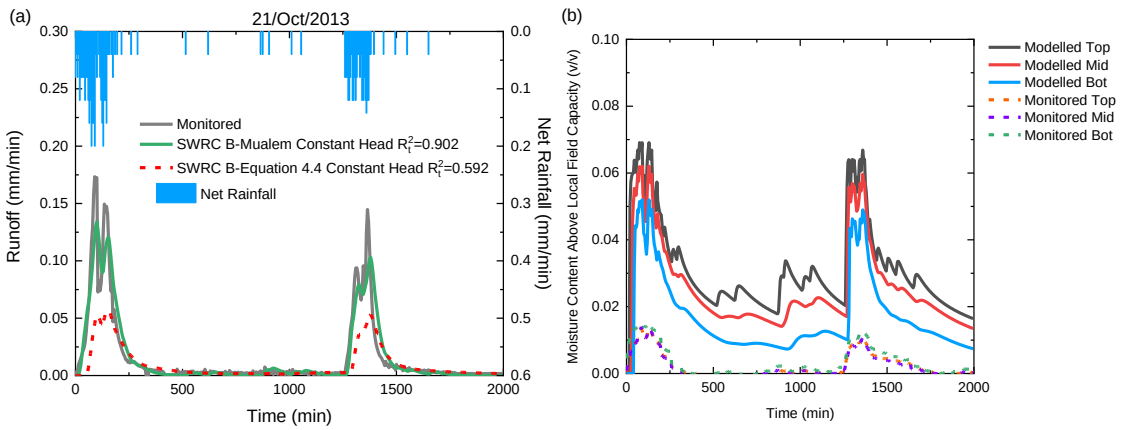

Figure 4.10. Validation of runoff and temporarily stored moisture. (a) monitored and modelled runoff; (b) monitored and modelled vertical moisture content profiles using the SWRC B-Equation 4.4 model.

4.8.3 Lower boundary condition

Based on the conceptual model outlined in **Figure 4.2**, the Richards Equation was applied only when the substrate moisture content was between field capacity and saturation (i.e. to model the detention). Based on field observations that the moisture content does not decrease below field capacity following a storm event, the lower boundary of the Richards Equation was set to a constant suction head. However, in some other studies, different approaches have been adopted. For example, the Richards Equation was used to model the retention and detention, and the lower boundary was set to be free drainage in the studies of Liu and Fassman-Beck, (2017) and Palla et al. (2009, 2012). The seepage boundary condition, in which the lower boundary is set as zero flux when the bottom boundary node is unsaturated and to zero pressure head when it is saturated (i.e. no bottom runoff is generated until the substrate is fully saturated), has also been applied to model green roof substrate with the Richards Equation (Brunetti et al., 2016; Hakimdavar et al., 2014). Model validation presented earlier has confirmed that the approach adopted in this study provides reasonable predictions of runoff and vertical moisture content profile (**Figure 4.7** and **Figure 4.8**). This section focuses on the influence of these alternative boundary conditions on the predictions. SWRC B was used for the SWRC, and the Mualem model was adopted to represent the HCF. The lower boundary was set to be free drainage (Equation 4.8) or seepage, and the runoff and the vertical moisture content profiles were regenerated for the event of 21/Oct/2013.

$$\frac{\partial h}{\partial z} = 0 \qquad \text{Equation 4.8}$$

Figure 4.11(a) shows the modelled runoff using the free drainage boundary condition. Compared with the runoff modelled with constant head boundary condition, the free drainage boundary condition underestimated the second runoff peak by 13.9% and the peak runoff was also delayed by 5 minutes. The drain down of the runoff responded slower and lasted longer, and the R_t^2 also dropped from 0.902 to 0.752. The long drain down curve was also observed in Liu and Fassman-Beck, (2017) when using a free drainage boundary condition. **Figure 4.11(b)** compares the monitored and modelled moisture content profile for the event. Following the storm event, the modelled moisture content dropped much faster than the monitored data, and the modelled moisture content fell well below the observed field capacity. Allowing the moisture content to drain below field capacity leads to an underestimation of water retained in the substrate. In the study of Palla et al. (2009), the same observation was made, using free drainage boundary condition with the Richards Equation, the model underestimated the moisture content for most of the studied storm events. However, compared with the vertical moisture content modelled with constant head boundary condition (**Figure 4.11(b)**), the vertical gradient is less significant, and therefore more similar to the monitored data.

The unrealistic drain-down observed here under the free drainage condition suggests that it is more appropriate to set the lower boundary condition to a constant suction head when applying the Richards Equation to model the runoff from green roof substrates.

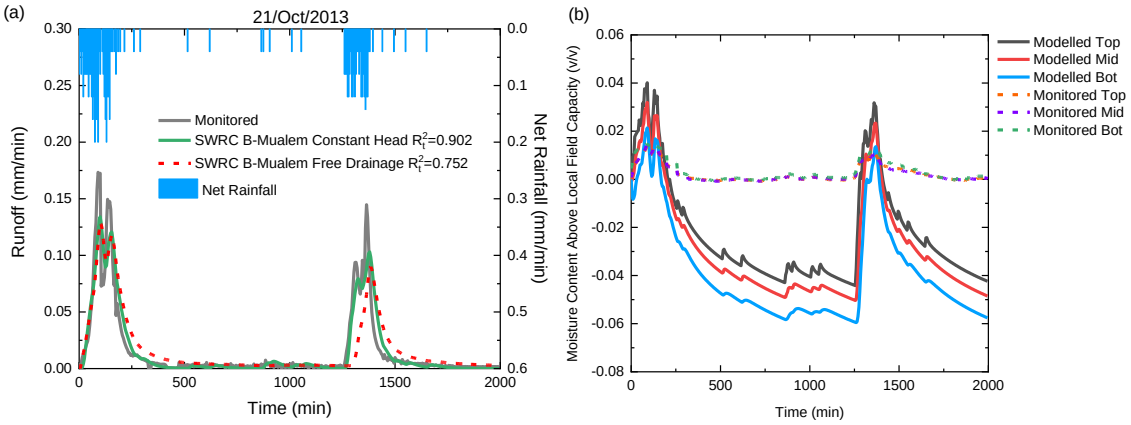

Figure 4.11. Validation of runoff and temporarily stored moisture. (a) Monitored and modelled runoff; (b) monitored and modelled vertical moisture content profiles using the SWRC B-Mualem model and free drainage boundary condition.

Figure 4.12(a) presents the modelled runoff using the seepage boundary condition. The timing of the runoff profile was incorrectly estimated by the model using the seepage boundary condition.

The time to start of runoff was delayed about 75 minutes and the time of peak runoff was also incorrectly predicted; 16.17% less runoff was estimated by the model compared with the constant head option. The R_t^2 also dropped from 0.902 to 0.691. As the seepage boundary assumes zero boundary flux when the bottom boundary is unsaturated, no outflow is generated until the lower boundary becomes saturated, and as a consequence, a delay in runoff was generated by the model. **Figure 4.12(b)** shows the modelled vertical moisture content profiles using the seepage boundary condition. More water was modelled to be stored in the substrate, which resulted in less runoff being generated. The moisture content at the bottom boundary corresponds to saturated moisture content. Following the storm event, the moisture content in the substrate was modelled to be kept at a high level, which is inconsistent with the observed moisture content data.

The incorrectly modelled timing of the runoff profile and the very unrealistic vertical moisture content profiles produced using the seepage boundary condition indicates that it is inappropriate to set seepage as the lower boundary condition when using the Richards Equation to model the detention effects of the type of green roof used in this study.

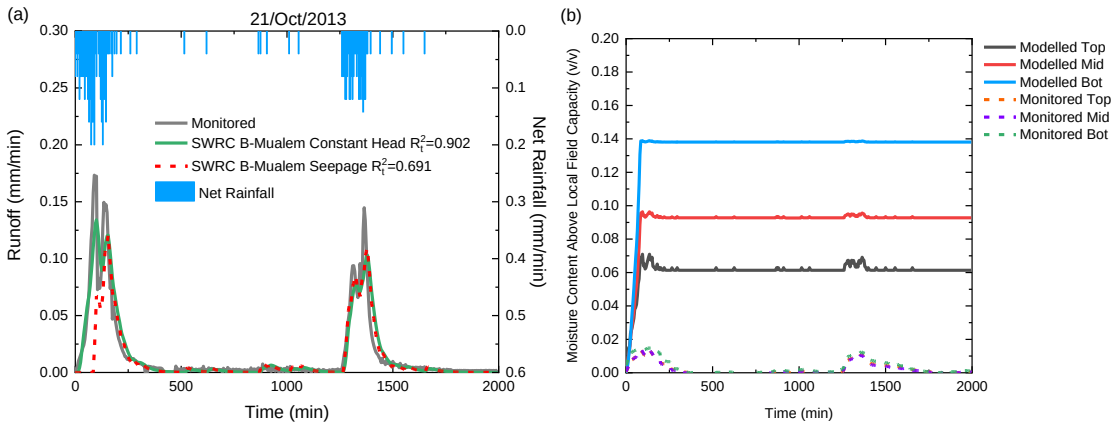

Figure 4.12. Validation of runoff and temporarily stored moisture. (a) Monitored and modelled runoff; (b) monitored and modelled vertical moisture content profiles using the SWRC B-Mualem model and the seepage boundary condition.

4.9 Conclusions

Based on the monitored moisture content data for a field green roof test bed, it was found that once the substrate reaches field capacity, moisture responses at all three depths in an 80 mm green roof substrate occur simultaneously, rather than as a wetting front moving downwards. The SWRC for HLS green roof substrate was characterised, and it has been confirmed that the

green roof substrate is more like a dual-porosity system and, therefore, the SWRC is better represented by the Durner equation (Equation 2.5).

Both the Richards Equation and the lumped Reservoir Routing model can provide reasonable predictions of runoff profiles and overall temporary storage dynamics. It should be noted that, whilst the Reservoir Routing model required calibration from observed rainfall-runoff performance data, the physically-based Richards Equation only required data based on the measurable physical characteristics of the substrate (i.e. SWRC, HCF and field capacity). Validated by five storm events, the approach of using the Richards Equation to represent temporary (detention) moisture storage between field capacity and saturation proposed in this chapter was proved to be capable of regenerating observed runoff profiles.

The lower boundary condition significantly impacts the model prediction of both runoff and vertical moisture content profile in the substrate. It is concluded that neither free drainage nor seepage boundary conditions are suitable boundary conditions to use with the Richards Equation to model the detention effects of the green roof used in this study. However, the constant suction head boundary condition was found to represent the observed behaviour better.

Investigations conducted with the Richards Equation suggested that the modelled runoff profile and vertical moisture content profile is sensitive to the HCF. Discrepancies between the measured and modelled (Richards Equation) profiles highlighted specific requirements for new laboratory data on the physical hydrological properties of green roof substrates and the hydrological detention responses of these substrates to imposed rainfall inputs.

5 Characterisation of Green Roof Substrate Physical Properties

5.1 Chapter overview

Chapter 4 emphasises the importance of hydrological properties to detention modelling with the Richards Equation. This chapter presents the experimental measurements of green roof substrates physical properties using the methods described in Chapter 3. Firstly, the four green roof substrates used for investigation are introduced. The substrate basic properties, including porosity, maximum water holding capacity, water permeability and particle size distribution, are determined using the FLL methods. The measured SWRC and HCF for the substrates are then presented. The Durner and van Genuchten models are fitted to the measured data, and the capability of the Durner-Mualem method for estimating the substrates' unsaturated hydraulic conductivity is investigated using the measured data. New hydraulic conductivity functions for the substrates are proposed based on the measured data. Further investigation into the substrates' detention performance is conducted with four design storms and two substrate depths.

This chapter forms part of the following publication:

Peng, Z., Smith, C., Stovin, V., 2020. The importance of unsaturated hydraulic conductivity measurements for green roof detention modelling. *J. Hydrol.* 590, 125273. https://doi.org/10.1016/j.jhydrol.2020.125273

5.2 The trial green roof substrates

Three representative green roof substrates from an external supplier and a homemade green roof substrate mixture were used in this study. Heather with Lavender Substrate (HLS) (which was also considered in Chapter 4) and Sedum Carpet Substrate (SCS) are manufactured by ZinCo, whereas the Marie Curie Substrate (MCS) was a comparable substrate developed between the University of Sheffield and ZinCo as part of a collaborative research project. These three substrates have been used in previous experimental and field studies, and they have shown the potential to provide hydrological benefits (Berretta et al., 2014; De-Ville et al., 2017; Stovin et al., 2015; Yio et al., 2013). The New Substrate Mix (NSM) is a homemade substrate that was designed to contain a higher percentage of fines. This was done with the intention of developing a substrate that would have contrasting characteristics compared to the other substrates. The components of NSM were separated out from HLS by sieving. As the organic matter was lost during the preparation processes, 5% (v/v) of John Innes No.1 compost was added to the mixture. **Figure 5.1**

shows photographs of the four green roof substrates. MCS shows the highest proportion of large particles. There is no significant difference between HLS and SCS, but as HLS contains perlite, it looks whiter than SCS; NSM contains more fines than MCS, HLS and SCS.

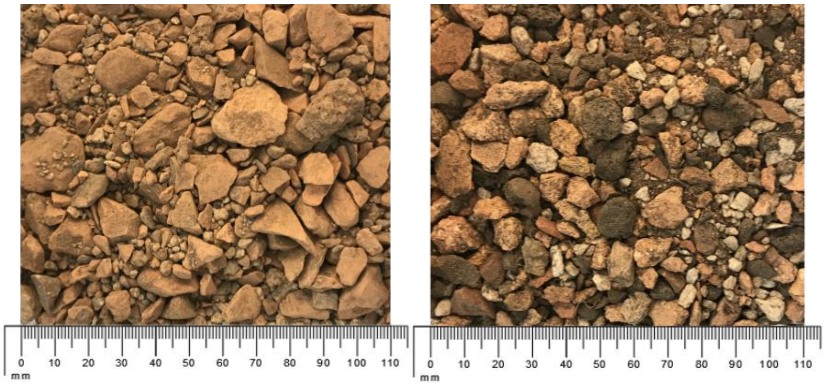

Marie Curie Substrate (MCS) Heather with Lavender Substrate (HLS)

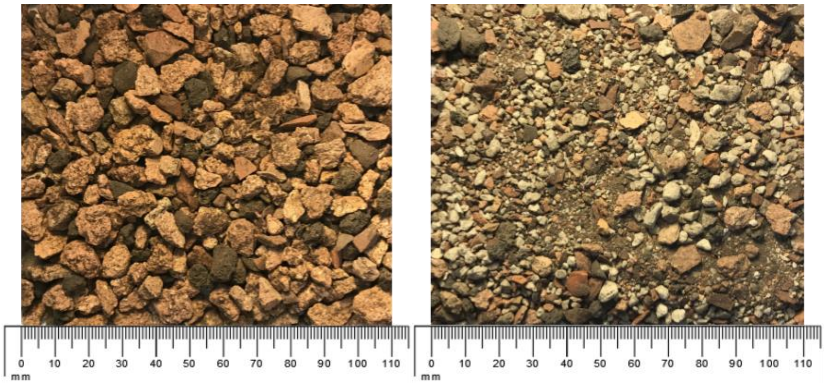

Sedum Carpet Substrate (SCS) New Substrate Mix (NSM)

Figure 5.1. Photographs of the four trial substrates.

5.3 Basic properties

In this chapter, properties determined for the substrates using the FLL methods (Section 3.2) included particle size distribution (PSD), d_{50}, bulk density, porosity, maximum water holding capacity (MWHC) and water permeability (saturated hydraulic conductivity). It should be noted that the FLL tests were conducted with HLS in Chapter 4. However, new tests with the substrate to determine the MWHC and water permeability were conducted in this chapter.

5.4 Soil water release curve (SWRC)

The Soil Water Release Curve (SWRC) for the substrates were determined using the hanging column and the pressure extractor methods (Section 3.3). The data points measured by the

pressure extractor method in this study were adopted from previous studies (Berretta et al., 2014). The SWRC for HLS was characterised in Chapter 4, and the results were brought to this chapter. As pressure extractor data for the NSM was unavailable, all the SWRC data for this substrate was determined by the hanging column method, with two additional suction heads at 200 cm and 300 cm.

The parameters of the van Genuchten model (Equation 2.6) and the Durner equation (Equation 2.5) models were determined in the SWRC Fit software (Seki, 2010) using the measured data points.

5.5 Hydraulic conductivity function (HCF)

The Hydraulic Conductivity Function for the four green roof substrates was measured using the steady-state and transient techniques in an infiltration column (Section 3.4). The Durner-Mualem model (Equation 2.9) is a conventional model to estimate soil unsaturated hydraulic conductivity. In the model, except for the saturated hydraulic conductivity, all the other model parameters are derived from an SWRC model. The capability of this conventional model of estimating the unsaturated hydraulic conductivity of green roof substrates were assessed based on the measured data points.

5.6 Detention tests with the substrates

Detention tests were conducted with the four green roof substrates at two depths (100 mm and 200 mm) and four design storms. The substrate was initially wetted with 1.2 mm/min of rainfall for 2 hours, and it was then left to drain for 2 hours to ensure that it was at field capacity (FLL, 2008; Yio et al., 2013). The moisture content and runoff data in the tests was recorded. Control tests were conducted without a substrate component, and three replications were conducted with the same sample of the substrates. Full descriptions of the substrate detention tests can be found in Section 3.5.1.

5.7 Model evaluation

The SWRC Fit software (Seki, 2010) was used to determine the parameters for the Durner and van Genuchten models. The software uses R^2 to assess the goodness of fit of the models to the measured SWRC data. A value of R^2 equals one corresponds to a perfect fit.

The root of the mean square error (RMSE) (Equation 5.1) was selected to assess the goodness of fit for the HCFs. RMSE yields a value higher than zero, and a smaller value of RMSE indicates a better prediction. The RMSE metric was also used in Liu and Fassman-Beck. (2018) to evaluate

the goodness of fit of the Durner-Mualem model to estimate the unsaturated hydraulic conductivity for green roof substrates.

$$\mathrm{RMSE} = \sqrt{\frac{1}{\mathrm{N}}\sum_{\mathrm{i}=1}^{\mathrm{N}}\left(\mathrm{K_m} - \mathrm{K_p}\right)^2} \qquad \text{Equation 5.1}$$

where N is the number of measured data points, $\mathrm{K_m}$ is the measured hydraulic conductivity and $\mathrm{K_p}$ is the predicted hydraulic conductivity.

5.8 Results and discussion

5.8.1 Basic properties

Table 5.1 lists the results of the FLL tests for the four substrates. SCS has the highest water permeability, suggesting that it may exhibit the worst detention effect during storm events. However, the static parameters measured by FLL methods have limited relevance to the dynamic behaviour of substrate moisture during storm events. It is also the case that the water permeability (saturated hydraulic conductivity) significantly overestimates the hydraulic conductivity experienced in actual, unsaturated conditions. Note that the Maximum Water Holding Capacity and Permeability values for HLS differ slightly from those reported in **Table 4.4**; this is due to additional repeat tests being undertaken concurrently with the three new substrates

Table 5.1. Substrate physical characteristics according to FLL (2008) test methods.

Properties	Unit	MCS		HLS		SCS		NSM	
		Mean	St.Dev	Mean	St.Dev	Mean	St.Dev	Mean	St.Dev
Particle size<0.063 mm	%	0.00	0.00	2.72	0.25	2.64	1.33	0.00	0.00
d_{50}	mm	3.97	0.49	5.05	0.07	7.25	0.35	2.58	0.39
Bulk density	g/cm^3	1.04	0.03	0.81	0.05	0.91	0.03	1.00	0.04
Porosity	%	55.15	0.02	55.60	0.85	53.99	0.45	48.64	0.02
Maximum water holding capacity	%	33.39	0.01	38.08	0.01	31.00	0.01	36.05	0.01
Permeability	mm/min	166.40	6.90	26.79	0.92	194.91	9.13	67.83	3.16

Particle Size Distributions (PSDs) for the four substrates are shown in **Figure 5.2**. All the substrates are FLL compliant. NSM was designed to contain more fine particles, and the PSD confirms this to be the case. The PSDs for HLS and SCS show differences in the percentages of large particles; SCS contains a higher proportion of particles larger than 1 mm. The particles in MCS are more evenly distributed, but it contains a slightly higher percentage of particles larger than 10 mm. The photographs of the four substrates in **Figure 5.1** are consistent with the PSD results shown in **Figure 5.2**.

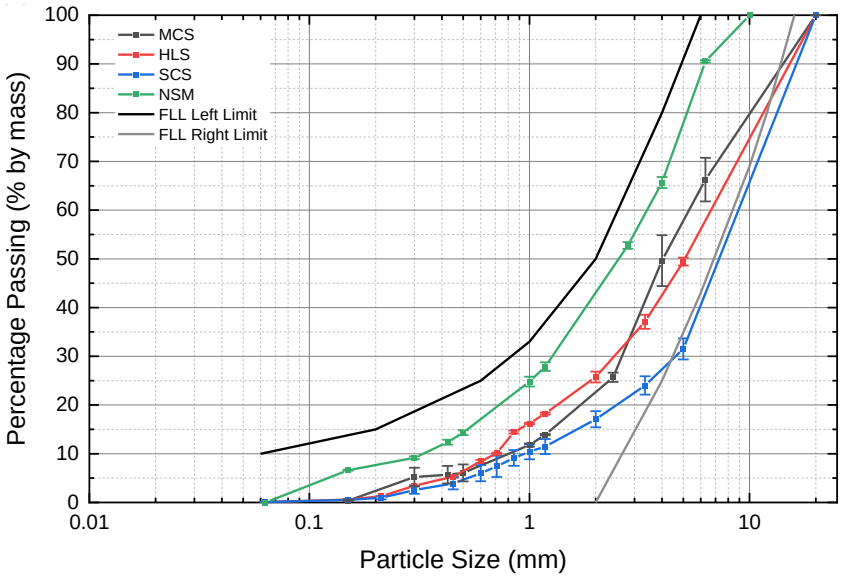

Figure 5.2. Particle Size Distribution (PSD) for the four green roof substrates (the graph is plotted with the errors to the average values of the three tests to show the variation between test samples).

5.8.2 Soil water release curve (SWRC)

Figure 5.3 presents the measured points on the SWRC for the four substrates. It should be noted that no pressure extractor data was obtained for NSM. However, data corresponding to high suction heads is not considered to be particularly critical for green roof detention modelling. The results for HLS were taken from Chapter 4. The results were plotted with error bars (± to the average values of three tests) to show the variation between tests. The results for the three replications confirm that little variation was present in the SWRCs. The amount of water retained in the substrate at low suction heads (i.e. 0 cm to 100 cm) depends mainly on capillary effects and the pore size distribution. However, at high suction heads, the substrate retains water due to adsorption, so it is influenced by the texture and the specific surface of the substrate (Hillel et al., 1998). HLS showed greater water retention than the other three substrates over the full range of suction heads; this indicates that it contains greater clay content. Compared with MCS and SCS, both HLS and NSM exhibited a more gradual decrease in wetness with an increase in the suction head; this suggests that a more uniform particle size distribution is present in HLS and NSM, which is consistent with the particle size distribution presented in **Figure 5.2**. For MCS and SCS, as most of the pores are large in these substrates, once these large pores are emptied (at suction head > 20 cm), only a small amount of water remains.

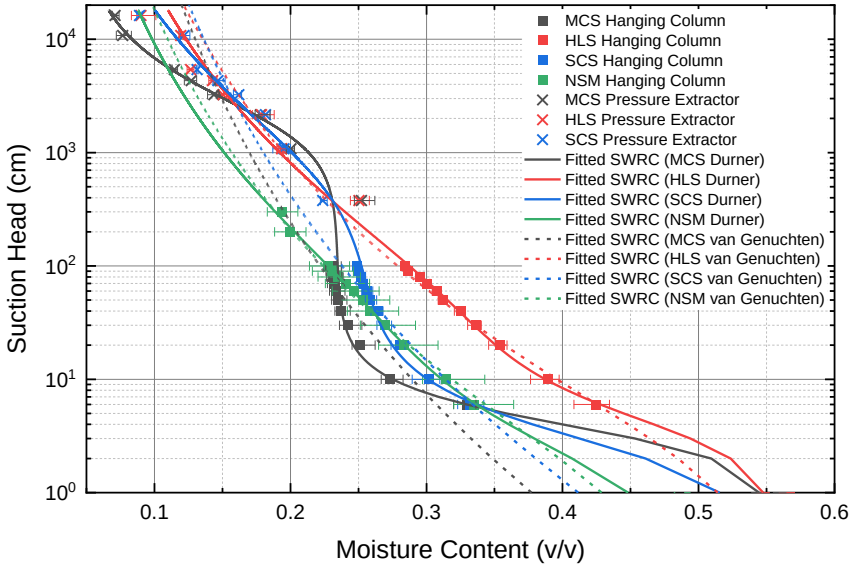

Figure 5.3. Soil Water Release Curve (SWRC) for the four green roof substrates (the graph is plotted with the errors to the average values of the three tests to show the variation between test samples, and the data for HLS is the same data presented in Chapter 4).

Table 5.2 lists the fitted parameters for the van Genuchten and Durner models for the SWRC. With all R^2 values for the Durner model higher than for the van Genuchten model, it is concluded that the Durner model provides a better fit to the measured SWRC for the four substrates. The same observation was also reported in Liu and Fassman-Beck (2018). **Figure 5.3** also shows the fitted SWRCs for the four substrates using the van Genuchten (Equation 2.6) and Durner (Equation 2.5) models. The MCS and SCS substrates exhibit significant dual-porosity characteristics, indicated by the occurrence of inflection points (0.23 v/v for MCS and 0.25 v/v for SCS) where the slope of the SWRC experiences a sudden change. For these substrates, the van Genuchten model fails to fit the measured points. On the other hand, the van Genuchten and Durner models show little difference for the HLS and NSM (R^2=0.988 versus R^2=0.995 for HLS and R^2=0.996 versus R^2=0.999 for NSM).

Table 5.2. Fitted Soil Water Release Curve (SWRC) parameters for the substrates.

	Durner				van Genuchten				
Parameter	MCS	HLS*	SCS	NSM	Parameter	MCS	HLS*	SCS	NSM
Θ_s	0.552	0.556	0.54	0.486	Θ_s	0.552	0.556	0.54	0.486
Θ_r	0.042	0	0	0	Θ_r	0	0	0	0
α_1	0.304	0.306	0.456	0.707	α	26.025	0.807	8.751	1.459
n_1	2.82	2.255	2.182	1.708	n	1.116	1.157	1.121	1.155
α_2	5.09E-04	0.02	0.002	0.021	R^2	0.933	0.988	0.979	0.996
n_2	1.926	1.194	1.267	1.184					
w_1	0.622	0.378	0.528	0.462					
R^2	0.996	0.995	0.997	0.999					

*Note: The parameters for HLS were also presented in Chapter 4.

5.8.3 Hydraulic conductivity function (HCF)

Figure 5.4 presents the measured hydraulic conductivity data for the four green roof substrates. The saturated hydraulic conductivity (the first data point on the HCF) was determined by the FLL tests, and the corresponding moisture content is the porosity (**Table 5.1**). The hydraulic conductivities were estimated using steady-state and transient techniques; within the transient technique, hydraulic conductivity was determined during drainage and evaporation. However, the tensiometers failed to capture the rapid change in the suction head in SCS, so no data was measured during the drainage process for SCS. It should be noted that the characterisations of HCF at the high moisture content (i.e. HCF determined by steady-state techniques) are more critical for detention modelling.

Significant variations between the two repeat tests are evident. This reflects the heterogeneous nature of green roof substrates. In addition, the unsaturated hydraulic conductivity is a property that is very sensitive to the pore size distribution (Masch and Denny, 1966; Rosas et al., 2014); differences in test column preparation could result in different pore size distributions and, therefore in differing HCFs.

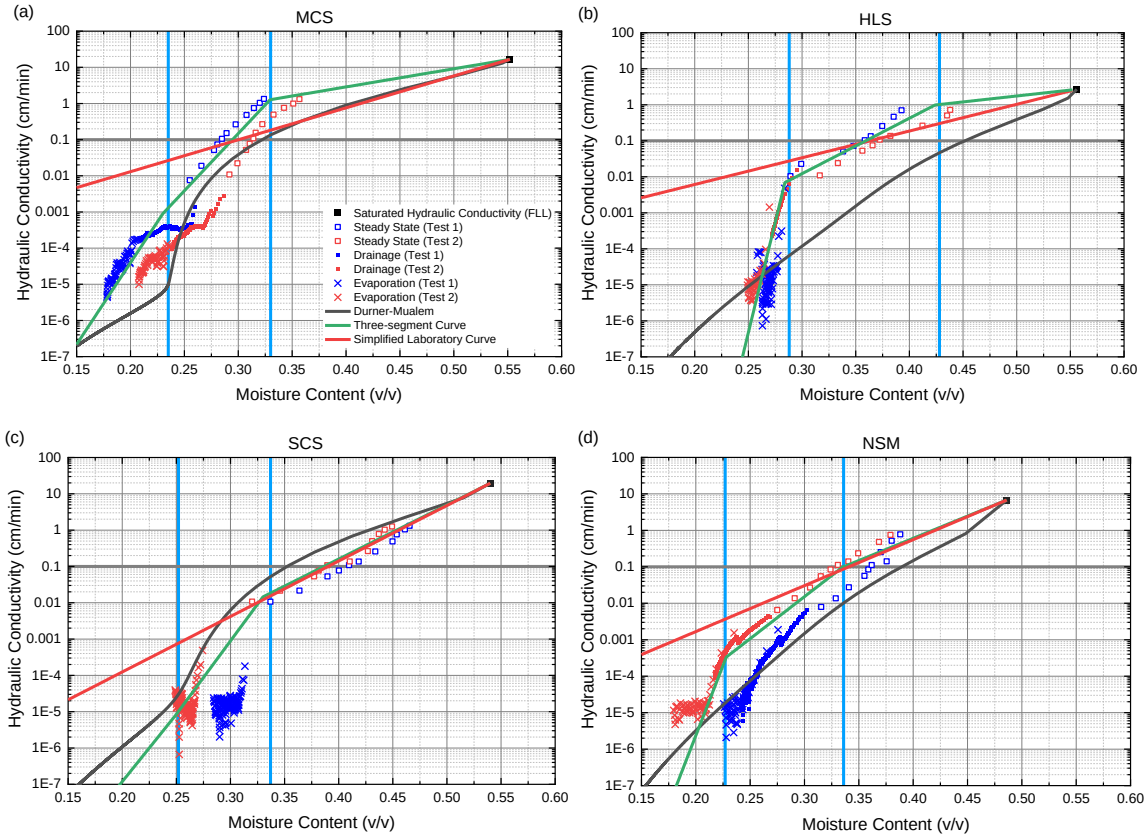

Figure 5.4. Measured unsaturated hydraulic conductivity, estimated (Durner-Mualem model) and fitted (three-segment curve and simplified laboratory curve) hydraulic conductivity functions (HCFs) for the four substrates (the two vertical lines indicate the intercepts: the moisture content corresponding to 6 cm (right line) and 100 cm (left line) suction head; the horizontal line indicates the hydraulic conductivity of 0.1 cm/min). Note: New measurements replace the preliminary data points for HLS reported in **Figure 4.6(b)**.

5.8.3.1 Durner-Mualem model

Figure 5.4 also compares the Durner-Mualem model with the measured data, and **Table 5.3** lists the statistics for the model fit. Consistent with Liu and Fassman-Beck (2018), the results indicate that the Durner-Mualem model is not suitable to represent the HCF for green roof substrates (with mean RMSE = 0.113, **Table 5.3**). The fit for HLS is particularly poor; it underestimated the unsaturated hydraulic conductivity by around two orders of magnitude at higher moisture contents (e.g. 9.67×10^{-5} cm/min was estimated by the Durner-Mualem compared with a measured value of 0.015 cm/min at 0.3 v/v).

Table 5.3. RMSE for the Durner-Mualem model and the three-segment curve.

Substrate	Test	Durner-Mualem	three-segment curve
MCS	1	0.146	0.060
	2	0.121	0.132
HLS	1	0.090	0.044
	2	0.095	0.089
SCS	1	0.238	0.057
	2	0.122	0.050
NSM	1	0.032	0.018
	2	0.059	0.033
Mean	-	0.113	0.060

5.8.3.2 Three-segment curve

Given the poor fit of the Durner-Mualem model, an alternative approach of estimating a continuous HCF from the laboratory data is required. Whilst some scatter in the data is evident, the laboratory measurements typically exhibit one or two changes in slope. This led to a proposal to fit a three-segment curve (Equations 5.2 to 5.4) to the measured data. It was noted that the two intercepts typically occurred at moisture contents associated with two specific suction heads, 6 and 100 cm (**Figure 5.3**). As indicated earlier (**Table 5.1** and **Figure 5.3**), these two values are associated with the MWHC (or practical field capacity) of these green roof substrates and with nominal field capacity in conventional soils, respectively. Vertical lines indicating the corresponding moisture contents from the SWRCs are included in **Figure 5.4** for reference. The use of a piecewise linear function to characterise the HCF is not novel. Poulsen et al. (2002) have shown that three-region models can be fitted to a wide range of natural soils. Furthermore, they assigned similar intercepts (at suction heads of 10 and 350 cm), suggesting that these intercept values delineate independent functions associated with the macropore, mesopore and micropore regions.

$$\text{if} \quad \theta_1 < \theta \leq \theta_s; \qquad K(\theta) = 10^{\beta_1 \cdot \theta + \gamma_1} \qquad \text{Equation 5.2}$$

$$\text{if} \quad \theta_2 < \theta \leq \theta_1; \qquad K(\theta) = 10^{\beta_2 \cdot \theta + \gamma_2} \qquad \text{Equation 5.3}$$

$$\text{if} \quad \theta < \theta_2 ; \qquad K(\theta) = 10^{\beta_3 \cdot \theta + \gamma_3} \qquad \text{Equation 5.4}$$

where θ_1, θ_2 are the two intercepts (v/v) on the HCF, β_1, γ_1, β_2, γ_2, β_3 and γ_3 are the empirical parameters.

The mean RMSE for the HCF decreased from 0.113 to 0.060 when the three-segment curves were adopted (**Table 5.3**). As two HCF characterisation tests were conducted with each substrate, two three-segment curves were derived from the measured data for each substrate. The three-segment curves presented in **Figure 5.4** are the average of the two tests, and **Table 5.4** lists the parameters for the three-segment curves in **Figure 5.4**.

Table 5.4. Parameters for the three-segment curves.

Substrate	θ_1	θ_2	β_1	γ_1	β_2	γ_2	β_3	γ_3
MCS	0.330	0.230	5.019	-1.550	31.667	-10.330	45.183	-13.439
HLS	0.424	0.284	3.292	-1.403	15.389	-6.531	122.44	-36.934
SCS	0.330	0.249	14.899	-6.755	40.387	-15.167	37.088	-14.344
NSM	0.335	0.228	12.185	-5.092	23.062	-8.736	76.800	-20.988

5.8.3.3 Simplified laboratory curve

Equations 5.2 to 5.4 require suitable values for the intercepts θ_1 and θ_2 to be identified to define the HCFs. However, this approach requires intensive measurement of moisture content, suction heads and infiltration rates, which is complex and time-consuming. A simplified approach is therefore proposed, whereby only two data points on the HCF are required to derive the HCF.

The saturated hydraulic conductivity (measured using the FLL method) and the averaged moisture content of the two tests corresponding to a hydraulic conductivity of 0.1 cm/min were selected to define the HCF using Equation 5.5. The justification for choosing 0.1 cm/min is that it represents a moderate infiltration rate which can be easily achieved by the apparatus, and the time for the substrate to reach equilibrium under this flow rate is relatively short. In addition, this value also typically falls within the range between field capacity and saturation, which is the range of interest for detention modelling.

$$K(\theta) = 10^{a \cdot \theta + b} \qquad \text{Equation 5.5}$$

where a and b are empirical parameters.

Figure 5.4 also shows the derived HCFs for the substrates using the simplified approach. **Table 5.5** lists the value of the empirical parameters derived for the substrates using Equation 5.5 and the measured HCF data points. Compared with the Durner-Mualem model, except for the case of MCS (**Figure 5.4(a)**), where the Durner-Mualem model and the simplified laboratory curve reached a good agreement at high moisture content, the simplified laboratory curve shows a better agreement with the measured HCF data points for high moisture content (i.e. above field capacity) than for low moisture content (**Figure 5.4**). However, during storm events, the moisture

content in the substrate does not fall below field capacity, and the HCF at high moisture content is of more relevance.

The investigation into the influence of these alternative HCFs on detention modelling will be presented in Chapter 6.

Table 5.5. Value of parameters for the simplified laboratory curve.

Substrate	a	b
MCS	8.8267	-3.6512
HLS	7.4203	-3.6977
SCS	15.284	-6.9636
NSM	12.609	-5.2981

5.8.4 Detention tests with the substrates

As high levels of consistency were observed (the mean Standard Deviation of each test for the three replications can be found in Appendix C), the results presented are the mean results of three replications.

5.8.4.1 Detention performance

Figure 5.5 presents the runoff profiles for the four substrates in response to four design storms. The left column presents the runoff profiles for the 100 mm substrates, and the right column corresponds to the 200 mm substrates. The runoff from the no substrate test confirms that the apparatus is capable of providing the desired rainfall rates.

In the shallow 100 mm substrates, as the detention tests started after initial wetting, with the substrate nominally at field capacity (Appendix C), none of the substrates showed a significant delay in the time to start of runoff. Interestingly, HLS and NSM showed similar responses to the storms, and MCS performed similarly to SCS. In Design Storm 1 it may be seen that runoff from the HLS and NSM substrates equilibrated with the rainfall relatively quickly (around 7 minutes) (**Figure 5.5(a)**). In contrast, runoff from the MCS and SCS substrates showed much greater detention (i.e. peak runoff is reduced by 10.7% compared with peak rainfall), and equilibrium was not reached before the end of the 30-minute rainfall (**Figure 5.5(a)**). The 100 mm substrates showed a minor difference in detention performance in response to the other design storms.

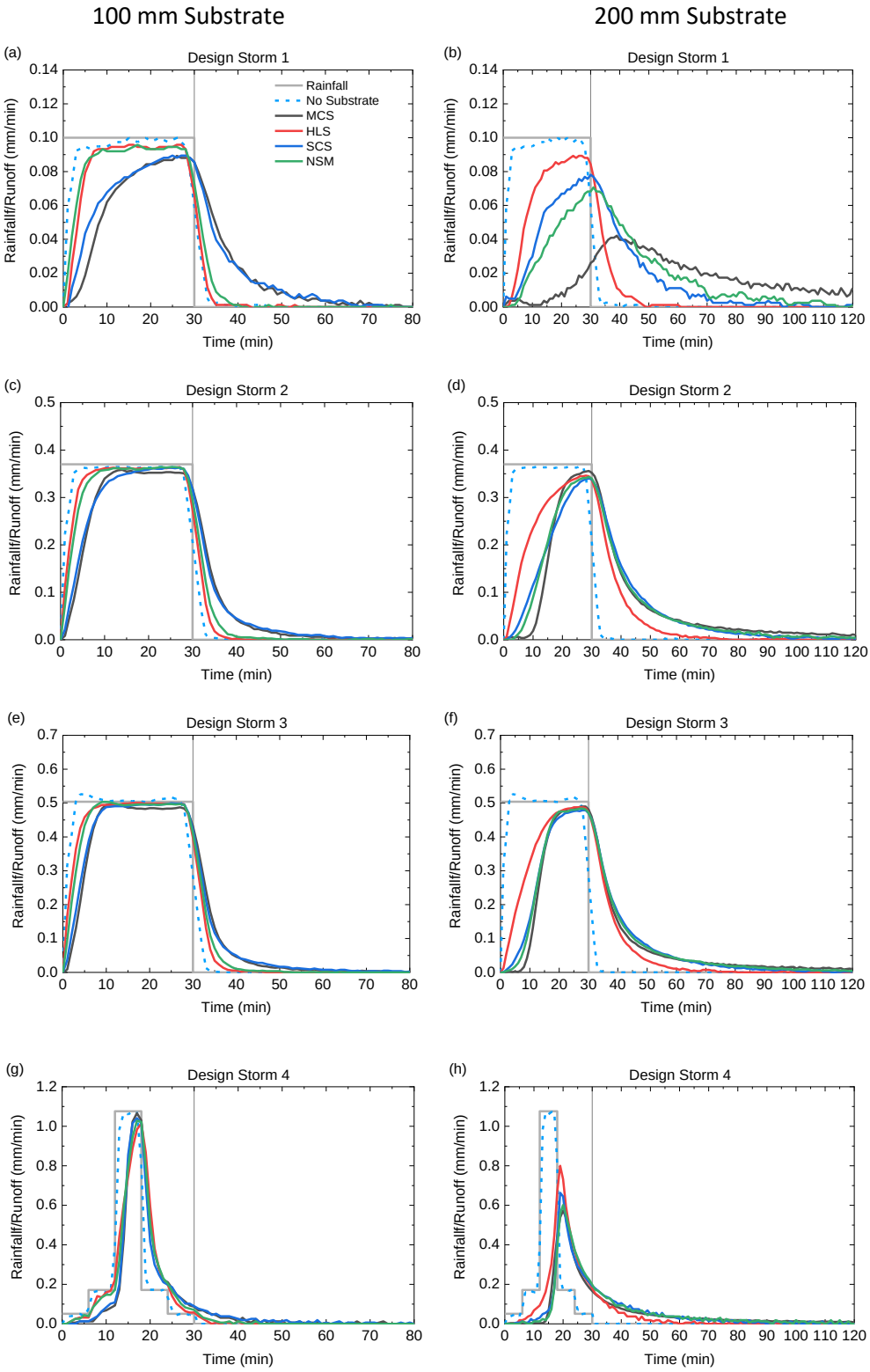

Figure 5.5. Measured runoff profiles for the substrate detention tests (the vertical line indicates the end of the rainfall event).

The differences between substrates detention performance are obvious in a deeper system (i.e. 200 mm substrate). In response to a low-intensity storm event (Design Storm 1) (**Figure 5.5(b)**),

MCS demonstrated the highest detention potential. It reduced the peak rainfall by 57.83% and extended the duration of runoff to beyond 120 minutes. In contrast, the HLS showed the lowest detention potential since it only reduced the peak rainfall by 9.67% and extended the duration of runoff to 60 minutes. Within the 200 mm substrates, in response to a peaked storm (Design Storm 4), HLS showed the lowest reduction in peak runoff (25.66%) and MCS showed the highest reduction (46.65%); HLS delayed the time to start of runoff by about 5 minutes, MCS delayed it by about 15 minutes (**Figure 5.5(h)**). There are no significant differences between SCS and NSM in response to Design Storms 2 and 3 (**Figure 5.5(d)** and (**Figure 5.5(f)**). SCS has a slightly lower peak runoff reduction in response to Design Storm 1 (21.87%) (**Figure 5.5(b)**).

Overall, HLS exhibits the worst detention performance, and MCS shows the best; detention performance is consistently improved by increasing the depth of the substrate. The observations here are consistent with the finding in Stovin et al. (2015) and Yio et al. (2013).

5.8.4.2 Moisture content behaviour during storms

Moisture content responses for all four substrates for all four design storms are shown in **Figure 5.6**, **Figure 5.7**, **Figure 5.8** and **Figure 5.9**. It should be noted that the secondary y-axis range is not consistent between sub-plots. The moisture content responses in the substrates showed significant differences between substrates and depths.

The moisture content profiles in the 100 mm substrates confirm that the moisture content increases simultaneously with the rainfall, and the moisture content returns to its initial value once the rainfall stops. The increase in moisture content is more significant in high rainfall intensity (Design Storm 3), and it is less significant in low rainfall intensity (Design Storm 1). The moisture content in the 100 mm SCS experienced the most dramatic change during Design Storm 3: it increased by about 0.03 v/v at the peak. In contrast, HLS showed the smallest increase in Design Storm 3, around 0.015 v/v.

The two moisture probes in the 200 mm substrates make it possible to investigate the vertical moisture content profiles during storms. **Figure 5.6**, **Figure 5.7**, **Figure 5.8** and **Figure 5.9** show the measured moisture content data at the top and bottom of the substrates during the design storms. Vertical gradients in moisture content were clearly present within the substrates. The top substrate was always wetter than the bottom substrate, and the top substrate always responded faster to the storm than the bottom substrate. The vertical gradient is significant in HLS and NSM (**Figure 5.7** and **Figure 5.9**); the moisture content at the bottom of these two substrates showed almost no increase even in the highest rainfall intensity (Design Storm 3) (about 0.001 v/v increase for HLS and less than 0.0005 v/v increase for NSM at the peaks) during the storm. The greater

gradient shown in HLS and NSM implies that they had a lower unsaturated hydraulic conductivity than MCS or SCS. Temporal variations in vertical substrate moisture content profiles were presented for shallow external green roof test beds in Peng et al. (2019) and Section 4.7.1. A greater peak to peak vertical moisture content gradient was observed in Peng et al. (2019) and Section 4.7.1 (2.4 v/v/m versus 0.8 v/v/m), and the gradient was also typically reversed. It has been suggested that the presence of vegetation and substrate consolidation over time may be contributed to the development of vertical gradients observed in external test beds (Berretta et al., 2014), but it is also acknowledged that other factors — including uncertainties associated with the calibration of moisture content probes and their siting within heterogeneous substrates — also impact on the absolute measured values. Acknowledging these uncertainties in absolute measured values, the moisture content profiles will be presented as values relative to the local initial moisture content later in Chapter 6.

Figure 5.6, **Figure 5.7**, **Figure 5.8** and **Figure 5.9** also show the runoff response to the storm. As the detention tests started from field capacity, runoff occurs immediately after the rainfall, and a wetting front was not present in every substrate. In the 200 mm MCS, some evidence of a wetting front was shown (**Figure 5.6**), with the response in the lower substrate layer occurring about 8 minutes later than the top in the Design Storm 3.

Liu and Fassman-Beck (2017) observed that preferential flow paths developed in the substrate during the storm when the substrate was initially relatively dry. However, based on the runoff and vertical moisture content profiles measured for the 200 mm substrates, there is no strong evidence for the occurrence of preferential flow within green roof substrates showed in this study. The runoff increases simultaneously with the rise in bottom moisture content, and in no case was runoff generated before the bottom moisture started to increase.

The measured moisture contents at the start and end of the detention tests are generally closer to the FLL MWHC values (e.g. 0.34 v/v was the measured value for the 200 mm NSM and 0.36 v/v for the FLL MWHC) than the SWRC values corresponding to 100 cm suction head, providing further indication that field capacity in these substrates may correspond to a lower suction head (i.e. 6 cm to 10 cm) than is the case for conventional soils. Any differences between the absolute values reported here and the MWHC values reported in **Table 5.1** are likely to result from slight discrepancies in the moisture probe calibration (moisture probe calibration can be found in Appendix A, and further discussion on the variations of moisture probes will be discussed in Chapter 10) and/or the use of different sub-samples for the specific tests.

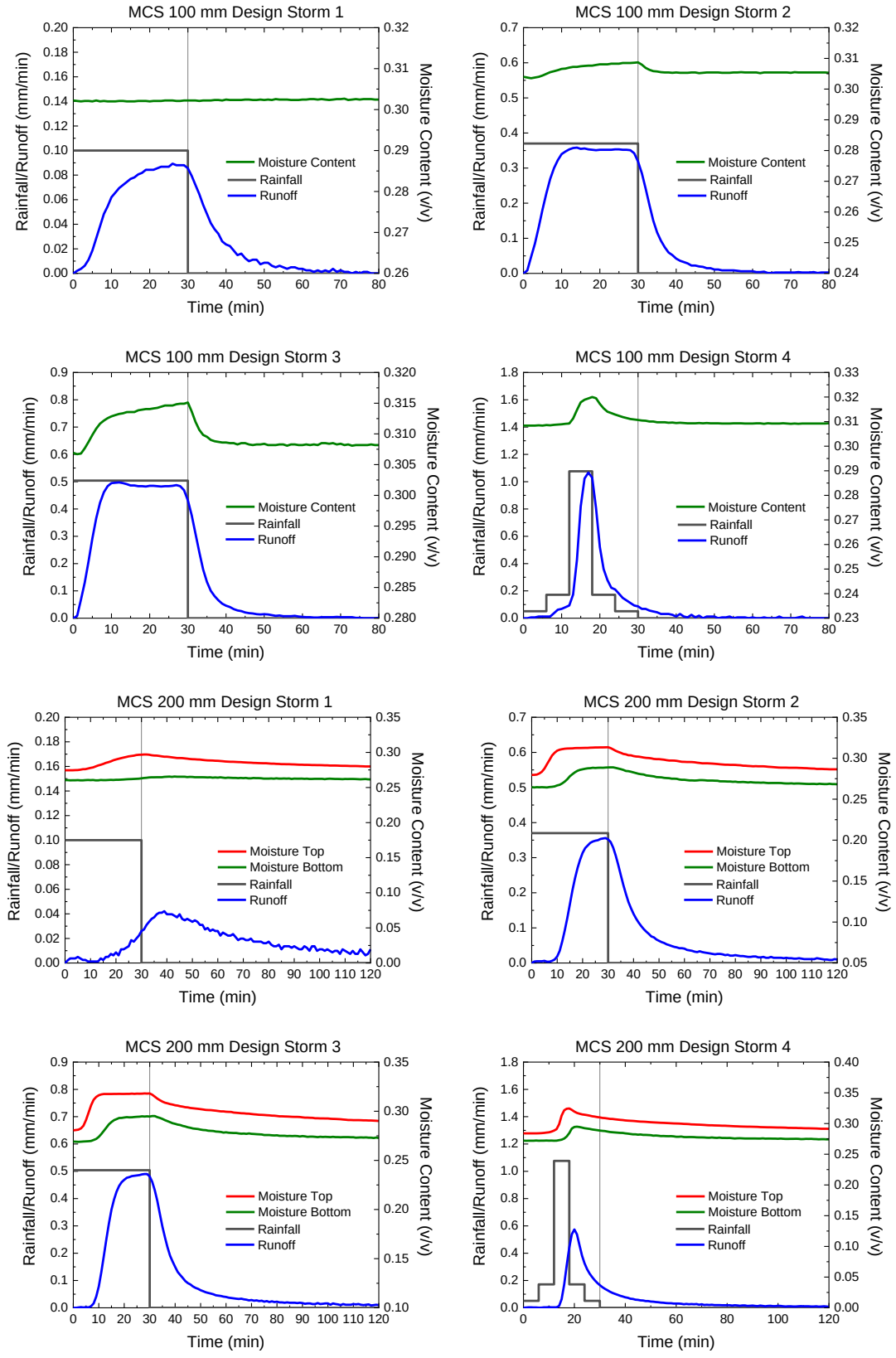

Figure 5.6. Measured runoff and moisture content profiles during the detention tests for MCS.

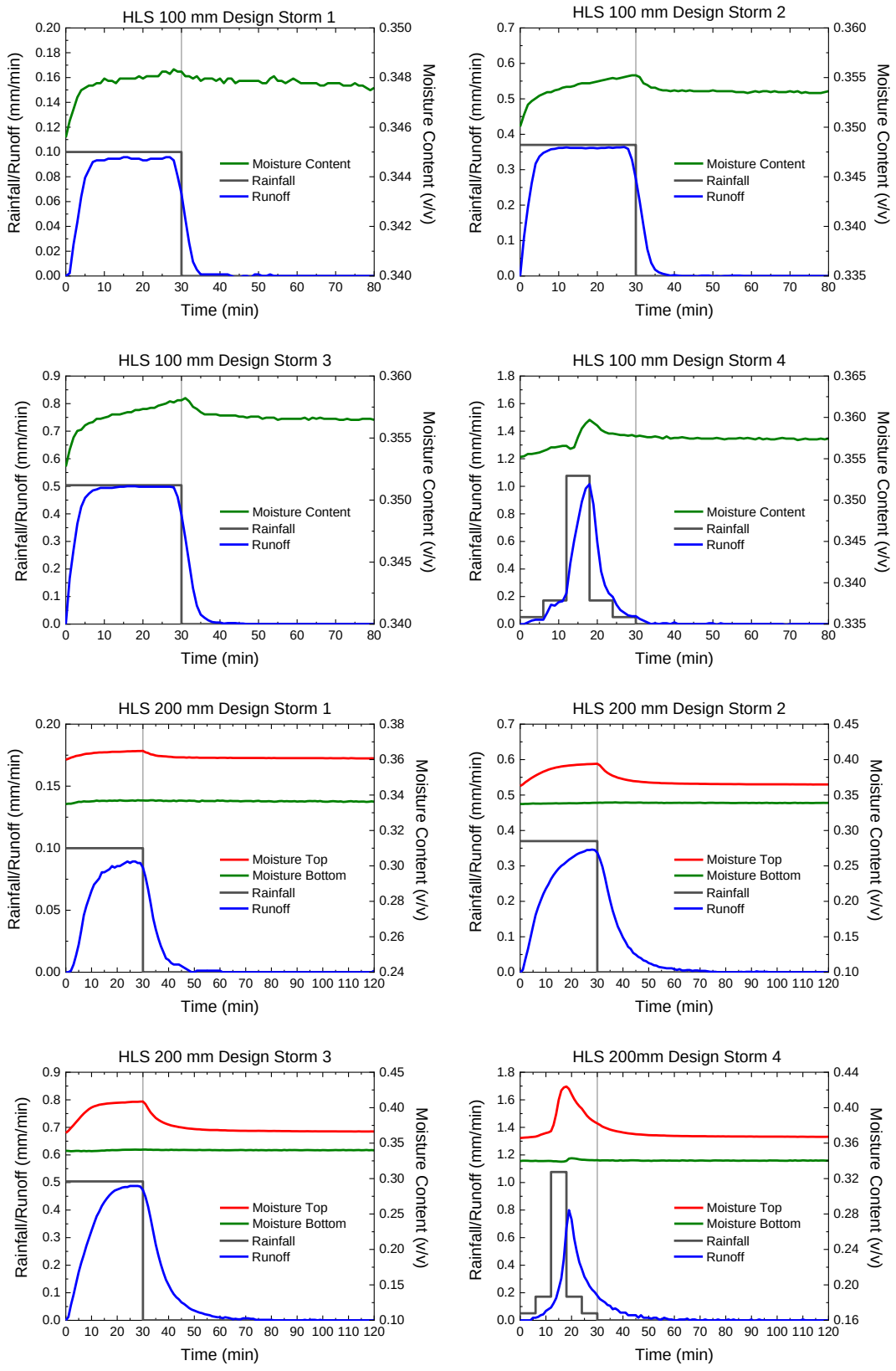

Figure 5.7. Measured runoff and moisture content profiles during the detention tests for HLS.

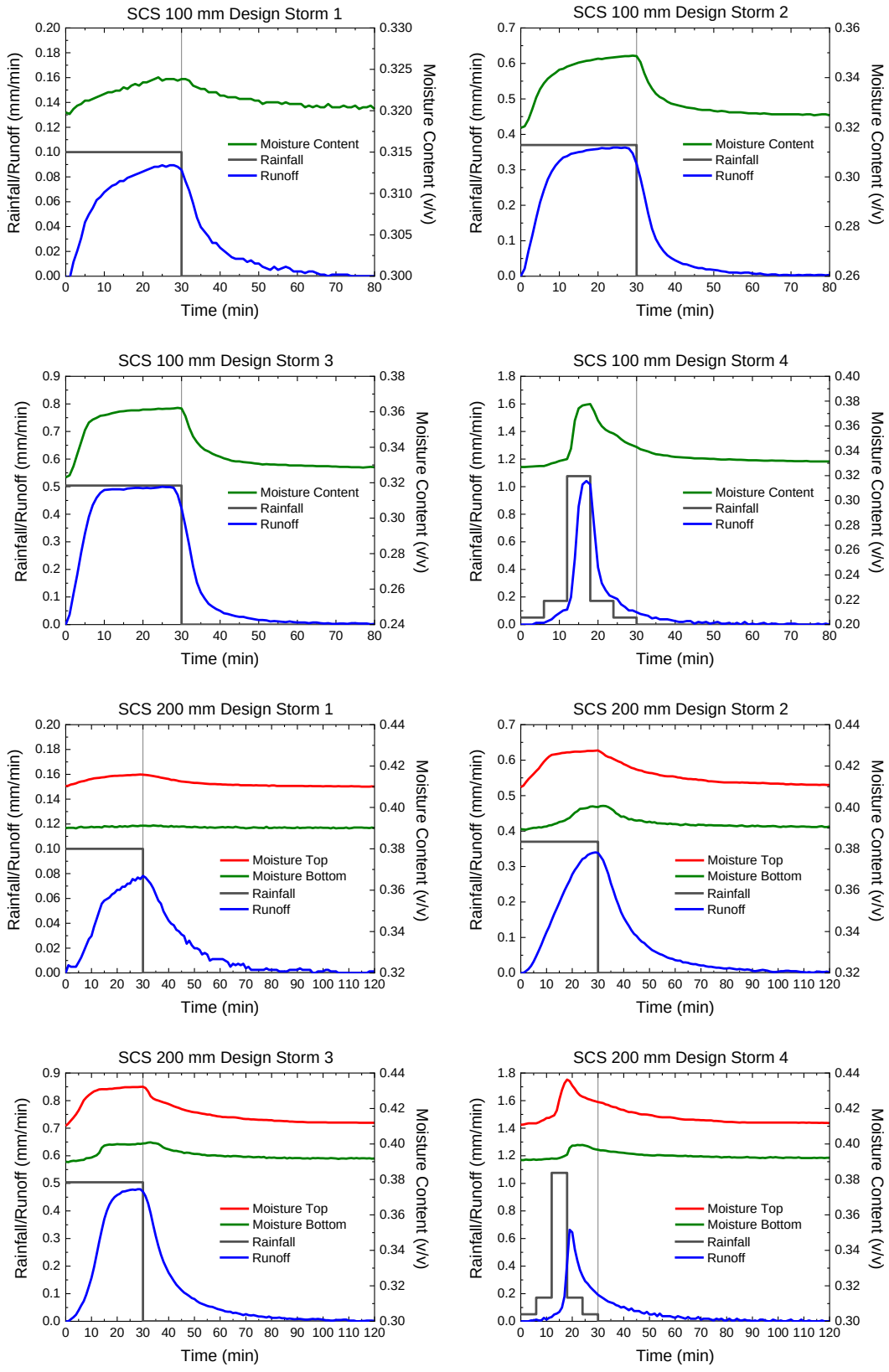

Figure 5.8. Measured runoff and moisture content profiles during the detention tests for SCS.

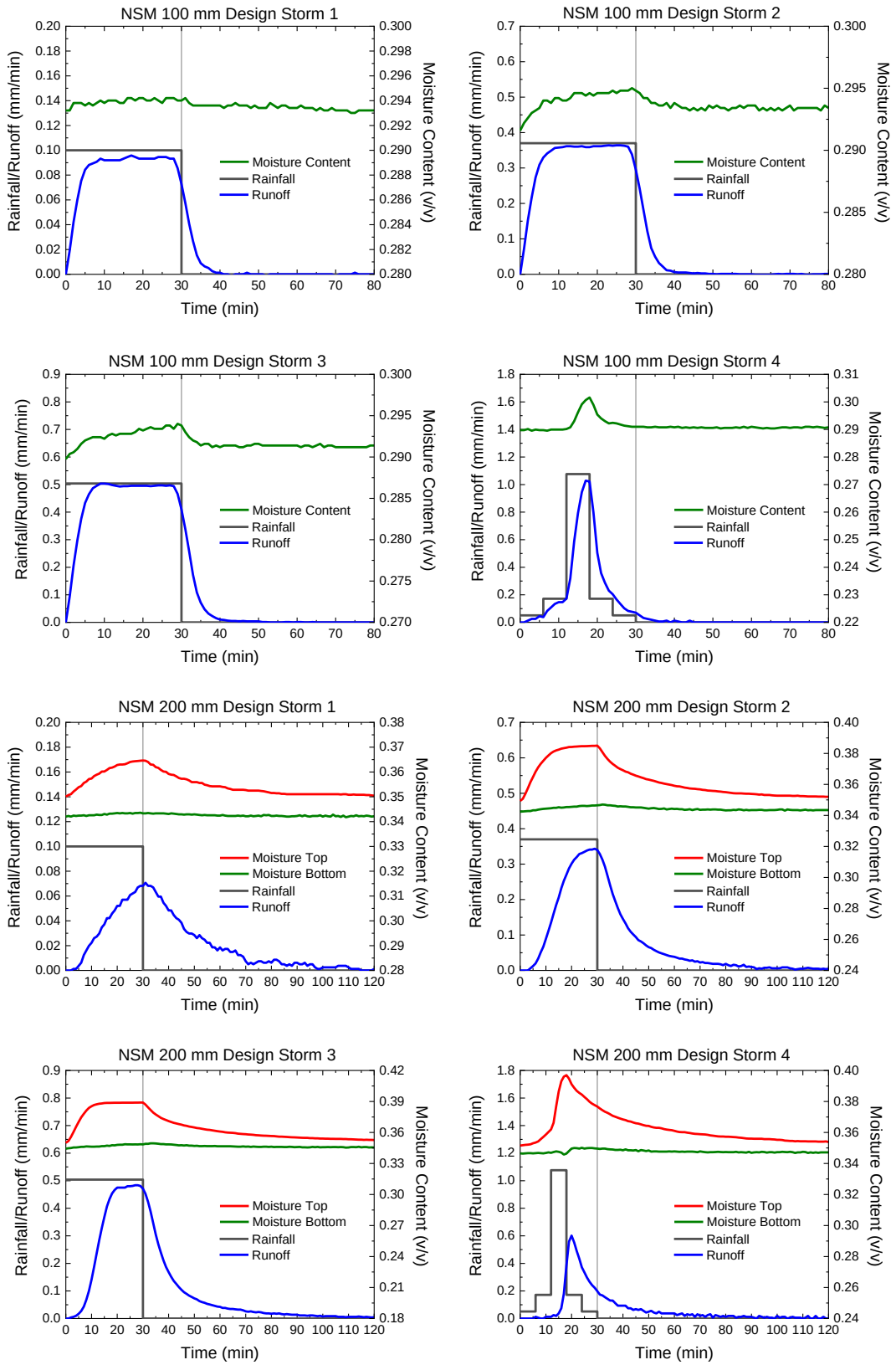

Figure 5.9. Measured runoff and moisture content profiles during the detention tests for NSM.

5.9 Conclusions

New SWRC data for four representative green roof substrates characterised in this chapter confirmed that the Durner model correctly represents the water release characteristics of the four representative green roof substrates. Variations observed in the HCF experiments highlighted the heterogeneous nature of green roof substrates. The comparison between measured and estimated HCF showed that the conventional approach for estimating hydraulic conductivity (Durner-Mualem) failed to represent the HCF for green roof substrates accurately. Therefore, a new three-segment curve form of HCF was proposed and shown to characterise the measured data well. A simplified form of HCF that requires two-point measurement of unsaturated hydraulic conductivity was also proposed for the substrates.

Comparisons between the SWRCs and actual moisture contents observed when the substrates were judged to have drained to field capacity suggest that moisture content measured at 6-10 cm suction head may provide a better practical estimate of field capacity in the brick-based green roof substrates than the 100 cm value typically assumed for natural soils.

The runoff and moisture content profiles measured for the substrates during simulated storm events clearly demonstrated different substrate responses. The measured vertical moisture content profiles in the 200 mm substrates indicated that vertical gradients exist within the substrate, and the change in moisture content in response to a storm is more rapid at the top of the substrate.

6 Modelling of Green Roof Substrate Detention Using the Richards Equation

6.1 Chapter overview

In Chapter 5, the physical properties of four representative green roof substrates were characterised. This chapter focuses on using the characterised properties within the Richards Equation to regenerate the runoff and moisture content profiles from the substrates during the detention tests presented in Chapter 5.

This chapter forms part of the following publication:

Peng, Z., Smith, C., Stovin, V., 2020. The importance of unsaturated hydraulic conductivity measurements for green roof detention modelling. *J. Hydrol.* 590, 125273. https://doi.org/10.1016/j.jhydrol.2020.125273

6.2 Green roof substrates and measured data

The measured physical properties (Chapter 5), including the saturated hydraulic conductivity, Soil Water Release Curve (SWRC) and the Hydraulic Conductivity Function (HCF), for the Marie Curie Substrate (MCS), Heather with Lavender Substrate (HLS), Sedum Carpet Substrate (SCS) and New Substrate Mix (NSM) were used within the Richards Equation to generate the runoff profiles. The measured runoff and moisture content profiles from the two depths of the substrates during the detention tests in response to the four design storms (Chapter 5) were used to validate and evaluate the model performance.

6.3 Model implementation

The Richards Equation (Equation 2.19) was used to model the detention effects in the substrates, following the approach described in Section 4.6.4. The Richards Equation model discretised the depth of substrate into 101 points and was run at 1-minute time steps. A fuller explanation of the model implementation is provided in Appendix B, where it is also demonstrated that the in-house model is capable of accurately reproducing the output from HYDRUS 1D. The model built in MATLAB allows the new characterised HCFs (i.e. the three-segment curve and the simplified laboratory curve) to be used in the Richards Equation.

6.3.1 Substrate parameters

The saturated hydraulic conductivity used within the HCFs was determined by the FLL tests (**Table 5.1**). Initial simulations were conducted with the Durner-Mualem Equation (Equation 2.9). For

further investigation, the three-segment curve and the simplified laboratory curve (Equations 5.2 to 5.4 and Equation 5.5) were used. Parameter values for these equations are listed in **Table 5.2**, **Table 5.4** and **Table 5.5**.

6.3.2 Boundary and initial conditions

For each design storm, the upper boundary was set as a Neumann condition (Equation 4.5). Following the approach adopted in Yio et al. (2013), the runoff collected from the control tests was used as rainfall input to the model. The initial condition was set to be a constant hydraulic head. The moisture content at the lower moisture probe was set to the measured value, and the suction head for this point was calculated from the fitted SWRC (the measured moisture content and corresponding suction head are listed in Appendix C. The suction heads for the rest of the vertical profile were calculated according to Equation 6.1.

$$h_i = h_p - Z_i + H_P \qquad \text{Equation 6.1}$$

where h_p is the suction head measured at the lowest probe and H_P is the elevation of the lowest moisture probe (P1, **Figure 3.2**).

Following the approach of Peng et al. (2019), the lower boundary was modelled as a constant suction head boundary, and the constant head was equivalent to the suction head of the lowest point at field capacity (the initial condition before design storms were applied).

6.4 Model evaluation

R_t^2 (Young et al., 1980) (Equation 4.1) is used to assess the model performance

6.5 Results and discussion

6.5.1 Modelled runoff profiles

6.5.1.1 Durner-Mualem model and three-segment curve

Figure 6.1, **Figure 6.2**, **Figure 6.3**, **Figure 6.4**, **Figure 6.5**, **Figure 6.6**, **Figure 6.7** and **Figure 6.8** compare modelled and measured runoff profiles from the substrates in response to the four design storms. The two HCF models led to different predictions of runoff profiles, and the performance of the models varied across substrates.

MCS

As both the Durner-Mualem model and the three-segment curve provided a good agreement with the measured HCF data points (**Figure 5.4**) for MCS, they both led to reasonable predictions of runoff profiles for MCS (**Figure 6.1** and **Figure 6.2**). Differences were present in the modelled

runoff profiles, with the Durner-Mualem model delaying the time to start of runoff (10 minutes) by about 5 minutes in response to the three constant design storms and about 10 minutes in Design Storm 4 compared with the three-segment curve for the 100 mm substrate (**Figure 6.1**). The time to start of runoff was reasonably modelled by the three-segment curve in the three constant design storms (Design Storms 1 to 3) for the 200 mm substrate, whilst it was delayed by between 20 minutes (Design Storms 2 and 3) and 40 minutes (Design Storm 1) by the Durner-Mualem model (**Figure 6.2**). For the 100 mm substrate, the two models provided close peak runoff rates in the design storms. However, the time to reach an equilibrium state in response to Design Storm 1, estimated by the Durner-Mualem model, was delayed about 10 minutes compared with the three-segment curve (**Figure 6.1**). For the 200 mm substrate, the three-segment curve gives a peak runoff rate about 100 % higher than the Durner-Mualem model in response to Design Storm 1 (0.069 cm/min versus 0.031 cm/min) and Design Storm 4 (0.797 cm/min versus 0.367 cm/min) (**Figure 6.2**). Comparing the modelled runoff profiles with measured profiles, the three-segment curve tends to overestimate the peak runoff rate, and the Durner-Mualem model is more likely to delay the time of peak runoff and the time to start of runoff for a deep substrate.

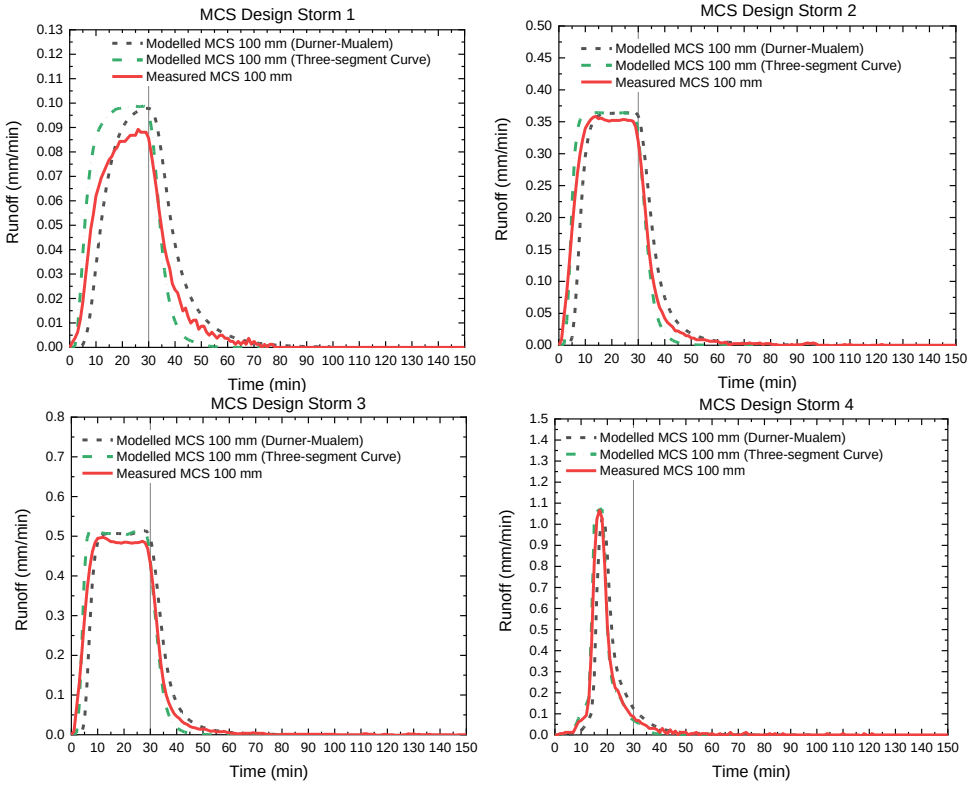

Figure 6.1. Measured and modelled runoff profiles for the 100 mm MCS using the Durner-Mualem model and three-segment curve.

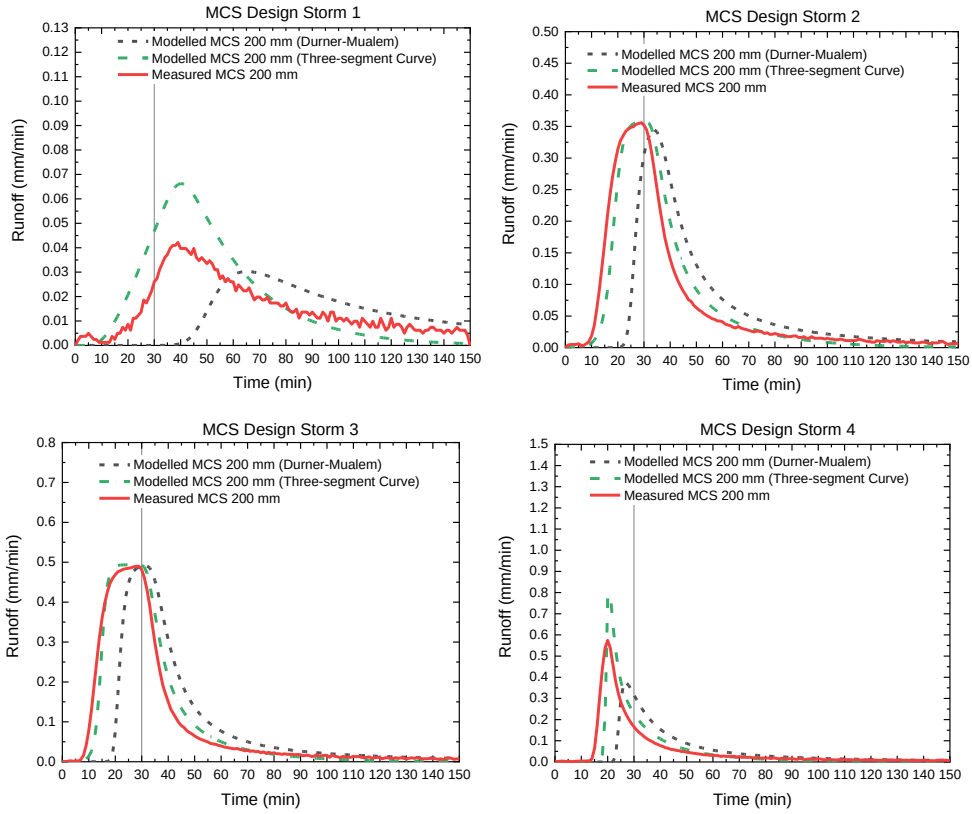

Figure 6.2. Measured and modelled runoff profiles for the 200 mm MSC using the Durner-Mualem model and three-segment curve.

HLS

The influence of the two different HCFs on modelled runoff is particularly striking for HLS (**Figure 6.3** and **Figure 6.4**). The Durner-Mualem model significantly overestimated the detention effects in response to all the design storms. For the 100 mm substrate, the time to start of runoff was delayed by up to 10 minutes in response to Design Storm 3; the peak runoff rate was underestimated by 38.9% in response to Design Strom 1 and by 42.8% in response to Design Storm 4 (**Figure 6.3**). The effects are particularly significant in the 200 mm substrate. The time to start of runoff was delayed by up to 50 minutes in response to Design Storm 1; in the case of Design Storm 4, the peak runoff rate was underestimated by 88% (**Figure 6.4**). The model results are significantly improved for both depths of the substrate when using the three-segment curve. The time to start of runoff and the rising and falling limbs are modelled well by the three-segment curve. However, for the 200 mm substrate, the three-segment curve slightly underestimated the peak runoff rate in Design Storms 1 (12.4%) and Design Storm 4 (13.3%) (**Figure 6.4**). It is not surprising that the two models showed noticeable differences; HCF influences the model results, and the two HCF models differed significantly for this substrate (**Figure 5.4**).

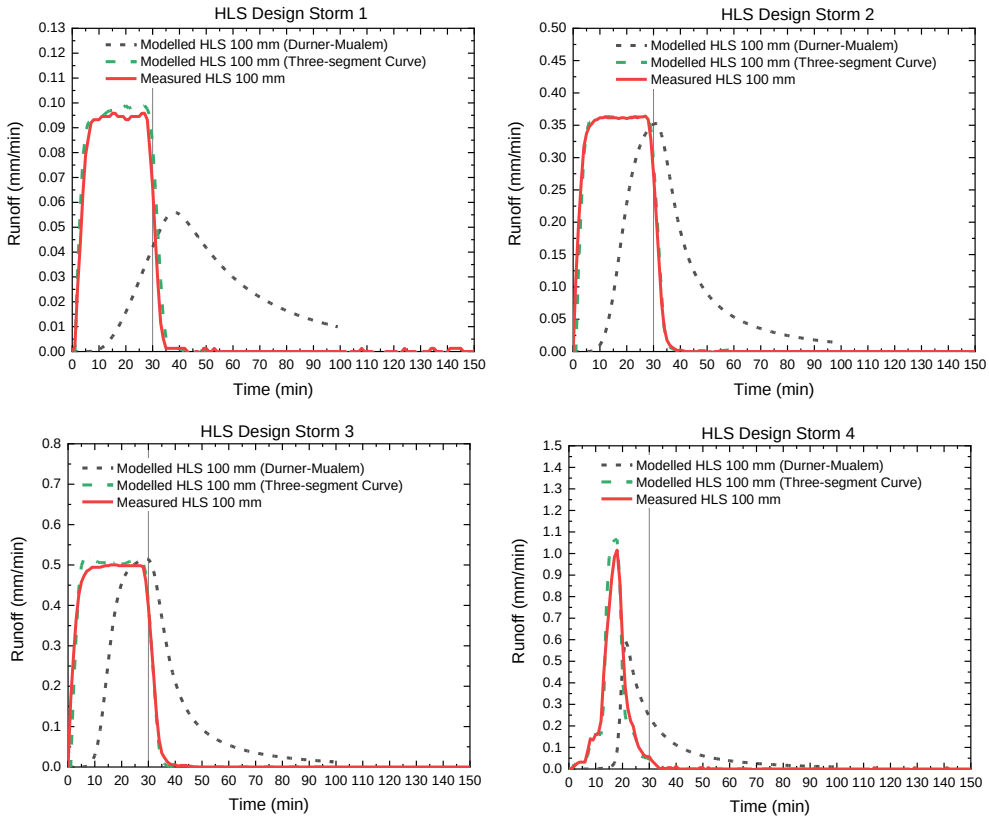

Figure 6.3. Measured and modelled runoff profiles for the 100 mm HLS using the Durner-Mualem model and three-segment curve.

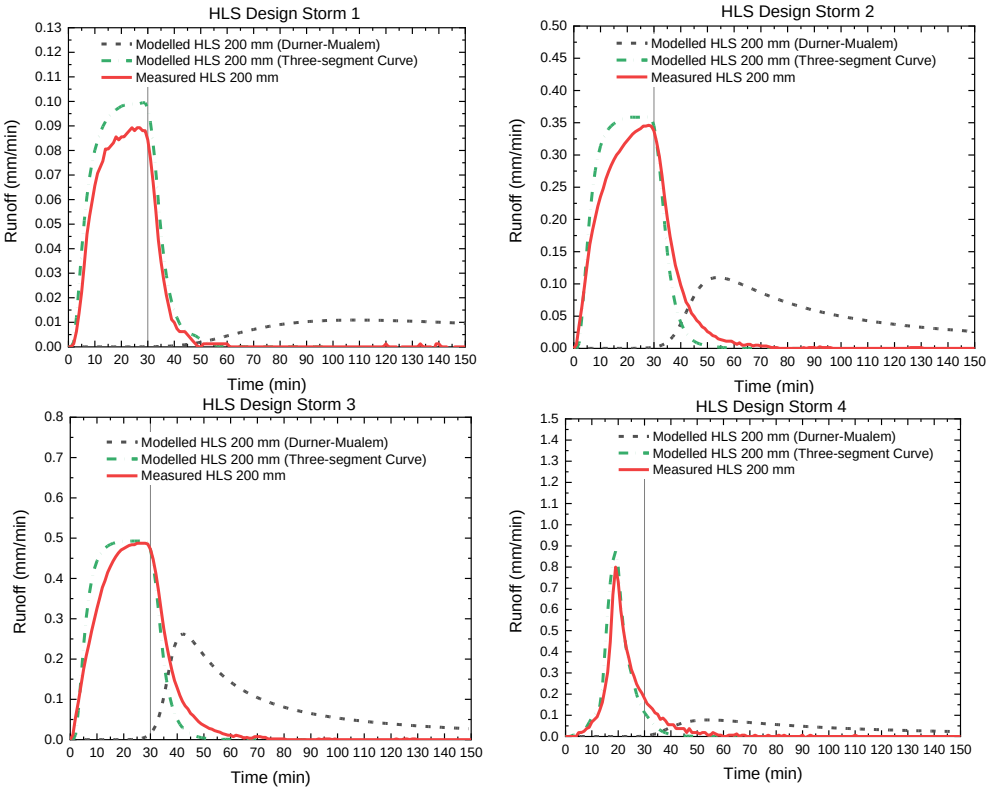

Figure 6.4. Measured and modelled runoff profiles for the 200 mm HLS using the Durner-Mualem model and three-segment curve.

SCS

SCS shows further interesting results (**Figure 6.5** and **Figure 6.6**). The two HCF models generated different runoff profiles. However, unlike HLS, the model results are worse when using the three-segment curve, which overestimated the detention effects. Both models modelled the peak runoff rates reasonably for the four design storms for the 100 mm substrate. However, the time to start of runoff was delayed by 10 minutes to 20 minutes using the three-segment model and by 5 to 10 minutes using the Durner-Mualem model for the 100 mm substrate (**Figure 6.5**). For the 200 mm substrate, peak runoff rates of the four design storms were not modelled well by the three-segment curve. It is possible that due to the heterogeneous nature of the substrates, neither of the infiltration column tests for the HCF characterisations was a good representation of the fresh sample utilised in the detention tests.

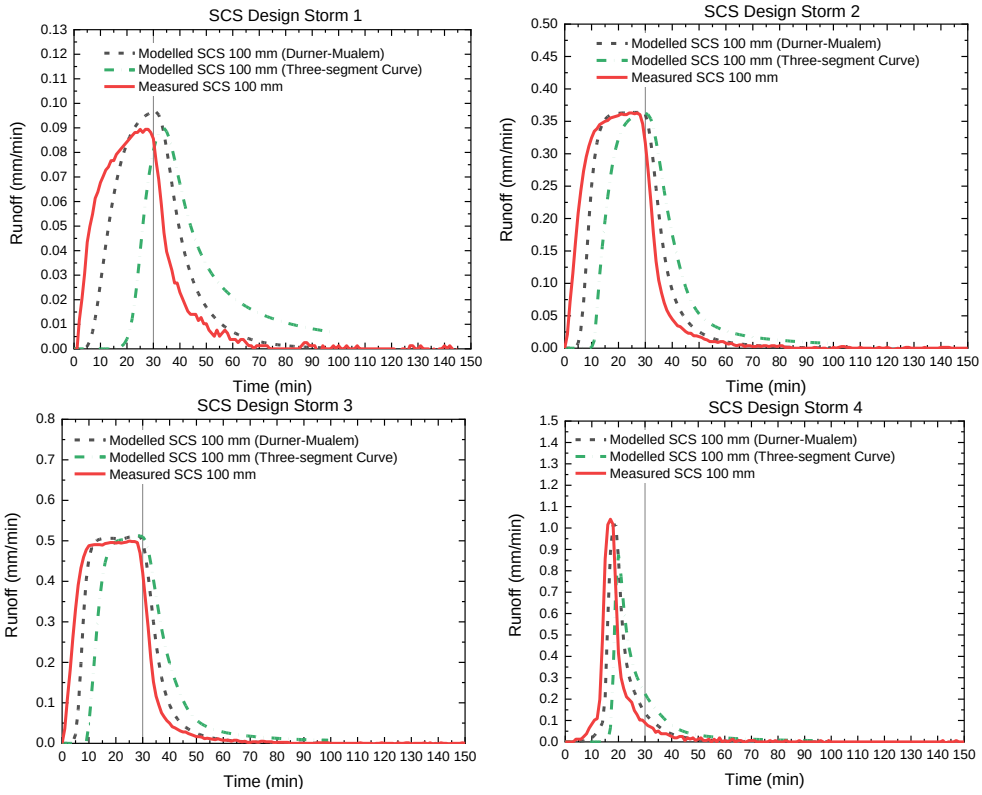

Figure 6.5. Measured and modelled runoff profiles for the 100 mm SCS using the Durner-Mualem model and three-segment curve.

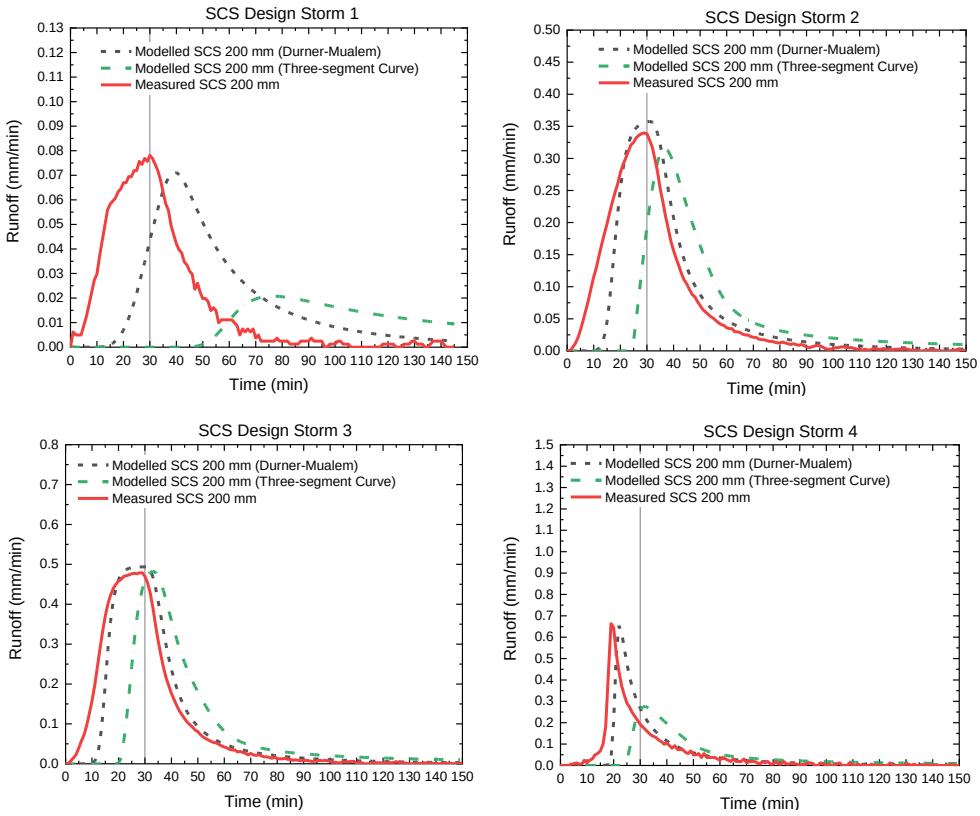

Figure 6.6. Measured and modelled runoff profiles for the 200 mm SCS using the Durner-Mualem model and three-segment curve.

NSM

The model results for NSM (**Figure 6.7** and **Figure 6.8**) are consistent with the results of HLS. Significant differences are presented in the results using the two HCF models. Although the three-segment curve tends to overestimate the substrate's detention effects, the model results were improved for both the 100 mm and 200 mm substrate when using the three-segment curve.

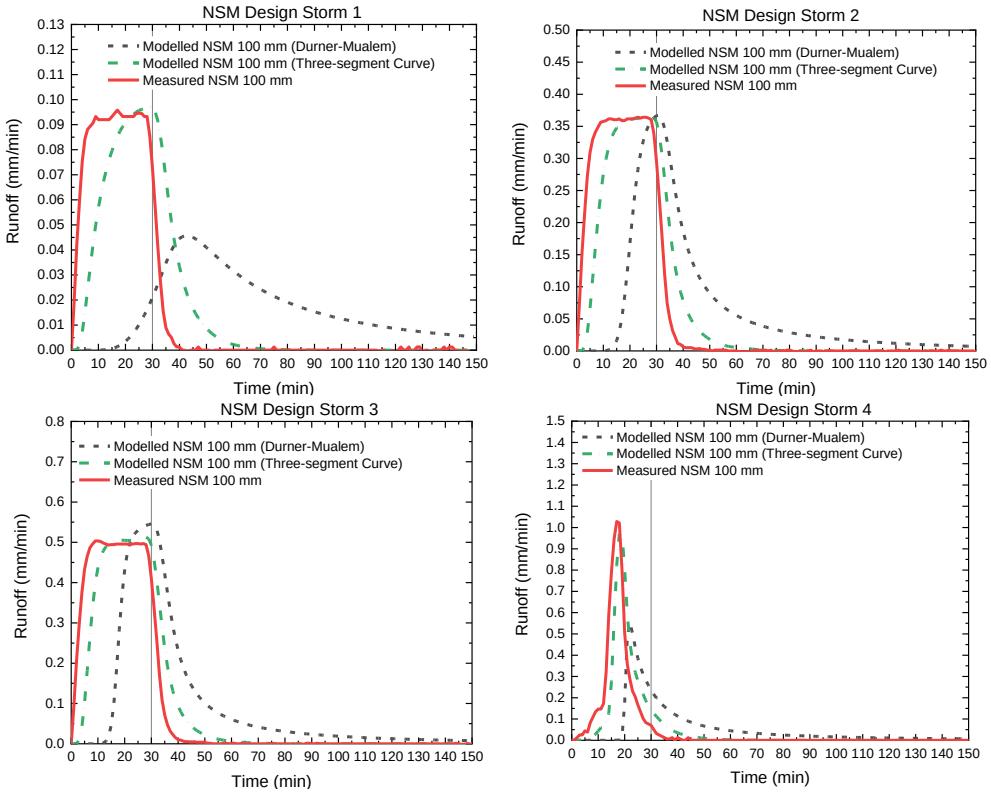

Figure 6.7. Measured and modelled runoff profiles for the 100 mm NSM using the Durner-Mualem model and three-segment curve.

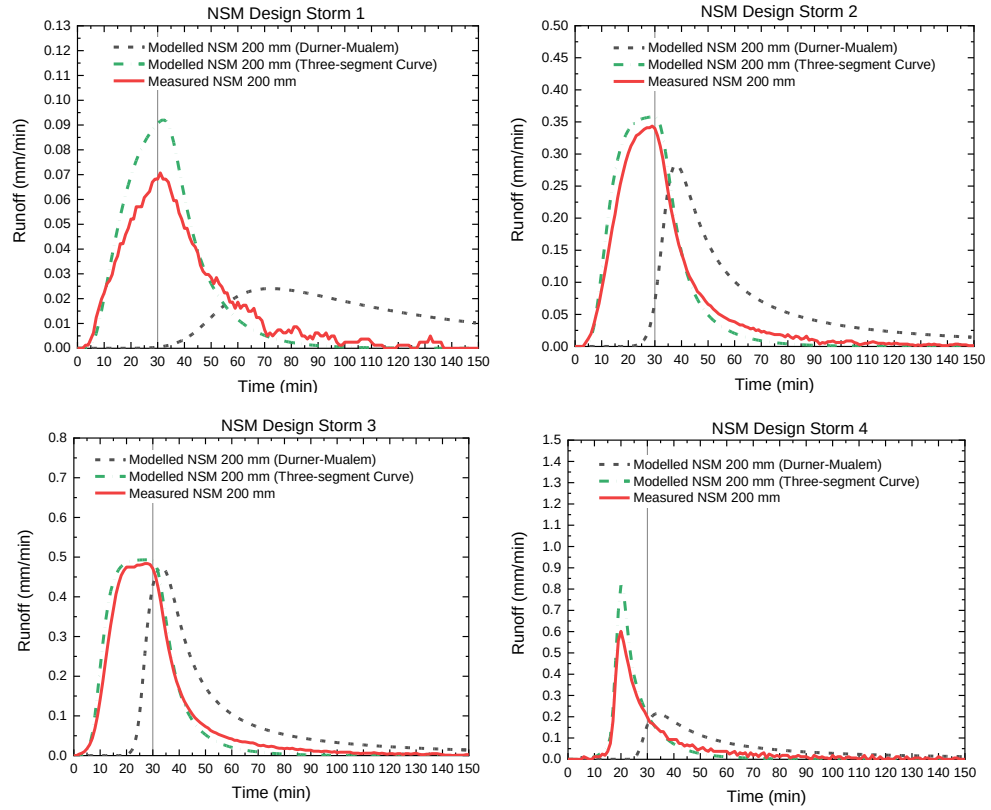

Figure 6.8. Measured and modelled runoff profiles for the 200 mm NSM using the Durner-Mualem model and three-segment curve.

6.5.1.2 Simplified laboratory curve

The performance of the simplified laboratory curve of modelling the runoff profiles from the substrates is assessed in this section.

The model results for all the substrates and depths in response to the design storms are presented in **Figure 6.9**, **Figure 6.10**, **Figure 6.11** and **Figure 6.12**. Except for the case of SCS, the runoff profiles for the 100 mm substrates were modelled well by the simplified laboratory curve. For the case of MCS, the model overestimated the detention effects in the 200 mm substrate in response to the design storms (**Figure 6.9**). This is because the substrate's moisture content during the storms is between 0.25 v/v and 0.27 v/v (**Figure 5.6**), and the simplified laboratory curve overestimated the unsaturated hydraulic conductivity in this range (**Figure 5.4**).

HLS and NSM are the two cases where the Durner-Mualem model significantly underestimated the HCF and resulted in poor performance of the model in regenerating the runoff profiles. However, although the simplified curve tends to underestimate the detention effects in the 200 mm substrates, the model results improved significantly when the simplified laboratory curve was utilised (**Figure 6.10** and **Figure 6.12**).

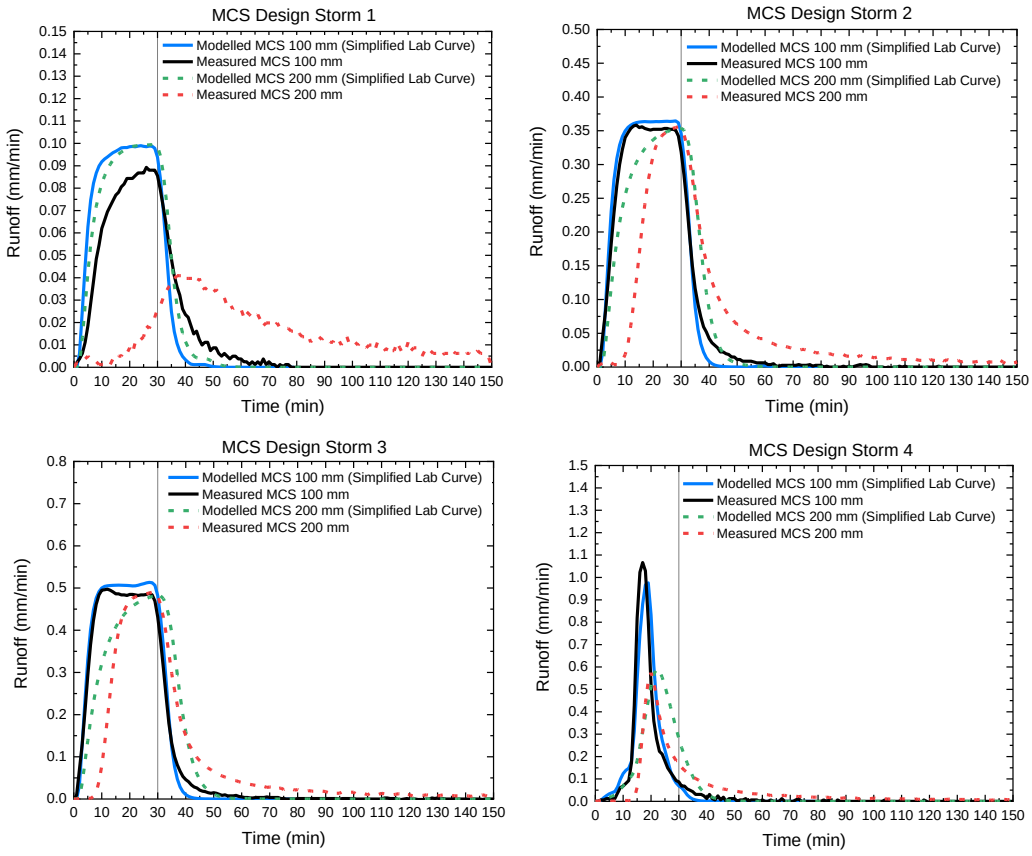

Figure 6.9. Measured and modelled runoff profiles using the simplified laboratory curve (MCS).

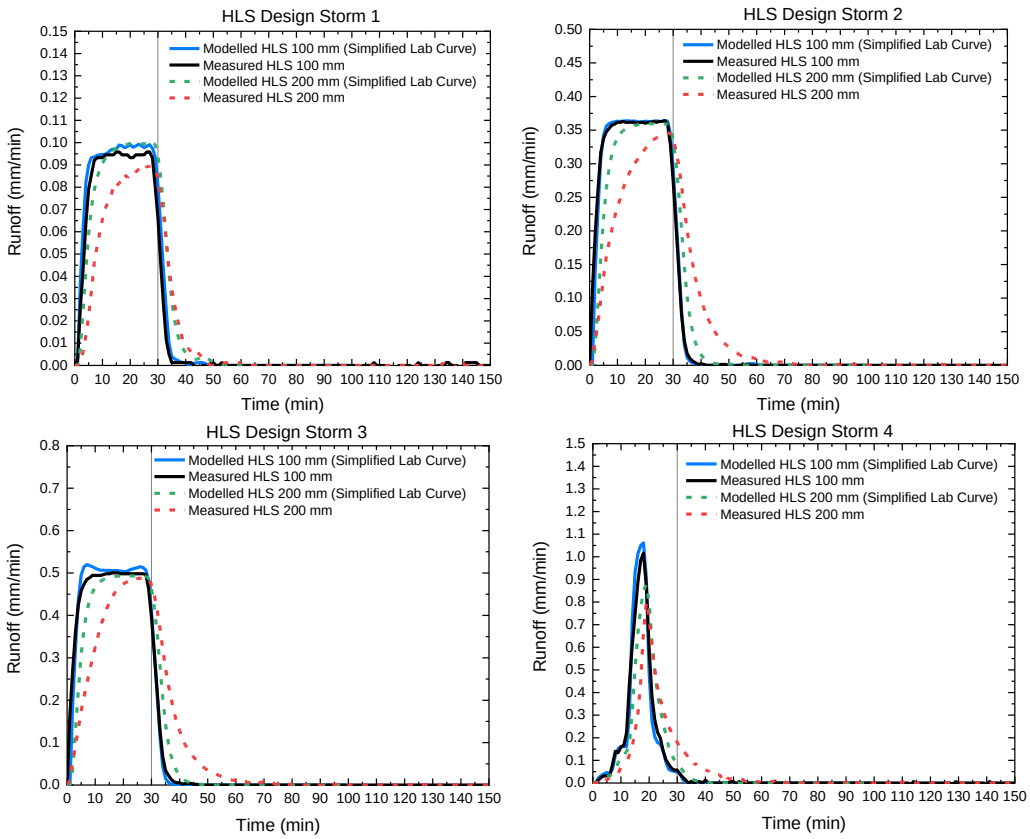

Figure 6.10. Measured and modelled runoff profiles using the simplified laboratory curve (HLS).

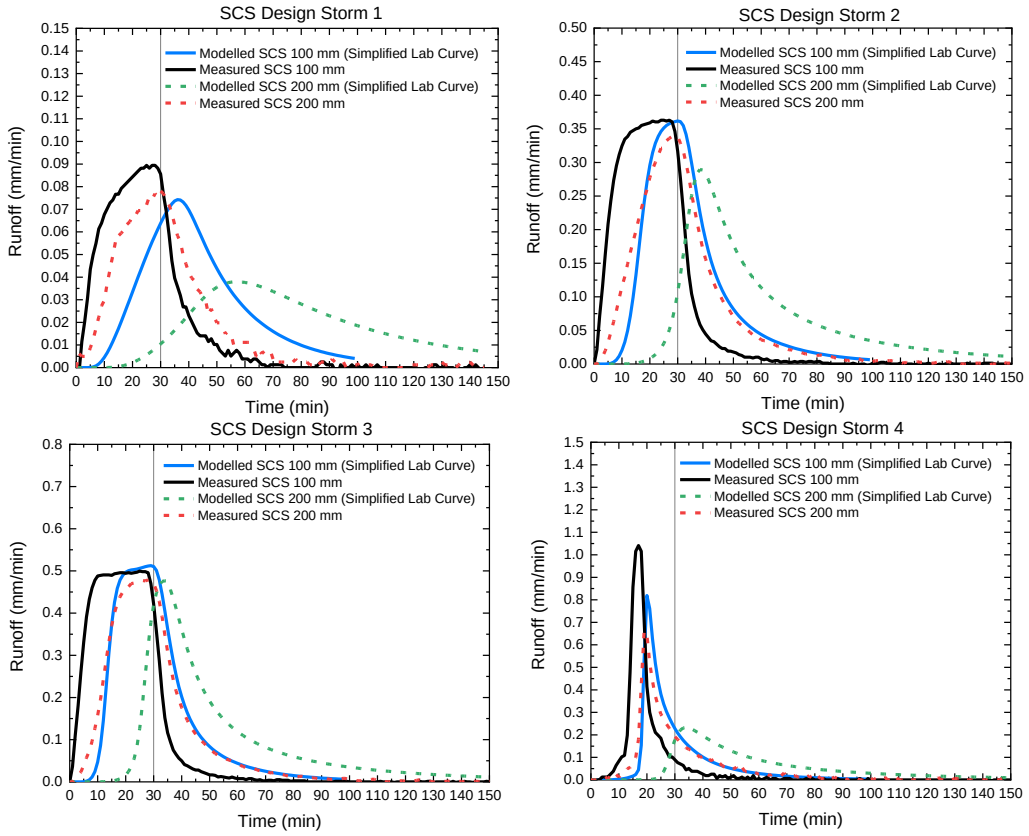

Figure 6.11. Measured and modelled runoff profiles using the simplified laboratory curve (SCS).

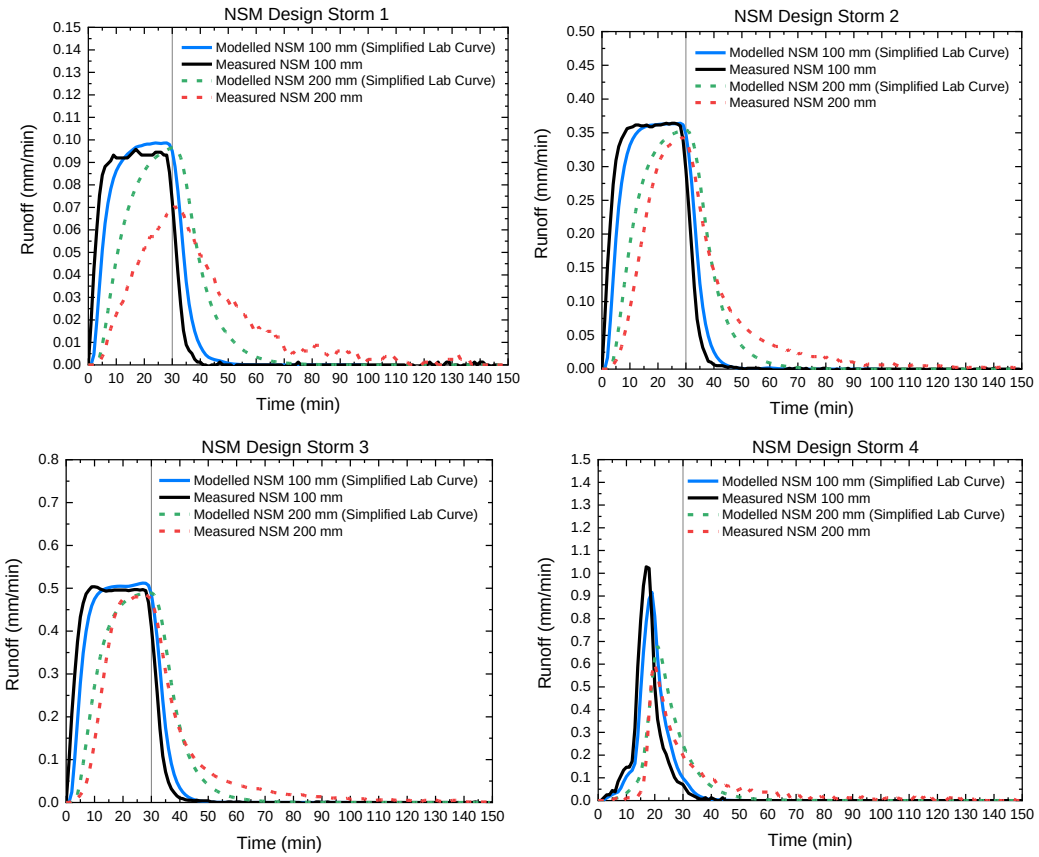

Figure 6.12. Measured and modelled runoff profiles using the simplified laboratory curve (NSM).

Figure 6.13 shows the distribution of the R_t^2 for the modelled runoff profiles of the two substrate depths in response to the four design storms using the three HCFs. The modelled for each design storms are provided in **Table 6.1**. Compared with the model results using the Durner-Mualem approach, the simplified laboratory curve provides a much better overall estimate of green roof detention performance (with a mean R_t^2 of 0.629 versus 0.409). However, the simplified laboratory curve has slightly worse performance than the three-segment curve (with a mean R_t^2 of 0.629 versus 0.754).

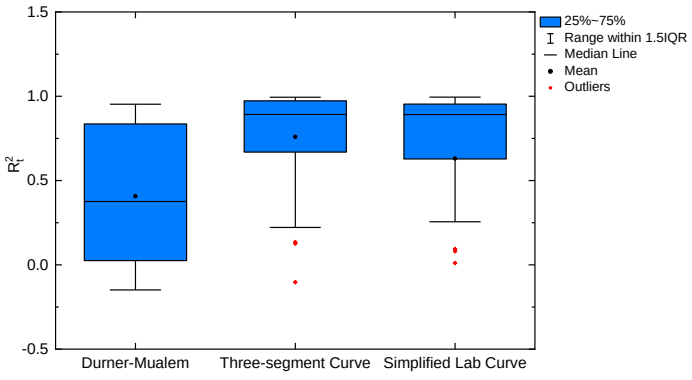

Figure 6.13. R_t^2 distributions for the modelled runoff profiles using the Durner-Mualem model, the three-segment curve and the simplified laboratory curve.

Table 6.1. R_t^2 for the modelled runoff profiles using the Durner-Mualem model, the three-segment curve and the simplified laboratory curve.

HCF	Design Strom	MCS		HLS		SCS		NSM	
		100 mm	200 mm	100 mm	200 mm	100 mm	200 mm	100 mm	200 mm
Durner-Mualem	1	0.918	0.366	-0.041	-0.092	0.831	0.386	-0.149	-0.023
	2	0.945	0.481	0.317	-0.127	0.907	0.899	0.261	0.174
	3	0.953	0.634	0.485	-0.091	0.919	0.924	0.422	0.366
	4	0.841	0.142	0.074	-0.055	0.743	0.554	-0.040	0.089
Three-segment Curve	1	0.937	0.650	0.989	0.965	0.222	-0.103	0.752	0.895
	2	0.990	0.947	0.994	0.963	0.641	0.357	0.865	0.978
	3	0.988	0.969	0.993	0.965	0.688	0.462	0.888	0.983
	4	0.987	0.711	0.861	0.791	0.135	0.126	0.796	0.907
Simplified Lab Curve	1	0.874	-3.126	0.989	0.930	0.397	0.011	0.936	0.714
	2	0.992	0.771	0.995	0.922	0.591	0.255	0.958	0.949
	3	0.994	0.893	0.993	0.933	0.665	0.377	0.961	0.968
	4	0.916	0.781	0.890	0.706	0.094	0.080	0.872	0.906

Liu and Fassman-Beck (2017) also obtained poor model predictions using Durner-Mualem HCF. They attributed this to preferential flow and demonstrated that improved predictions could be obtained when a mobile-immobile dual-porosity model was applied. In contrast, in this study, the model results were improved by using an HCF that better represents the measured unsaturated hydraulic conductivity data without increasing the complexity of the unsaturated flow model (Richards Equation).

The combination of results also provides some support for the application of a simplified approach to determining the HCF. As the simplified laboratory curve can provide reasonable estimations of HCF between field capacity and saturation (the range where detention dominated the flow processes) and runoff profiles, the HCF characterisation can be reduced to the measurement of just two data points: the saturated hydraulic conductivity and the steady moisture content under an infiltration rate of 0.1 cm/min. Although the model results based on the simplified laboratory curve are not as good as those based on the three-segment curve, the simplified approach reduces the complexity and time (from 5 weeks to one day) required for the HCF measurement, which offers considerable benefits in terms of practical application.

6.5.2 Modelled moisture content profiles

The moisture probe placed in the 100 mm substrate (P1, **Figure 3.2**) and the two moisture probes (P1 and P2, **Figure 3.2**) placed in the 200 mm substrate column provide the opportunity to

validate the models from the perspective of the moisture content variations during the storm events. The modelled vertical moisture content profiles (using the Durner-Mualem model and the three-segment curve) at the locations where the moisture probes are located are discussed in this section.

Figure 6.14, **Figure 6.15**, **Figure 6.16** and **Figure 6.17** compare the modelled and measured moisture content profiles in response to the four design storms for the 100 mm substrates. Due to the heterogeneous nature of the green roof substrates, uncertainties exist in the moisture probe calibration. It is not easy to measure the moisture content value precisely (with ±0.003 v/v accuracy). However, it may be argued that the dynamic of moisture content profiles is more important than absolute values. In response to Design Storm 1, for the cases of MCS, HLS and NSM, the modelled moisture content is more dynamic than measured. This is because the increase in the moisture content during the storms is minor such that the moisture probe failed to detect such change.

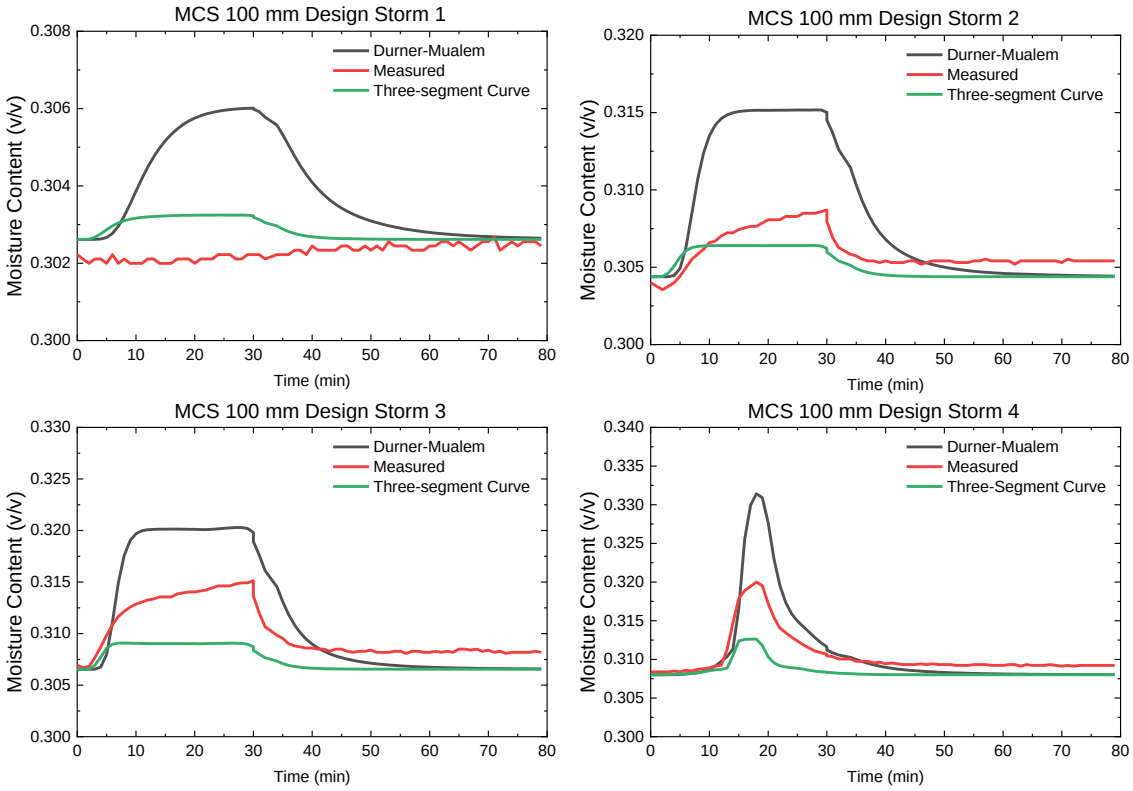

Figure 6.14. Measured and modelled moisture content profiles for the 100 mm MCS using the Durner-Mualem model and three-segment curve.

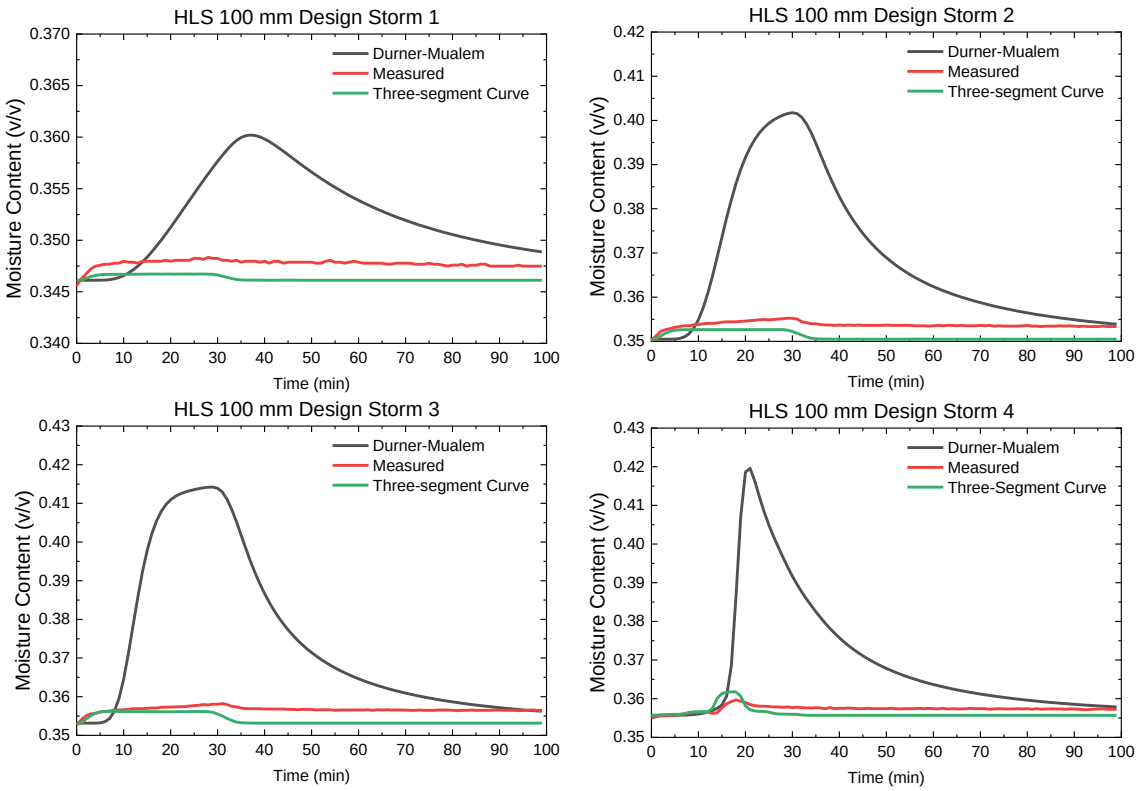

Figure 6.15. Measured and modelled moisture content profiles for the 100 mm HLS using the Durner-Mualem model and three-segment curve.

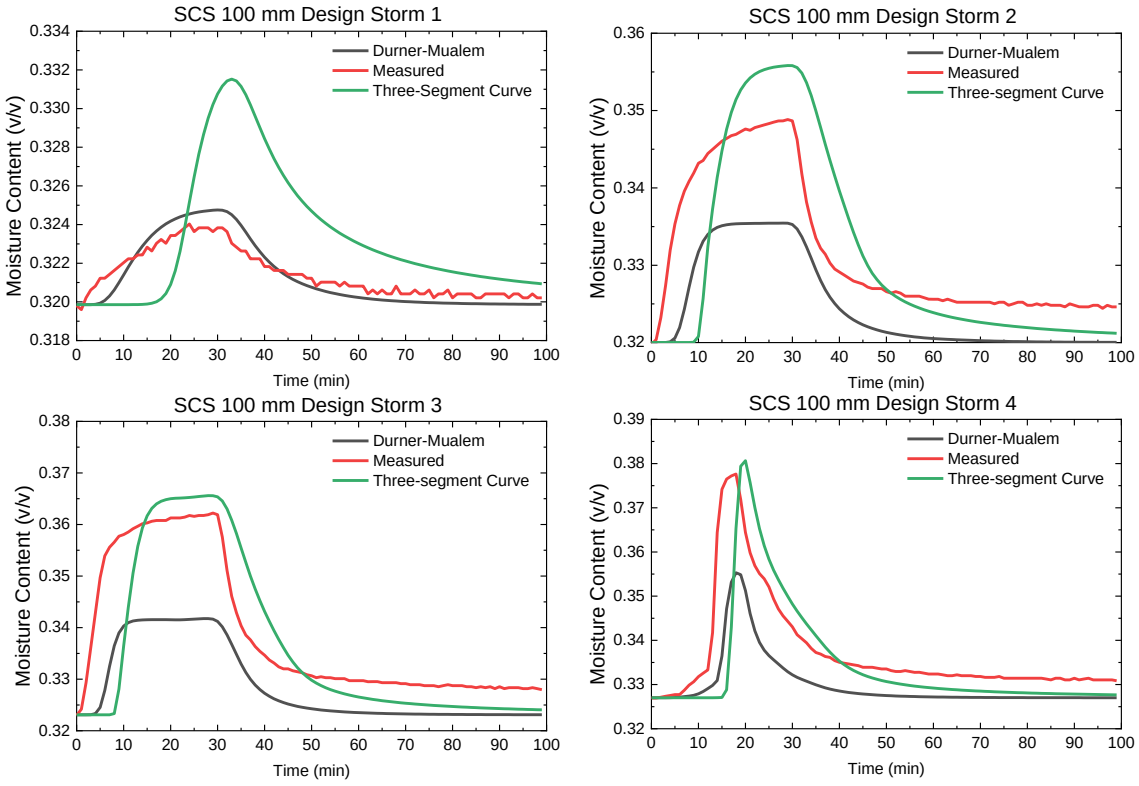

Figure 6.16. Measured and modelled moisture content profiles for the 100 mm SCS using the Durner-Mualem model and three-segment curve.

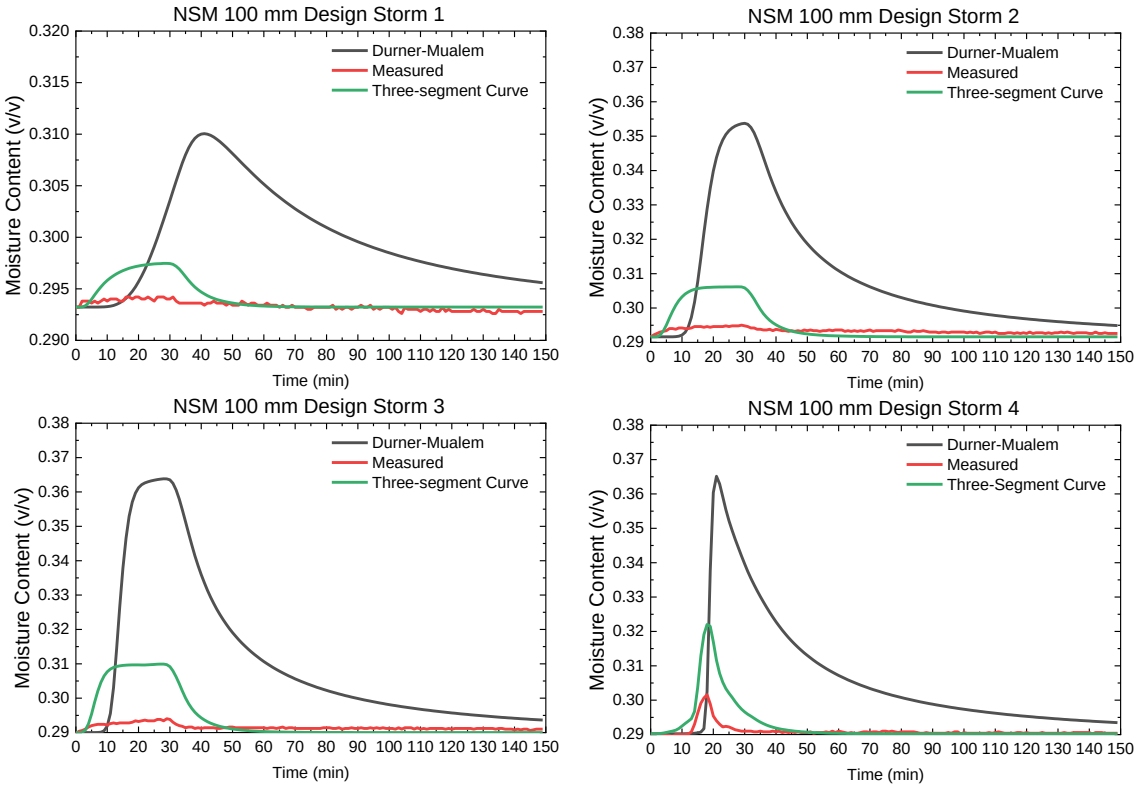

Figure 6.17. Measured and modelled moisture content profiles for the 100 mm NSM using the Durner-Mualem model and three-segment curve.

Figure 6.18, **Figure 6.19**, **Figure 6.20** and **Figure 6.21** compare the modelled and measured vertical moisture content profiles in response to the design storms in the 200 mm substrates. The moisture content at any depth returns to its initial moisture content when the rainfall stops. Therefore, to highlight the dynamics of moisture changes in the substrate, the moisture content presented in the figures is relative to the initial moisture content. Consistent with what was observed, the change in moisture content at the upper part of the substrates is modelled to be more dramatic than the lower part.

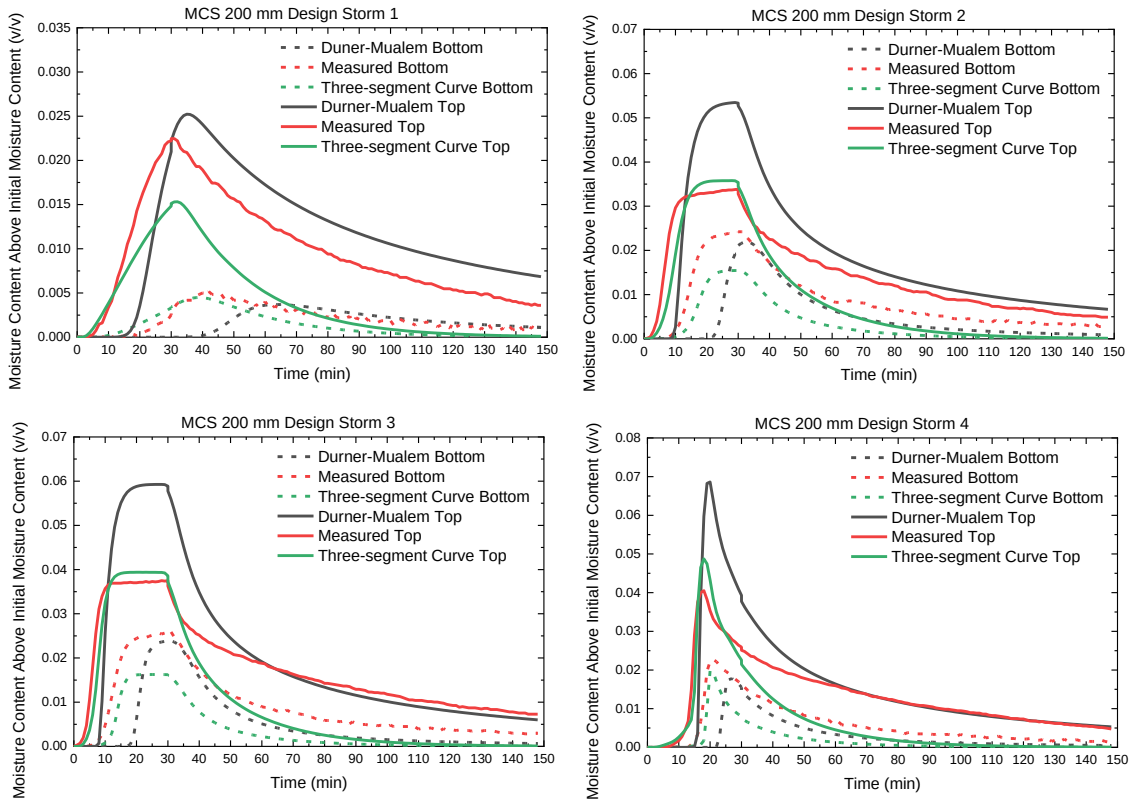

Figure 6.18. Measured and modelled moisture content profiles for the 200 mm MCS using the Durner-Mualem model and three-segment curve.

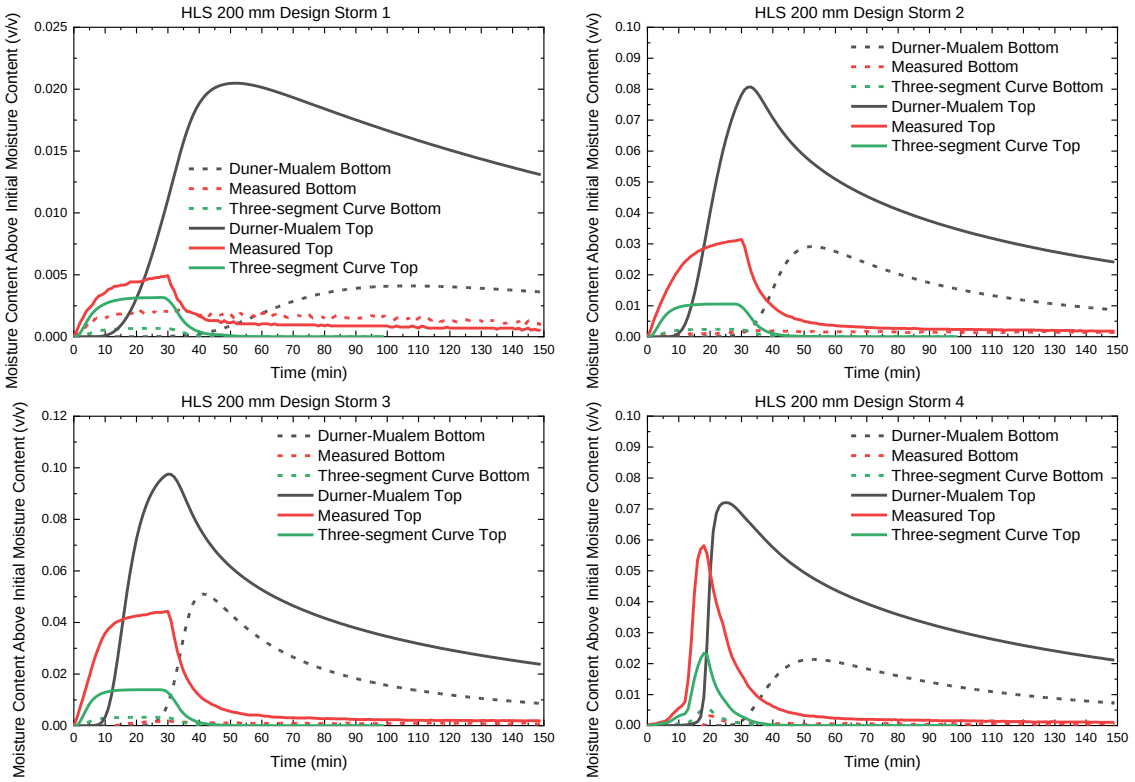

Figure 6.19. Measured and modelled moisture content profiles for the 200 mm HLS using the Durner-Mualem model and three-segment curve.

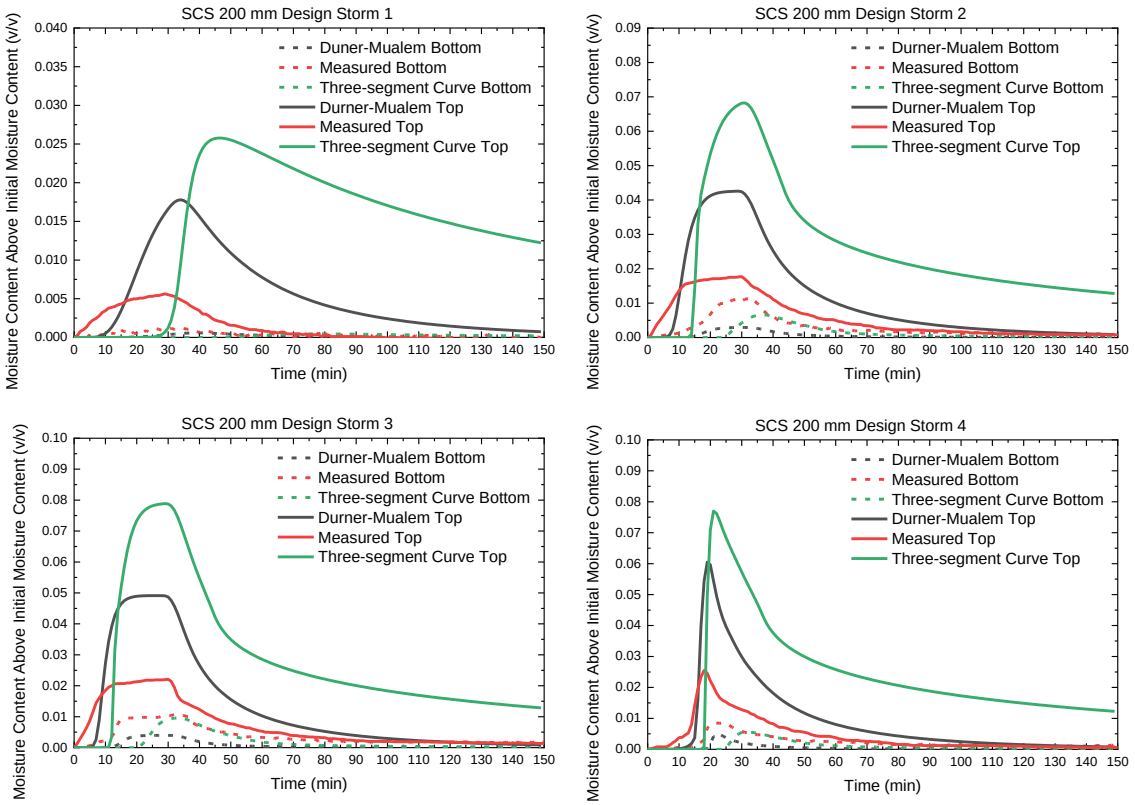

Figure 6.20. Measured and modelled moisture content profiles for the 200 mm SCS using the Durner-Mualem model and three-segment curve.

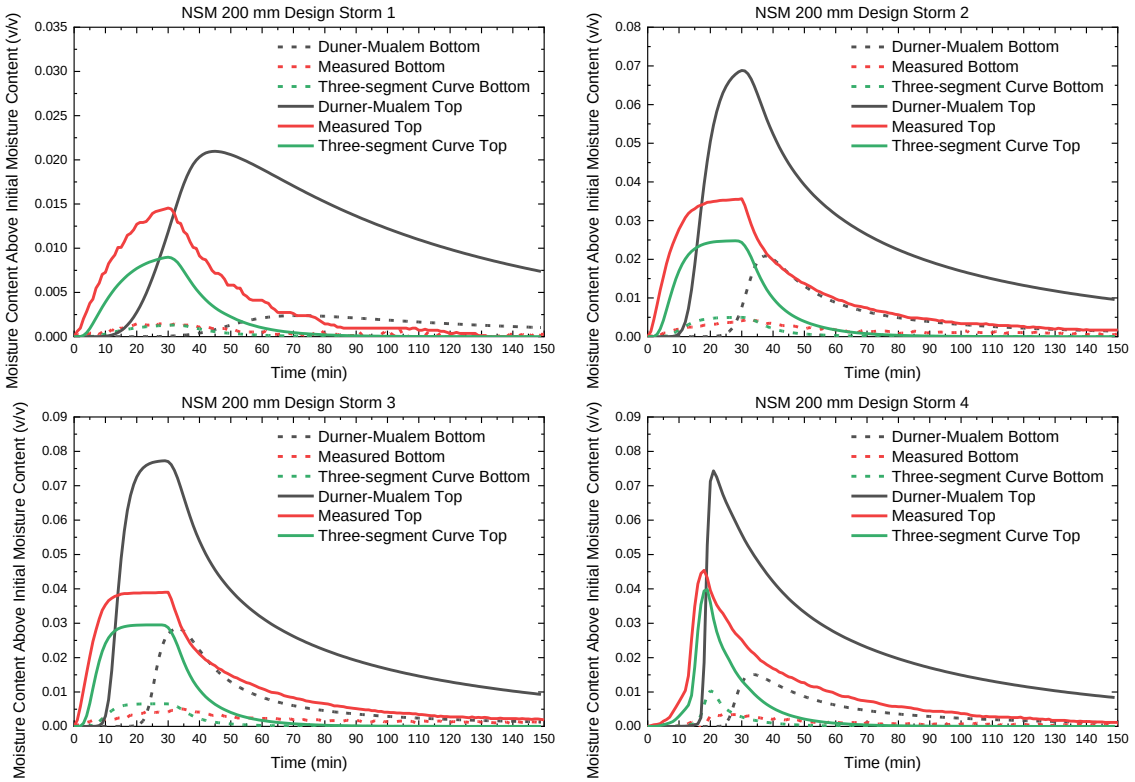

Figure 6.21. Measured and modelled moisture content profiles for the 200 mm NSM using the Durner-Mualem model and three-segment curve.

Similar to the modelled runoff profiles, for both depths of the substrate, the differences in modelled vertical moisture content profiles between the two models are minor, where the two models give close predictions for HCFs (the case for MCS) (**Figure 6.14** and **Figure 6.18**), and the model gives reasonable predictions of vertical moisture content profiles when the HCF is correctly modelled. The Durner-Mualem model tends to overestimate the vertical gradient in the substrate (**Figure 6.18**, **Figure 6.19** and **Figure 6.21**), and the three-segment curve leads to better overall model performance compared with the Durner-Mualem model (**Figure 6.14**, **Figure 6.15**, **Figure 6.17**, **Figure 6.18**, **Figure 6.19** and **Figure 6.21**). The differences between modelled (three-segment curve) and measured moisture contents are minor for the cases of MCS and NSM. The worst case was for SCS, where the three-segment curve gives a peak moisture content value that is higher than measured (**Figure 6.16** and **Figure 6.20**). However, it should be noted that for the case of SCS, any difference between the measured and modelled moisture content could be due to the uncertainties associated with the subsampling of the substrate.

6.6 Conclusions

Comparisons between measured and modelled runoff profiles confirmed that Richards Equation based models are capable of modelling detention effects within green roof substrates. The results also showed that the moisture content profiles could be accurately regenerated by Richards Equation based models if the HCF is reasonably represented. HCF curves derived from measured HCF data points result in better performance than the conventional Durner-Mualem approach. The simplified HCF proposed in Chapter 5 also showed reasonable estimations of runoff profiles. This approach simplifies the procedures and saves time for HCF determination, which has practical implications for the application of the Richards Equation in modelling the detention effects due to green roof substrates. The detention model comparisons highlight the importance – in this context – of correctly characterising unsaturated hydraulic conductivities in the ‘wet’ range between field capacity and saturation.

7 A Two-Stage Physically-Based Green Roof Detention Model

7.1 Chapter overview

Detention processes in a complete green roof system can be modelled by two stages. The first stage of detention is mainly in the substrate and the second stage of detention is mainly in the drainage layer. This chapter presents a two-stage physically-based green roof detention model. The Richards Equation, which has been considered in detail in earlier chapters, is combined with the Saint Venant equation to represent the detention effects in a complete green roof system. An initial value for the model coefficient is derived from drainage layer isolated detention tests, and the sensitivity of the model results to the parameter is assessed. Finally, the two-stage model is validated using the measured runoff profiles from a laboratory and a field green roof test bed. The performance of the two-stage model is evaluated based on the accuracy of regenerated runoff profiles. Limitations of the two-stage physically-based model are also discussed in this chapter.

This chapter forms part of the following publication:

Peng, Z., Garner, B., Stovin, V., 2021. Two green roof detention models applied in two green roof systems. *J. Hydrol. Eng.* (under review).

7.2 Green roof drainage layer model

A typical green roof system consists of (from top to bottom) vegetation layer, substrate layer, filter sheet and drainage layer. In earlier chapters, the focus was on the physical properties of engineered green roof substrates and the modelling approach that considers the detention effect in the substrate. However, when a green roof is functioning as a complete system, the drainage layer plays an essential role in its overall hydrological performance. In this section, a physically-based model will be proposed for modelling the detention effects in green roof drainage layers. The proposed model will be used to simulate different scenarios to test the stability and feasibility of the model for generic use.

7.2.1 A physically-based model for the drainage layer

The Saint Venant equation describes 1D gradually varied unsteady flow in an open channel, and it is usually used to model overland flow problems. The mass balance of the equation is given in Equation 7.1 (Chow, 1959). It is the fundamental basis for the model developed in this chapter.

$$\frac{\partial h_s}{\partial t} + \frac{\partial h_s U_s}{\partial x} = R(x,t) \qquad \text{Equation 7.1}$$

where h_s is the unit storage of water depth, U_s is the depth-averaged flow velocity, t is time, x is the distance coordinate and R(x,t) is the rate of recharge. In the case of a green roof drainage layer, recharge represents the outflow from the overlying substrate layer.

7.2.1.1 Governing equation

The velocity term (U_s) in the Saint Venant equation, can be estimated using Manning's equation (Chow, 1959):

$$U_s = \frac{{h_s}^{2/3}}{n_f}\sqrt{s_f} \qquad \text{Equation 7.2}$$

where n_f is the Manning's roughness coefficient (Manning's n). s_f is the friction slope, which can be estimated using the following equation (Chow, 1959).

$$s_f = -\frac{\partial(h_s+z)}{\partial x} \qquad \text{Equation 7.3}$$

where z is the surface elevation.

Under the assumption that the water depth gradient is much smaller than the surface elevation gradient, the following equations can be obtained.

$$U_s = -\frac{{h_s}^{2/3}}{n_f\sqrt{s}}\frac{\partial(h_s+z)}{\partial x} \qquad \text{Equation 7.4}$$

And by substituting Equation 7.4 into Equation 7.1 the following equation can be obtained:

$$\frac{\partial h_s}{\partial t} = \frac{\partial h_s}{\partial x}\left[\frac{{h_s}^{\frac{2}{3}}}{n_f\sqrt{s}}\left(\frac{\partial h_s}{\partial x} - \tan\theta\right)\right] + R(x,t) \qquad \text{Equation 7.5}$$

where s is the mean local slope, and the other symbols are as defined before.

Equation 7.5 constitutes the basis of the physically-based model used to simulate the detention effects in green roof drainage layers.

7.2.1.2 Boundary and initial conditions

Equation 7.5 is a partial differential equation; initial and boundary conditions need to be defined to obtain numerical solutions. **Figure 7.1** shows the longitudinal section of a green roof drainage layer. L is the drainage length of the drainage layer, and θ is the slope of the system. The shaded area in **Figure 7.1** illustrates the possible water level distribution in the system during storms. The drainage layer receives the recharge (inflow) from the upper layers and discharges the water at $x = L\cos\theta$. In this sloped system, water added at the remotest point generates flow quickly due to gravity; water, therefore, accumulates at the outlet resulting in an increase in the water level

at this point. The left boundary was treated as a constant head boundary (Equation 7.6), and the right boundary was treated as a free drainage condition (Equation 7.7) to represent the conditions in **Figure 7.1**.

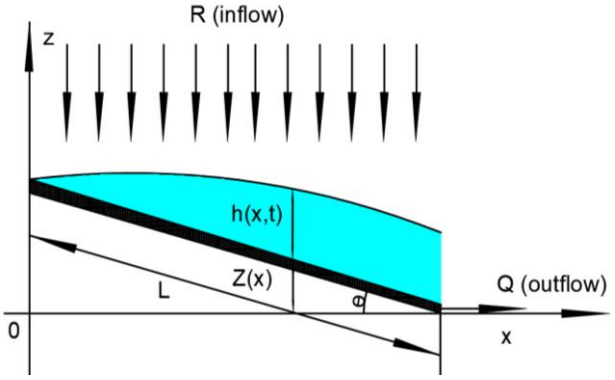

Figure 7.1. Schematic diagram for the horizontal flow in a green roof drainage layer.

$$h_s(t, x = 0) = 0 \qquad \text{Equation 7.6}$$

$$\frac{\partial h_s(x=L\cos\theta)}{\partial x} = 0 \qquad \text{Equation 7.7}$$

where θ is the slope of the bed, and the other symbols are as defined before.

It is assumed that the initial water level in the drainage layer is zero. Therefore, the initial condition for the model can be represented by the following equation:

$$h(t = 0, x) = 0 \qquad \text{Equation 7.8}$$

7.2.1.3 Model implementation

The time and spatial steps used in this study were 1 minute and 100 mm, respectively. The simulation was conducted in MATLAB R2017b using the *pdepe* function.

The runoff profile from the drainage layer in mm/min was calculated based on the modelled water level distribution. As the change in water level in the drainage layer is due to recharge, runoff can be calculated from the difference between the recharge and storage. The following equations were used to calculate the runoff.

$$v(x, t) = R - [h_s(x, t) - h_s(x, t - 1)] \qquad \text{Equation 7.9}$$

$$\text{Runoff}(t) = (\sum_1^{L/dx} v(x, t))/[L/dx] \qquad \text{Equation 7.10}$$

where $v(x,t)$ is the velocity distribution (mm/min), R is the recharge (mm/min), $\mathrm{Runoff}(t)$ is the longitude-averaged runoff from the layer (mm/min), L is the length of the layer (mm), and dx is the spatial step (mm).

7.2.2 Parametric study

The objective of this section is to test whether Equation 7.5 can provide a reasonable prediction of the runoff profiles from a green roof drainage layer. The system to be simulated in this section consists of only a drainage layer. During the storm, rainfall directly drops on the surface of the drainage layer, and the simulated runoff is the flow per unit length at the outlet of the drainage layer. Different rainfall intensities, rainfall durations, drainage layer slopes, drainage lengths, and Manning's n (reflecting the roughness of different materials) will be used to test the model with constant rainfall inputs.

Table 7.1 lists the value of parameters that were used to test the model. A slope of 0.02 was chosen to represent a typical green roof slope. The slope was increased to 0.1 to investigate the influence of the slope on the runoff response. It is expected that a reduced detention effect would be obtained by increasing the slope. Manning's n is an indicator of a material's surface roughness, and 0.05 was used here as suggested in She and Pang (2009) for a green roof drainage layer. A lower value of 0.02 was also used in the simulation with an expectation of a higher peak runoff rate. A drainage length of 6.1 m was used to represent a typical length of a green roof in the field. The drainage length was decreased to 3 m to investigate its influence on the model results. A rapid rising and falling in runoff profiles would be expected in a short system. A 2 mm/min 15-minute rainfall event was used in the simulation to represent a short, intense rainfall event. A long-duration rainfall (30 minutes) and a high-intensity rainfall (20 mm/min) were used in the simulation to investigate the response of the drainage layer to different rainfall events. It is expected that a reduced detention effect would be observed in a longer duration rainfall or a heavy rainfall.

Table 7.1 Value of parameters set for the models

Simulation No.	Slope	Manning's n	Drainage Layer Length	Rainfall Intensity	Rainfall Duration
	$\tan\theta$	-	m	mm/min	min
1	0.02	0.05	6.1	2	15
2	0.1	0.05	6.1	2	15
3	0.02	0.05	3	2	15
4	0.02	0.02	6.1	2	15
5	0.02	0.05	6.1	2	30
6	0.02	0.05	6.1	20	15

7.2.3 Results and Discussion

Figure 7.2 shows the modelled runoff profiles for the simulation cases 1 to 4. A significant detention effect was modelled in a drainage layer of 6.1 m long and roughness of 0.05 (S1): in response to a 15-minute 2 mm/min rainfall event, the peak runoff rate was modelled to be reduced to 1.3 mm/min. When the slope of the drainage layer was increased from 0.02 to 0.1 (S2), the peak runoff rate reached the peak rainfall rate within 15 minutes of rainfall. As expected, the peak runoff increased from 1.3 mm/min to 1.8 mm/min when the drainage length was decreased from 6.1 m to 3 m (S3). Decreasing Manning's n is equivalent to decreasing the roughness of the drainage layer, and the flow is faster over a smoother material. As modelled in S4, detention was reduced (with a peak runoff of 1.3 mm/min versus 1.9 mm/min) in a drainage layer with a smooth surface.

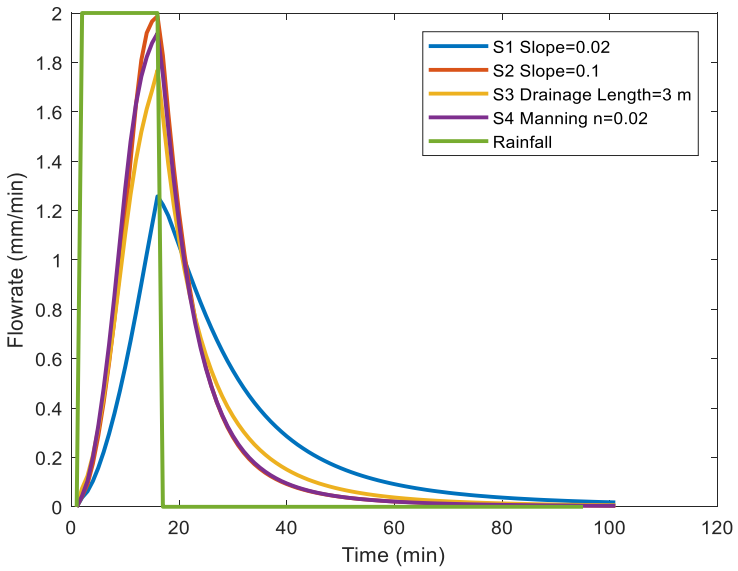

Figure 7.2. Modelled runoff profiles for simulations 1 to 4 using the physically-based drainage layer model.

Figure 7.3 shows the modelled runoff profiles for simulation cases 5 and 6. The results are for a drainage layer of 6.1 m long with a roughness of 0.05 and 2% slope. Increasing the storm duration resulted in reduced detention; as shown in **Figure 7.3(a)**, the peak runoff rate increased from 1.3 mm/min (simulation case 1) to 1.9 mm/min when the duration of the rainfall was extended to 30 minutes.

Figure 7.3(b) shows the model results in response to a 20 mm/min rainfall. Reduced detention can be observed in the drainage layer in this intensive rainfall event with a significantly less reduction in peak rainfall (35% in the 2 mm/min rainfall and 5% in the 20 mm/min rainfall).

The model results in **Figure 7.2** and **Figure 7.3** all conform with expected physical behaviour. It can be concluded that the model proposed for the drainage layer could provide a reasonable prediction of the runoff profiles for different drainage layer materials and drainage lengths in response to various storm events. Further investigation on the model will be conducted to compare the model results with laboratory-measured results in section 7.3.

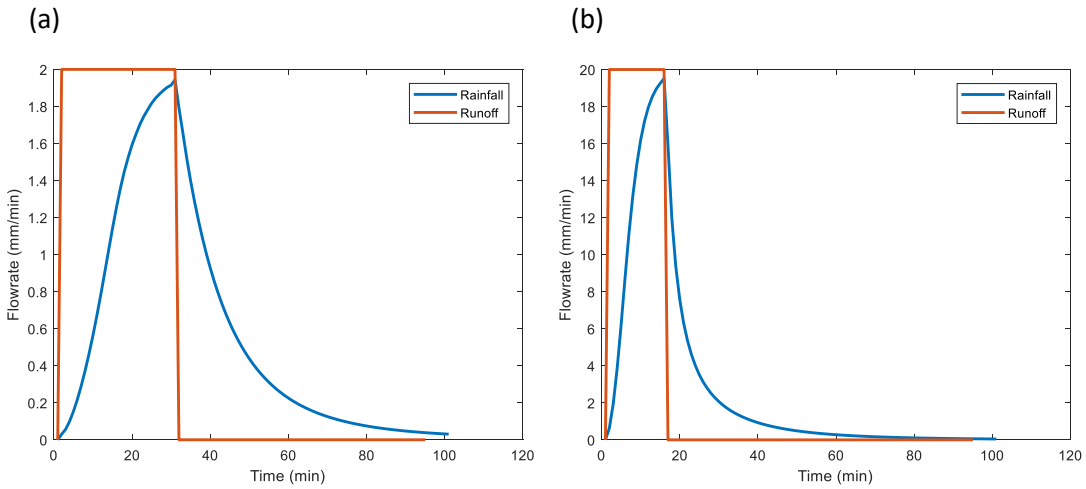

Figure 7.3. Modelled runoff profiles for simulations 5 and 6 using the physically-based drainage layer model.

7.3 Modelling of green roof drainage layers

The preliminary studies on the physically-based green roof drainage layer model proposed in Section 7.2.2 have demonstrated that the model can provide a prediction of the runoff profiles from the drainage layer. In this section, further investigation will be conducted with the model to test its capability of accurately predicting runoff profiles from different drainage layers. Laboratory runoff profiles from three typical green roof drainage layers will be used to determine Manning's n (the only empirical parameter that relates to the properties of the drainage layer materials) in the model. The capability of the model to simulate the runoff from the drainage layers will be evaluated based on the modelled and measured runoff profiles. Limitations of the model will be discussed at the end of this section.

7.3.1 Drainage layer detention tests

7.3.1.1 Representative drainage layers

Figure 7.4 shows the three drainage layers that were considered in the tests. **Figure 7.4(a)** is a ZinCo Floradrain FD 25 drainage layer; it is an egg-box style Polyolefin module with a thickness of 25 mm. **Figure 7.4(b)** is a ZinCo Floradrain FD 40 drainage layer; it has the same design as ZinCo Floradrain FD 25 with a thickness of 40 mm. **Figure 7.4(c)** is a ZinCo Floraset FS 75 drainage layer;

it is an expanded polystyrene component with water storage cells and a multi-directional channel system on both sides.

(a) (b) (c)

Figure 7.4. Drainage layers used for investigation in this study; (a) ZinCo Floradrain FD 25; (b) ZinCo Floradrain FD 40; (c) ZinCo Floraset FS 75 (Vesuviano, 2014)**.**

7.3.1.2 Test programme

The detention tests on the green roof drainage layers were conducted by Dr Gianni Vesuviano at ZinCo GmbH international headquarters in 2011 (Vesuviano, 2014). The descriptions of the test can be found in Section 3.5.2 and Vesuviano (2014). The full test programme with the drainage layers consisted of 100 configurations of drainage layers, protection mats, and rainfall intensities. However, only the tests with the three drainage layers in **Figure 7.4** were considered in the present study. Three replications were conducted with the same rainfall intensity and system configuration, and in total, this makes 180 independent tests.

7.3.2 Derivation of Manning's n

The modelling method described in Section 7.2 was used to generate the runoff profiles from the drainage layers in response to the rainfall events at 1-second time steps. The measured inflow rate was used as the rainfall input to the model. R_t^2 (Young et al., 1980) was used to evaluate the goodness of fit between the modelled and measured runoff profiles. A series of Manning's n values were tested to obtain the best estimation of Manning's n that achieves the highest overall averaged R_t^2 for all the detention tests with the same drainage layer. In total, for each drainage layer, 60 tests were used to determine Manning's n.

7.3.3 Results and discussion

7.3.3.1 Derivation of Manning's n

Assessments of the drainage layer performance can be found in Vesuviano (2014); the focus of this study is on the drainage layer modelling. **Figure 7.5** shows the relationship between the value of Manning's n and averaged R_t^2 of the model results for the same drainage layer. Averaged R_t^2 is

the mean value of the R_t^2 for all the tests with the same drainage layer (i.e. 60 tests). A peak value of R_t^2 was used to identify the best-fit Manning's n for each drainage layer. The same best-fit coefficients were obtained for the FD 25 and FS 75 drainage layers, and a slightly higher value was obtained for the FD 40 drainage layer. The best-estimated value of Manning's n for FD 25 and FS 75 drainage layers is 0.0017, and it is 0.002 for the FD 40 drainage layer. Referring to the value for Manning's n for different surfaces listed in Chow (1959), the values for the drainage layers determined here are in the low range of suggested values; they are equivalent to a very smooth surface. The FD 25 and FD 40 drainage layers should have the same surface roughness as they are made from the same material. However, the flow over the two layers is different as the thickness is different. The 'form roughness' due to higher obstacles in FD 40 will slow down water flow and increase the equivalent roughness. FS 75 and FD 25 are made from different materials, and FS 75 is expected to have a rough surface. However, as the FS 70 has significant water storage capacity, water is more likely to travel over a thin film of water, which may smoothen the surface roughness. Although the model could achieve a high value of R_t^2 (i.e. R_t^2 are all above 0.96) for all the drainage layers, it performs the best with the FD 25 drainage layer and the worst with the FS 75 drainage layer. The high value of R_t^2 for all the drainage layers confirms that the drainage layer-specific Manning's n is independent of system configuration and rainfall intensity, which confirms the feasibility of the model for generic use.

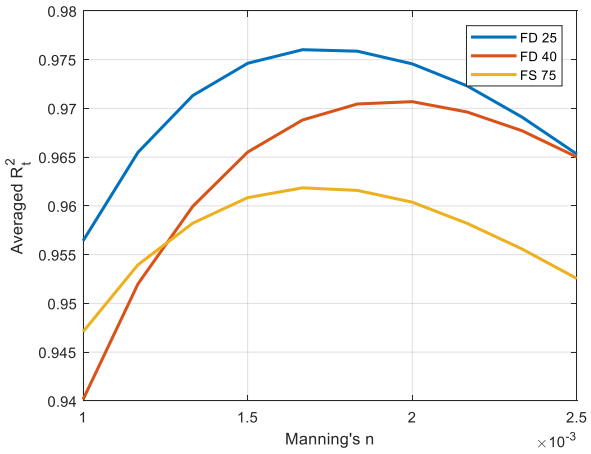

Figure 7.5. The relationship between Manning's n and the averaged R_t^2 for each drainage layer.

The drainage layer model performance will now be considered with respect to rainfall intensity, drainage length and slope. **Figure 7.6** shows the R_t^2 for all the tests using the determined drainage-layer specific Manning's n (i.e. 0.0017 for FD 25 and FS 75, and 0.002 for FD 40). The performance of the model is classified by the type of drainage layer in **Figure 7.6(a)**. Consistent with **Figure 7.5**, the model performs best in representing flow over FD 25 and worst in FS 75.

Figure 7.6(b) shows the R_t^2 grouped according to rainfall intensity. The model performs better in a high rainfall event. This could because that the drainage layers provide specific storage capacity, and the flow condition is more likely to be overland flow (the flow condition that the model is intended to represent) with high flow rates. **Figure 7.6(c)** groups the R_t^2 by drainage length. The model performs equally well (with a medium R_t^2 above 0.95 for both lengths) in the drainage length of 2 m and 5 m. However, more outlier points are shown in the 2 m drainage length. Those outlier points are mostly in response to the lowest rainfall intensity. **Figure 7.6(d)** shows the model R_t^2 for different slopes. The model performs slightly better for a steep system (17.6%), with a higher mean R_t^2. **Figure 7.7** shows the R_t^2 for each configuration; the model performs better in the 2% slope 2m and 17.6% slope 5 m configurations for all the drainage layers. This could because that the flow condition in those configurations is more likely to be overland flow.

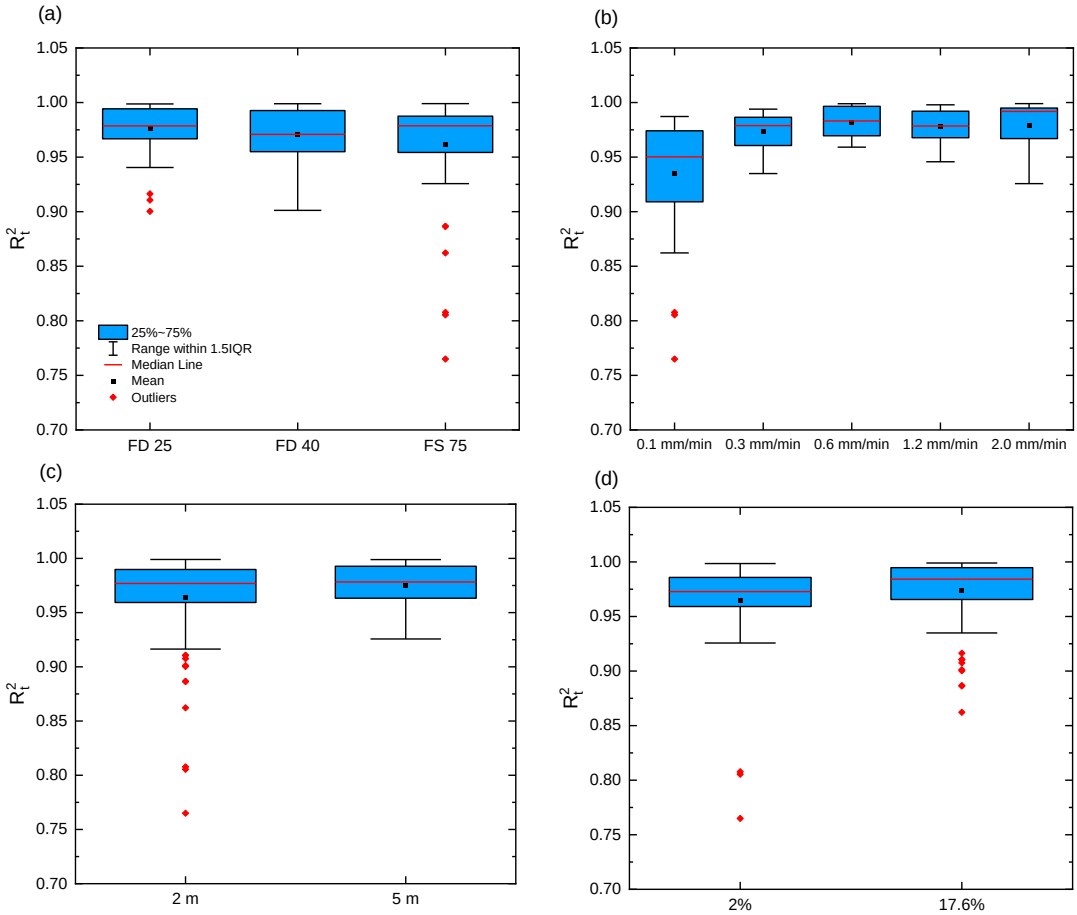

Figure 7.6. R_t^2 for all the model results using the best-estimated Manning's n in different categories; (a) in drainage layer types; (b) in rainfall intensities; (c) in drainage lengths; (d) in slopes.

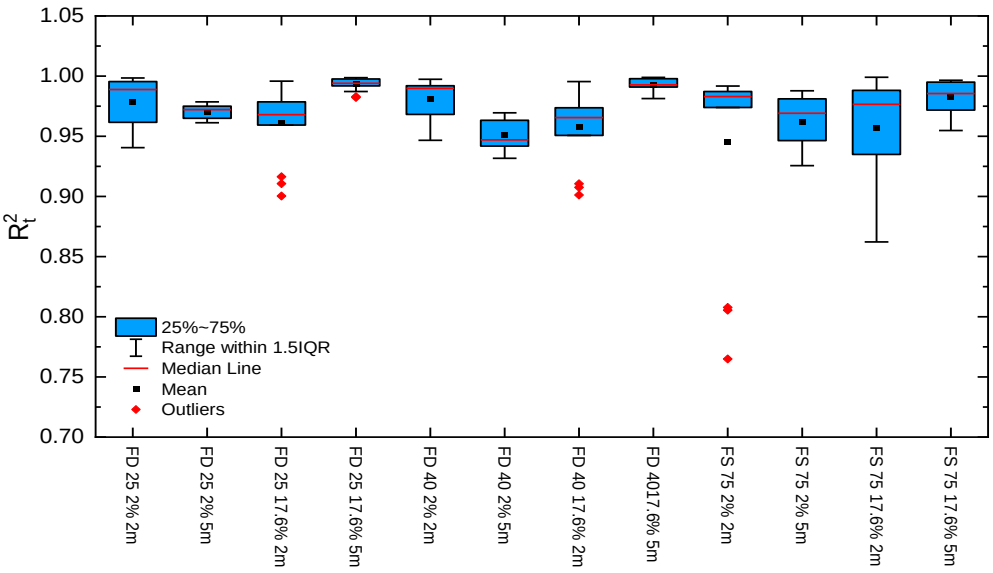

Figure 7.7. R_t^2 for all the modelled tests using the best-estimated Manning's n grouped in different configurations (the drainage layer are labelled as drainage layer type, slope and drainage length).

The R_t^2 values provide information about overall model performance, but they hide any systematic errors or limitations that only become evident through the direct comparison of modelled and measured runoff profiles. Among the 15 tests with the same configuration, a best and a worst-case were identified. **Figure 7.8** shows the best and the worst fit cases using the characterised Manning's n (i.e. Manning's n = 0.0017) for the FD 25 drainage layer. The best fit cases are all in moderate to high rainfall intensities (i.e. 0.6-2.2 mm/min). In the best fit cases, all runoff profiles are modelled well except for the configuration of 2% slope, 5 m drainage length, where the model tends to overestimate the detention effects in the drainage layer. When drainage length is long, and the slope is gentle, a thin film of water can be developed, and water flows over this film rather than over the surface of the drainage layer directly. This decreases the equivalent surface roughness. The worst cases are mostly with the lowest rainfall intensities, where background noise was evident in the measured runoff profiles. Unstable numerical solutions were also observed in the lowest rainfall intensities. Further discussion on the unstable numerical solutions will be provided in Section 7.3.3.2.

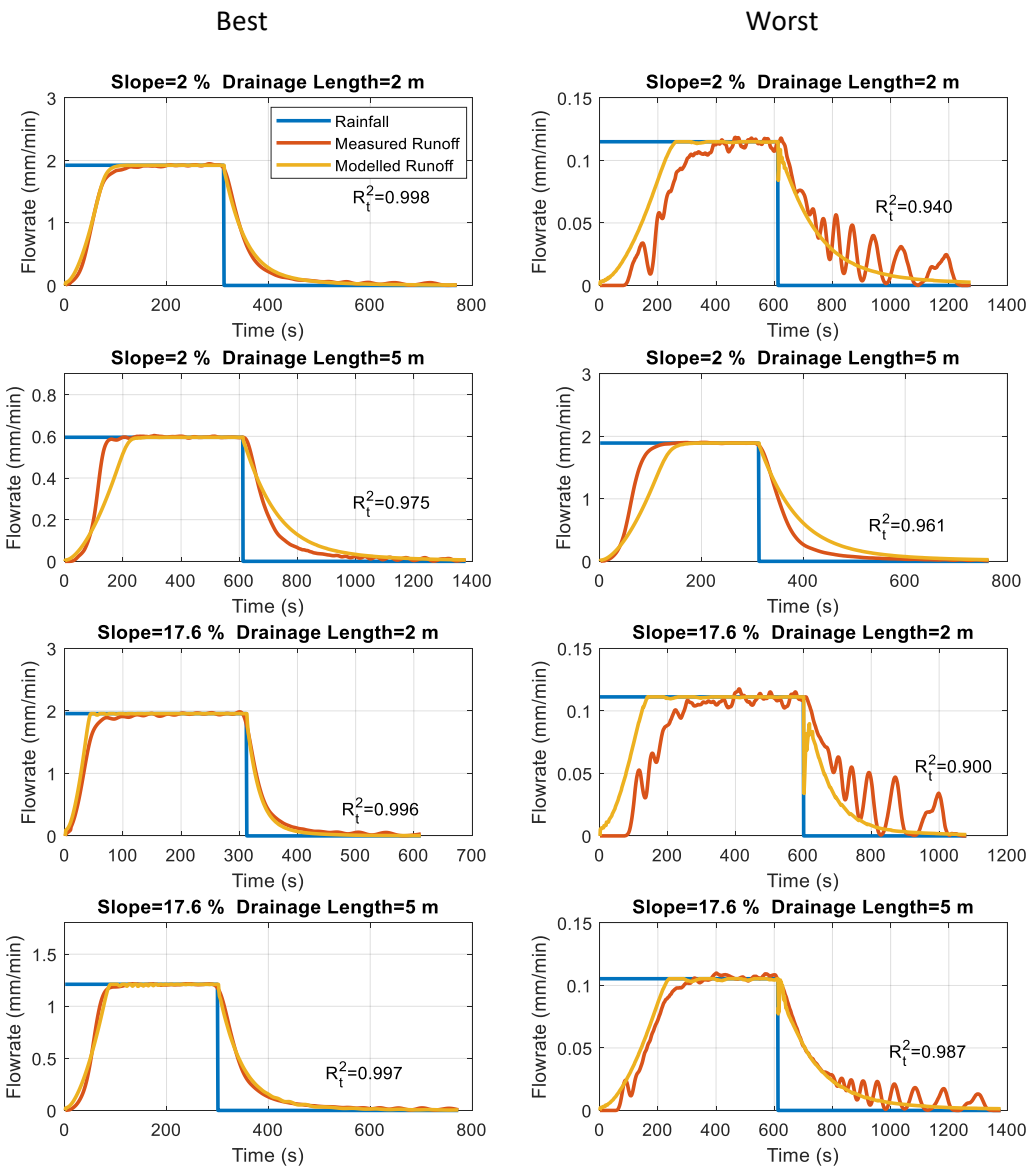

Figure 7.8. Cases where the physically-based drainage layer model achieves the best and the worst fit for the FD 25 drainage layer (with Manning's n = 0.0017); left column: the best fit; right column: the worst fit.

Figure 7.9 shows the best and the worst fit cases using the characterised Manning's n (i.e. Manning's n = 0.002) for the FD 40 drainage layer. The results here are consistent with the results for the FD 25 drainage layer. The model overestimated the detention effects for the configuration of 2% slope, 5 m drainage length. The model also performs better in moderate to high rainfall intensities. The worst fit cases are all with the lowest rainfall intensities, and unstable numerical solutions were observed in the results of the lowest rainfall intensity.

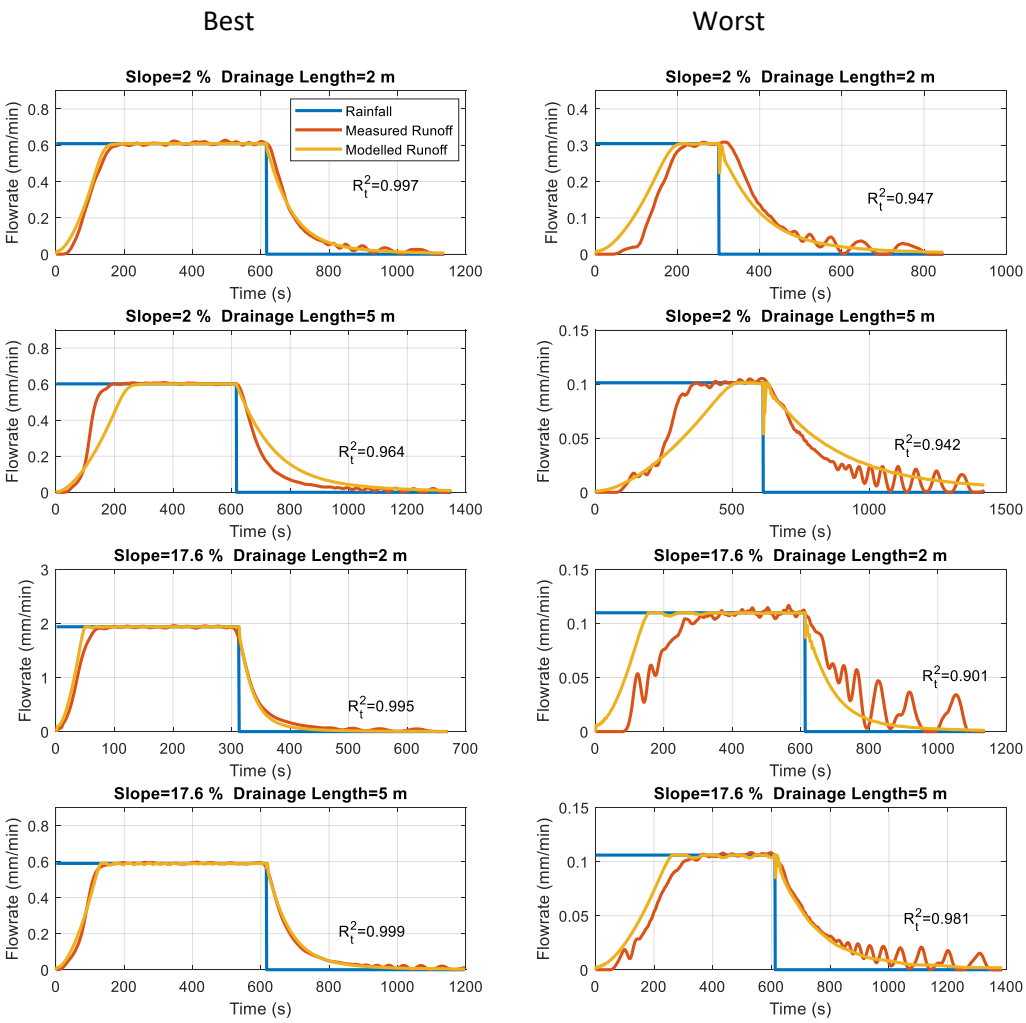

Figure 7.9. Cases where the physically-based drainage layer model achieves the best and the worst fit for the FD 40 drainage layer (with Manning's n = 0.002); left column: the best fit; right column: the worst fit.

Figure 7.10 shows the best and the worst fit cases using the characterised Manning's n (i.e. Manning's n = 0.0017) for the FS 75 drainage layer. The results here are similar to the results of FD 25 and FD 40 drainage layers. However, the worst fit cases are not all with the lowest rainfall intensity for the FS 75 drainage layer; they occur at different rainfall intensities as well (i.e. 2.0 mm/min and 1.2 mm/min).

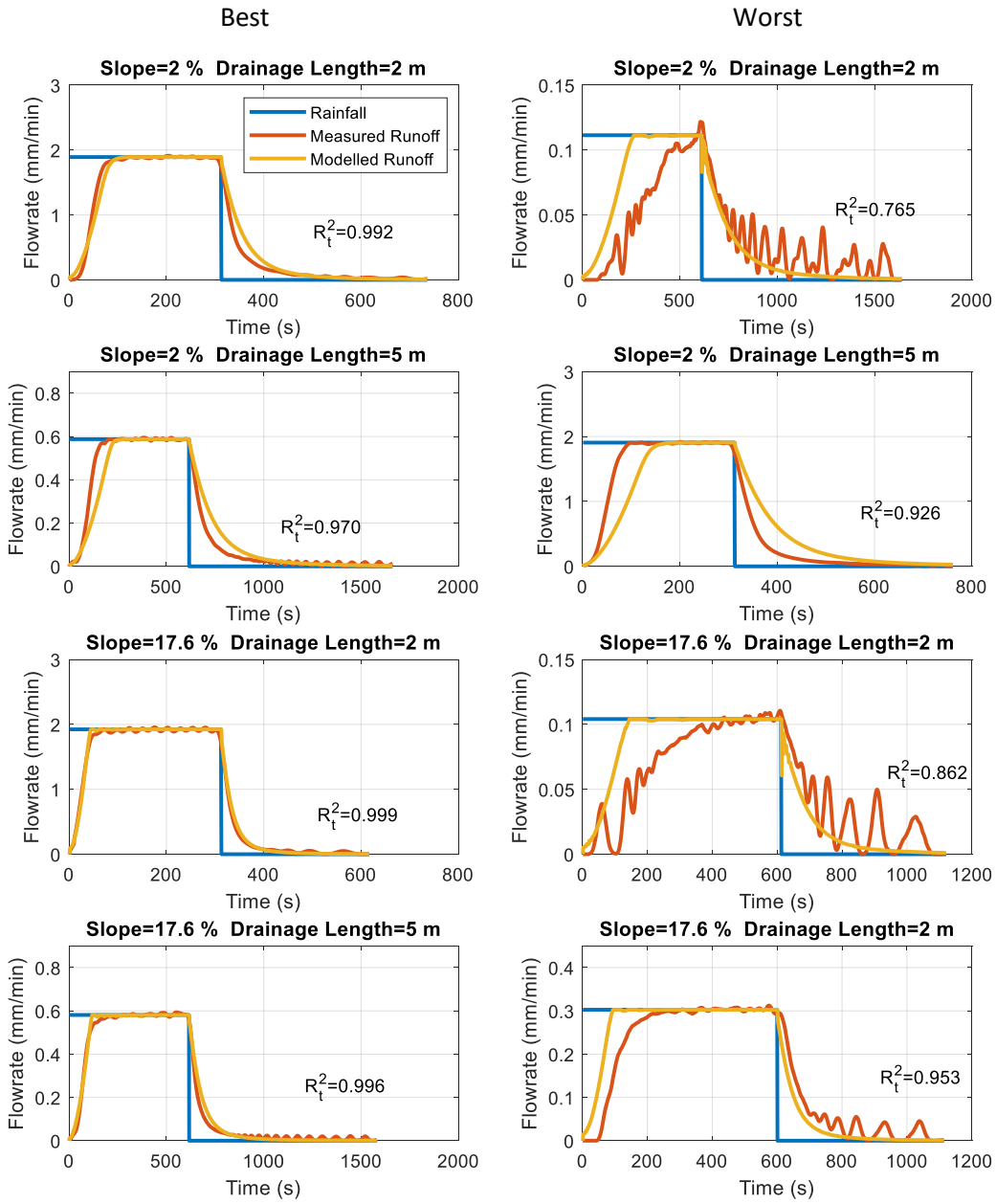

Figure 7.10. Cases where the physically-based drainage layer model achieves the best and the worst fit for the FS 75 drainage layer (with Manning's n = 0.0017); left column: the best fit; right column: the worst fit.

7.3.3.2 Model limitations

As shown in **Figure 7.8**, **Figure 7.9** and **Figure 7.10**, the model exaggerated the influence of drainage length for all the drainage layers. The reason for this could be that the model models the water flowing over the drainage layer surface, but, in reality, it could be the water flowing over a thin layer of water film in long drainage lengths. Unstable numerical solutions were observed in the falling limb of the modelled runoff profiles in response to the lowest rainfall intensity (0.1 mm/min) for all the drainage layers, and an unstable numerical solution was also

observed at the equilibrium stage in a steep system (17.6%) (**Figure 7.11**). However, it should be noted that a slope of 2% is a standard slope for a green roof system (FLL, 2008) and the response of the system to a moderate rainfall intensity is of more interest to detention performance. The unstable model solution may be caused by the numerical scheme adopted in the *pdepe* function in MATLAB or the method used to discretise time and spatial steps. Investigating the numerical scheme is beyond the scope of this research, and it will not be discussed here. However, an unstable numerical solution for this type of model is not unusual; Šimůnek (2015) also reported the same problem when the same model was used to model the water flow over different types of land. With this limitation on board, a careful selection of time and spatial steps are needed to utilise this model.

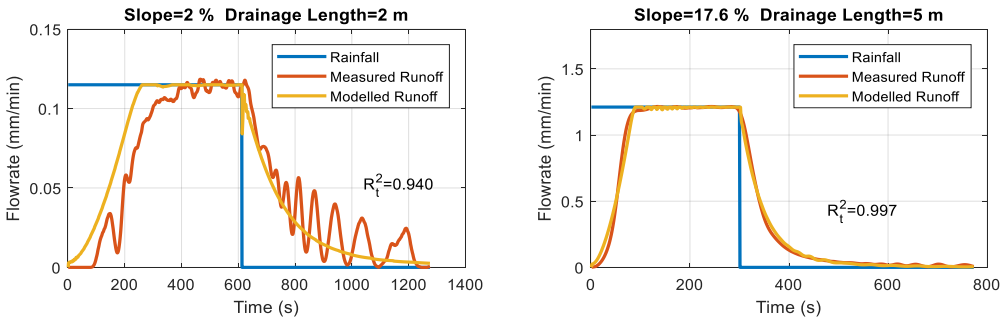

Figure 7.11. Examples of cases where the physically-based drainage layer model provides unstable solutions.

7.3.4 Conclusions

Based on the model results above, it can be concluded that the proposed drainage layer model provided reasonable and accurate predictions of the runoff profiles from the drainage layers when the material-specific Manning's n was determined. However, it should be acknowledged that the model may overestimate the detention effects in a long and shallow sloped system. In addition, special attention should be given to the model results when it is used to model the runoff profiles in response to a low rainfall intensity or from a steep system as unstable numerical solutions may be obtained from these cases.

7.4 A two-stage green roof detention model

The model discussed in previous sections is for the drainage layer only. A model for the substrate is also required to simulate the runoff from a complete green roof system. In this section, a two-stage physically-based green roof detention model is proposed.

The concept of modelling a complete green roof using two or more independent models that represent the performance of each independent component is not new. The LID module in SWMM and the two-stage Reservoir Routing model developed in Vesuviano et al. (2014) have already adopted this concept. In these models, the detention effect in the substrate and drainage layer are modelled independently by different models, and the models are connected through the flux from the upper layer to the lower. The two-stage green roof detention model proposed in this study shares the same concept with previous existing studies. However, different models for the substrate and drainage layer are used in this study. **Figure 7.12** shows the concept of the two-stage physically-based model developed in this study. In this model, the Richards Equation is used to represent the flow in the substrate (Equation 2.19), and the Saint Venant model developed in Section 7.2 (Equation 7.5) is used to model the performance of the drainage layer.

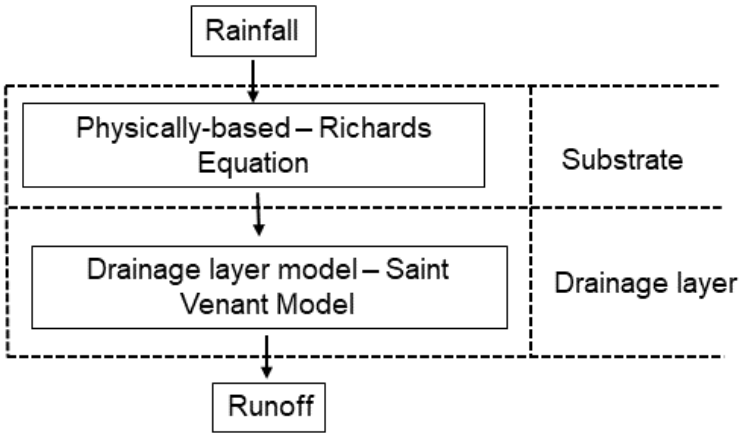

Figure 7.12. The concept of the two-stage physically-based green roof detention model.

7.5 Validation of the two-stage physically-based model using laboratory data

The capability of the two-stage physically-based green roof detention model (proposed in section 7.4) to regenerate runoff profiles from a laboratory green roof test bed will be tested in this section. The substrate and drainage layer parameters derived in Chapter 5 and Section 7.3 will be used in the model to generate the runoff profiles in response to five design storms. The performance of the model will be evaluated based on the modelled and measured runoff profiles using R_t^2 (Young et al., 1980).

7.5.1 Laboratory green roof test bed

The laboratory green roof system was built at ZinCo GmbH international headquarters. It consisted of 100 mm Marie Curie Substrate (MCS) above a ZinCo Floradrain FD 25 drainage layer. A ZinCo Systemfilter SF particle filter sheet was used to separate the substrate and drainage layer,

and the filter sheet was taped to the internal walls of the simulator to prevent any movement of it during the tests. A fibrous ZinCo SSM 45 protection mat was laid under the drainage layer (**Figure 7.13**). The two additional layers in the complete green roof system have the potential to provide extra detention and retention effects. The whole system was placed at a slope of 2%. The rainfall simulator in **Figure 3.3** was used for the detention tests with the green roof system, and the full length (i.e. 5 m) of the rainfall simulator was used in all the tests. A full description of the laboratory green roof test bed can be found in Vesuviano et al. (2014). The test programme with this green roof system can be found in Section 3.5.3.

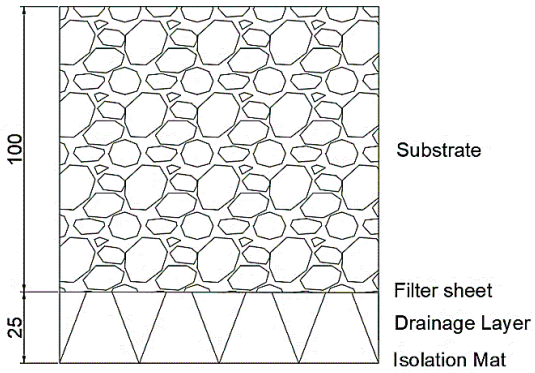

Figure 7.13. Configuration of the laboratory green roof system (dimensions in mm).

7.5.2 Model implementation

The *pdepe* function in MATLAB was used to solve the substrate Richards Equation and the drainage layer Saint Venant equation. The rainfall was used as an input to the Richards Equation to simulate the runoff from the substrate using the approach described in Chapter 4. The modelled runoff from the substrate was then used as the input to the Saint Venant model to model the runoff from the drainage layer (the runoff from the green roof system) using the method described in Section 7.2.1 at 1-minute time steps. It should be noted that the other two layers (the filter sheet and the protection mat) were not represented in the model.

7.5.2.1 Substrate model parameters

The substrate (MCS) used in the laboratory green roof test bed has been studied in detail in Chapter 5. The characterised SWRC (Durner model) and HCF (three-segment curve) in Chapter 5 for the MCS (**Table 5.2** and **Table 5.4**) were used here to model the runoff from the substrate. As no moisture probe was used in the detention tests to determine the moisture content at initial stages, the moisture content corresponding to a suction head of 10 cm was set for the bottom boundary of the Richards Equation for all the tests. The 10 cm suction head is approximately

equivalent to the averaged suction head of the lower boundary conditions of the detention tests with the MCS conducted in Chapter 5.

7.5.2.2 Drainage layer model parameters

The Manning's n for the ZinCo Floradrain FD 25 drainage layer (i.e. Manning's n = 0.0017) has been determined based on the drainage layer isolated test in Section 7.3, and the same value was used here for the drainage layer in the complete green roof system.

7.5.3 Results

Evaluation of the green roof system performance can be found in Vesuviano et al. (2014) and Vesuviano (2014); the focus of this study is on the capability of the two-stage model to regenerate the runoff profiles from the green roof test bed. In all of the 15 simulations, no unstable numerical solutions were observed. As a good consistency has been observed in the three repeat tests, the model results of one test were presented.

Figure 7.14 shows the modelled runoff profiles from the green roof system using the parameters derived from previous sections. It should be noted that the duration of the storm events was 16 hours (60 minutes of rainfall followed by 15 hours' dry period). However, the measured runoff rate was insignificant after 100 minutes. 100 minutes was used for the time-series plot, and 200 minutes was used for the cumulative plots. This could account for cases where the total measured runoff depth is lower than the total rainfall depth. With all R_t^2 higher than 0.91, the model provides an accurate prediction of runoff profiles from the green roof test bed. The falling limb of the runoff profiles was accurately modelled in all the tests. However, the rising limb of the measured runoff profile, especially in low rainfall intensities, is slightly shallower than those of the modelled runoff profile, which indicates that the model underestimated the detention effect of the green roof in the period from time zero to steady-state. For example, in response to the lowest rainfall intensity (i.e. 0.3 mm/min), the system runoff reached a steady-state condition approximately 30 minutes after the start of the rainfall. However, it was modelled to reach a steady-state condition approximately 18 minutes after the rainfall. In the two time-varying rainfall events, the model tends to underestimate the time to start of runoff. In the 1-in-10 year rainfall event, the measured runoff started approximately 20 minutes after the rainfall. However, it was modelled to be 10 minutes. In terms of peak attenuation, the model also underestimated the peak attenuation in the two time-varying rainfall events. No peak attenuation was modelled in either case, whilst approximately 4.9% attenuation was observed in the 1-in-10 year rainfall event, and 10.3% was observed in the 1-in-100 year rainfall event. **Figure 7.14** also shows the

modelled runoff profiles from the substrate; it is evident that both the substrate and the drainage layer contribute detention effects to the whole green roof system.

Figure 7.14 shows that the modelled cumulative runoff depth at the final time is equal to the total rainfall depth. This means that all the rainfall is modelled to leave the system as runoff, and the model is unable to retain any water.

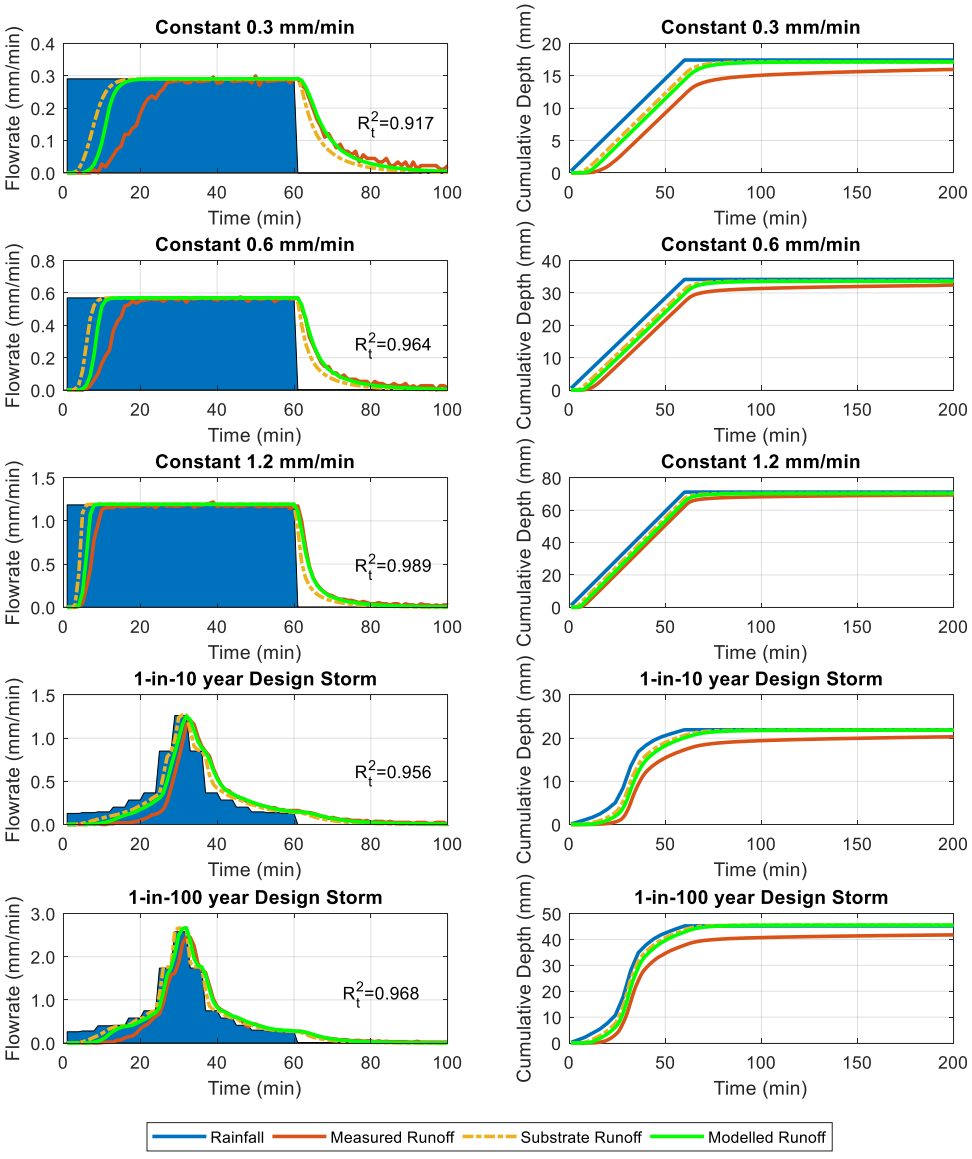

Figure 7.14. Modelled and measured runoff profiles and cumulative depths using the two-stage physically-based model with the parameter identified from drainage layer isolated tests (i.e. Manning's n = 0.0017).

7.5.4 Discussion

The model results in 7.5.3 show a noticeable difference in the rising limb runoff profiles between the modelled and measured results. This difference may be caused by a) hysteresis effects in the substrate; b) the retention capacity of the filter sheet or the moisture mat below the drainage layer; c) variation in drainage layers. In this section, the three hypotheses will be investigated independently. Model modifications will be made to represent the proposed effect, and the model results will be compared to the measured data to evaluate the mentioned effect.

7.5.4.1 Impact of the substrate hysteresis effect

The soil hysteresis effect refers to the phenomenon that soil shows different behaviour in the wetting and drying processes (Hillel et al., 1998). The hysteresis effect is believed to be caused by the nonuniformity of pores space and the variation in the liquid-solid contact angle (Hillel et al., 1998; Rudiyanto et al., 2013). As the contact angle and the radius of curvature are greater in the water advancing processes than the water receding processes, to reach the same moisture content, a higher suction head is required in the drying curve than the wetting curve (Hillel et al., 1998). As a green roof substrate is a mixture of aggregates consisting of various pore sizes, the hysteresis effects also apply. In reality, the hysteresis effects are complicated as the soil could experience several loops between the main wetting and drying curves to reach an equilibrium stage eventually (Hillel et al., 1998). However, to simplify the problem, it is assumed that no hysteresis cycle occurs in the green roof substrate during the storms.

Figure 7.15 proposes the SWRCs for the MCS corresponding to the drying and wetting processes. The drying curve is the fitted Durner model using the measured SWRC data in **Table 5.2**. The wetting curve is a constructed curve formed by increasing the α_1 in Durner model from 0.3044 to 0.9. A value of 0.9 was used here to construct a comparable wetting curve for the MCS such that the suction head in the wetting curve is three times lower than in the drying curve at the same moisture content. It should be noted that the purpose of the constructed wetting curve is to investigate the influence of SWRCs on the model results; more experimental measurements are needed to characterise the actual wetting curve for the MCS substrate. The wetting and drying processes of the substrate were modelled independently by two SWRCs to account for the substrate hysteresis effects. In the model, the wetting curve was used to model the runoff profiles from the substrate in the first 30 minutes of the rainfall, and the drying curve was used to model the runoff from 30 minutes until the end (i.e. 200 minutes). The modelled substrate runoff profiles were then used as inflow to the drainage layer model to generate the runoff profiles from the whole system.

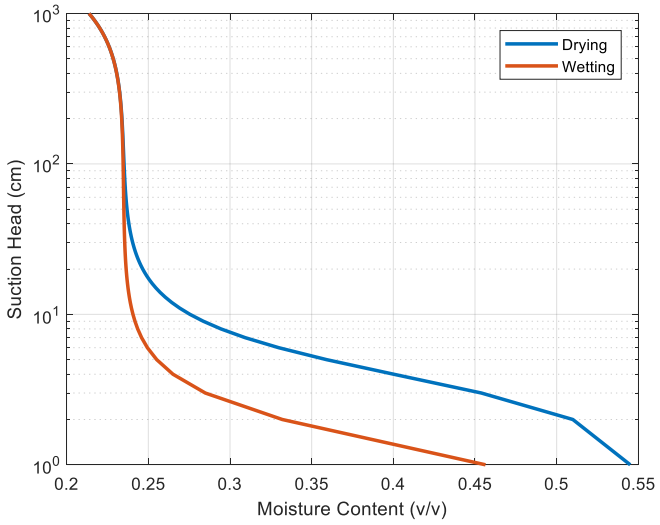

Figure 7.15. Hysteretic SWRCs for the MCS substrate (the wetting curve is a constructed curve).

Figure 7.16 shows the model results when the substrate hysteresis effects are considered. The hysteresis effect only applied to the substrate model, the modelled substrate runoff profile was changed, and consequently, the modelled runoff from the whole system. As two SWRCs were used for the wetting and drainage processes, the rising and falling limbs of the substrate runoff and modelled runoff profiles are not symmetrical; they show more detention in the rising limb. Although the detention effect in the rising limb of the modelled runoff profile is more significant when hysteresis was considered, the time for the system to reach an equilibrium stage was not modelled well. The modelled time of equilibrium is approximately 5 minutes earlier than it was measured both in the lowest and medium rainfall intensities (i.e. 0.3 mm/min and 0.6 mm/min). This could be due to the fact that the substrate could go into several hysteresis loops before reaching an equilibrium stage, which was not fully considered in the model. The time to start of runoff was modelled well in most tests except for in the medium rainfall intensity (i.e. 0.6 mm/min), where the model delayed the time to start of runoff by approximately 5 minutes. The model underestimated the peak attenuation in the two time-varying rainfall events. No peak attenuation was modelled in either case, whilst 4.9% and 10.3% peak attenuation was observed in the two cases, respectively. The mean value of R_t^2 increased from 0.959 to 0.985, indicating that the model results are improved when hysteresis was considered.

The cumulative depth of modelled runoff in **Figure 7.16** shows a close match to the measured runoff for the duration of the simulation (i.e. 200 minutes), followed by a lower cumulative depth than the total rainfall in the long-term. However, as this detention model is unable to retain water, the under-prediction is caused by the insufficient time being allowed for the modelled

runoff rate to decline to zero. The modelled cumulative runoff depth at the final time point should be assumed equal to the total rainfall depth.

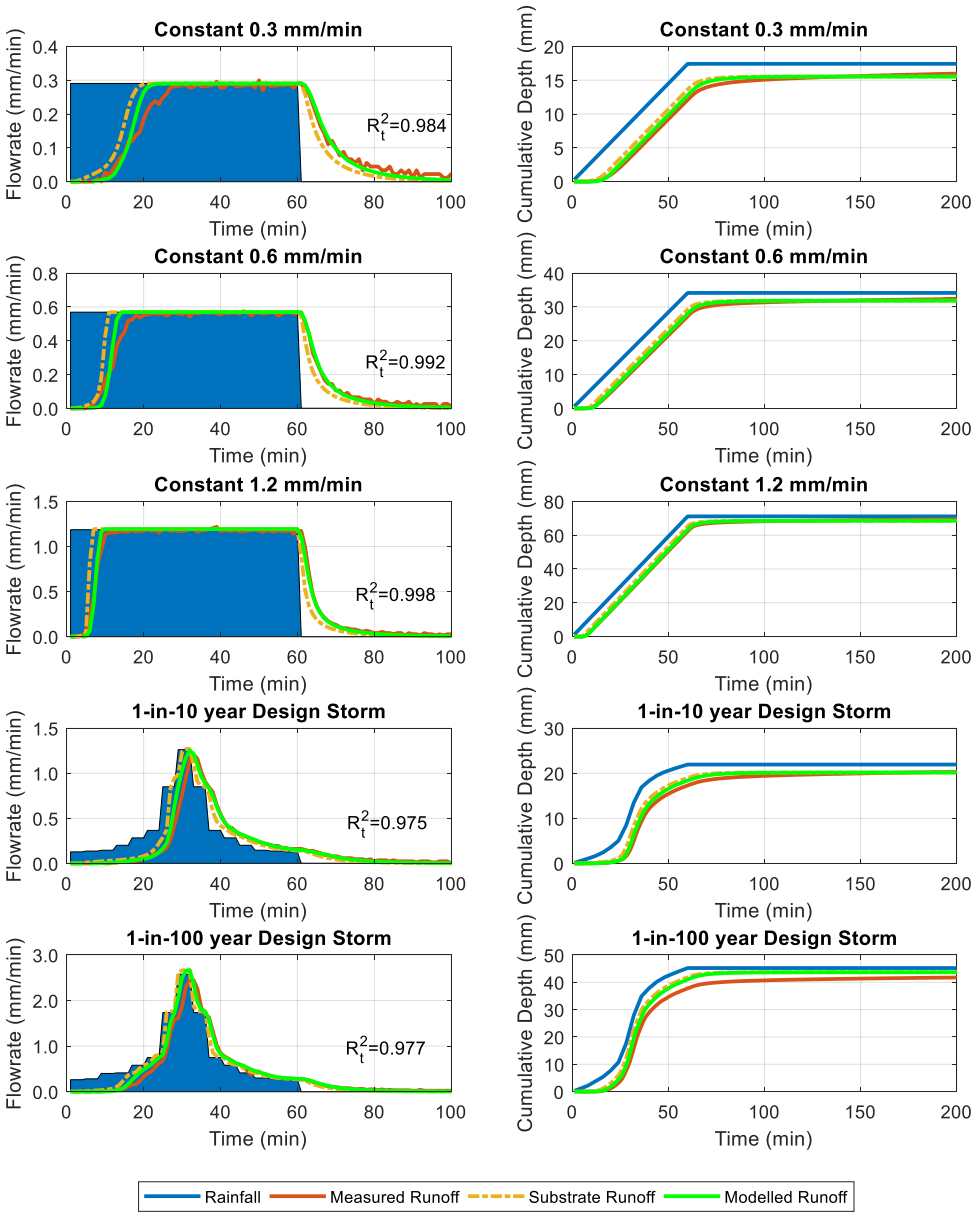

Figure 7.16. Measured and modelled runoff profiles and cumulative depths that considers substrate hysteresis effects.

7.5.4.2 Retention capacity of the filter sheet and moisture mat

The filter sheet, placed between the substrate and the drainage layer, and the moisture mat, placed beneath the drainage layer, may have a certain storage capacity that can influence the model result. The retention capacity of the filter sheet was represented as initial losses at the beginning of the rainfall. The retention capacity was calculated based on the difference between the total depth of rainfall and runoff at the end of 200 minutes. This practice was conducted under

the assumption that all rainfall has left the system two hours after the storm (De-Ville et al., 2018; FLL, 2008), and any difference between the total rainfall and runoff at this point is due to the retention associated with the filter sheet and moisture mat. **Figure 7.17** shows the model results with the retention capacity was excluded from the rainfall. The mean value of R_t^2 is increased from 0.959 to 0.980, which indicates an improvement of the model results. As only the rainfall input was changed, the parameters for the substrate and the drainage layer are unchanged, the falling limb of the modelled runoff profiles was not influenced and was still modelled well in all the tests. The modelled time to start of runoff is close to the measured in all the tests. However, the modelled time for the system to reach a steady-state is always earlier than the measured.

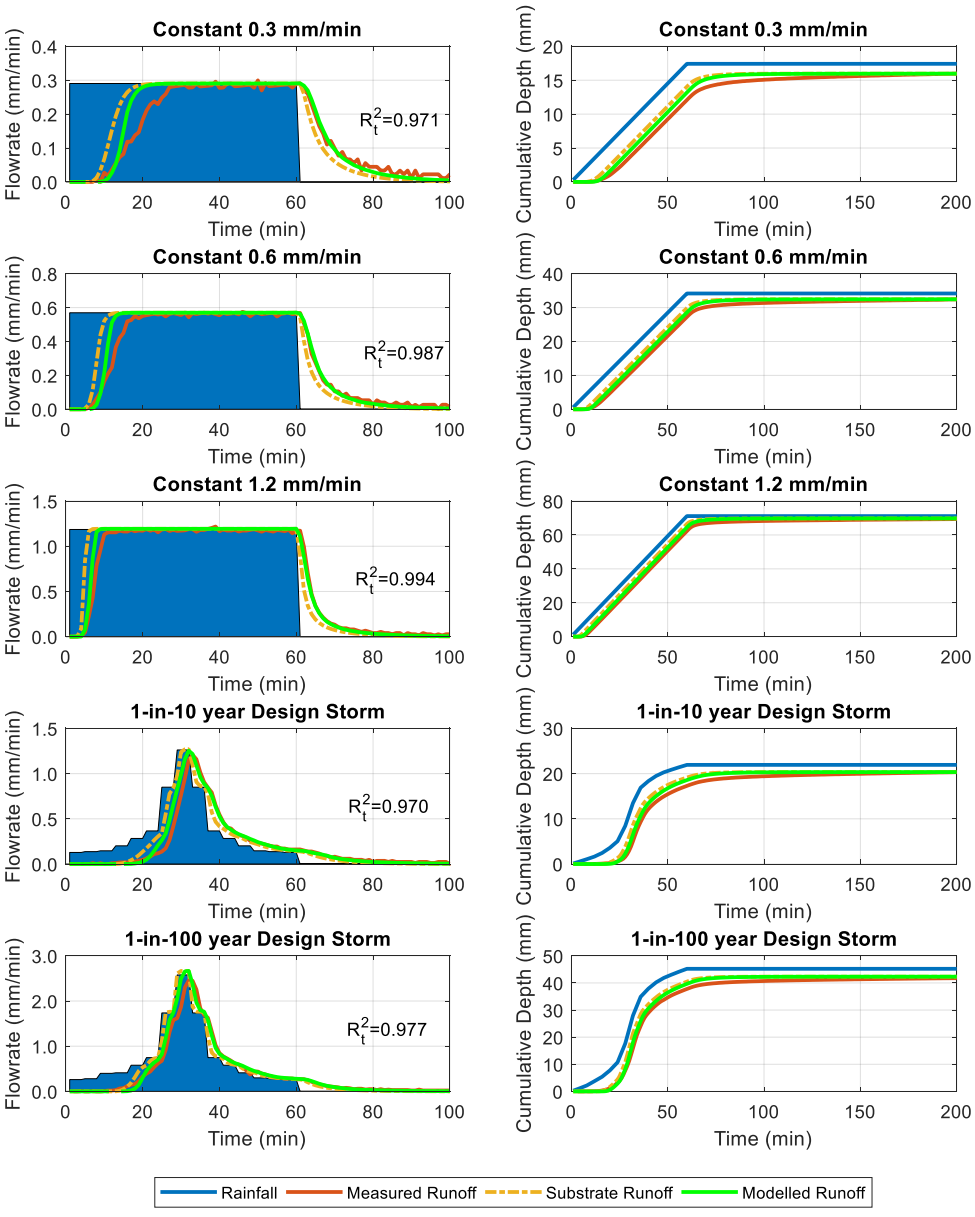

Figure 7.17. Measured and modelled runoff profiles and cumulative depths that excluded the retention capacity of the filter sheet and moisture mat.

7.5.4.3 Influence of drainage layer roughness

The model results in **Figure 7.14** show that the model underestimated the detention performance. This could be caused by the change in the roughness of the drainage layer. In this section, the influence of the drainage layer roughness is considered (note that hysteresis and initial losses were not considered here). Manning's n for the drainage layer model was recalibrated to achieve the highest mean R_t^2 over the 15 full-system tests. **Figure 7.18** shows the calibration results. A peak R_t^2 of 0.983 was achieved with Manning's n = 0.006. The original value of Manning's n, determined from isolated drainage layer tests, was 0.0017, which is significantly lower than the value calibrated here.

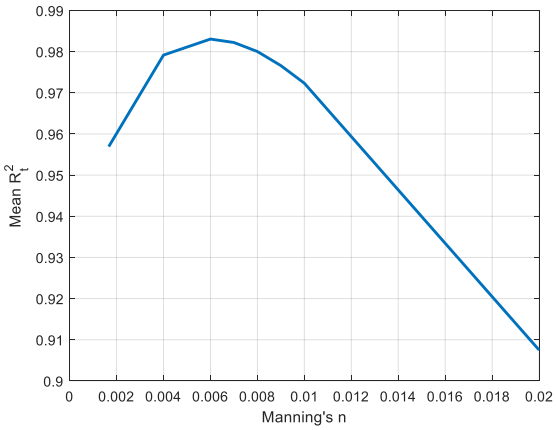

Figure 7.18. The relationship between Manning's n and the mean R_t^2 of the 15 tests.

Figure 7.19 shows the model results using Manning's n of 0.006 for the drainage layer. Comparing to the model results of Manning's n = 0.0017 (**Figure 7.14**), the model provided a better overall estimation of the runoff profiles. This may indicate that the drainage layer behaves slightly differently when it was tested alone compared with when it was tested in a complete green roof system. The influence of the filter sheet and the moisture mat was not modelled in the model. However, the detention effects in these layers could increase the roughness and result in a higher value of calibrated Manning's n. The time to start of runoff was modelled well in all cases, and the peak attenuation for the two time-varying rainfall events was also close to the measured value. The model provided more detention effects in the rising limb of the runoff profiles than before. However, at the same time, more significant detention effects were modelled for the falling limb of the runoff profiles. Increasing the drainage layer roughness influenced the detention effect in the whole system, and this is reflected in both the rising and falling limbs of the runoff profiles.

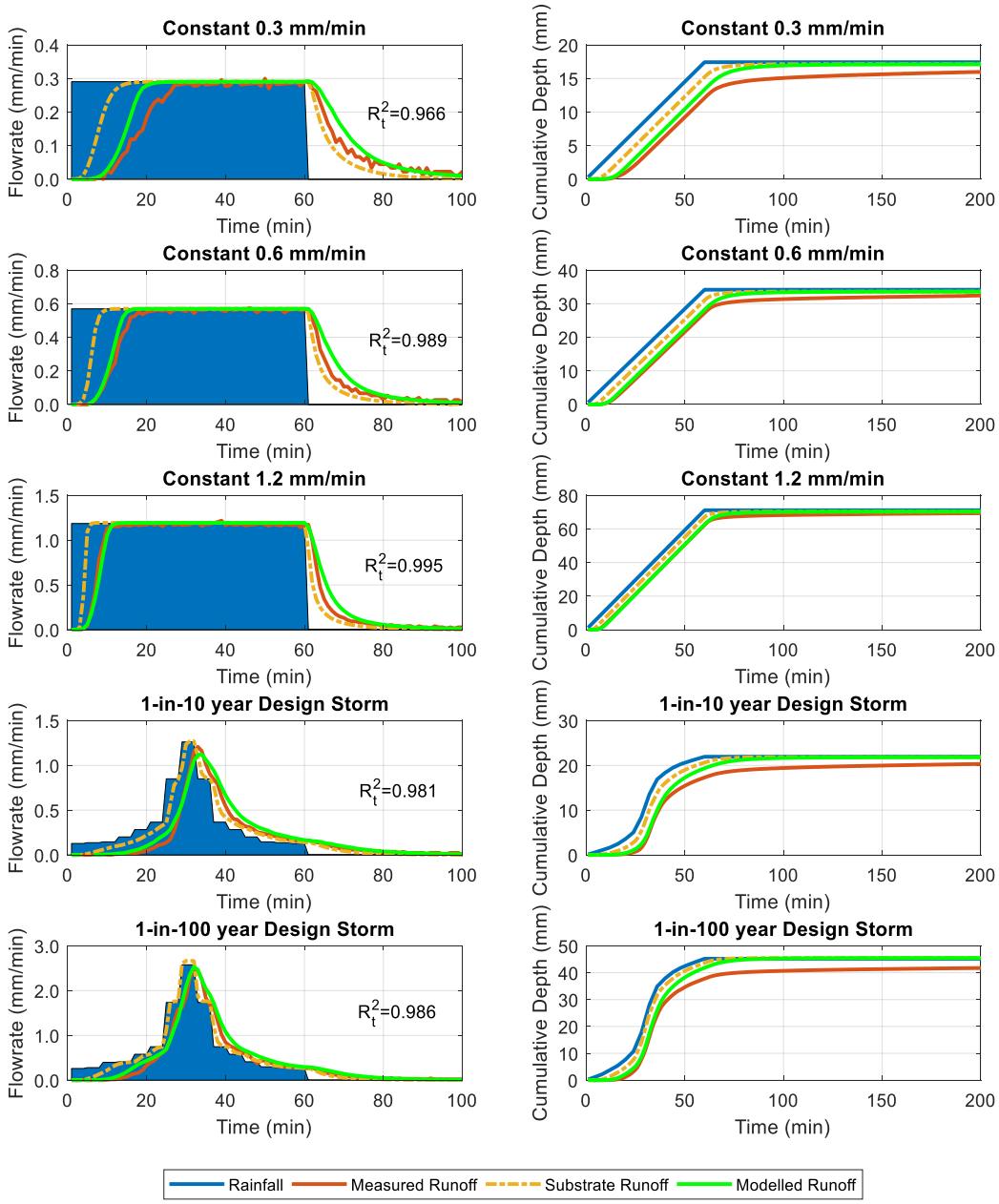

Figure 7.19. Measured and modelled runoff profiles and cumulative depths using the physically-based model and calibrated Manning's n (i.e. n = 0.006).

The model results were improved when each of the three effects (Section 7.5.4) were taken into consideration in the model. As the hysteresis hypothesis provided the highest mean R_t^2 (0.985), it is believed that the difference between the modelled and measured runoff profiles in the rising limb is more likely to be caused by the hysteresis effect in the substrate. However, the three hypotheses were tested independently; namely, only one effect was considered a time; there is a possibility that two or more of the effects could influence the behaviour of the system at the same time. However, considering multiple factors at the same time increases the model complexity, and no evidence has been shown that there is a need to increase the complexity of

the model. The model has already provided accurate estimations of the runoff profiles using the parameters determined in the isolated component experiments, significant improvement in the model results would not be expected with further modifications to the model framework.

7.5.5 Conclusions

The two-stage physically-based green roof detention model provides an accurate prediction of runoff profiles (with a mean $R_t^2 = 0.959$) from a conventional laboratory green roof test bed using the parameters determined in isolated component experiments. It was, however, noted that the detention effects on the rising limb were generally underestimated. The model results were improved when the substrate hysteresis effect was taken into consideration. However, to balance the model complexity and model accuracy, the original model is judged to be fit-for-purpose for this type of modelling (i.e. a shallow green roof system).

7.6 Validation of the two-stage physically-based model using field data

In Section 7.5, the two-stage model was validated using the measured rainfall-runoff data from a laboratory green roof test bed. In this section, further investigation into the two-stage model will be conducted with a field green roof test bed. The parameters determined in previous sections will be used in the two-stage physically-based model to regenerate the runoff profiles from the test bed in response to five selected real rainfall events. The influence of model parameters on the model results will also be explored.

7.6.1 The field green roof test bed and rainfall events

Test bed 1 (TB1), which was introduced in Chapter 4, was used here to validate the two-stage green roof detention model. The five representative storm events (Chapter 4, **Table 4.1**) were used for model validation. The characteristics of the five selected storm events, the performance of TB1 in response to the storms and the observed initial moisture content can be found in **Table 4.1** and **Table 4.3**.

7.6.2 Model implementation

The method described in Section 4.6.4.2 was used for the substrate Richards Equation, and the method described in Section 7.2.1 was for the drainage layer model to generate the runoff from the TB1 at 5-minute time steps.

7.6.2.1 Substrate parameters

To model the detention for each selected event, the retention (initial losses), which was calculated as the difference between the monitored rainfall and runoff depths, was removed from the start of the rainfall profile such that only net rainfall was routed to runoff. The physical

properties of HLS have been characterised and studied in Chapter 4, and the characterised SWRC (Durner model) and HCF (three-segment curve) were used to represent the detention effects in the substrate (**Table 5.2** and **Table 5.4**).

7.6.2.2 Drainage layer parameters

The value of Manning's n determined for the ZinCo Floradrain FD 25 in Section 7.3 (i.e. Manning's n = 0.0017) was used here for preliminary investigation.

7.6.3 Results

Figure 7.20 shows the measured and modelled runoff profiles for the field green roof test bed in response to the five selected rainfall events. The model significantly underestimated the detention effect in the green roof system in all the events, and the modelled runoff profiles showed a more rapid response to the rainfall than the measured profiles. In the events on 6/Dec/2012 and 26/Aug/2015, the model doubled the peak runoff rate. In response to the low rainfall rates during the storms (e.g. around 500 minutes to 1000 minutes in the event on 21/Oct/2013 and 600 minutes to 700 minutes in the event on 26/Aug/2015), no runoff was observed from the test bed, while a significant high runoff rate was estimated by the model. However, the model did provide reasonable predictions of the runoff profiles in that the rising and falling of the runoff profiles occur simultaneously with the rainfall. The unsatisfactory modelling results here is likely to be caused by the potential variations in drainage layers and the change in substrate and drainage layer characteristics over time. Further investigation into the improvement of the model results will be considered in Section 7.6.4.

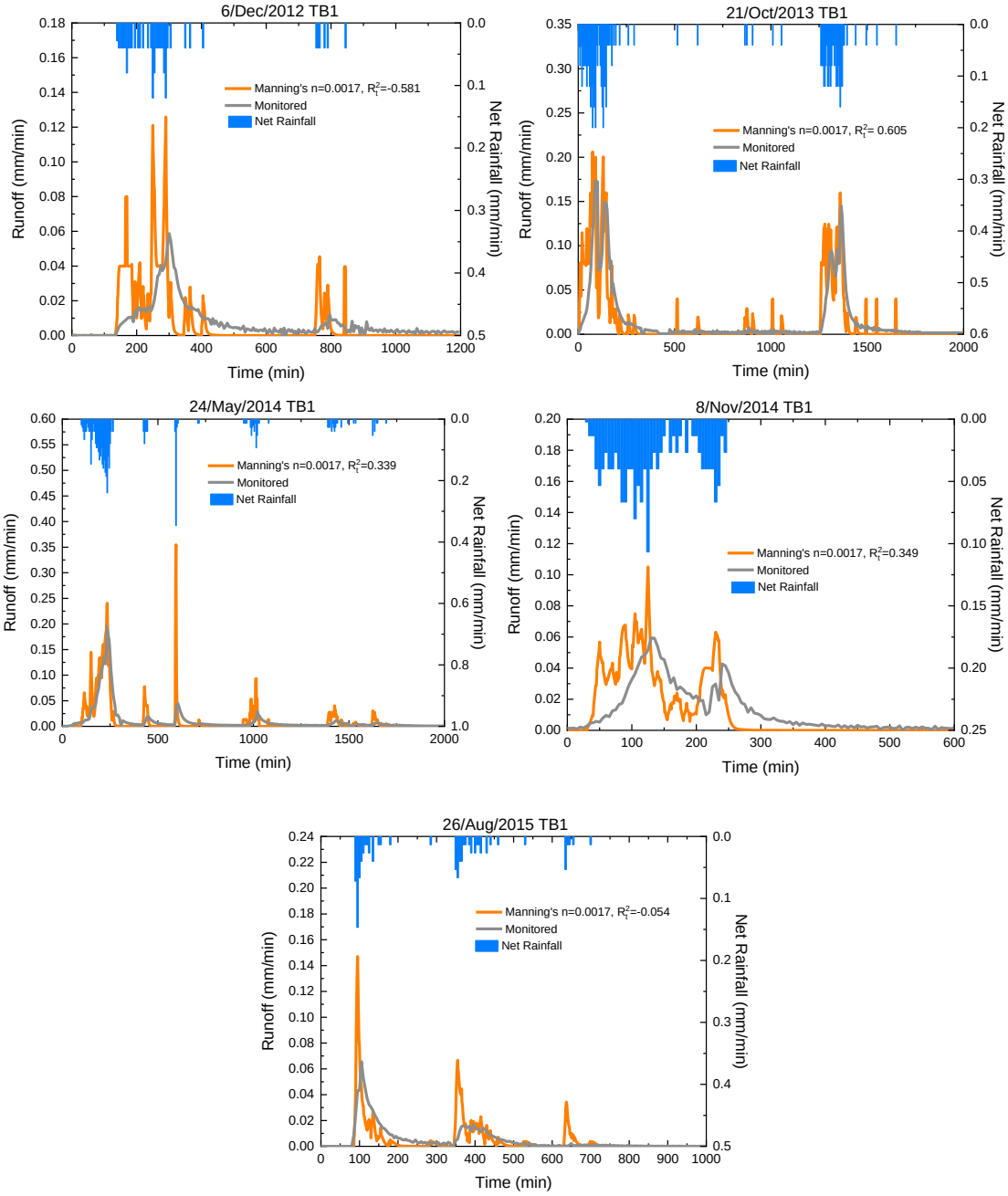

Figure 7.20. Modelled and measured runoff profiles for the five selected rainfall events (**Table 4.3**) using the physically-based model and model parameters determined in isolated component experiments in the laboratory.

7.6.4 Further investigations on the two-stage physically-based detention model

The influence of parameters on the two-stage physically-based model results was assessed in this section. Firstly, sensitivity analysis on Manning's n was conducted with the model using two of the design storms presented in Section 7.5. Manning's n for the FD 25 drainage layer was then recalibrated based on the measured rainfall-runoff data from the field green roof test bed in

response to the five selected rainfall events (Section 7.6). Lastly, alternative model options and model parameters were explored.

7.6.4.1 Sensitivity of model results to Manning's n

Manning's n in the Saint Venant model is a parameter that needs careful characterisation. The influence of Manning's n on the model results was explored independently with the drainage layer model in Section 7.2. In this section, the influence of Manning's n was explored within the two-stage detention model (Section 7.4). Two of the design storms presented in Section 7.5 (a constant rainfall event (i.e. 0.3 mm/min for 60 minutes) and a time-varying rainfall (1-in-10 year 75% summer storm profile)) were used to conduct the analysis. The same test bed configuration and modelling approaches described in Section 7.6.2 were used to regenerate the rainfall profiles in response to the two design storms. A range of Manning's n from 0.001 to 0.1 was tested.

Figure 7.21 shows the model results of using the values of Manning's n. As expected, the detention effect increases with an increase in Manning's n. In the constant storm, the difference between model results is not significant when low values of Manning's n were used. For example, the model results of Manning's n = 0.001 and Manning's n = 0.01 showed no difference in peak attenuation. The time to reach a steady-state condition was delayed by approximately 5 minutes when a higher value was used. However, when Manning's n increased to 0.1, significant detention effects were observed in the modelled runoff profiles: peak attenuation of 7% was modelled, and the duration of runoff was extended to 200 minutes.

Figure 7.21 also shows the model results in response to a time-varying storm. The difference in model results is evident in the time-varying rainfall event. The peak attenuation and peak lag showed an increasing trend with an increase of Manning's n. No peak attenuation was modelled when Manning's n = 0.001 was used; in contrast, it increased to 15.4% when Manning's n = 0.01 was used. The duration of runoff was extended to 120 minutes for the result of Manning's n = 0.1. Up to 50% of peak attenuation and 10 minutes peak lag were modelled when a high value of Manning's n was used.

The sensitivity analysis conducted above illustrates that the model results are sensitive to Manning's n, and this parameter needs to be carefully characterised.

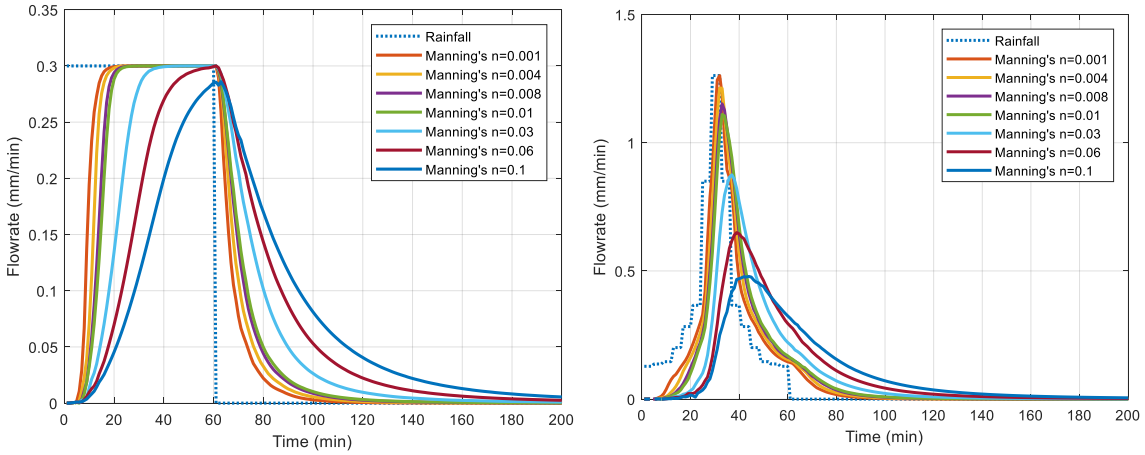

Figure 7.21. The sensitivity of the model results (two-stage physically-based model) to Manning's n.

7.6.4.2 Calibration of Manning's n based on the measured field data

In this section, Manning's n for the drainage layer was recalibrated based on the measured rainfall-runoff data from the field green roof test bed in response to the five selected real rainfall events (Section 7.6).

Figure 7.22 shows the relationship between Manning's n and the mean value of R_t^2 for the five selected rainfall events. A significant improvement was witnessed in the model results following calibration. The best estimated Manning's n, based on the five selected rainfall events, is 0.05, and the corresponding mean R_t^2 is 0.869. The improved model results confirm that the difference between the modelled and measured runoff profiles in Section 7.6.3 is likely to be caused by the physical variations in the synthetic drainage layer. The calibrated Manning's n for the field green roof drainage layer (i.e. 0.05) is significantly higher than the value determined for the same drainage layer in the isolated tests (i.e. 0.0017). However, it should be noted that the growing environment for the field green roof test bed is different from the laboratory test bed. TB1 is a vegetated test bed. The roots system developed in the substrate could change the physical properties of the substrate (De-Ville et al., 2017). At the same time, root networks could extend to the filter sheet and reduce its water permeability. If the roots keep developing into the drainage layer, then the roughness of the drainage layer could increase. **Figure 7.23** shows an aged green roof in which the root system penetrated through the filter sheet and reached the drainage layer. This explains why the calibrated Manning's, based on the field data, is higher than the one that was determined for the clean laboratory drainage layer.

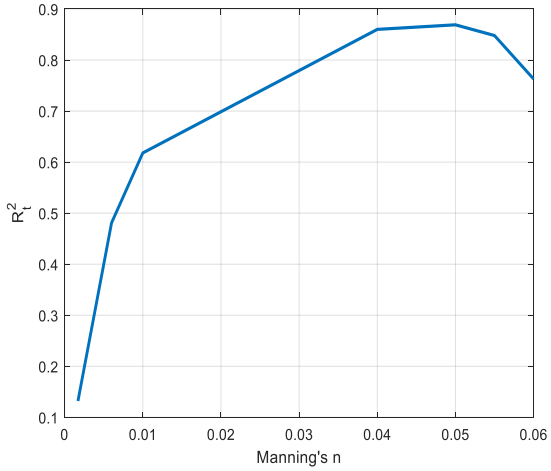

Figure 7.22. The relationship between Manning's n and the mean R_t^2 of the five selected rainfall events.

Figure 7.23. Example of a sedum vegetated green roof system that roots system reached drainage layer (Source: https://www.gtspecifier.co.uk/green-roofs-living-walls/green-roof-garden-vegetation/sedum-green-roof-trays).

Figure 7.24 shows the model results for the five selected rainfall events using Manning's n of 0.006 and 0.05. 0.006 is the calibrated value for the FD 25 drainage layer using the detention tests conducted with a complete, new, green roof test bed in the laboratory. 0.05 is the calibrated value for the FD 25 drainage layer using the runoff data from the established field test bed in response to the five selected rainfall events. More significant detention was modelled when Manning's n was increased from 0.0017 to 0.006 (**Figure 7.20** and **Figure 7.24**). The model provided the best overall estimations of the runoff profiles with Manning's n = 0.05. However, the model still slightly underestimated the detention in some cases. For example, in the event on 8/Nov/2014, the modelled peak runoff due to the first rainfall peak is 5 minutes earlier than measured, and in the event on 26/Aug/2015, the model underestimated the peak runoff rate by approximately 50 % and delayed the peak runoff by approximately 20 minutes in response to the

first rainfall peak. The model showed some problems in response to short-duration rainfalls. For example, in the event on 21/Oct/2013, several short rainfall events (5 minutes to 10 minutes) happened between the two main rainfall events; the model tends to skip those small rainfalls and provides a high runoff rate. This is a problem caused by the modelling time-step (5 minutes time-step was used in the model as the data was collected at 5 minutes interval), and a shorter time step may help solve this problem. However, for a long-term simulation, decreasing modelling time step means an increase in computational cost.

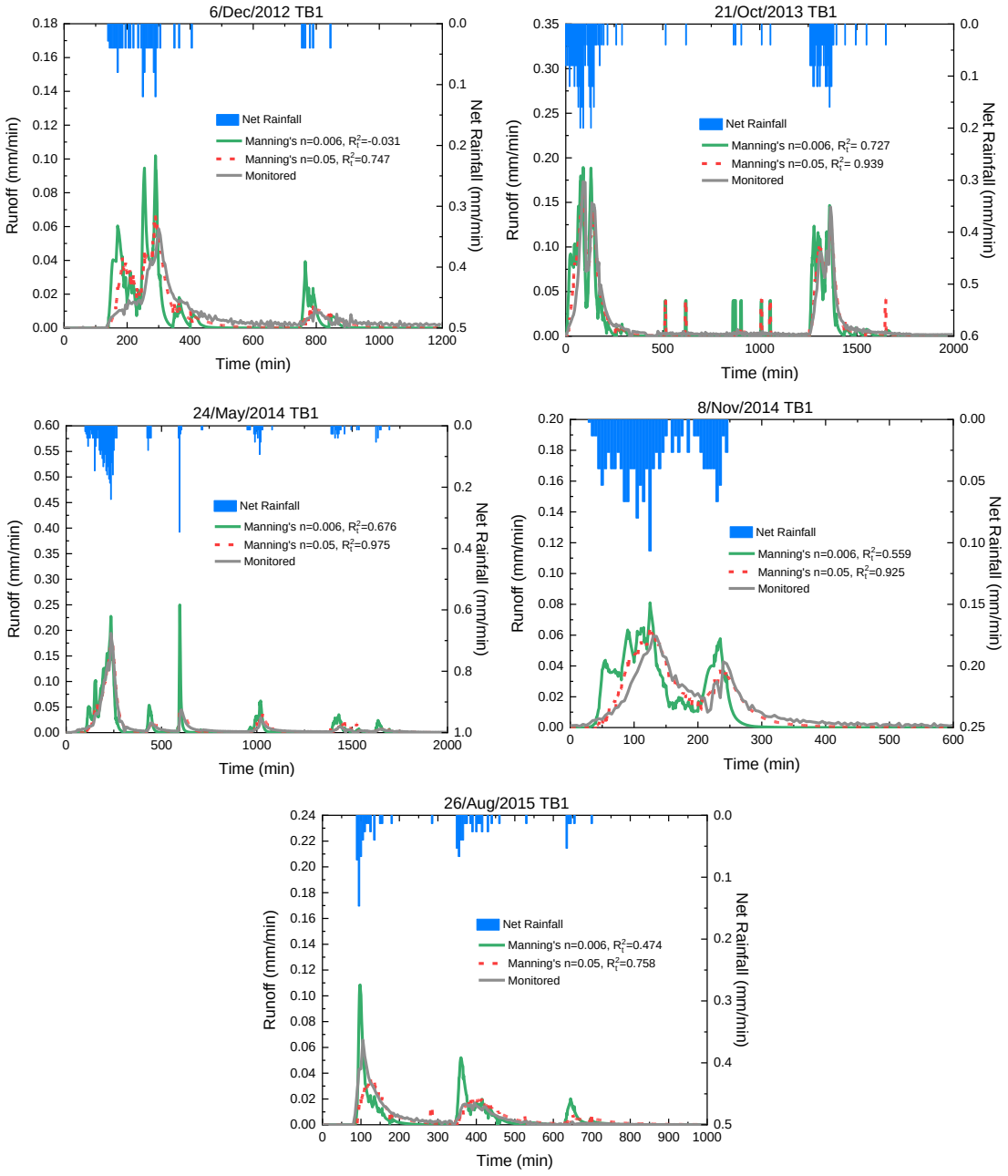

Figure 7.24. Modelled and measured runoff profiles for the five selected rainfall events using the physically-based model and different values of Manning's n.

7.6.4.3 Influence of model and model parameters

In Section 7.5, it has been found that the model parameters determined from laboratory tests do not represent the behaviour of a field green roof test bed. The influence of model combinations and model parameters on the model results will be explored in this section.

The two-stage physically-based model (Section 7.4) consists of two independent models for the substrate and the drainage layer. The two-stage model developed in Vesuviano (2014) (Equations 4.2 and 4.3) is a model that represents the substrate and the drainage layer detention using two Reservoir Routing models independently. In this section, 12 model combinations were used to investigate the influence of model types and model parameters.

Table 7.2 gives the value of parameters and model combinations of the 12 models. The value of parameters (substrate parameters and drainage layer parameters) for Model 1 was determined in this study in Section 7.5; the value of parameters for the drainage layer model in Model 2 were calibrated based on the field test bed data by fixing the substrate parameters to $n_G = 2.0$ and $k_G = 0.212$ (Peng et al., 2019). The drainage layer parameters in Model 3 were the reported values for the 3 m FD 25 drainage layer in Vesuviano (2014). The value for Manning's n in Model 4 was the calibrated value based on the measured rainfall-runoff date from the field test bed. The substrate parameters in Model 5 were calibrated for a 100 mm MCS substrate based on the substrate isolated detention tests (Yio et al., 2013). The substrate parameters in Model 9 were the estimated values for the 80 mm HLS substrate in Vesuviano (2014) based on the measured data for the 50 mm and a 100 mm MCS in the laboratory. It should be noted that the parameters for the substrate Reservoir Routing model were derived from the 100 mm MCS due to a lack of information on the 80 mm HLS substrate. However, it is acknowledged that this practice could introduce uncertainties to the model results. The two design storms in Section 7.5 were used to investigate the difference between models, and the 12 models were then used to generate the runoff profiles from the field test bed in response to the five selected rainfall events.

Table 7.2. Model parameters for the 12 models.

Substrate Model	Drainage Layer Model			
	Saint Venant Model (n =0.0017) (Lab*)	Reservoir Routing (Peng et al., 2019), (n_D=1.196; k_D=0.026) (Field*)	Reservoir Routing (Vesuviano, 2014), (n_D=1.72; k_D=0.652) (Lab*)	Saint Venant Model (n=0.05) (Field*)
Richards Equation (HLS, Three-segment Curve) (Lab*)	Model 1	Model 2	Model 3	Model 4
Reservoir Routing (Yio et al., 2013), (n_G=2.0; k_G=0.212) (Lab*)	Model 5	Model 6	Model 7	Model 8
Reservoir Routing (Vesuviano, 2014), (n_G=2.27; k_G=0.436) (Lab*)	Model 9	Model 10	Model 11	Model 12

*Note: Lab indicates the value of parameters were determined based on the component isolated laboratory tests, and field indicates the value of parameters were characterised based on the measured field green roof test bed data.

Figure 7.25 shows the results of the 12 models. In the constant rainfall event (i.e. 0.3 mm/min), Model 1 and Model 3, Model 5 and Model 7, Model 9 and Model 11 provide the same runoff profiles, which is not surprising as the parameters for the drainage layer in these paired models were derived from the same drainage layer tests. When the same models were used for the drainage layer, the model results were solely influenced by the substrate model. However, based on the results using the models in the same column of **Table 7.2**, it may be seen that the impact of the substrate models is minor, and the differences observed between models are primarily due to the drainage layer parameters. The models provided very close model results when the same model parameters were used for the drainage layer. However, the Richards Equation did provide slightly more significant detention effects than the two Reservoir Routing models. Comparing the results of the models in the same row, the models using parameters of n_D = 1.196 and k_D = 0.026 for the drainage layer provided the most detention effects (models 2, 6 and 10), followed by the Manning's n of 0.05 in the Saint Venant model. Although the parameters of n_D = 1.196, k_D = 0.026 and Manning's n = 0.05 were calibrated for the drainage layer based on the field test bed data, the model results of the two are not totally equivalent. This is because a much larger dataset (i.e. 444 events) was used to calibrate the parameters for the substrate Reservoir Routing model. In

contrast, only five events were used to calibrate Manning's n in the Saint Venant model. In response to the time-varying rainfall event, Model 7 and model 11 experienced stability problems due to the high value of drainage layer parameters (i.e. $n_D = 1.72$; $k_D = 0.652$).

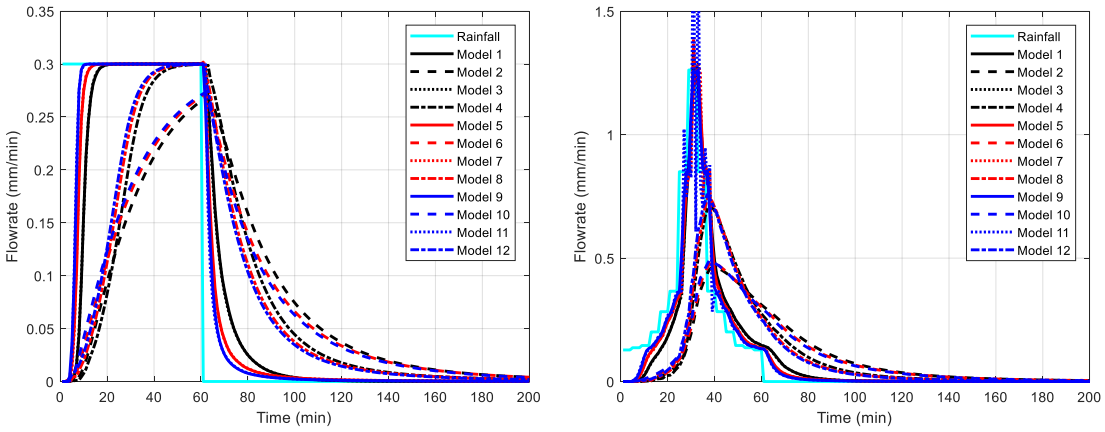

Figure 7.25. Model results of the 12 models (**Table 7.2**) in response to two design storms (the measured runoff profiles for these two events can be found in **Figure 7.14**).

Figure 7.26 shows the value of R_t^2 for the modelled runoff profiles in response to the five selected rainfall events using the 12 models in **Table 7.2**. As discussed earlier, the differences in model results are primarily due to the parameters of the drainage layer; the models using the same drainage layer parameters showed similar results. The models using the drainage layer parameters that were calibrated from field green roof test bed data (i.e. Models 2, 4, 6, 8, 10, 12) generally had better performance than the models using the parameters determined based on the drainage layer isolated experiments in the laboratory (i.e. Models 1, 3, 5, 7, 9, 11). This may indicate that the parameters characterised in the drainage layer isolated tests are not suitable to represent the performance of the component in a complete field green roof system. Calibration is needed to characterise the model parameters based on the field data in order to obtain an accurate prediction of the field green roof system behaviour.

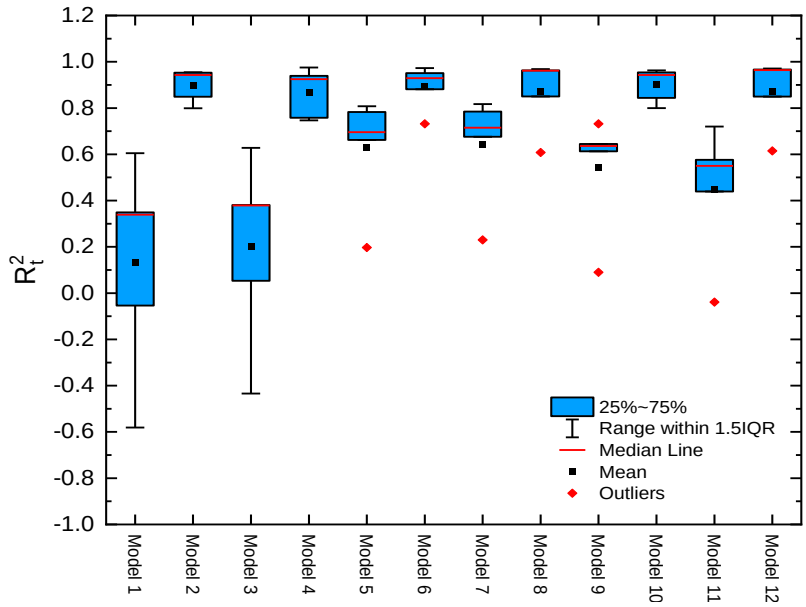

Figure 7.26. R_t^2 distribution of the modelled runoff profiles in the five selected rainfall events (**Table 4.3**) using the 12 models in **Table 7.2**.

7.6.5 Conclusions

The two-stage physically-based green roof detention model was used to regenerate the runoff profiles from a field green roof test bed. It was found that the model failed to provide accurate predictions of the runoff profiles using the parameters determined from the laboratory component isolated tests. Due to root development, the roughness of the drainage layer of the field test bed is believed to be changed, and the drainage layer used in the laboratory cannot represent its behaviour in the field anymore. Sensitivity analysis on the two-stage physically-based found that the model results are sensitive to the Manning's n, and the model provided acceptably accurate model results after the Manning's n was recalibrated based on the measured field data. Further investigation into the substrate and drainage layer model combinations revealed that no matter which model was used, model parameters need to be calibrated based on the field data to accurately predict the performance of a field green roof.

8 Validation of the Physically-based Green Roof Detention Model with an Innovative Green Roof System

8.1 Chapter overview

In Chapter 7, a two-stage green roof detention model was developed and validated against a conventional green roof system. In this chapter, the same model is used to simulate the detention performance of an innovative green roof system. The model performance is assessed based on the measured runoff profiles from the complete system set-up, and further calibration of model parameters is conducted to improve model results. Limitations of the physically-based detention model to model the innovative green roof system are discussed at the end of the chapter.

This chapter forms part of the following publication:

Peng, Z., Garner, B., Stovin, V., 2021. Two green roof detention models applied in two green roof systems. *J. Hydrol. Eng.* (under review).

8.2 The innovative green roof system

Figure 8.1 shows the configuration of the innovative green roof system used in this study. The innovative green roof system refers to a system developed based on testing and research performed by Green Roof Diagnostics, which is commonly referred to as "the Purple-Roof Concept" (https://www.purple-roof.com/). One embodiment of this green roof system consists of 20 mm sedum vegetation, 50 mm Moerings Mix #9 Substrate (MMS), 50 mm needled mineral wool, 50 mm honeycomb detention reservoir and 5 mm detention layer (**Figure 8.1**). The Moerings Mix #9 Substrate was developed and blended to be representative of an ideal green roof substrate for the eastern USA. The tested system is 6.1 m long, 1.1 m wide, and it was placed on a base of 2% slope. The concept of this innovative system is to maximise the retention and detention capacity by adding extra storage and detention layers to the system. The mineral wool is made from lightweight mineral fibre. In the green roof system, the mineral wool increases plant-available water for a longer period of time after rainfall compared with an aggregate substrate. The primary hydrological function of the mineral wool is to increase retention at the beginning of rainfall events. During storms, once the rainfall exceeds the maximum water retention capacity of the mineral wool, the mineral wool conducts water without any significant detention effects. The honeycomb detention reservoir is a panel of small diameter (10 mm in this study), vertically oriented, solid-wall tubes. In the green roof system, the honeycomb holds water inside the array of tubes, thereby preventing horizontal flow and increasing the storage capacity

of the system. The detention layer at the bottom of the system is a flexible layer comprising vertically oriented polyester threads between two knitted layers of tightly woven polyester fabric. The detention layer increases detention performance by reducing the outflow rate, thus allowing water to backfill into the overlying honeycomb.

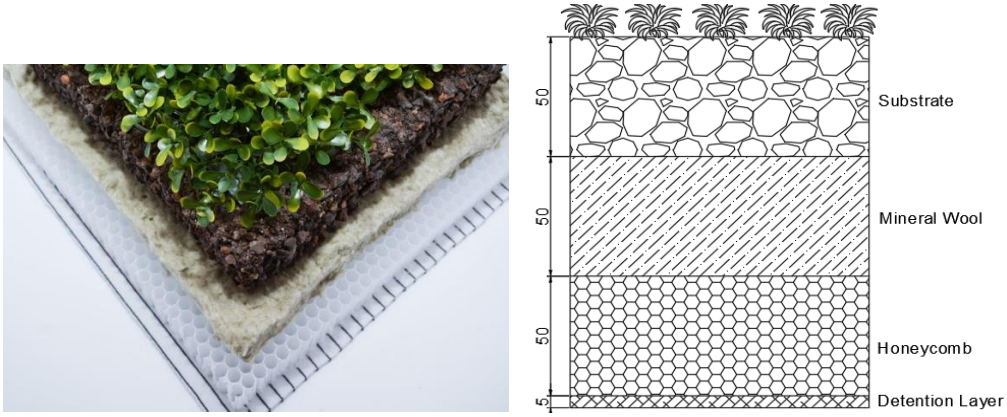

Figure 8.1. The configurations of the innovative green roof system (dimensions in mm) (source: https://www.purple-roof.com/).

8.3 Experimental set-up and test programme

Two types of detention test were undertaken in the laboratory with the innovative green roof system, and the full description of the test programme can be found in Section 3.5.4.

8.4 Model implementation

8.4.1 Model representation

Although the innovative green roof system consists of multiple layers, not every layer in the system contributes to detention. The detention impact of mineral wool was neglected in the model, and the honeycomb and the detention layer were combined and modelled by one model. The physically-based detention model that represents detention in the substrate using the Richards Equation and in the detention layer by the Saint Venant Equation was illustrated in **Figure 8.2** and used to model the detention processes in the innovative green roof system.

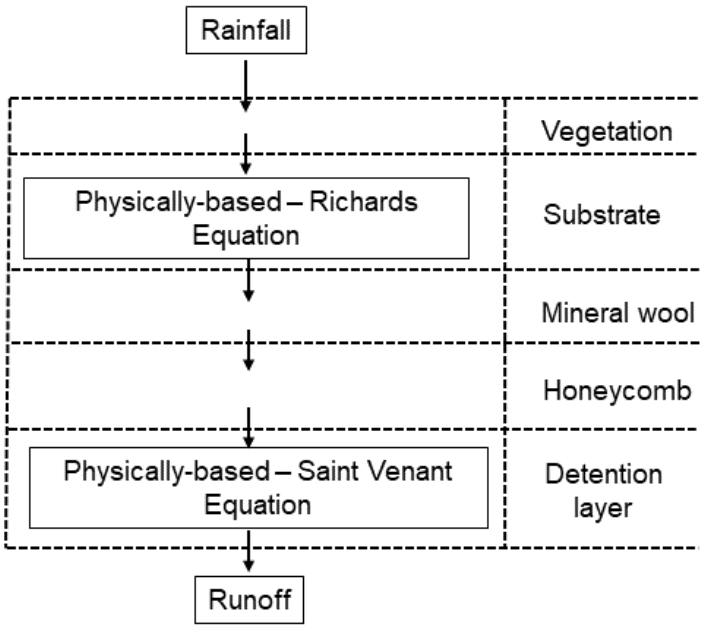

Figure 8.2. The physically-based detention model for the innovative green roof system.

8.4.1.1 Substrate layer — Richards Equation

The substrate layer of the system is modelled by the Richards Equation (Equation 2.19). Previous chapters have demonstrated that the Durner model (Durner, 1994) provides the best representation of the Soil Water Release Curve (SWRC) for green roof substrates (Chapters 4 and 5), and a three-segment curve provides the best estimation of a green roof substrate Hydraulic Conductivity Function (HCF) (Chapter 5). However, as the HCF for the substrate used in the innovative green roof system has not been experimentally determined, the conventional approach of Durner-Mualem (Equations 2.5 and 2.9) was used for this substrate. Whilst using an estimated HCF for the substrate introduces uncertainty into the model, the substrate in the innovative green roof system is only 50 mm deep, the influence of the substrate model is minor on the final model results.

Following the approach described in Chapter 4, a constant head (equivalent to the suction head at field capacity) boundary condition was used for the lower boundary, a time-varying flux condition (equivalent to the rainfall input) was assigned for the upper boundary condition, and a constant hydraulic head was set for the initial conditions.

8.4.1.2 Detention layer — Saint Venant Equation

The 1D gradually varied unsteady flow Saint Venant equation (as developed in Chapter 7, Equation 7.5) was used to model the detention layer.

Simulations were implemented in MATLAB with 1-minute time-steps, and 0.5 mm vertical spatial steps were used for the Richards Equation, and 100 mm horizontal spatial steps were used for the Saint Venant equation. Simulations started from field capacity to exclude retention effects, and the initial storage in the detention layer at the beginning of the simulation was set to be zero.

8.4.2 Model parameters

Table 8.1 lists the value of parameters used in the model for the innovative green roof system. The SWRC parameters for the substrate used in the innovative green roof system were based on the Durner model (Equation 2.9), for which the parameters were fitted to data points measured using the hanging column method (**Figure 8.3**, test data provided by Green Roof Diagnostics).

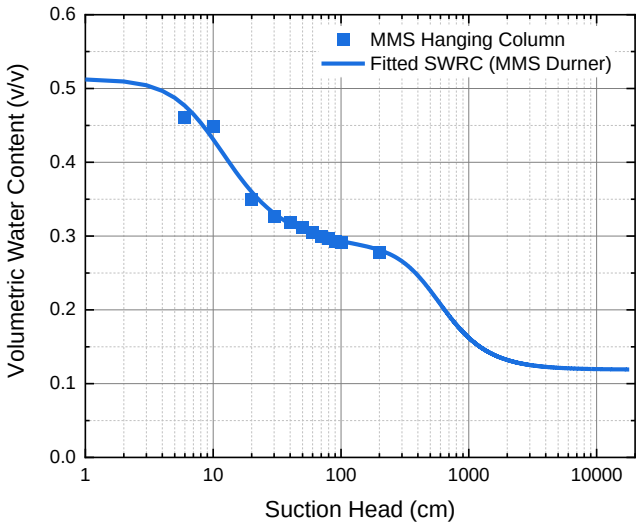

Figure 8.3. Measured SWRC and fitted Durner model for the MMS.

Table 8.1 Value of parameters for the MMS substrate.

Parameter	Value
Θ_s	0.513
Θ_r	0.119
α_1	0.108
n_1	2.344
α_2	0.002
n_2	2.834
w_1	0.579
Permeability	14.7 mm/min
R_t^2	0.988

8.5 Model validation and calibration

R_t^2 was used to evaluate the goodness-of-fit of the modelled runoff. Comparisons between the model predictions and measured laboratory data are presented in two stages. Firstly, the measured and modelled runoff profiles for the detention layer isolated tests are introduced. Secondly, the substrate layer model is introduced to evaluate the multi-layered models' abilities to reproduce the runoff profiles observed in the complete system. It is possible that the detention layer will perform differently within the complete system due to interactions with the overlying layers. Further calibration of Manning's n was conducted using the measured runoff data from the complete system to improve the model results.

8.6 Results

8.6.1 Detention performance

8.6.1.1 Detention layer

Figure 8.4, **Figure 8.5** and **Figure 8.6** show the measured runoff from the detention layer in isolation in response to the three rainfall intensities (with two replications of each intensity). The rainfall was designed to apply for 15 minutes at a constant rate; however, fluctuations, especially in the lowest rainfall intensity, were observed. The duration of the applied rainfall is slightly longer than 15 minutes in all the tests, and this could be due to the delay in the electronic control system.

The total cumulative runoff is slightly lower than the total applied rainfall in the two events at the lowest rainfall intensity (0.17 mm/min, **Figure 8.4**). This could be because the detention layer releases water slowly after the storms, and without giving sufficient time for drainage, some water was still temporarily stored in the detention layer. In response to the other rainfall intensities (**Figure 8.5** and **Figure 8.6**), almost all rainfall has left the detention layer as runoff. Variations were also observed between the two repeat tests (both in the rainfall profiles and cumulative rainfall depths), such that the total runoff from the detention layer is slightly different in the two repeat tests. This could be caused by the unstable performance of the rainfall simulator and/or the accuracy of the runoff measurement instrument.

As the duration of the rainfall was short, an equilibrium state was not achieved in all tests. The detention performance, in this case, was assessed based on the peak attenuation. The detention layer reduced the peak rainfall intensity by approximately 18% to 50% in the storms. Even in the highest rainfall intensity (1.9 mm/min, **Figure 8.6**), the peak runoff is significantly lower than the peak rainfall, which indicates that the detention layer has the potential to provide detention effects.

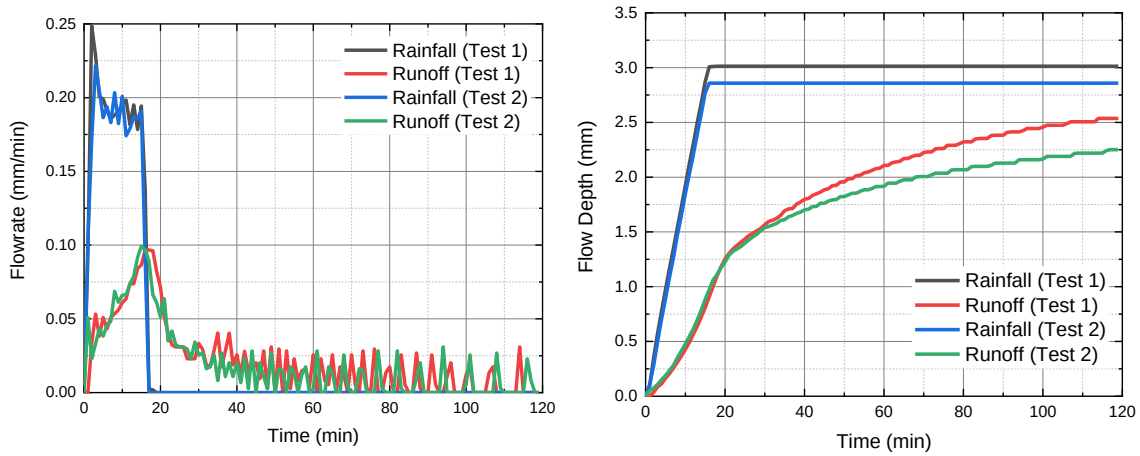

Figure 8.4. Measured runoff from the detention layer in response to the low rainfall intensity (0.17 mm/min).

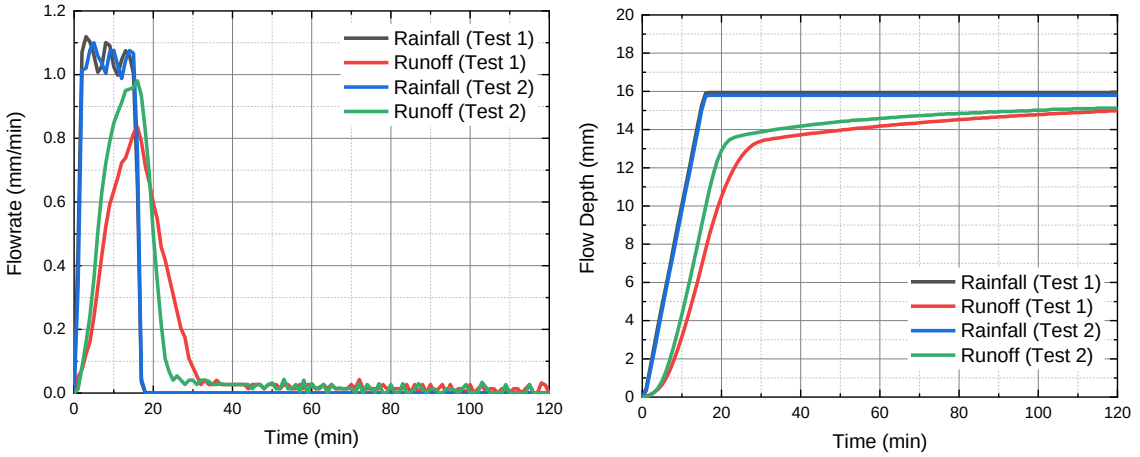

Figure 8.5. Measured runoff from the detention layer in response to the medium rainfall intensity (0.78 mm/min).

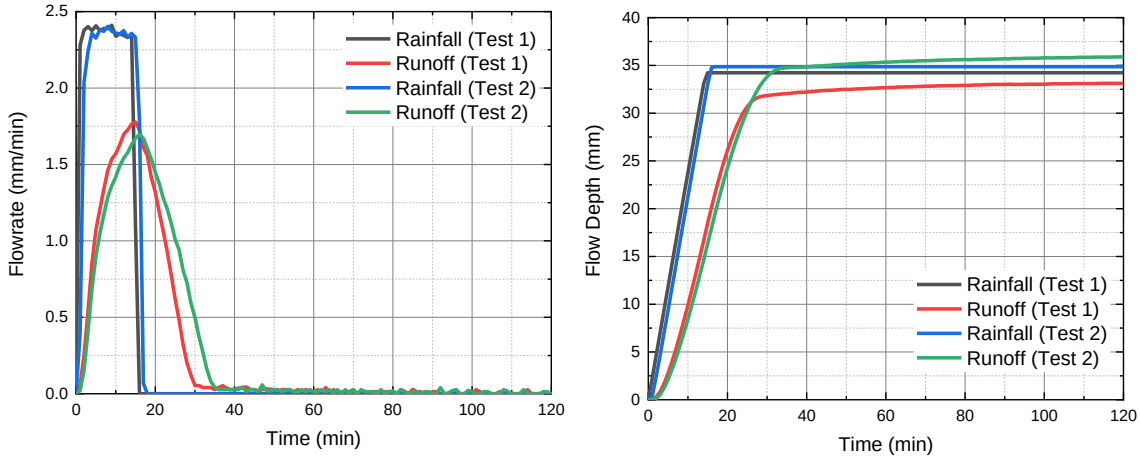

Figure 8.6. Measured runoff from the detention layer in response to the high rainfall intensity (1.9 mm/min).

Figure 8.7 shows the temporary storage in the detention layer calculated from the difference between the cumulative rainfall and runoff depth at each time step. At the two low rainfall intensity events (0.17 mm/min, Tests 1 and 2), the storage in the layer is below 5 mm (the thickness of the detention layer), which indicates the water is flowing through the layer. During the two medium rainfall events (0.78 mm/min, Tests 1 and 2), temporary storage in the detention layer exceeded 5 mm 10 minutes after the rainfall, indicating water flowing over the surface of the detention layer may have occurred. In the two high rainfall intensity events (1.9 mm/min, Tests 1 and 2), temporary storage in the detention layer exceeded the thickness of the detention layer shortly after the rainfall, and water built up to 12 mm above the surface of the detention layer in the storms. This may indicate that a substantial proportion of water flowed over the surface of the detention layer in these high rainfall intensity events. It should be noted that the figure here only shows the length averaged temporary storage; it does not provide any information on the water distribution over the length of the detention layer.

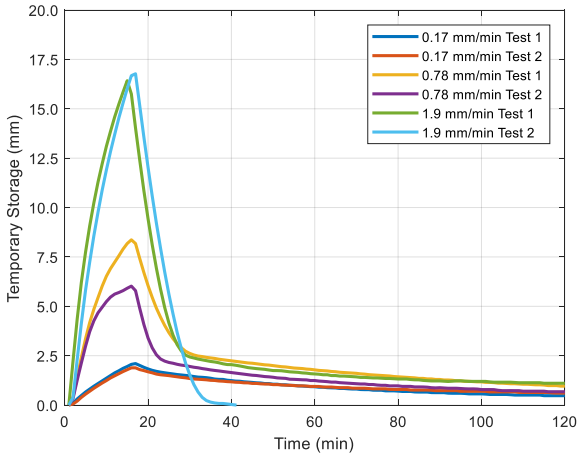

Figure 8.7. Temporary storage in the detention layer in response to the storms.

8.6.1.2 Complete system

Figure 8.8, **Figure 8.9** and **Figure 8.10** show the measured runoff from the complete green roof system in response to the storms. As variations in rainfall were observed continuously, four replications were conducted with the low rainfall intensity (**Figure 8.8**). Two replications were conducted with the medium rainfall intensity (**Figure 8.9**), and three replications were conducted with the high rainfall intensity (**Figure 8.10**). The fluctuation in rainfall, which was caused by the rainfall simulator, is significant at the low rainfall intensity. However, the rainfall was relatively stable at medium and high rainfall intensities (**Figure 8.9** and **Figure 8.10**). The runoff profiles from the two repeat tests are consistent, which indicates good repeatability of the tests. The total depth of rainfall and runoff are consistent in most cases. However, slightly higher runoff (0.5 mm)

was measured for the first two repeat tests at the lowest rainfall intensity (**Figure 8.8**), and slightly lower runoff (2 mm) was observed in the test with the medium rainfall intensity (**Figure 8.9**).

An equilibrium state was not achieved due to the short duration of the rainfall events. The green roof system reduced the peak rainfall by approximately 45% to 75% in the storms. Given higher percentages of peak runoff reduction were achieved by the complete green roof system (45% to 75% peak attenuation) than the isolated detention layer (18% to 50% peak attenuation), it can be included that by adding additional layers to the green roof system, the detention performance was improved. However, it should also be noted that the rainfall profiles measured during the detention tests with the detention layer and the complete system tests were not exactly the same; the peak reduction is influenced by the actual applied rainfall.

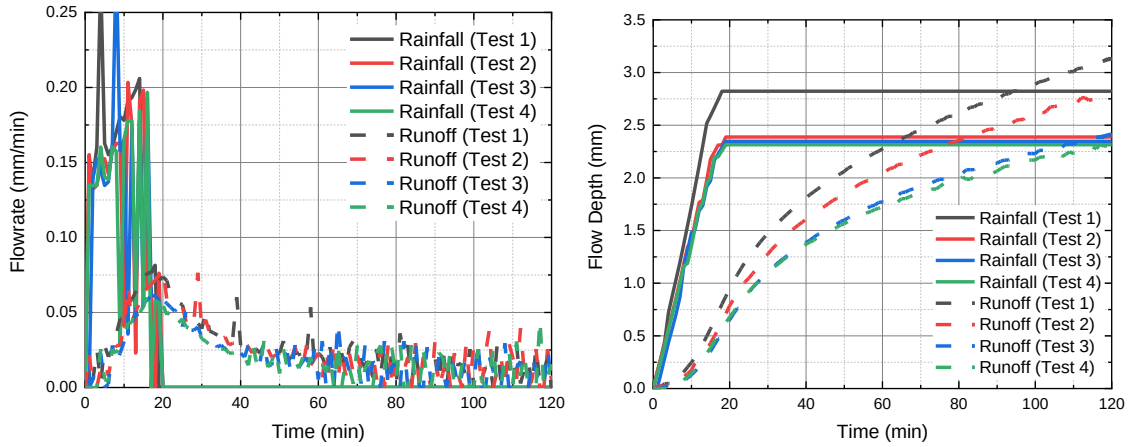

Figure 8.8. Measured runoff from the complete innovative green roof system in response to the low rainfall intensity (0.17 mm/min).

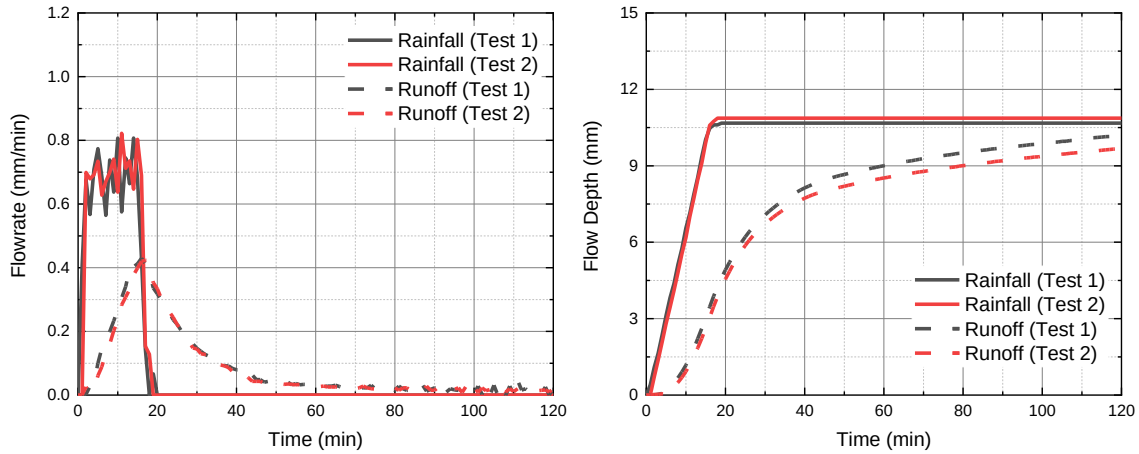

Figure 8.9. Measured runoff from the complete innovative green roof system in response to the medium rainfall intensity (0.78 mm/min).

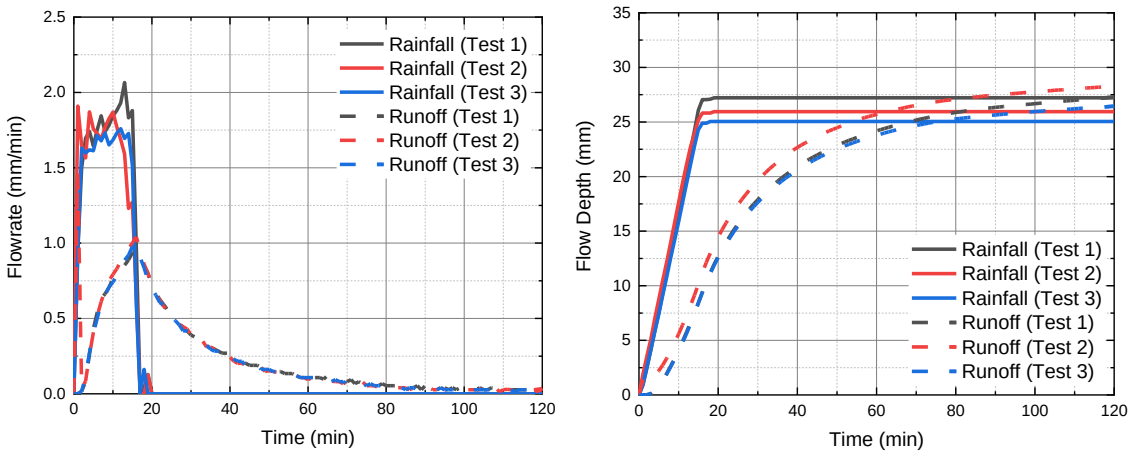

Figure 8.10. Measured runoff from the complete innovative green roof system in response to the high rainfall intensity (1.9 mm/min).

Figure 8.11 show the temporary storage within the complete green roof system during the storms. The temporary storage was calculated from the measured cumulative rainfall-runoff data. The temporary storage here includes the water stored in the substrate and honeycomb and/or detention layer. However, without more detailed information, it is impossible to know where and how much water is stored in each layer. Comparing with the temporary storage measured during the detention layer isolated tests, a slightly higher temporary storage was measured within the complete green roof. This could be due to the additional storage capacity provided by the substrate.

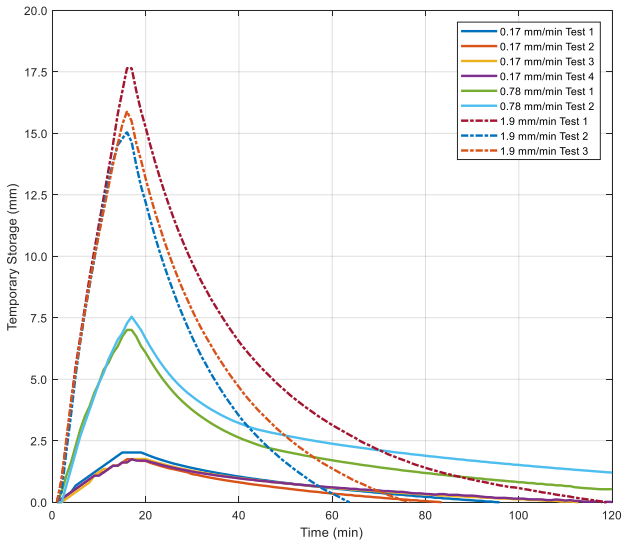

Figure 8.11. Temporary storage in the complete innovative green roof system in the storms.

8.6.2 Model validation

8.6.2.1 Detention layer

Figure 8.12 shows the relationship between Manning's n and the mean R_t^2 of the six tested events. The Manning's n identified for the detention layer in isolation was 0.017, and the highest mean R_t^2 of 0.8 was achieved by the model using this value.

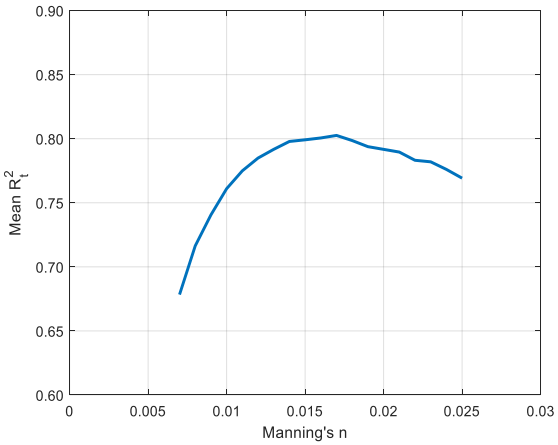

Figure 8.12. The relationship between Manning's n and mean R_t^2 of the modelled runoff from the detention layer in response to the six tests.

Figure 8.13, **Figure 8.14** and **Figure 8.15** show the modelled runoff from the innovative detention layer component in response to the three rainfall intensities using the identified value of Manning's n (0.017). As the rainfall applied to the two repeat tests was slightly different, two model results were obtained for each rainfall intensity. The model was able to simulate the runoff from the detention layer to some extent. At the low rainfall intensity (0.17 mm/min, **Figure 8.13**), the model appeared to overestimate detention effects. As the model accounts for the effects of horizontal flow, the peak runoff rate was maintained for a prolonged period. Although the model achieved high values of R_t^2 in the medium and high rainfall intensities, it is more meaningful to assess the model's performance based on the modelled runoff profiles. The model performed the best in the medium rainfall intensity (0.78 mm/min, **Figure 8.14**). However, the model overestimated the peak runoff by about 15.2% in the first test. In response to the high rainfall intensity (1.9 mm/min, **Figure 8.15**), the model significantly overestimated the peak (by approximately 40%).

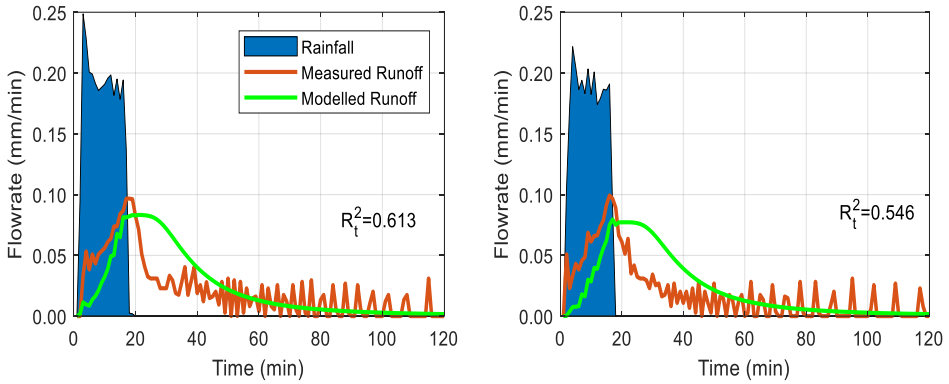

Figure 8.13. Measured and modelled runoff from the detention layer using the physically-based model (Manning's n = 0.017, at the low rainfall intensity, 0.17 mm/min).

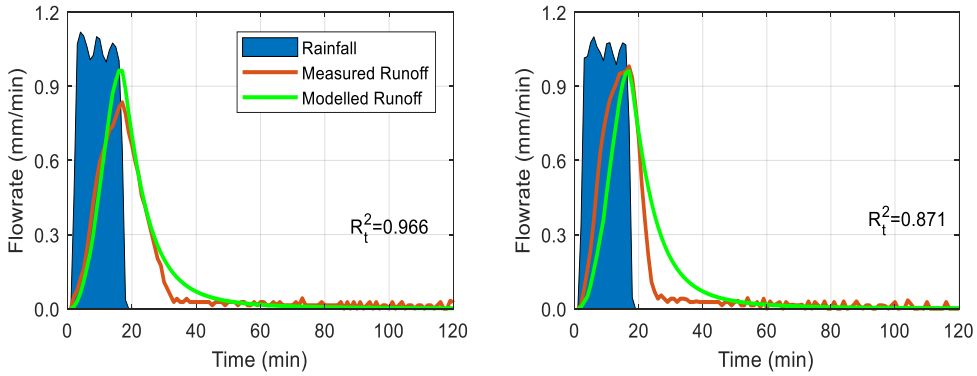

Figure 8.14. Measured and modelled runoff from the detention layer using the physically-based model (Manning's n = 0.017, at the medium rainfall intensity, 0.78 mm/min).

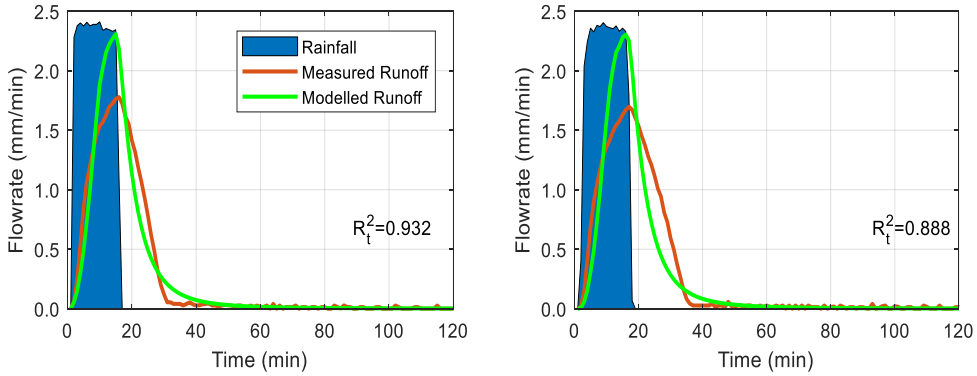

Figure 8.15. Measured and modelled runoff from the detention layer using the physically-based model (Manning's n = 0.017, at the high rainfall intensity, 1.9 mm/min).

Figure 8.13, **Figure 8.14** and **Figure 8.15** are the results of using a rainfall intensity independent Manning's n. However, It was observed that the best-fit parameter values for Manning's n increased with rainfall intensity (**Figure 8.16**). This suggests that the flow conditions in the

innovative detention layer are complicated, such that a constant value for the parameters may not be sufficient to fully describe the relevant processes.

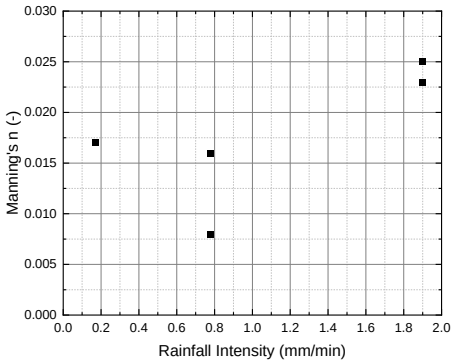

Figure 8.16. Optimised Manning's n for the detention layer in response to different rainfall intensities.

Figure 8.17, **Figure 8.18** and **Figure 8.19** show the modelled water level distribution within the detention layer using Manning's n of 0.017. As the rainfall applied to the two repeat tests was not identical, two model results were obtained for each rainfall intensity. The temporary storage in the detention layer in these cases is due to the direct rainfall dropped on the detention layer. Due to the free drainage boundary condition set for the outlet of the detention layer, the water builds up at the outlet of the layer. Consistent with the measured data (**Figure 8.7**), water was modelled to be kept within the detention layer during the low rainfall intensity (**Figure 8.17**), and it exceeded the upper boundary of the layer during the medium and the high rainfall intensity (**Figure 8.18** and **Figure 8.19**). However, limited by the measured data, it is not possible to assess the model performance in modelling the water level distribution along the length of the detention layer.

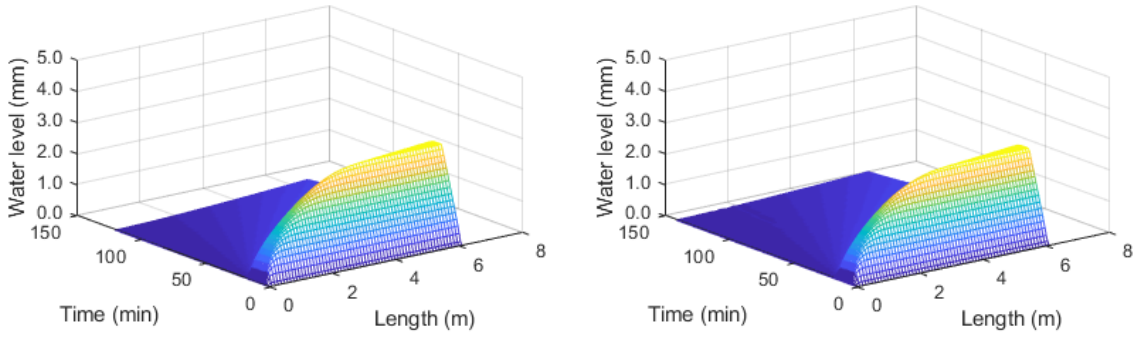

Figure 8.17. Modelled water level distribution within the detention layer in response to the low rainfall intensity (0.17 mm/min) using the physically-based model (Manning's n = 0.017).

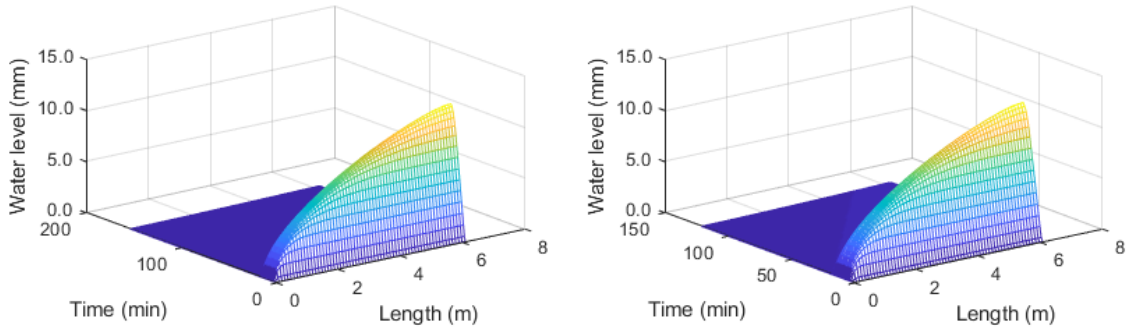

Figure 8.18. Modelled water level distribution within the detention layer in response to the low rainfall intensity (0.78 mm/min) using the physically-based model (Manning's n = 0.017).

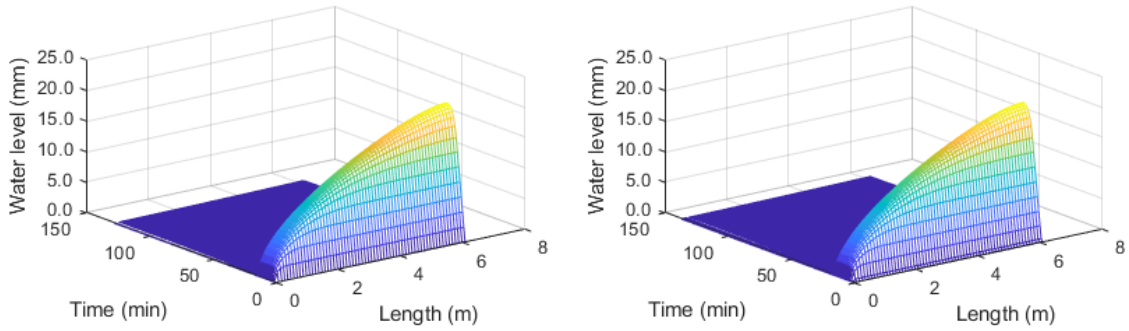

Figure 8.19. Modelled water level distribution within the detention layer in response to the low rainfall intensity (1.9 mm/min) using the physically-based model (Manning's n = 0.017).

8.6.2.2 Complete system

Figure 8.20, **Figure 8.21** and **Figure 8.22** show the measured and modelled runoff profiles from the complete innovative green roof system. The parameters used in the model for the substrate are listed in **Table 8.1**, and Manning's n used in the model (0.017) was as identified in Section 8.6.2.1. As the model is a two-stage model, the runoff from the substrate can be provided by the model (**Figure 8.20**, **Figure 8.21** and **Figure 8.22**). The model suggests that the 50 mm substrate provides very limited detention such that it did not show any detention effect in response to the high rainfall intensity (**Figure 8.22**).

The model provided reasonable estimations of the measured runoff profiles (i.e. R_t^2 ranges from 0.7 to 0.88). However, in response to the low rainfall intensity (0.17 mm/min, **Figure 8.20**), the model delayed the time of peak runoff. This is caused by the consideration of horizontal flow in the model; it takes time for the water added at the upstream end to flow to the outlet in the detention layer. In the two medium rainfall intensity events (0.78 mm/min, **Figure 8.21**), the

model overestimated the peak runoff by around 30%. In the three high rainfall intensity events (1.9 mm/min, **Figure 8.22**), the model overestimated the peak runoff by about 60%.

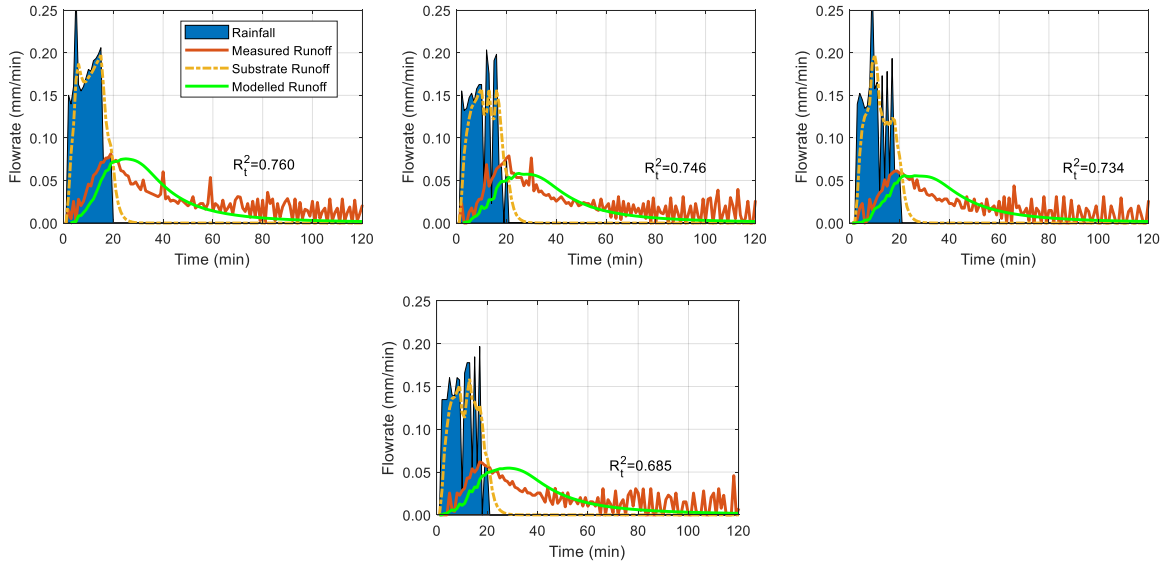

Figure 8.20. Measured and modelled runoff from the complete system using the physically-based model (Manning's n = 0.017, at the low rainfall intensity, 0.17 mm/min).

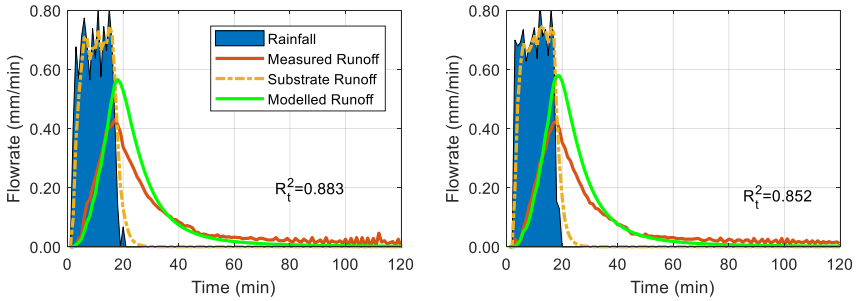

Figure 8.21. Measured and modelled runoff from the complete system using the physically-based model (Manning's n = 0.017, at the medium rainfall intensity, 0.78 mm/min).

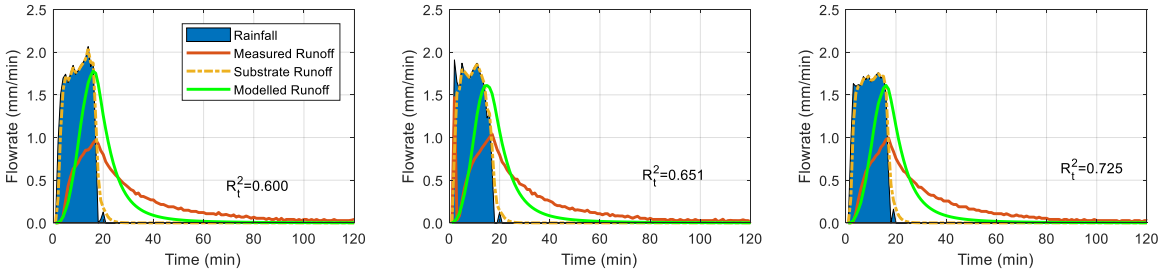

Figure 8.22. Measured and modelled runoff from the complete system using the physically-based model (Manning's n = 0.017, at the high rainfall intensity, 1.9 mm/min).

Figure 8.23, **Figure 8.24** and **Figure 8.25** show the modelled water level distribution in the detention layer and honeycomb. Water temporarily stored in the detention layer and/or honeycomb in these cases is due to the inflow from the substrate. As the water level was modelled to be lower than 5 mm in response to the low rainfall intensity events, water in these events was temporarily stored only within the detention layer (**Figure 8.23**). However, during the medium and high rainfall intensity events (**Figure 8.24** and **Figure 8.25**), the water level in the detention layer was modelled to exceed the depth of the detention layer and to be stored in the honeycomb. Due to the slope of the system, the water was modelled to enter the honeycomb at the middle length of the detention layer, and the stored water was quickly emptied after storms stopped. The maximum water level in these events was modelled to be significantly lower than 55 mm, which indicates that no backflow from the honeycomb to the substrate was modelled to occur. No measured data was obtained to validate the modelled water level distribution within the detention layer and honeycomb.

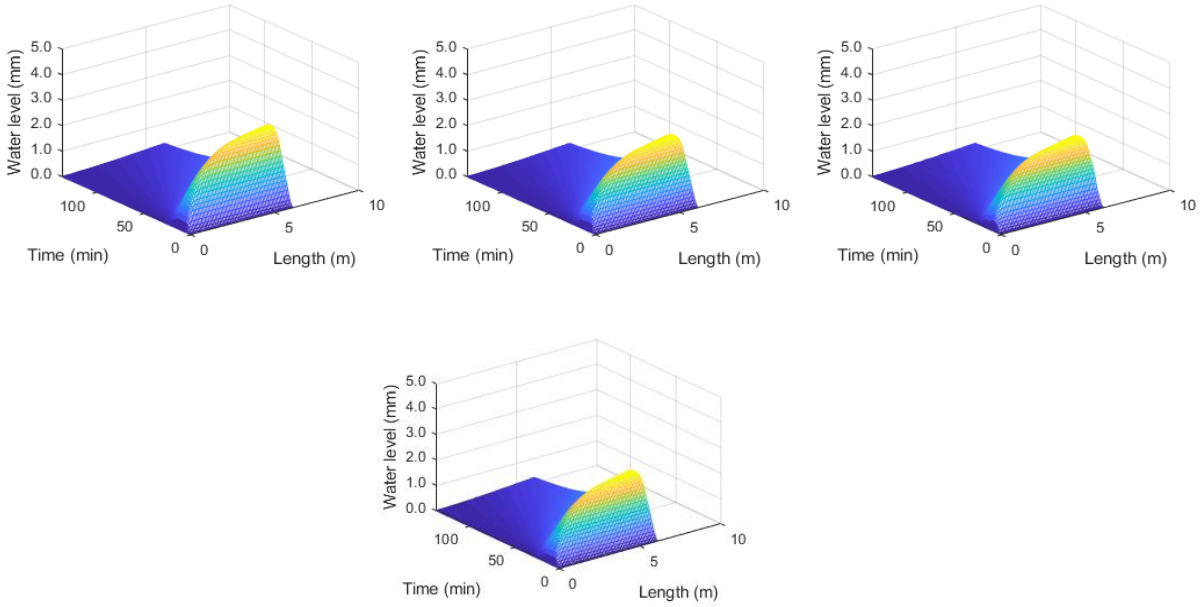

Figure 8.23. Modelled water level distribution within the detention layer in the complete system in response to the low rainfall intensity (0.17 mm/min) using the physically-based model (Manning's n = 0.017).

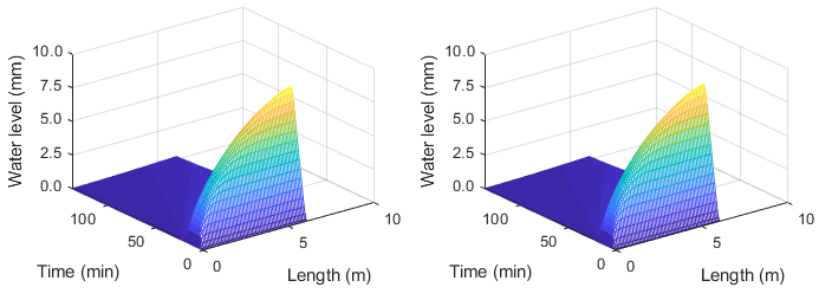

Figure 8.24. Modelled water level distribution within the detention layer in the complete system in response to the low rainfall intensity (0.78 mm/min) using the physically-based model (Manning's n = 0.017).

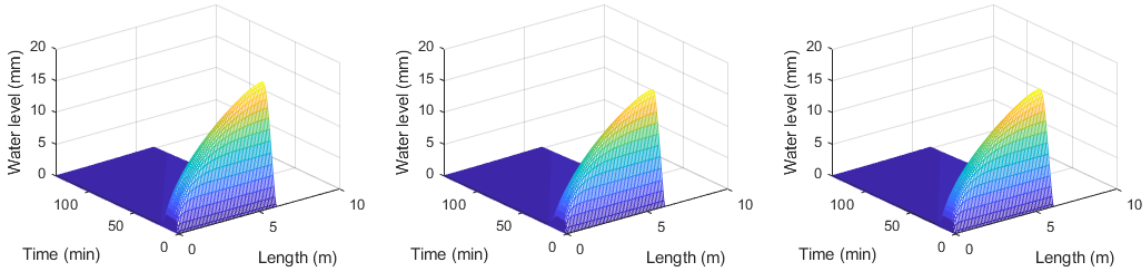

Figure 8.25. Modelled water level distribution within the detention layer in the complete system in response to the low rainfall intensity (1.9 mm/min) using the physically-based model (Manning's n = 0.017).

8.6.3 Model calibration

Figure 8.26 shows the relationship between the value of Manning's n and the mean R_t^2 of the nine tests. The highest R_t^2 of 0.78 was achieved by the model using Manning's n=0.028. A minor increase in R_t^2 (from 0.74 to 0.78) was observed when Manning's n was increased from 0.017 to 0.028. It should be noted that Manning's n in the model is a representation of the detention effect in the honeycomb and the detention layer. It is assumed that the honeycomb does not influence the horizontal flow in the detention layer. However, when the water level in the system exceeds the depth of the detention layer and reaches the honeycomb, the honeycomb will prevent horizontal flows due to the vertical obstacle, and this results in a higher Manning's n.

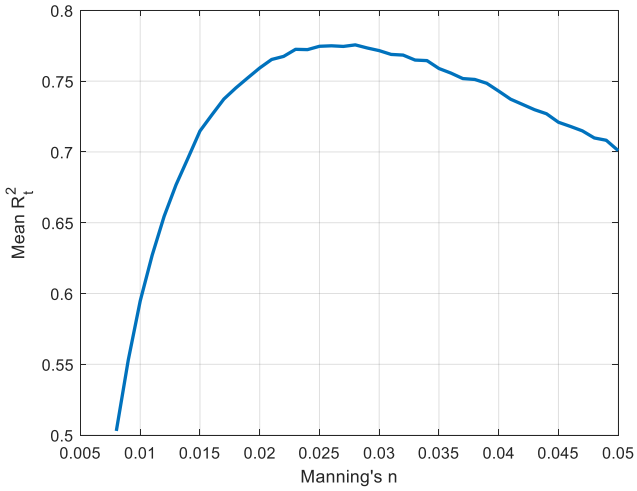

Figure 8.26. The relationship between Manning's n and mean R_t^2 of the modelled runoff from the complete green roof system in response to the nine tests.

Figure 8.27, Figure 8.28 and **Figure 8.29** show the modelled runoff from the complete green roof system using the calibrated Manning's n (0.028). The modelled substrate runoff is also presented in the figures. However, as Manning's n is a parameter for the detention layer, the modelled runoff from the substrate has not been changed. The peak runoff rate decreased in all cases when a higher value of Manning's n was used. In response to the low rainfall intensity events, the model underestimated the peak runoff rate by about 28% (**Figure 8.27**), and consistent with the model results with the detention layer, the model overestimated the influence of the drainage length in that the peak runoff rate was maintained for a long duration. The peak runoff in response to the medium rainfall intensity was estimated well (**Figure 8.28**). However, the model slightly overestimated the detention effects in the falling limb of the runoff profiles, and the time of peak runoff was also delayed about 3 minutes. In response to the high rainfall intensity (**Figure 8.29**), the model overestimated the peak runoff. Overall, after calibration, the model results were improved slightly. However, noticeable differences between the modelled and measured runoff profiles were still observed.

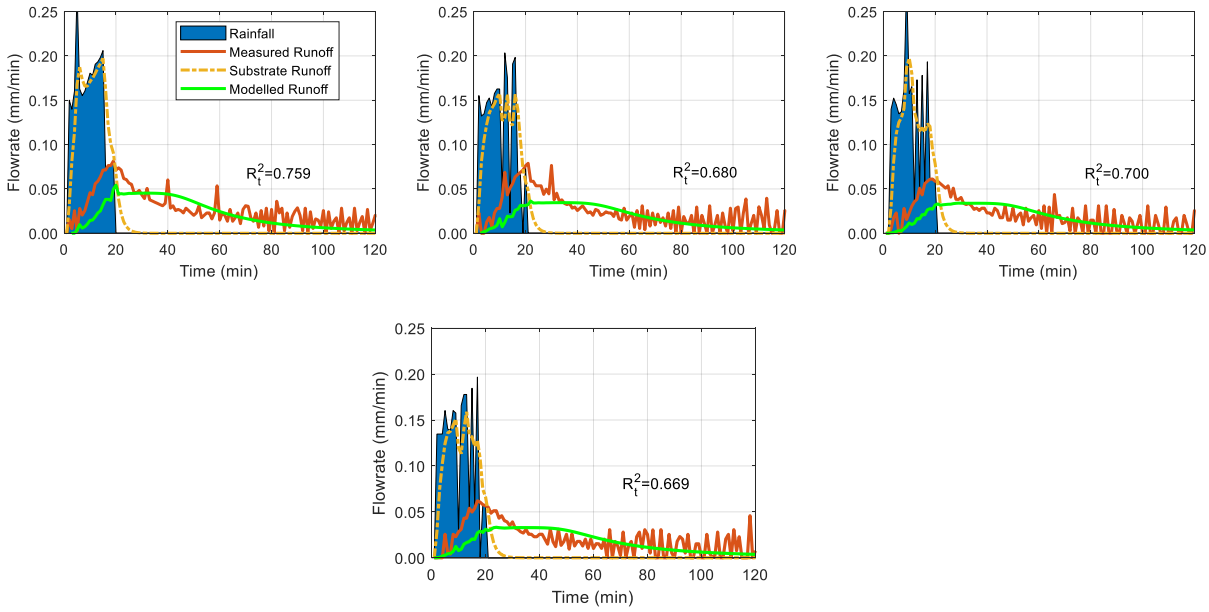

Figure 8.27. Measured and modelled runoff from the complete system using the physically-based model (Manning's n=0.028, at the low rainfall intensity, 0.17 mm/min).

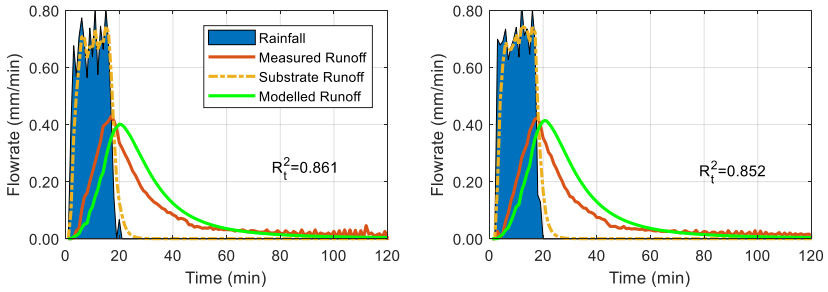

Figure 8.28. Measured and modelled runoff from the complete system using the physically-based model (Manning's n=0.028, at the medium rainfall intensity, 0.78 mm/min).

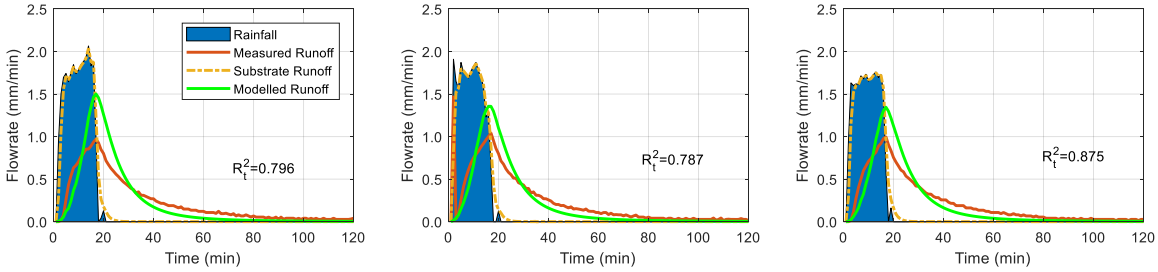

Figure 8.29. Measured and modelled runoff from the complete system using the physically-based model (Manning's n=0.028, at the high rainfall intensity, 1.9 mm/min).

Figure 8.30, **Figure 8.31** and **Figure 8.32** show the modelled water level distribution during the storms using the calibrated Manning's n of 0.028. Compared with the results of 0.017 (**Figure 8.23**, **Figure 8.24** and **Figure 8.25**), the maximum water depth in the detention layer and

honeycomb was increased in all storm events. However, the maximum water level is less than the total thickness of the detention layer and the honeycomb (55 mm).

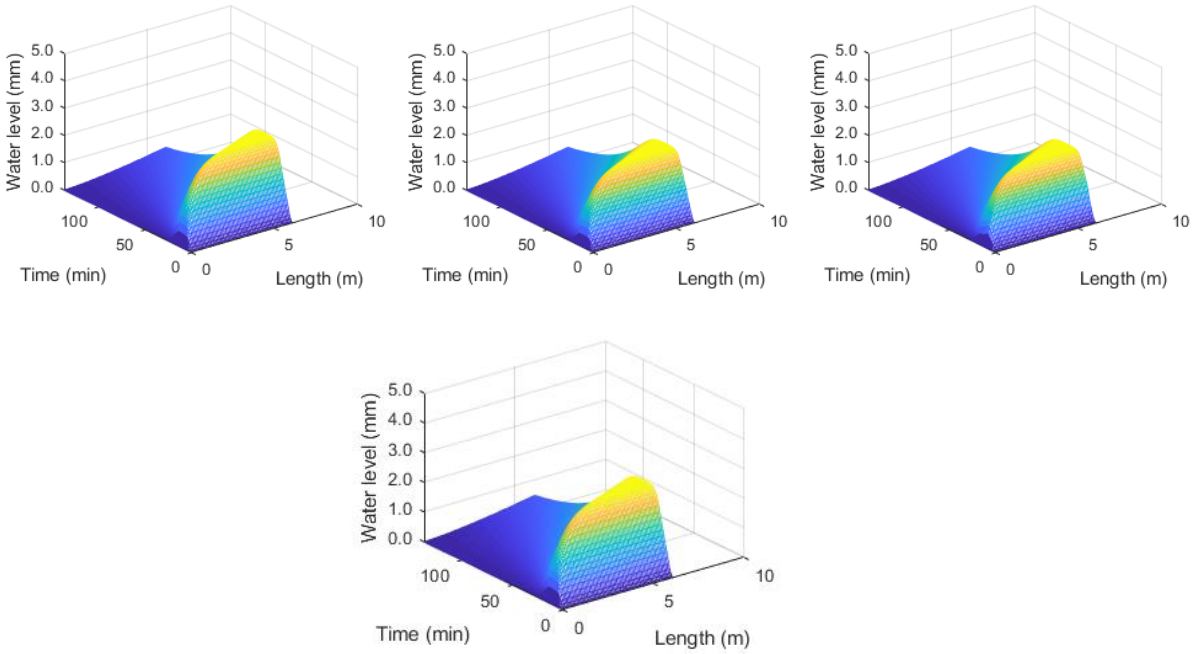

Figure 8.30. Modelled water level distribution within the detention layer in the complete system in response to the low rainfall intensity (0.17 mm/min) using the physically-based model (Manning's n = 0.028).

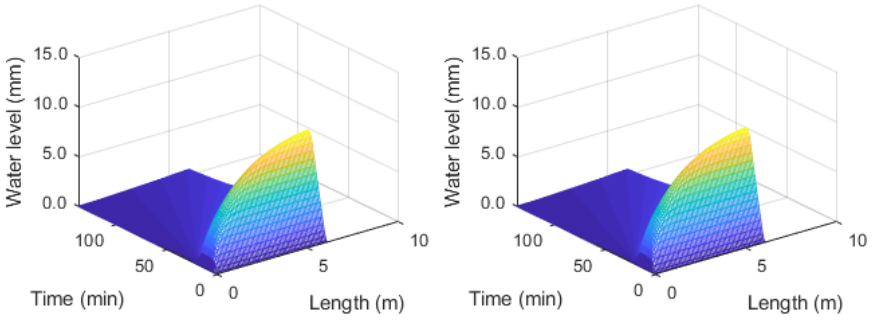

Figure 8.31. Modelled water level distribution within the detention layer in the complete system in response to the low rainfall intensity (0.78 mm/min) using the physically-based model (Manning's n = 0.028).

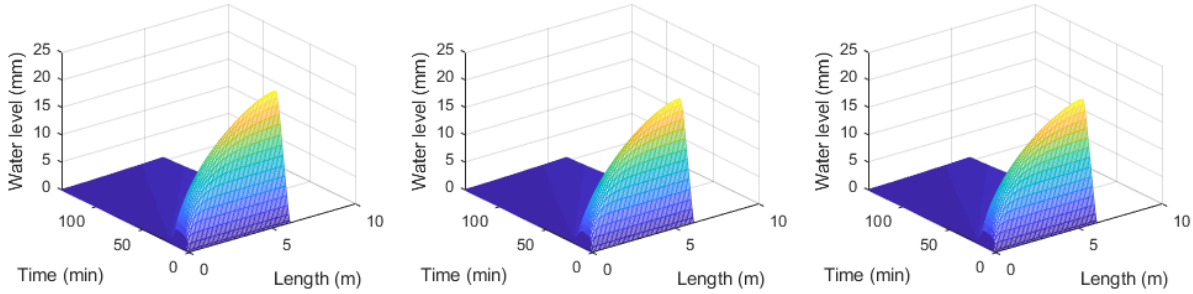

Figure 8.32. Modelled water level distribution within the detention layer in the complete system in response to the low rainfall intensity (1.9 mm/min) using the physically-based model (Manning's n = 0.028).

8.7 Discussion

One of the goals for this modelling exercise was to develop a physically-based model that can be parametrised from independent laboratory tests of the separate components without the need for any calibration. The work documented in this chapter accomplishes much of that goal. Transferability of parameter values from detention layer isolated tests did not generally lead to good model predictions. However, the recalibration of Manning's n did not fully address the problems highlighted when attempting to model the detention effects in the complete system. The less satisfactory model results (comparing to the model results for the conventional grenn roof system presented in Section 7.5) may indicate that flow conditions in the detention layer vary with rainfall intensity, which has not been fully represented by the model.

Manning's n for the detention layer showed an increasing trend with rainfall intensity. This may indicate that the actual flow conditions in the detention layer are more complicated than the model assumes. The model for the detention layer was derived based on over surface flow conditions. However, water is likely to flow through the detention layer as well. The vertically oriented polyester threads act as obstacles in the flow path; when the rainfall intensity is low, the flow velocity is low, and the flow around the obstacles is more likely to be laminar, and the distance travelled for the water to reach the outlet is short. In contrast, when the rainfall intensity is high, higher flow velocities in the layer may lead to a more turbulent, chaotic flow with increased travel distance and energy loss. The model in this chapter does not consider the effects of turbulent flow in the detention layer, and the unrealistic representation of the flow condition in the innovative green roof detention layer can contribute to the less satisfactory performance of the model with the innovative green roof system.

Whilst the depth of the substrate used in the system is only 50 mm, the substrate parameters maybe do not have a significant influence on the model results. However, as previous chapters (Chapters 5 and 6) have discussed, the Durner-Mualem model is not a good representation of the substrates HCF, using the Durner-Mualem model introduced uncertainties to the substrate HCF estimations.

8.8 Conclusions

The two-stage physically-based model developed in Chapter 7 provided a reasonable prediction of runoff profiles from the innovative green roof system. However, the model tends to overestimate the influence of the drainage length and overestimate the peak runoff. Whilst the model results were improved slightly using calibrated parameters, the calibration did not lead to an accurate estimation of the runoff profiles from the innovative green roof system. The unsatisfactory performance of the model could be due to the effects of turbulent flow in the detention layer, which has not been considered by the model. Further exploration of a robust model capable of modelling the detention performance of the innovative green roof system is needed.

9 Modelling of Two Green Roof Detention Using SWMM

9.1 Chapter overview

SWMM (Storm Water Management Model) (Rossman and Huber, 2016) is a widely used model for practitioners to estimate or test the hydrological response of green infrastructure designs. In this chapter, the SWMM green roof model is used to model the detention effects of the two green roof systems studied in Chapter 7 and Chapter 8. Firstly, the model is reproduced in MATLAB and is validated against the model results from the SWMM software with the same model inputs. Sensitivity analysis is conducted with the model to investigate the influence of model parameters on the model result. Then the model is used to regenerate the runoff profiles from the two green roof systems in the detention test. Further calibration is conducted to minimise the differences between modelled and measured results. Discussion on the limitations and implications of the SWMM green roof model is presented at the end.

This chapter forms part of the following publication:

Peng, Z., Garner, B., Stovin, V., 2021. Two green roof detention models applied in two green roof systems. *J. Hydrol. Eng.* (under review).

9.2 The SWMM green roof model

9.2.1 Introduction

From a practitioner point of view, a model that could provide rapid results with few parameter inputs is preferable. However, the physically-based green roof detention model discussed in earlier chapters requires intensive computational calculations; therefore, it is not a widely adopted approach in practice for green roof detention modelling. In contrast, the Storm Water Management Model (SWMM), which uses simple modelling approaches and few model inputs, is a widely used model in the industry. The main objective of this chapter is to validate the SWMM green roof model against the data from two green roof systems considered in Chapter 7 and Chapter 8. The SWMM model results will be compared with the two-stage physically-based detention model results to evaluate the model performance.

The Storm Water Management Model (SWMM) is a dynamic rainfall-runoff simulation model used for a single rainfall event or long-term (continuous) simulation of runoff quantity and quality from primarily urban areas. The LID (Low Impact Development) module in SWMM simulates the hydrological performance of various SuDS devices. SWMM considers SuDS controls to be part of the catchment, and each control is assigned a fraction of the catchment's impervious area whose

runoff it captures. The variables that affect the hydrologic performance of SuDS controls include the properties of the media (soil and gravel), the vertical depth of its media layers, the hydraulic capacity of the underdrain system, and the surface area of the unit itself (Rossman and Huber, 2016). The retention model in SWMM considers evapotranspiration from the SuDS controls during the dry weather period, and the detention model predicts the timing and the rate of runoff. The focus of this chapter is on the SWMM green roof detention model.

9.2.2 Green roof detention processes representation

In SWMM, a green roof is represented by three horizontal layers (**Figure 9.1**). During storms, the surface layer (which also includes the vegetation layer) receives direct rainfall. Then the rainfall infiltrates into the soil or becomes surface runoff if ponding occurs. The soil layer (or the substrate) receives infiltration from the surface layer and loses water through percolation into the drainage layer below it. The drainage layer receives percolation from the soil layer, and the rainfall leaves the system as runoff through this layer.

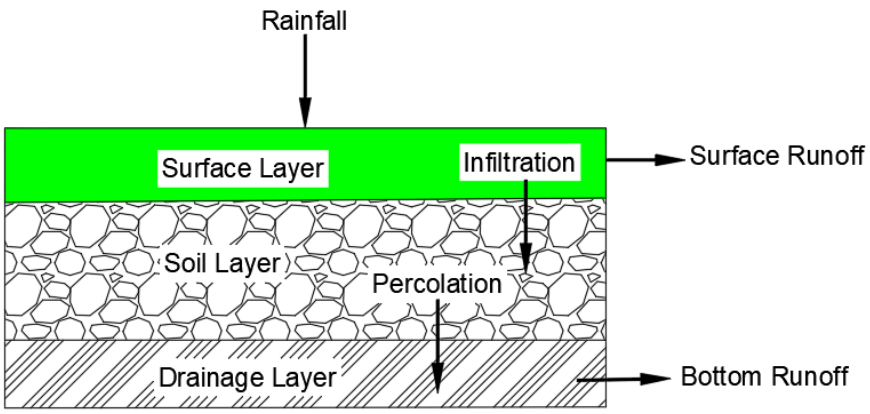

Figure 9.1. Representation of green roof detention processes in SWMM.

The following simplified assumptions are made by SWMM to model the detention performance of a green roof system:

- The cross-sectional area remains constant throughout the depth of the system.
- Flow in the system is 1D vertical flow.
- Rainfall is evenly distributed over the surface layer of the system.
- Moisture content is uniformly distributed throughout the depth of the soil layer (no vertical gradient is present).

Under the simplifying assumptions above, three continuity equations (Equations 9.1 to 9.3) are used to model the behaviour of a green roof system. The change of water level in the surface

layer is modelled as the difference between the rainfall and infiltration plus surface runoff (Equation 9.1). Moisture content in the soil layer is determined by the difference between infiltration and percolation (Equation 9.2). The temporary storage in the drainage layer is simulated as the difference between the percolation and bottom runoff (Equation 9.3).

$$\emptyset_1 \frac{\partial d_1}{\partial t} = i - f_1 - q_1 \quad \text{Equation 9.1}$$

$$D_2 \frac{\partial \theta_3}{\partial t} = f_1 - f_2 \quad \text{Equation 9.2}$$

$$\emptyset_3 \frac{\partial d_3}{\partial t} = f_2 - q_3 \quad \text{Equation 9.3}$$

where d_1 is the depth of water stored on the surface, d_3 is the depth of water in the storage layer (mm), i is the precipitation rate falling directly on the surface layer (mm/min), q_1 is the surface layer runoff (mm/min), q_3 is the drainage layer outflow rate (mm/min), f_1 is the infiltration rate (mm/min), f_2 is the percolation rate (mm/min), $\emptyset_1$ is the void fraction of surface volume, $\emptyset_3$ is the void fraction of the drainage layer, D_2 is the soil thickness (mm), θ_3 is the soil moisture content (volume of water/total volume of soil).

For each layer, different models are used to represent the flux. Manning's equation for uniform flow (Equation 9.4) is used to model the surface runoff from the vegetation layer; the Green-Ampt model (Equation 9.5) is used to model the infiltration of surface water into the soil layer; the percolation from soil layer to drainage layer is modelled using Darcy's Law for a steady-state flow (Equation 9.6), and the runoff from the drainage layer is modelled by Manning's equation for uniform flow (Equation 9.7).

$$q_1 = \frac{0.6017}{n_s}\sqrt{S_1}(W_1/A_1)\emptyset_1(d_1 - D_1)^{\frac{5}{3}} \quad \text{Equation 9.4}$$

$$f_1 = K_s\left(1 + \frac{(\emptyset_2 - \theta_3)(d_1 + \varphi_2)}{F}\right) \quad \text{Equation 9.5}$$

$$f_2 = \begin{cases} 0, & \theta_3 < \theta_{FC} \\ K_s \exp\left(-HCO(\emptyset_2 - \theta_3)\right), & \theta_3 \geq \theta_{FC} \end{cases} \quad \text{Equation 9.6}$$

$$q_3 = \frac{0.6017}{n_3}\sqrt{S_1}(W_1/A_1)\emptyset_3(d_3)^{\frac{5}{3}} \quad \text{Equation 9.7}$$

where n_s is the surface roughness coefficient, n_3 is the drainage layer roughness coefficient, S_1 is the system slope (m/m), W_1 is the total length along the edge of the roof where runoff is collected (m), A_1 is the roof surface area (m^2), K_s is the soil saturated hydraulic conductivity (mm/min), θ_{FC} is the soil field capacity, φ_1 is the suction head at the infiltration wetting front

formed in the soil (mm), F is the cumulative infiltration volume per unit area over a storm event (mm), and HCO is the soil hydraulic slope. It should be noted that empirical units are used in SWMM, a coefficient of 0.6017 is used in Equations 9.4 and 9.7 to convert empirical units to SI units.

The flux from the surface layer to the soil layer is limited by the amount of empty pore space in the soil and the volume removed by drainage (Equation 9.8). Soil percolation rate is limited by the amount of drainable water plus the water added to the soil layer (Equation 9.9). The soil percolation rate is also limited by the available storage volume in the drainage layer and the amount of water removed from the drainage layer (Equation 9.10). The runoff rate from the drainage layer is limited by the amount of water that can be stored plus any inflow from the soil layer.

$$f_1 = \min[f_1, (\emptyset_2 - \theta_3)D_2 + f_2] \quad \text{Equation 9.8}$$

$$f_2 = \min[f_2, (\theta_2 - \theta_{FC})D_2 + f_1] \quad \text{Equation 9.9}$$

$$f_2 = \min[f_2, (D_3 - d_3)\emptyset_3 + q_3] \quad \text{Equation 9.10}$$

$$q_3 = \min[q_3, (d_3 - D_3)\emptyset_3 + f_2] \quad \text{Equation 9.11}$$

where D_3 is the drainage layer thickness (mm).

9.2.3 Comparison between the SWMM and the physically-based models

Table 9.1 lists the models used in the SWMM green roof model and the two-stage physically-based model (Chapter 7) to represent the detention processes in a green roof system. Surface runoff is not considered in the physically-based model as surface runoff is not normally expected in a green roof system. Infiltration and substrate runoff are modelled by the Richards Equation in the physically-based model. However, the two processes are modelled separately by two models in the SWMM green roof model. Surface infiltration is modelled by the Green-Ampt model in the SWMM green roof model under the assumption that the infiltration rate is driven by the water head ponding on the surface of the substrate layer. The percolation model in SWMM is a simplified model of the Richards Equation under the assumption of a steady-state flow condition. Drainage layer runoff is modelled by the Saint Venant Equation in the physically-based model, and it is modelled via Manning's Equation in the SWMM green roof model. Both drainage layer models are physically based, but Manning's Equation in the SWMM green roof model is a simplified model under the assumption of a uniform steady flow condition.

Table 9.1. Comparison of the SWMM and the physically-based models.

Process	Physically-based model (Chapter 7)	SWMM green roof model
Surface runoff	Not considered	Surface Manning's Equation
Infiltration from the surface layer to the deep substrate	Richards' Equation	Green-Ampt infiltration model
Percolation from the substrate to the drainage layer	Richards' Equation	Percolation model
Drainage layer runoff	Saint Venant Equation	Drainage layer Manning's Equation

9.2.4 Validation of the MATLAB SWMM green roof model

The green roof detention model in SWMM was built in MATLAB in order to be able to conduct systematic sensitivity analysis and calibration on model parameters. The model built in MATLAB was validated against the SWMM software. The same values of model parameters were put into the MATLAB model and the SWMM software, and the model results, including surface infiltration, substrate percolation, bottom runoff, substrate moisture content and temporary storage in the drainage layer, were then compared.

The green roof system to be modelled in the two interfaces consists of 20 mm vegetation, 50 mm substrate and 55 mm drainage layer; the length of the system is 6 m, and the width of the system is 1.1 m. The value of surface layer, substrate and drainage layer parameters used in the model are listed in **Table 9.2**. The parameters for the surface layer were all assumed for the following two reasons: a) such parameters are difficult to characterise in practice; b) the surface layer parameters are not crucial to the model results; the saturated hydraulic conductivity of the soil layer of a green roof substrate is usually higher than the rainfall such that no surface runoff will be generated. For test purposes, the value for the soil layer and drainage layer physical properties were also assumed within the range of suggested values. An arbitrary rainfall was used as the rainfall input to the models. The initial moisture content in the substrate was set to be at field capacity, and the initial water storage in the drainage layer was set to be zero.

Table 9.2. Values of parameters put into the model for the MATLAB code validation.

Symbol	Description	Value	Unit	Source
$\emptyset_1$	The void fraction of surface volume	0	-	Assumed
D_1	Surface depression storage depth	0	mm	Assumed
n_s	Surface roughness coefficient	0.1	-	Assumed
φ_2	Suction head at the infiltration wetting front	50	mm	Assumed
K_{ss}	Soil saturated hydraulic conductivity	14.7	mm/min	Assumed
D_2	The thickness of the soil layer	50	mm	Configuration specific
ϕ_2	The porosity of the soil layer	0.52	-	Assumed
θ_{FC}	Field capacity	0.34	-	Assumed
HCO	Soil hydraulic slope	35	-	Assumed
S_1	Slope	0.02	-	Configuration specific
n_3	Drainage layer roughness coefficient	0.3	-	Assumed
$\phi 3$	The void fraction of the drainage layer	0.5	-	Assumed
W_1	Width	1.1	m	Configuration specific
A_1	Roof surface area	6.71	m^2	Configuration specific
D_3	The thickness of the drainage layer	55	mm	Configuration specific

Figure 9.2 shows the model results of the SWMM software and the MATLAB code with the same model inputs. **Figure 9.2(a)** is the modelled flux. As the rainfall intensity did not exceed the saturated hydraulic conductivity of the substrate, all of the rainfall infiltrated into the substrate. A good agreement between the model results was achieved by the two approaches. **Figure 9.2(b)** shows the modelled water storage in the drainage layer. The water storage modelled by the SWMM green roof model at the beginning of the storm is slightly higher than that modelled by the MATLAB code. This is because the initial water storage in the drainage layer cannot be assigned separately from the initial moisture content in the substrate in the SWMM software. Even when 24 hours of simulation without rainfall were conducted in SWMM to empty the storage in the drainage layer, about 0.03 mm of storage was still filled in the drainage layer at the beginning of the storm. **Figure 9.2(c)** shows the modelled moisture content in the substrate during the storm; the two approaches obtained very close results. The model results shown here confirm that the code built in MATLAB is equivalent to the SWMM model results of SWMM. Therefore, the following simulations with the SWMM green roof model will be implemented in MATLAB.

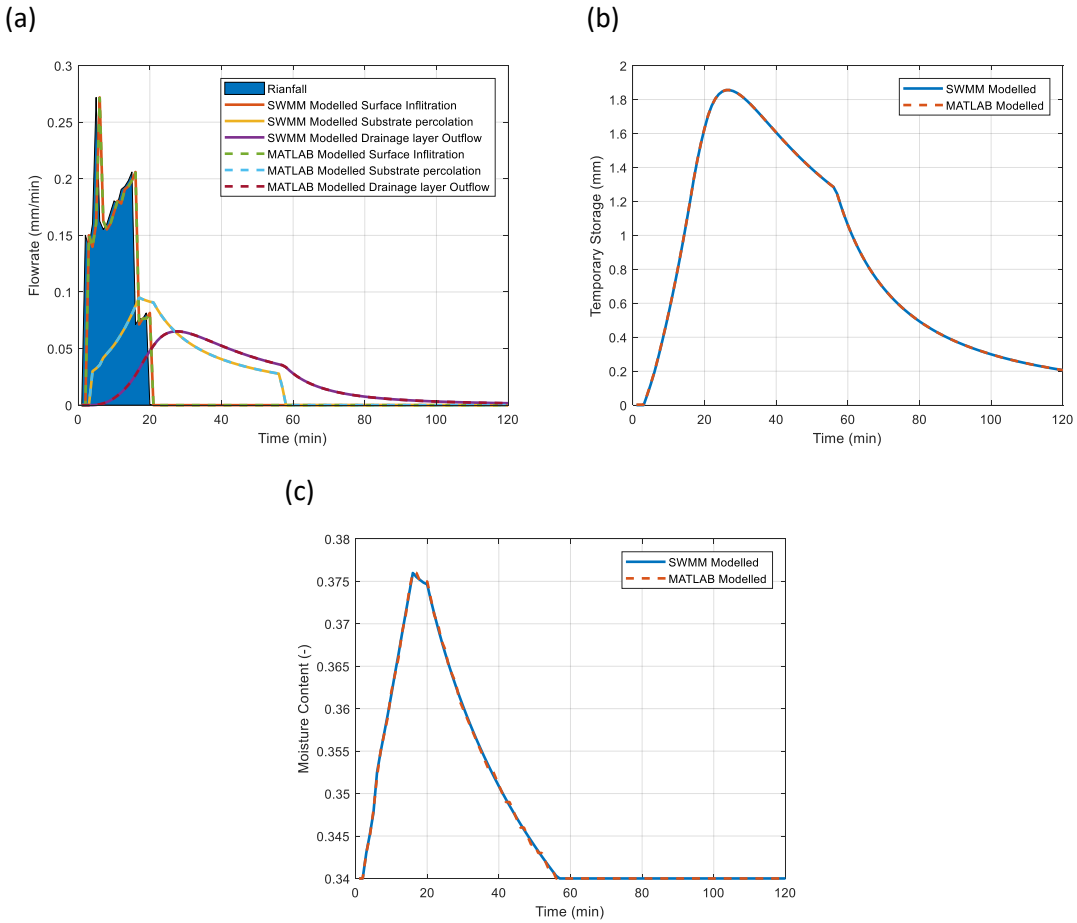

Figure 9.2. Model results generated by the SWMM software and the MATLAB code; (a) water flux; (b) temporary storage in the drainage layer; (c) moisture content in the substrate.

9.2.5 Sensitivity analysis

Several parameters are required to implement the SWMM green roof model. However, some of the parameters are not critical to the model results (for example, the parameters for the surface layer); some are configuration specific (i.e. the slope, the thickness of the soil and drainage layer and the area and width of the system); some can be determined from a routine test for a green roof substrate (i.e. saturated hydraulic conductivity, porosity, field capacity and soil hydraulic slope (can be estimated from particle size distribution)). The drainage layer roughness coefficient and void fraction are the two parameters that are hard to characterise and may need calibration. Therefore, a sensitivity analysis was conducted on the two parameters to investigate their influence on the model results. A series of drainage layer roughness and drainage layer void fraction values were put into the model built in MATLAB, and the modelled runoff profiles were compared.

The drainage layer roughness values, ranging from 0.05 to 2.5, were tested in the model to investigate the influence of drainage layer roughness on the model result. In each test, the

remaining parameters are listed in **Table 9.2**. The drainage layer roughness of 0.05 is within the range of typical values for a green roof drainage layer roughness (Rossman and Huber, 2016), but values above 1.8 are outside the suggested range. The purpose of testing such high values is to account for the high detention effects that may present in the innovative detention layer.

The drainage layer void fraction values, ranging from 0.3 to 0.6, were tested in the model to investigate the influence of the void fraction on the model result. The remaining parameters are listed in **Table 9.2**. Void fraction values of 0.3 and 0.6 are the lower and upper boundaries of the suggested values for a green roof drainage layer's (Rossman and Huber, 2016).

Figure 9.3 shows the modelled runoff profiles using different values of drainage layer roughness coefficient and void fraction. **Figure 9.3(a)** shows the sensitivity of the modelled runoff profiles to the drainage layer roughness. Unsurprisingly, the modelled runoff profile is sensitive to the drainage layer roughness. The peak flow rate was reduced by about 71% when the roughness was increased from 0.05 to 2.5. **Figure 9.3(b)** suggests that the value of drainage layer void fraction does not have a significant influence on the model results. The peak flow rate decreased from about 0.68 to 0.6 mm/min when the drainage layer void fraction increased from 0.3 to 0.6.

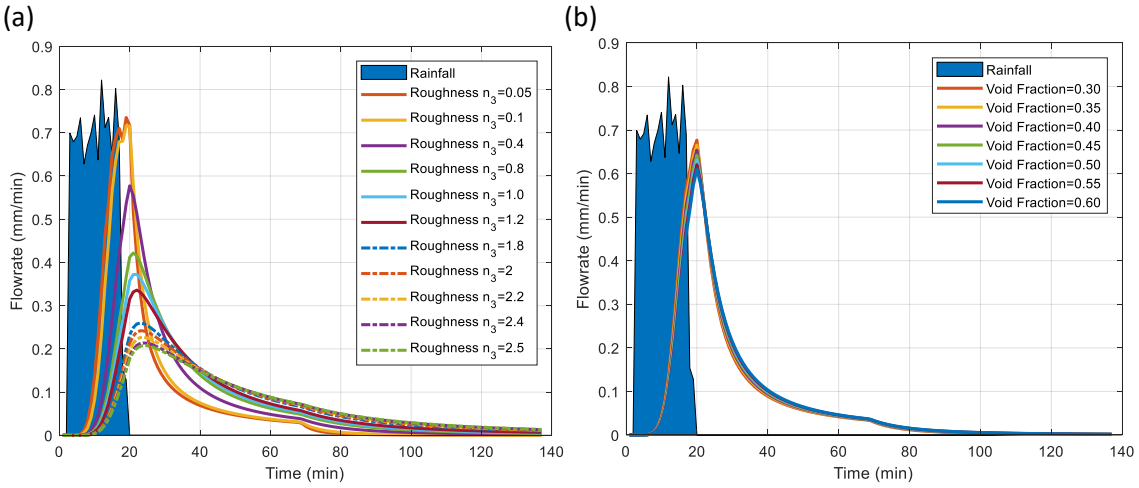

Figure 9.3. Modelled runoff profiles from a green roof system using different values of drainage layer roughness and the void fraction using the SWMM green roof model; (a) drainage layer roughness coefficient; (b) drainage layer void fraction.

9.3 Validation of the SWMM green roof model

9.3.1 Green roof systems

Two green roof systems (conventional and innovative) were considered. The conventional green roof system was as described in Section 7.5.1, and the innovative green roof system was as described in Section 8.2.

9.3.2 Laboratory detention tests

The detention tests with the drainage layer and the complete conventional green roof system can be found in Sections 3.5.2 and 3.5.3, and the tests with the detention layer and the complete innovative green roof system can be found in Section 3.5.4.

9.3.3 Substrate parameters

9.3.3.1 Conventional green roof system

The physical properties of the substrate used in the conventional green roof system (MCS) have been intensively characterised in Chapter 5, and the value of parameters used in the SWMM green roof model are listed in **Table 9.3**. The value of the suction head at the infiltration wetting front, in this case, is an assumed value as no test was conducted to determine this value. However, this parameter is not critical to the model results as no ponding is expected on the surface of the green roof system in storms. The saturated hydraulic conductivity, porosity and field capacity of the substrate were determined through FLL methods (**Table 5.1**). The hydraulic slope refers to the slope of the HCF curve in log scale space. As the HCF of the MCS has been determined (**Figure 5.4(a)**), the hydraulic slope was calculated from the measured HCF data.

9.3.3.2 Innovative green roof system

Table 9.3 lists the value of parameters for the substrate used in the innovative green roof system (MMS). The suction head at the infiltration wetting front for this substrate is also an assumed value. Parameters including saturated hydraulic conductivity, porosity and field capacity of the substrate were determined through the ASTM E2399 method (FLL equivalent method), and the data was provided by Green Roof Diagnostics. As the HCF of the MMS has not been determined, the hydraulic slope was determined based on the characterised particle size distribution using Equation 9.12 (Saxton and Rawls, 2006).

$$\mathrm{HCO} = 0.48 \times \%\mathrm{sand} + 0.85 \times \%\mathrm{clay} \qquad \text{Equation 9.12}$$

9.3.4 Drainage layer parameters

The drainage layer parameters required by the SWMM model are drainage layer roughness coefficient and void fraction. The results of the sensitivity analysis showed that the model results are not sensitive to the drainage layer void fraction (**Figure 9.3**). Therefore, a value of 0.5 was used for the void fraction for both the FD 25 drainage layer (conventional green roof system) and the detention layer (innovative green roof system). The roughness coefficient of the drainage layer and the detention layer were parameterised from component isolated tests.

9.3.4.1 Conventional green roof system

The conventional green roof system uses ZinCo Floradrain FD 25 drainage layer at the bottom of the system to effectively convey excess water. Based on the detention tests with the drainage layer (Section 3.5.2), a roughness coefficient of 0.0578 was determined for the 5 m drainage length and 2% slope configuration using the *Isqcurvefit* function in MATLAB (**Table 9.3**).

9.3.4.2 Innovative green roof system

The innovative green roof system uses an innovative detention layer to enhance the detention performance of the whole system. The detention tests with the detention layer were conducted by Green Roof Diagnostics (Section 3.5.4). Based on the experimental results, a roughness coefficient of 0.952 was determined for the detention layer using the *Isqcurvefit* function in MATLAB (**Table 9.3**).

Table 9.3. Value of parameters for the SWMM green roof model.

	Parameter	Conventional Green Roof	Innovative Green Roof
System Configuration	W_1	1 m	1.1 m
	A_1	5 m^2	6.71 m^2
	S_1	0.02	0.02
Surface layer	$\emptyset_1$	0	0
	D_1	0	0
	n_s	0.1	0.1
	φ_2	50	50
Substrate layer	K_s	166.4 mm/min	14.7 mm/min
	D_2	100 mm	50 mm
	Soil wilting point	0.01	0.01
	$\emptyset_2$	0.552	0.513
	θ_{FC}	0.334	0.38
	HCO	20	25.59
	Initial substrate saturation	64.10%	72.55%
Drainage/detention layer	n_3	0.0578	0.952
	$\emptyset_3$	0.5	0.5
	D_3	25 mm	55 mm
	Initial water storage	0	0

As all the detention tests started from field capacity, the initial moisture content in the substrate in the model was set to be at field capacity, and the water storage in the drainage layer was set to be zero.

9.3.5 Model validation and calibration

R_t^2 was used to evaluate the goodness-of-fit of the modelled runoff. Comparisons between the model predictions and measured laboratory data are presented in two stages: component isolated tests and complete system tests. Further calibration of the drainage layer roughness coefficient was conducted as the drainage layer could perform differently within the complete system due to interactions with the overlying layers.

9.3.6 Results

9.3.6.1 Model validation

Drainage layer in the conventional green roof system

Figure 9.4 shows the measured and modelled runoff profiles from the 5 m FD 25 drainage layer at a 2% slope using the SWMM model with a drainage layer roughness of 0.0578. As good consistency was achieved between replicate tests, only one test for each rainfall intensity is presented in the figure. With all R_t^2 higher than 0.95, the model is capable of modelling the runoff from the FD 25 drainage layer. Whilst the model delayed the time for the system to reach an equilibrium state in all cases, the falling limb of the runoff profile was modelled well by the model. It should be noted that the time-step here is 1-second; the difference between the measured and modelled results will be minor if a 1-minute time-step is used (e.g. for complete system modelling).

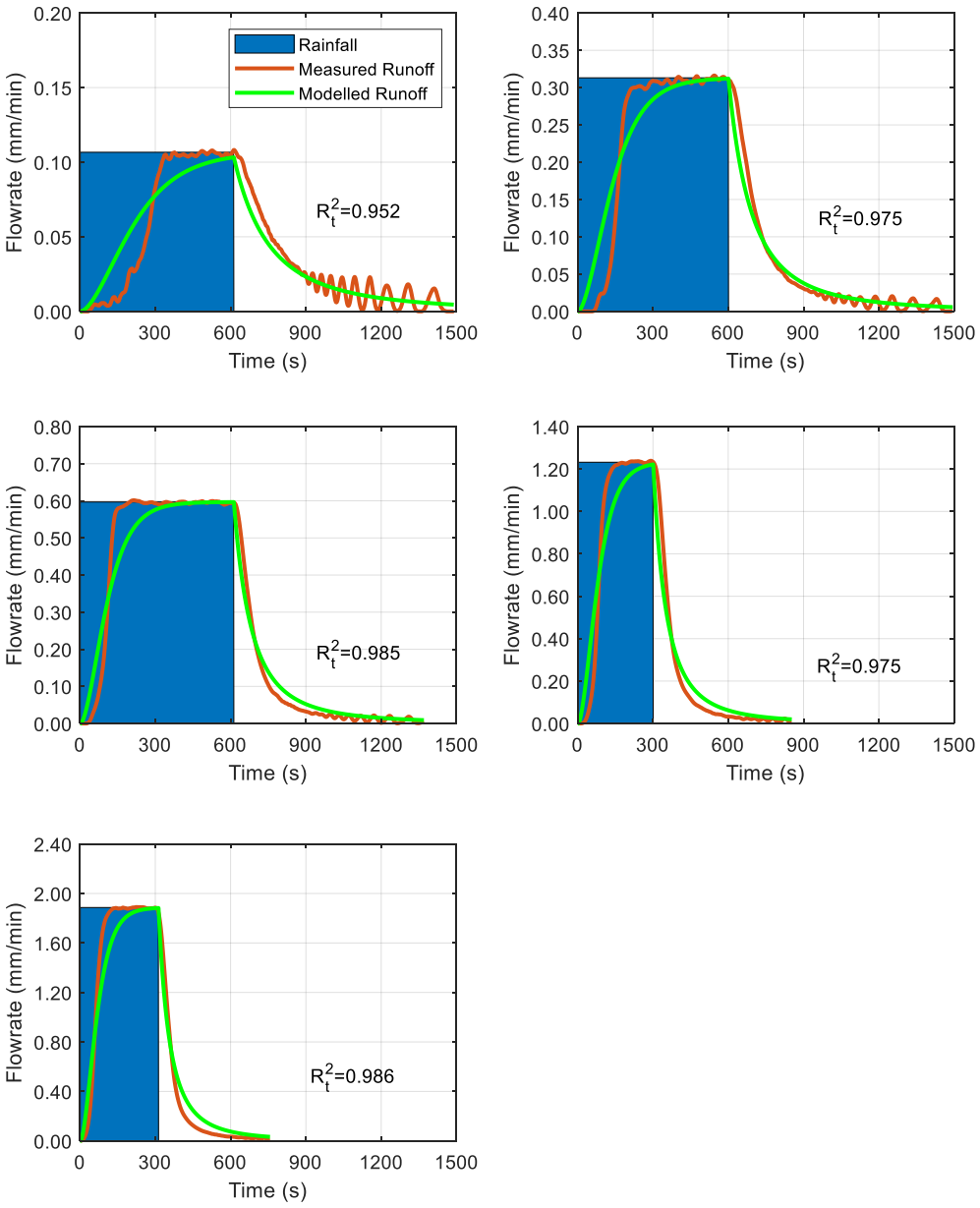

Figure 9.4. Measured and modelled runoff profiles from the conventional green roof drainage layer using the SWMM green roof model (with a roughness coefficient of n_3=0.0578).

Detention layer in the innovative green roof system

Figure 9.5, **Figure 9.6** and **Figure 9.7** show the modelled runoff from the innovative detention layer component in response to the three rainfall intensities using the identified drainage layer roughness coefficient (0.952). The identified drainage layer roughness coefficient is significantly higher than the typical value for a green roof drainage layer (0.01-0.03) suggested in Rossman and Huber (2016), which indicates the high detention potential of the detention layer. The model is able to simulate the runoff from the detention layer to some extent. At the low rainfall intensity (0.17 mm/min, **Figure 9.5**), the model appeared to overestimate detention effects. The model

has the best performance in the medium rainfall intensity (0.78 mm/min, **Figure 9.6**), with R_t^2 higher than 0.96. In response to the high rainfall intensity (1.9 mm/min, **Figure 9.7**), the model significantly overestimated the peak. Whilst **Figure 9.5**, **Figure 9.6** and **Figure 9.7** show the results of using a single parameter value, independent of rainfall intensity. It was observed that the best-fit parameter values for the drainage layer roughness coefficient increased with rainfall intensity (**Figure 9.8**).

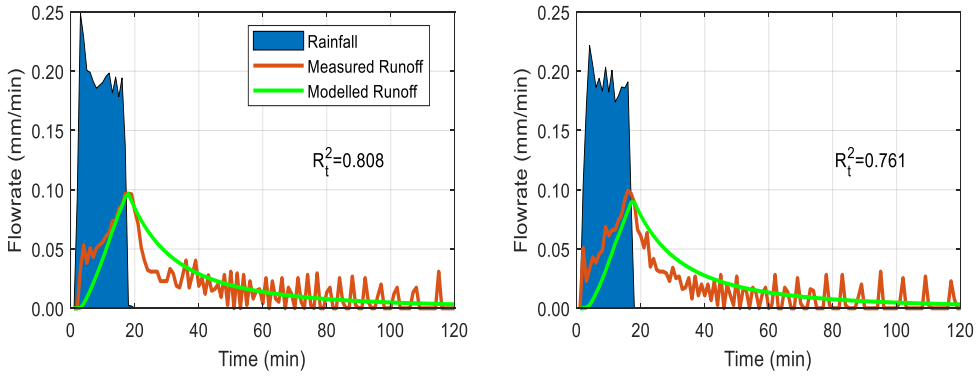

Figure 9.5. Measured and modelled runoff profiles from the innovative green roof detention layer using the SWMM green roof model (with a roughness coefficient of n_3=0.952, rainfall intensity of 0.17 mm/min).

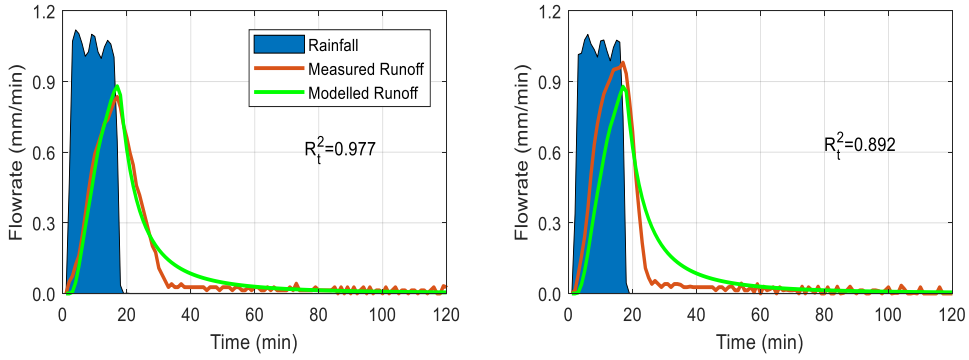

Figure 9.6. Measured and modelled runoff profiles from the innovative green roof detention layer using the SWMM green roof model (with a roughness coefficient of n_3=0.952, rainfall intensity of 0.78 mm/min).

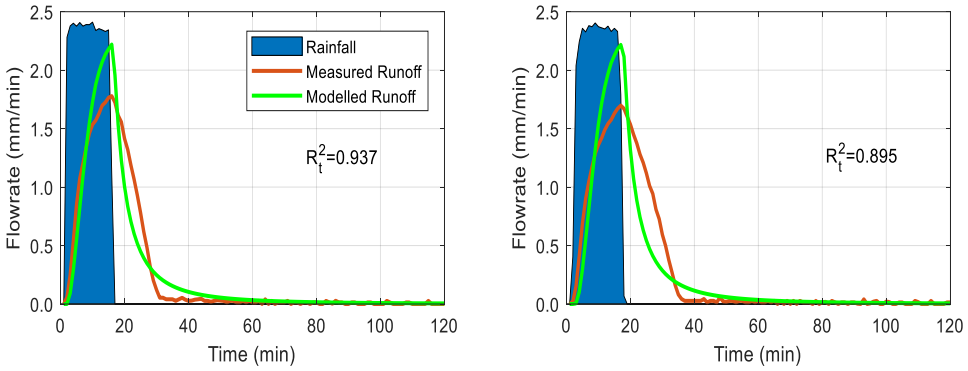

Figure 9.7. Measured and modelled runoff profiles from the innovative green roof detention layer using the SWMM green roof model (with a roughness coefficient of n_3=0.952, rainfall intensity of 1.9 mm/min).

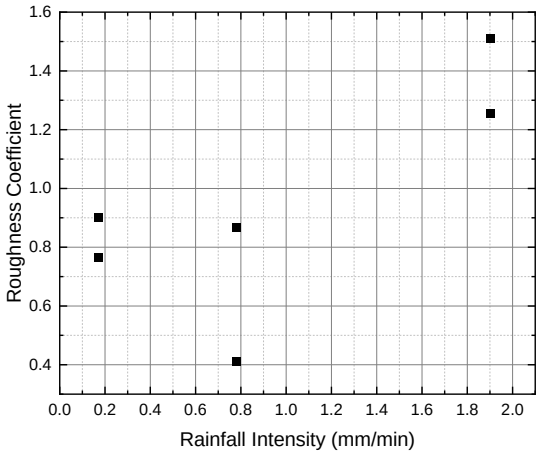

Figure 9.8. Relationship between optimised drainage layer roughness coefficient and rainfall intensity for the detention layer in the innovative green roof system.

As the rainfall intensities used in the detention tests with the FD 25 drainage layer and the detention layer are not identical, no direct comparison can be made between their detention performance. However, Stovin et al. (2015) demonstrated that the calibrated parameters in a detention model could be used to characterise the detention performance of a system. Based on the identified drainage layer roughness coefficient (0.0578 for the FD 25 drainage layer and 0.952 for the detention layer), the parameters indicate that the detention layer has the potential to provide more significant detention effects than the FD 25 drainage layer.

Complete conventional green roof system

Figure 9.9 shows the measured and modelled runoff profiles from the complete conventional green roof system. The parameters used in the models are as listed in **Table 9.3**. As good

consistency was achieved between replicate tests, one test for each design storm is presented in **Figure 9.9**.

The SWMM green roof model underestimated the detention effects of the system in all five design storms, and some numerical stability problems were also observed at high rainfall intensities (**Figure 9.9**). In the constant intensity design storms, the time for the system to reach equilibrium was modelled to be between 6 minutes (1.2 min/mm, **Figure 9.9**) and 20 minutes (0.3 mm/min, **Figure 9.9**) earlier than measured. The SWMM green roof model also overestimated the peak runoff rate by 7.3% (**Figure 9.9**) in the two time-dependent design storms. The modelled substrate runoff suggested that the substrate provided very limited detention effects in the storms. The modelled cumulative runoff depth at the final time in **Figure 9.9** is equal to the total rainfall depth, indicating that the model is only modelling the runoff routing.

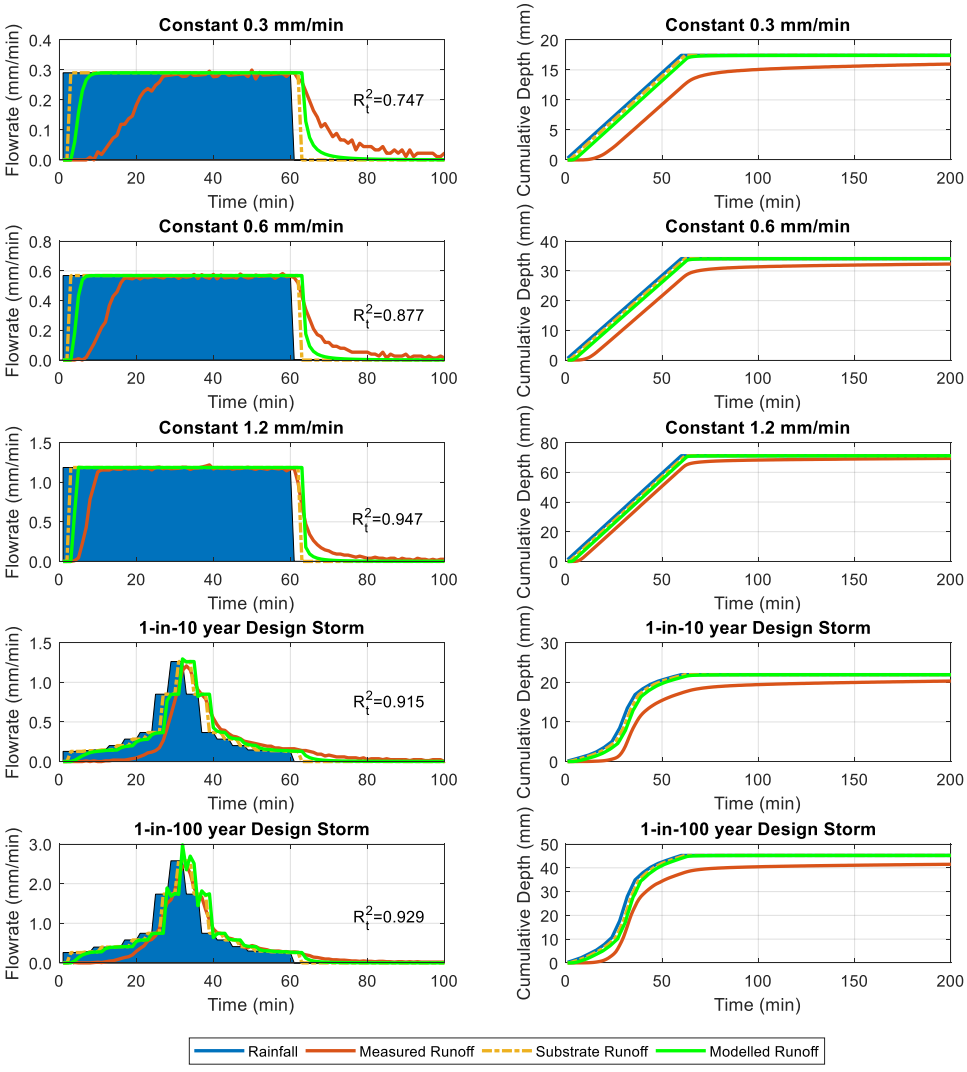

Figure 9.9. Measured and modelled runoff profiles from the conventional green roof system using the SWMM green roof model (n_3=0.0578).

Whilst the drainage layer model in the SWMM green roof model appeared capable of regenerating the runoff from the drainage layer in the drainage layer isolated tests; it failed to regenerate the runoff profiles from the complete system accurately. This could be caused by limitations in the way the overlying substrate layers are modelled in SWMM. Further discussion on the SWMM green roof percolation model will be provided in Section 9.4.

Complete innovative green roof system

Figure 9.10, **Figure 9.11** and **Figure 9.12** show the measured and modelled runoff profiles from the complete innovative green roof system. The parameters used in the models are as listed in **Table 9.3**. The model provided reasonable estimations of the measured runoff profile (i.e. R_t^2 ranges from 0.6 to 0.9). However, in the medium rainfall intensity (0.78 mm/min, **Figure 9.11**), the model overestimated the peak runoff by about 23%. In the high rainfall intensity (1.9 mm/min, **Figure 9.12**), the model overestimated the peak runoff by 50 % to 80% and delayed the time of peak runoff by about 2 minutes.

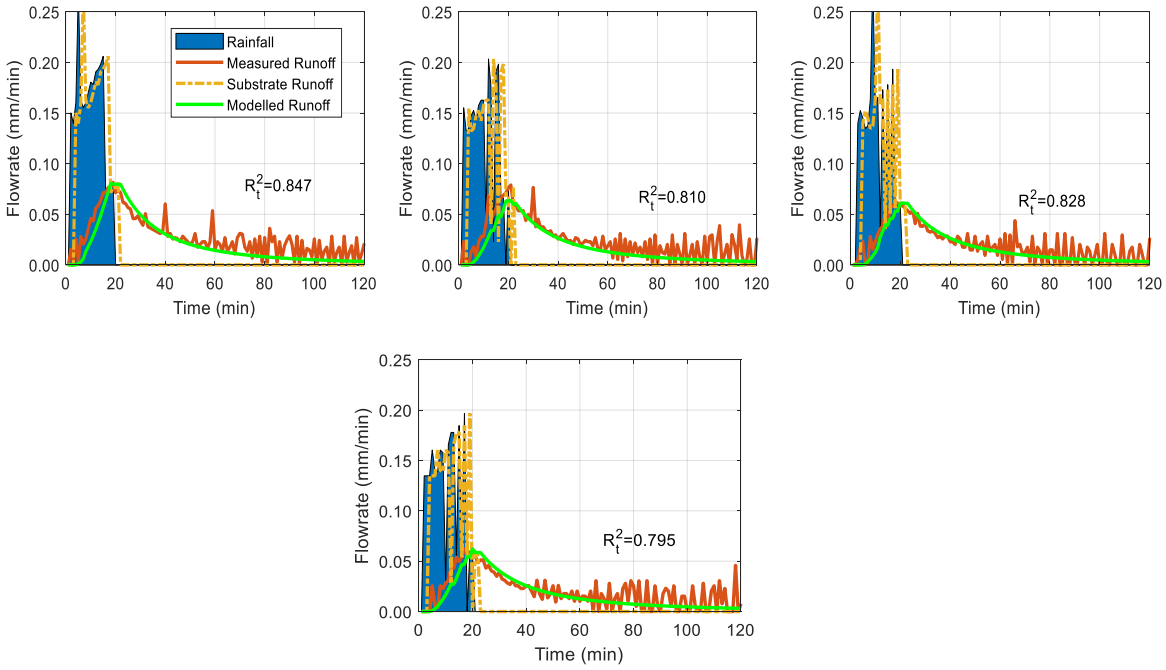

Figure 9.10. Measured and modelled runoff profiles for the innovative green roof system using the SWMM green roof model (with a roughness coefficient of n_3=0.952, rainfall intensity of 0.17 mm/min).

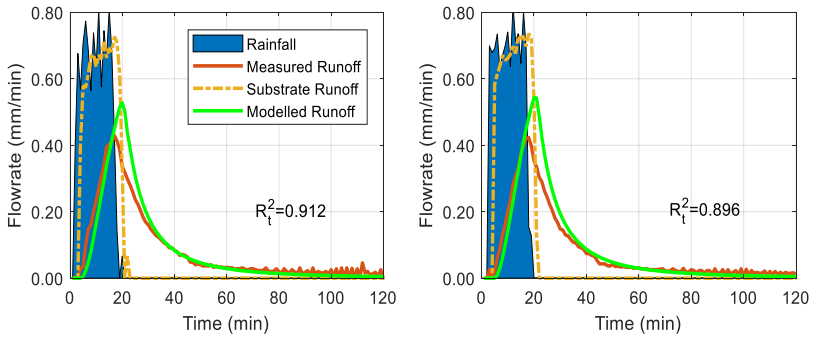

Figure 9.11. Measured and modelled runoff profiles for the innovative green roof system using the SWMM green roof model (with a roughness coefficient of n_3=0.952, rainfall intensity of 0.78 mm/min).

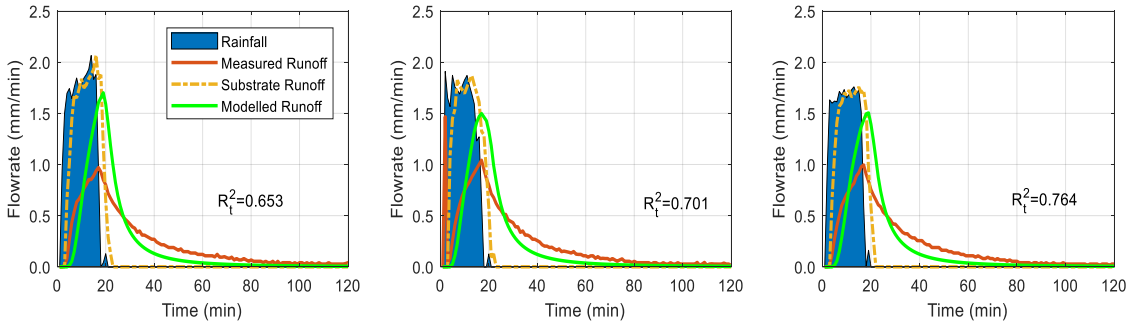

Figure 9.12. Measured and modelled runoff profiles for the innovative green roof system using the SWMM green roof model (with a roughness coefficient of n_3=0.952, rainfall intensity of 1.9 mm/min).

The time to start of runoff was delayed by 3 minutes by the model in all cases. This is because a backwards numerical scheme was used in the SWMM green roof model, and the three models for the three processes in the substrate and the drainage layer resulted in the three-minute delays. The model results for the detention layer isolated tests suggested that a higher value of drainage layer roughness coefficient needs to be used in the high rainfall intensity to fit the measured runoff; this is consistent with the observation that detention is underestimated for the complete system when a universal coefficient value is applied here.

9.3.6.2 Model calibration

Conventional green roof system

A drainage layer roughness of 0.502 was calibrated using the measured runoff from the complete conventional green roof system, and **Figure 9.13** shows the modelled runoff profiles using the calibrated value. With mean R_t^2 increased from 0.883 to 0.950, a significant improvement in model results has been observed following calibration. The drainage layer roughness determined for the drainage layer based on the component isolated tests was 0.0578, which is significantly

lower than the calibrated value (0.502) using the measured runoff from the complete green roof system. This may indicate that the parameters determined from the component isolated tests cannot represent the behaviour of the component in a complete system. The possible reasons leading to an increase in drainage layer roughness have been discussed in Chapter 7.

As the drainage layer roughness only influences the model results from the drainage layer, the runoff from the substrate has not been changed after calibration (**Figure 9.13**). Whilst a high value of R_t^2 was obtained after calibration, differences between the modelled and measured runoff profiles are still noticeable (**Figure 9.13**). In response to the three constant rainfall events, the falling limb of the runoff profile was modelled well; the difference between the modelled and measured runoff profiles was mainly in the rising limb. In response to the lowest rainfall intensity (0.3 mm/min), the modelled and measured time for the system to reach the equilibrium state are the same. However, the modelled time to start of runoff was about 8 minutes earlier than the measured. In the medium rainfall intensity (0.6 mm/min), the time to start of runoff was modelled to be 5 minutes ahead of the measured runoff, and the time for the system to reach equilibrium state was delayed about 5 minutes by the model. In the highest rainfall intensity (1.2 mm/min), the model delayed the time for the system to reach the equilibrium state by about 10 minutes. The model significantly underestimated the peak runoff rate by 20% to 23% in the two events with time-dependent rainfall inputs. The observations here indicate that the detention performance of the conventional green roof is not accurately represented by the model.

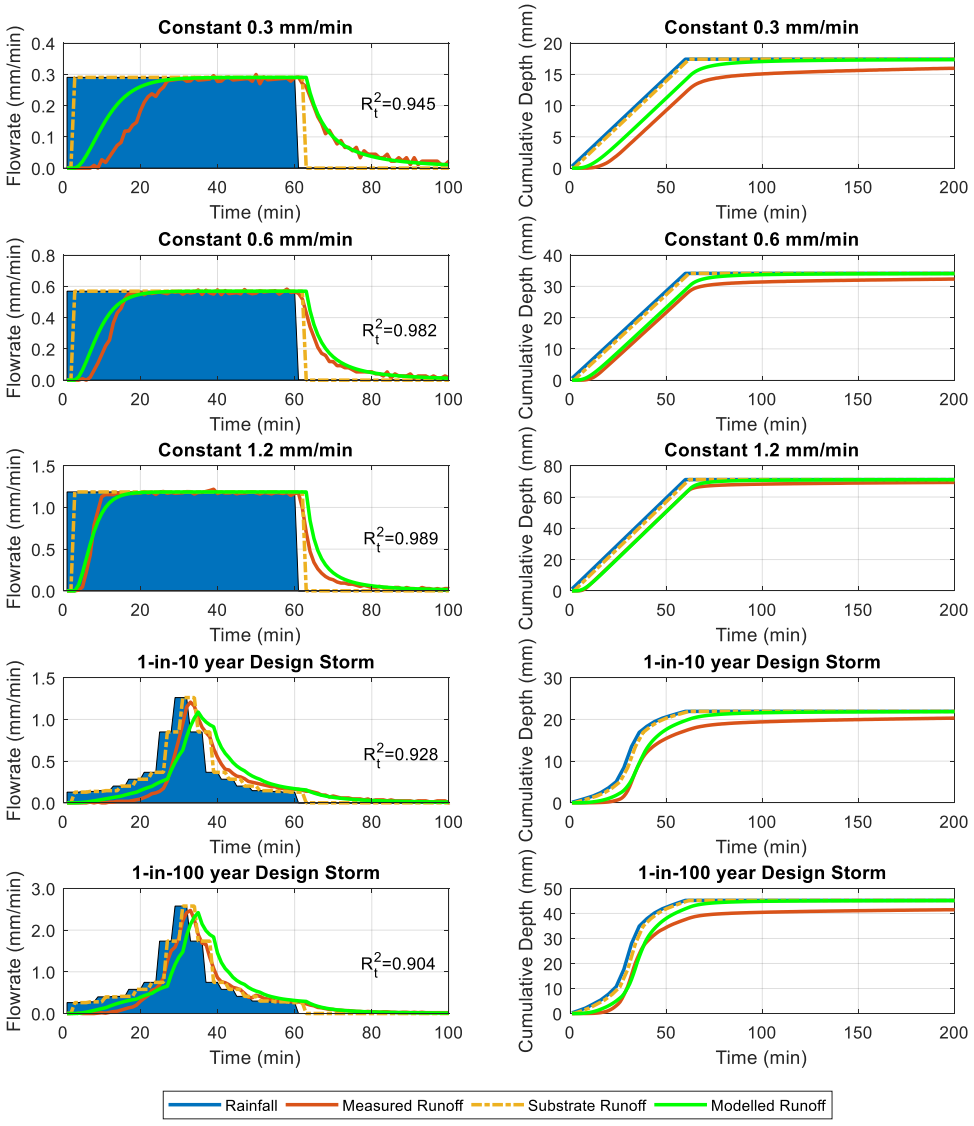

Figure 9.13. Measured and modelled runoff profiles from the conventional green roof system using the SWMM green roof model and calibrated roughness coefficient (n_3=0.502).

Innovative green roof system

Calibration of the detention layer roughness coefficient was conducted using the measured runoff from the complete innovative green roof system, and a value of 1.416 was obtained. As the innovative material used for the detention layer is different from the typical green roof drainage layer. The value of 1.416 is outside the typical range for a green roof drainage layer (Rossman and Huber, 2016). **Figure 9.14**, **Figure 9.15** and **Figure 9.16** show the modelled runoff profiles using the roughness coefficient of 1.416. The overall model performance was slightly improved following the calibration (with the mean value of R_t^2 was increased from 0.80 to 0.814). However, only the model results with the high rainfall intensity were significantly improved (**Figure 9.16**). The model results for the low and medium rainfall intensities are worse than before (**Figure 9.14**,

Figure 9.15, **Figure 9.10** and **Figure 9.11**). The peak runoff rates were estimated well in the low and medium rainfall intensities when using the uncalibrated roughness (n_3=0.952, **Figure 9.10** and **Figure 9.11**), while the model underestimated the peak runoff when the calibrated value (n_3=1.416, **Figure 9.14** and **Figure 9.15**) was used. In the high rainfall intensity (**Figure 9.16**), the model still overestimated the peak runoff rate, but it was decreased from more than 50% to less than 50% when the calibrated value (n_3=1.416) was used. The observations presented here may indicate that the flow within the detention layer is more complicated than the model assumed. Further discussions on the model will be in Section 9.4.

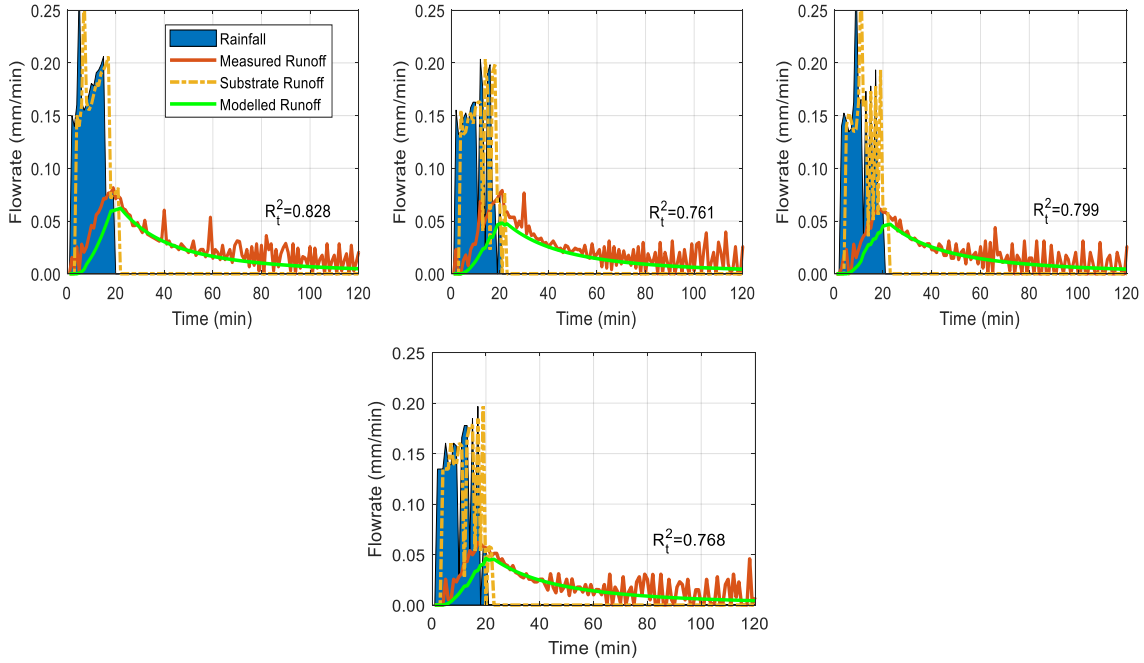

Figure 9.14. Measured and modelled runoff profiles for the innovative green roof system using the SWMM green roof model (with a calibrated roughness coefficient of n_3=1.416, rainfall intensity of 0.17 mm/min).

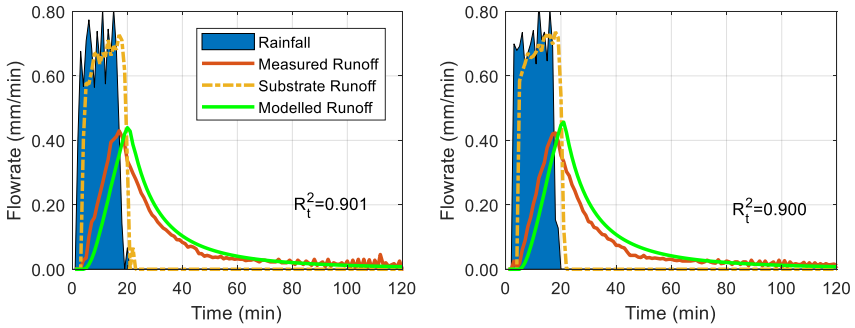

Figure 9.15. Measured and modelled runoff profiles for the innovative green roof system using the SWMM green roof model (with a calibrated roughness coefficient of n_3=1.416, rainfall intensity of 0.78 mm/min).

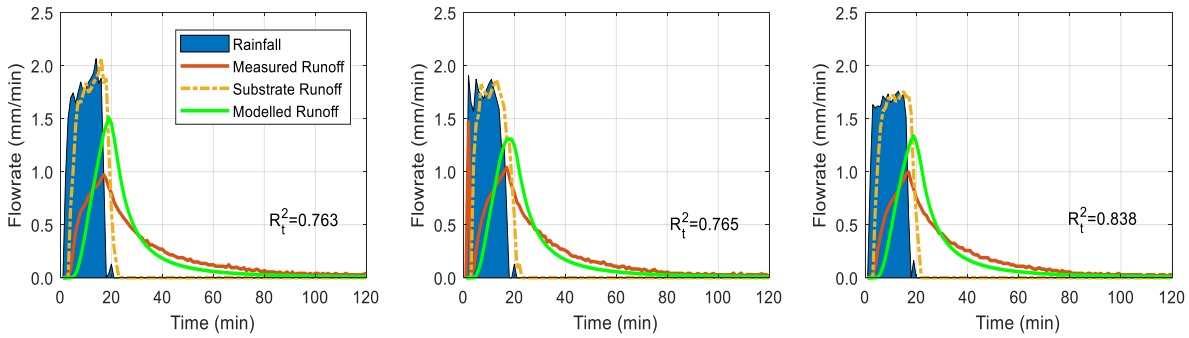

Figure 9.16. Measured and modelled runoff profiles for the innovative green roof system using the SWMM green roof model (with a calibrated roughness coefficient of n_3=1.416, rainfall intensity of 1.9 mm/min).

9.4 Discussion

In this section, the results of the SWMM green roof model (SWMM-GR) presented in previous sections will be compared with the model results of the two-stage physically-based model (2SPB) presented in Chapter 7 and Chapter 8. Based on the model results for the two green roof systems, the limitations of the SWMM green roof detention model will be discussed.

9.4.1 Comparison of models

Both the two-stage physically-based model (2SPB, presented in Chapters 7 and 8) and the SWMM green roof model (SWMM-GR) were applied in the conventional green roof system and the innovative green roof system. Whilst both models have presented a certain level of capability of modelling the runoff profiles from the green roof systems, the two models showed some difference in model performance. This section compares the model results of the two models using the model parameters identified from component isolated tests. The performance of the models will be evaluated based on the modelled runoff profiles from the two green roof systems.

9.4.1.1 Conventional green roof system

Figure 9.17 shows the measured and modelled runoff profiles from the complete conventional green roof system. The parameters used in the models were characterised in independent component tests and are listed in **Table 7.1** and **Table 9.3**. Both models are capable of generating credible runoff profiles from the conventional green roof system. However, with consistently higher values of R_t^2, the 2SPB model provides better estimations of the runoff profiles than the SWMM-GR model.

In the two lowest constant intensity design storms (0.3 mm/min and 0.6 mm/min, **Figure 9.17(a)** and **(b)**), both models underestimated the detention effects in the rising limb of the runoff

profiles. However, the falling limb was modelled well by the 2SPB model. In the highest constant intensity design storm (1.2 mm/min, **Figure 9.17(c)**), the runoff profile was modelled well by the 2SPB model, while the time for the system to reach equilibrium modelled by the SWMM-GR model was 6 minutes earlier than measured. In the two time-dependent design storms (**Figure 9.17(d)** and **(e)**), both the 2SPB and SWMM-GR model overestimated the peak runoff.

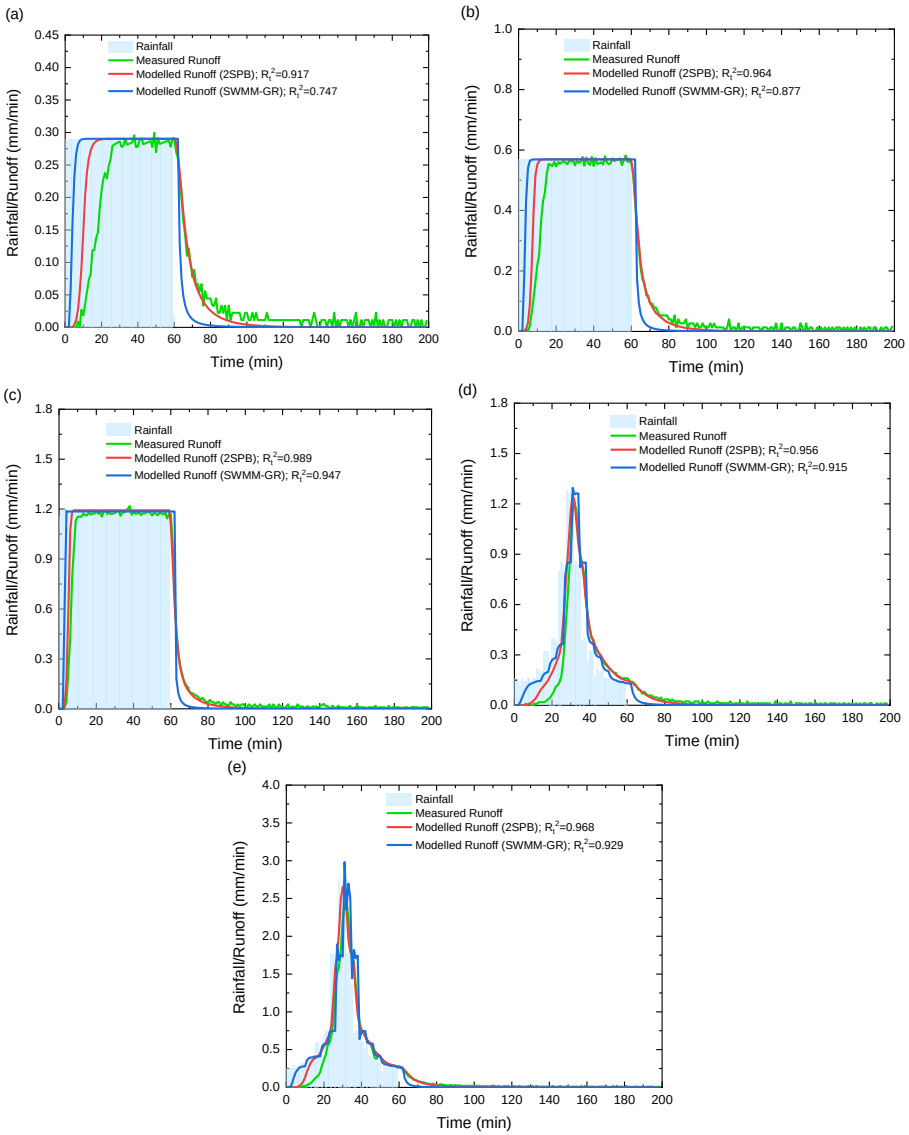

Figure 9.17. Measured and modelled runoff from the complete conventional green roof system using the identified parameters from the drainage layer isolated detention tests (2SPB: the two-stage physically-based model developed in Chapter 7 and the results have been presented in **Figure 7.14**; SWMM-GR: SWMM green roof model presented in this chapter and the results have been presented in **Figure 9.9**).

The substrate model and the drainage layer model in the 2SPB model were independently parametrised using component isolated detention tests, and the model performs well when

applied to a complete system. This indicates that the proposed model has the potential for generic application in modelling detention in a conventional green roof system. Whilst the drainage layer model in the SWMM-GR model appeared capable of regenerating the runoff from the drainage layer in the drainage layer isolated tests; it failed to regenerate the runoff profiles from the complete system accurately. This could be caused by the limitations in the way the overlying substrate layers are modelled in SWMM.

9.4.1.2 Innovative green roof system

Figure 9.18 shows the measured and modelled runoff profiles from the complete innovative green roof system using the two models. The parameters used in the models are as listed in **Table 8.1** and **Table 9.3**. Only one test for each rainfall intensity is presented in **Figure 9.18**. Both models provided reasonable estimations of the measured runoff profile (i.e. R_t^2 ranges from 0.7 to 0.9). In the medium rainfall intensity (0.78 mm/min, **Figure 9.18(b)**), the models overestimated the peak runoff by 31.7% (2SPB model) and 22.9% (SWMM-GR model). In the high rainfall intensity (1.9 mm/min, **Figure 9.18(c)**), the 2SPB model overestimated the peak runoff by 61.9%, whilst the SWMM-GR model overestimated the peak runoff by 51.1% and delayed the time of peak runoff about 2 minutes.

The SWMM-GR model underestimated detention at the start of a runoff event in the conventional green roof system, and both the 2SPB and SWMM-GR models overestimated the peak runoff associated with the innovative detention system. The underestimated detention effects noted above suggest that the SWMM-GR failed to accurately estimate the detention performance in the conventional green roof system; both models failed to accurately estimate the runoff profiles from the innovative green roof system.

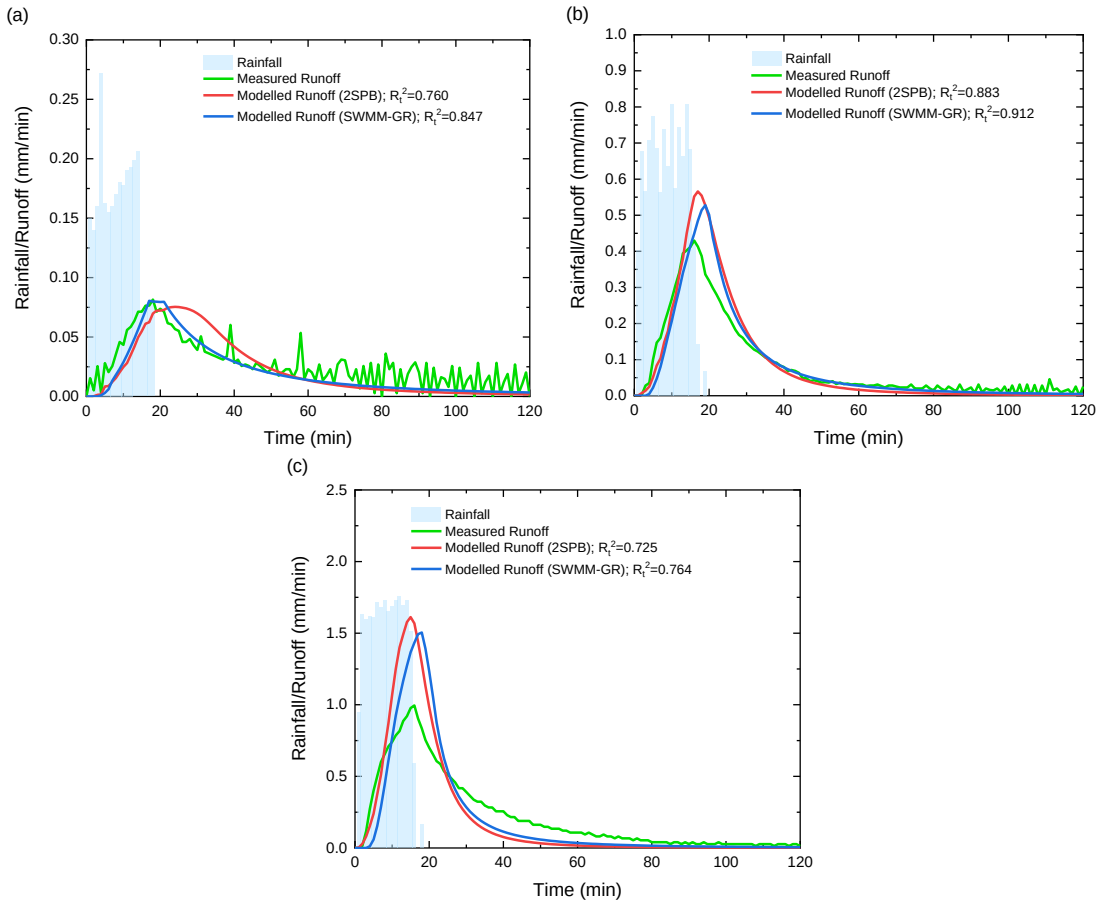

Figure 9.18. Measured and modelled runoff from the complete innovative green roof system using the identified parameters from the detention layer isolated detention tests; (2SPB: the two-stage physically-based model explored in Chapter 8 and the results have been presented in **Figure 8.20**, **Figure 8.21** and **Figure 8.22**; SWMM-GR: SWMM green roof model introduced in this chapter and the results have been presented in **Figure 9.10**, **Figure 9.11** and **Figure 9.12**).

9.4.1.3 Transferability of model parameters

A generic green roof detention model should have the characteristic of good parameter transferability. In this study, parameters determined from component isolated characterisation tests were used to model the runoff from the complete systems. When the newly-derived drainage layer model and parameters were combined with the independently parametrised physically-based substrate model, this approach (two-stage physically-based model) led to reasonable estimates of runoff from a conventional green roof system, without the need for further calibration. In the case of the SWMM green roof model, however, the full system was not modelled satisfactorily.

For the innovative green roof system, the parameters identified from the detention layer isolated tests for both models provided a reasonable estimation of the runoff profiles in response to the

low and medium rainfall intensities. However, both models failed to regenerate the runoff profile in the high rainfall intensity accurately, potentially reflecting more complex flow processes and layer interactions than conventional green roof systems, which neither model is capable of representing.

9.4.2 Infiltration model

The SWMM green roof model uses the Green-Ampt model (Equation 9.5) to represent the water infiltrating from the substrate surface to the deeper substrate. In this model, the infiltration rate is controlled by the water head ponding on the surface of the substrate. However, as the two substrates used in the two green roof systems are highly permeable (higher than the highest tested rainfall intensity), no water ever ponded on the surface of the substrate, and no detention effects were modelled due to this process. Green roof substrates commonly have high water permeability (e.g. 0.6 mm/min to 70 mm/min (FLL, 2008)), which generally prevents surface runoff. As it had been foreseen that the detention effects due to surface infiltration would not be significant, this process was not considered in the physically-based model.

9.4.3 Percolation model

The SWMM green roof model uses a percolation model (Equation 9.6) to represent the runoff from the substrate. This model assumes the substrate is at a steady-state condition, such that the moisture content is uniform throughout the depth of the soil layer. At this condition, the flow in the substrate is driven only by gravity, and the runoff rate from the substrate is equivalent to the unsaturated hydraulic conductivity corresponding to its moisture content. However, in response to low rainfall intensities, the substrate does not reach steady-state condition instantaneously, and the detention effects due to the vertical moisture content gradient are significant. Therefore, this model is not appropriate to model the response of the substrate to low rainfall intensities. **Figure 9.19** shows the modelled substrate runoff from the two systems in response to low rainfall intensities. For the conventional green roof system, **Figure 9.19(a)** shows that no detention effects are modelled by the SWMM green roof model. In contrast, the Richards Equation in the 2SPB model accounts for the non-uniform wetting process, and the detention effects in the substrate are more realistically modelled. The same unrealistic estimation of the substrate runoff profiles was also observed for the SWMM green roof model in the innovative green roof system in response to the low rainfall intensity (**Figure 9.19(b)**). It should be noted that the substrate in the conventional green roof system is twice as deep as in the innovative green roof system (100 mm versus 50 mm); therefore, the impact of the substrate model is more significant in the conventional green roof system. The comparisons made between the Richards Equation in the 2SPB model and the percolation model in SWMM indicate that the Richards Equation provides a

better representation of the substrate detention effects. However, it is acknowledged that the use of the Richards equation would significantly increase the computational cost.

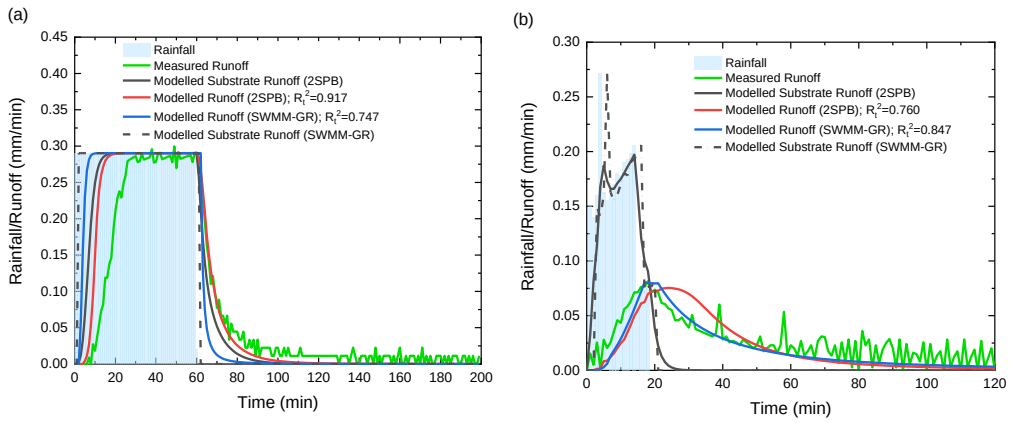

Figure 9.19. Measured and modelled substrate and bottom runoff from a conventional and an innovative green roof systems using the calibrated parameters; (a) conventional green roof system; (b) innovative green roof system.

9.4.4 Drainage layer model

The drainage layer model in the SWMM green roof model assumes that the water level in the drainage layer is constant throughout the length of the layer and that the outflow rate is determined by the water temporarily stored in the drainage layer. In the physically-based model, the water level in the drainage layer is assumed to be spatially varied, and the outflow rate is determined by the horizontal flow. Despite the fact that the physically-based model is more 'complete' than the SWMM green roof model, both models provided reasonable predictions of the runoff profiles from the drainage layer in the conventional green roof system, and there is not a strong case to be made that the new model performs better than the SWMM green roof model (**Figure 9.20**). However, both models depend on the correct characterisation of a drainage layer roughness coefficient.

For the detention layer in the innovative green roof system, both models did not provide accurate estimations of the runoff profiles from this layer (**Figure 8.13**, **Figure 8.14**, **Figure 8.15**, **Figure 9.5**, **Figure 9.6** and **Figure 9.7**). Manning's n and the drainage layer roughness coefficient for the detention layer showed an increasing trend with rainfall intensity (**Figure 8.16** and **Figure 9.8**). This may indicate that the actual flow conditions in the detention layer are more complicated than the model assumes.

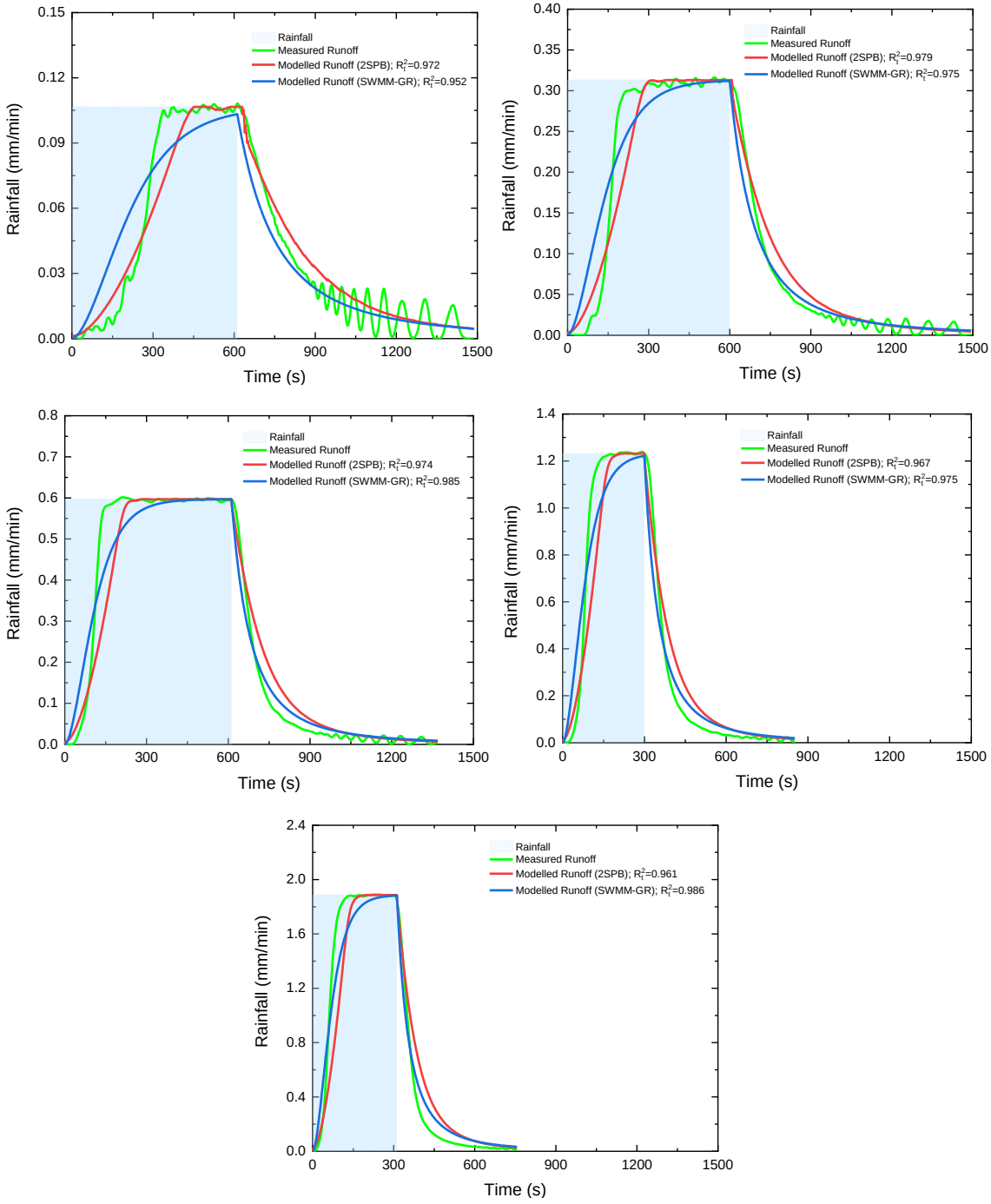

Figure 9.20. Measured and modelled runoff from the FD 25 drainage layer using the tow-stage physically-based model (2SPB) and the SWMM green roof model (SWMM-GR) (the model results for the SWMM-GR model have been presented in **Figure 9.4**).

9.5 Conclusions

The SWMM green roof detention model was found to be able to provide an accurate estimation of runoff profiles from the drainage layer in the conventional green roof system. However, the model fails to provide accurate estimations of the runoff from the complete system due to

limitations in the way that percolation in the substrate is modelled. When using the parameters identified from the detention layer isolated tests to regenerate runoff profiles from the innovative green complete system, the model significantly overestimated the peak runoff in response to the medium and high rainfall intensities, suggesting that the model has not fully captured the flow conditions occurring in the innovative detention layer.

Whilst the performance of the SWMM green roof model can be improved via further calibration of the model parameters based directly on full system build-up tests, this defeats the objective of applying physically-based models to explore design opportunities associated with unseen systems made up of different component layers.

It is also found that the physically-based model developed in Chapter 7 provides a better estimation of the runoff from the conventional green roof system than the SWMM green roof model. However, neither the model equation in the two-stage physically-based model nor the SWMM green roof model considers the effects of turbulent flow in the detention layer. This limits the accuracy of the runoff estimations for the innovative system.

10 Discussion

10.1 Chapter overview

Several discussion points related to specific findings have already been considered in previous chapters. This chapter considers the questions that have arisen from the experimental and modelling methods adopted in this study. Suggestions on how the methods employed in this study could be enhanced are discussed. A discussion of research questions arising from the findings of this study is also presented in this chapter.

10.2 Field capacity

Field capacity describes the ability of a system to hold water against gravity, and it is a critical parameter for assessing the retention capacity of a green roof system. The methods that can be used to measure field capacity and the different metrics used to define the field capacity have been discussed in Section 2.5.2.1. Results in Chapter 5 have shown that the moisture content corresponding to 6 to 10 cm suction head is more representative of green roof substrate practical field capacity than the 100 cm suction head typically used for natural soil. The moisture content profiles measured for the substrates in the detention tests (**Figure 5.6** to **Figure 5.9**) demonstrated that the rainfall intensity does not have a significant influence on the local field capacity. This section considers the field capacity measured in the field green roof test bed and the field capacity measured using the FLL method.

From the green roof hydrology perspective, field capacity is the boundary between retention and detention; runoff is generated when the system water content exceeds its field capacity. Several approaches have been developed to determine the field capacity for green roof substrates under laboratory conditions or in the field. The field capacity determined for the green roof system in the field is termed local field capacity, and it is the moisture content in the green roof system observed two hours after a rainfall event has finished. Maximum water holding capacity (field capacity) in the FLL test methods is the moisture content in the system 2 hours after the substrate has been fully saturated and allowed to drain (FLL, 2008). This section discusses the difference between local field capacity and maximum water holding capacity (FLL field capacity).

In this additional study, two sets of data were used to investigate the difference between the local field capacity and FLL field capacity. A preliminary investigation was conducted with the moisture content and runoff data collected from four field green roof test beds located in Sheffield (De-Ville et al., 2018) (TB1, TB2, TB3 and TB7). TB1 to TB3 are vegetated systems with

different substrate treatments. Heather with Lavendar substrate was used in TB1, and Sedum Carpet substrate and Light Expanded Clay were used in TB2 and TB3, respectively. TB7 is an unvegetated system with Heather with Lavender substrate. All four test beds include an egg-box style drainage layer (ZinCo FD 25). The field data includes 444 rainfall events that generated runoff, spanning a six-year monitoring period. In each test bed, three moisture probes, inserted at three depths (top: 20 mm below the surface; middle: 40 mm below the surface; and bottom: 60 mm below the surface) in an 80 mm deep green roof substrate, were used to record continuous moisture content data. Details on the collected moisture content data for analysis can be found in De-Ville et al. (2018).

Further investigation was carried out with the moisture content data collected during laboratory detention tests for four green roof substrates – Marie Curie Substrate (MCS), Heather with Lavender Substrate (HLS), Sedum Carpet Substrate (SCS) and New Substrate Mix (NSM) (reported in Chapter 5). For each substrate, four design storms ranging from 0.1 mm/min to 0.57 mm/min were applied to 100 mm and 200 mm substrates with three replications. A moisture probe in the 100 mm substrates (40 mm above the bottom) and two moisture probes (40 mm and 125 mm above the bottom) in the 200 mm substrates were used to measure the moisture content continuously. Initial wetting was conducted on the substrates with 1.2 mm/min applied for 90 minutes to 150 until steady runoff was observed before the design storms were applied to the substrate.

FLL maximum water holding capacities (FLL field capacity) for the substrates used in the green roof test beds (Chapter 4) and substrate detention tests (Chapter 5) were determined in the laboratory using the FLL method (FLL. 2008).

The moisture content data measured for the field green roof test beds is firstly considered.

Figure 10.1 compares the measured moisture content two hours after rainfall events with the FLL field capacity (the triangle markers). A vertical gradient in moisture content was clearly observed in the vegetated green roof test beds (TB1 to TB3). Different local field capacities are evident in different test beds due to the different physical properties of the substrates. Due to the vertical gradient, the local field capacity is not a static value at different substrate depths. The FLL field capacity represents the local field capacity at the lower part of the substrate. However, overall, the FLL method for determining maximum water holding capacity tends to overestimate the field capacity measured in the field. It should be noted that the FLL method measures the moisture content 2 hours after fully saturation. However, in response to real rainfall events, the green roof substrates rarely get saturated, and it takes longer for the substrate to reach its field capacity

from saturation in the FLL tests. Therefore, the FLL field capacity may not fully reflect the local field capacity of field green roofs.

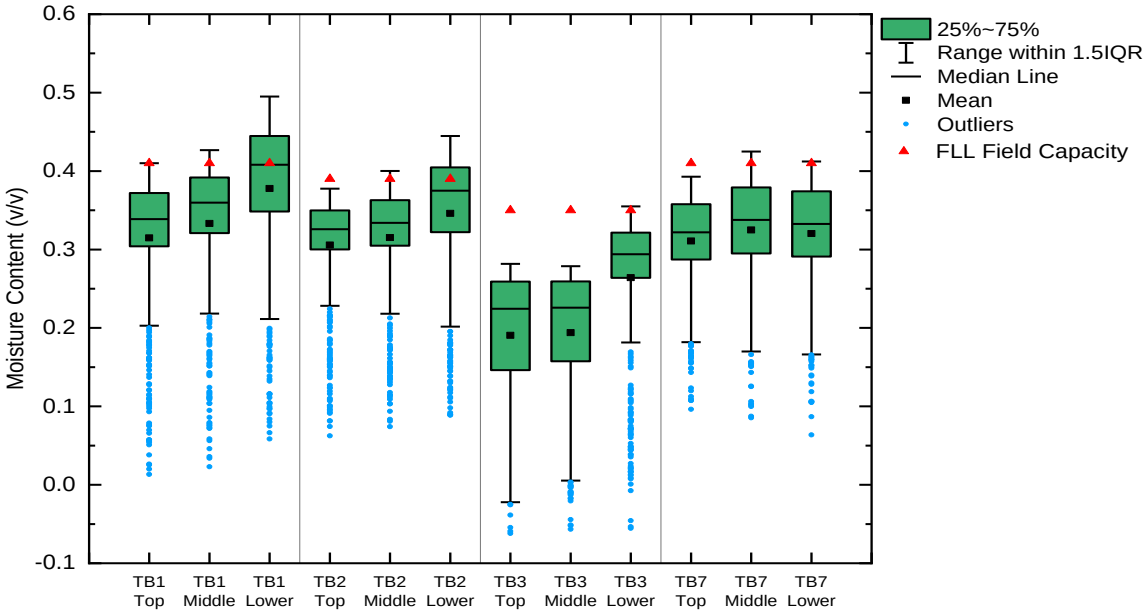

Figure 10.1. The FLL field capacity and the measured moisture content for four field green roof test beds 2 hours after rainfall events (adopted based on the moisture content data in De-Ville et al., 2018).

The field capacity measured for the four substrates in the detention tests reported in Chapter 5 is then considered.

Figure 10.2 shows the measured moisture content in the substrate detention tests 2 hours after the design storms were applied (Chapter 5). (Note that, although two of the substrates considered here – HLS and SCS – were also considered in the field test bed analysis, different batches of the materials were used, so new values for FLL Field Capacity are reported here.) The shaded areas in the figure are the FLL field capacity, determined for the substrate in Chapter 5. The wide range for the FLL field capacity may indicate uncertainties associated with subsampling and compaction. In the 200 mm substrates, the vertical gradient in moisture content is evident. However, a gradient is less significant than in the vegetated field green roof test bed (**Figure 10.1**). The field capacity varies according to the depth of the substrate. Except for SCS, The FLL field capacity is higher than the local field capacity of the substrates. In the case of SCS, the FLL method underestimated the local field capacity. This may be caused by fine losses during the FLL tests. The particle sizes in the SCS are less uniformly distributed than the other three substrates (**Figure 5.2**), resulting in a loose connection between particles. When applying high water pressure to the substrate (i.e. allowing ponding on the surface of the substrate), the fines tend to be flushed

away, which reduces the water holding capacity of the substrate. As the FLL field capacity was determined following the falling head permeability test, the loss of fines in the permeability test may have resulted in a lower value of FLL field capacity for the SCS. Compared with the variation shown in FLL field capacity, the variation in local field capacity, determined for the substrates after different rainfall intensities, is not significant.

In the field green roof test bed, the moisture content at the lower part of the substrate is higher than the top part (**Figure 10.1**). However, in the detention tests with the substrate columns, the lower part of the substrate is slightly drier than the upper part of the substrate (**Figure 10.2**). The reversed vertical moisture gradient may be caused by uncertainties associated with the moisture probe calibration, which will be discussed in Section 10.4.

Based on the results from the field and laboratory data, it is found that the FLL method tends to overestimate the local field capacity. This observation is thought to be caused by the way the system is wetted. With the free drainage boundary condition at the bottom of the system in the field, during the rainfall events, the water flows through mainly coarse pore space. While during the soaking process for the FLL approach, all the pore space is occupied by the water, including the small pore space that holds water tightly. As it is hard for the water trapped in the fine pore space to be drained under gravity, more water is retained in the material due to soaking. Therefore, the FLL method results in a higher estimate of field capacity. However, it is believed that the local field capacity is more relevant in practice, as saturated conditions are rarely observed in the field. For representative and reproducible controlled detention tests, it is suggested that the moisture content in the green roof system should be brought up to local field capacity through the application of relatively high-intensity rainfall. Rainfall should be applied to the system until steady runoff is observed, and the system should then be left to drain for 2 hours.

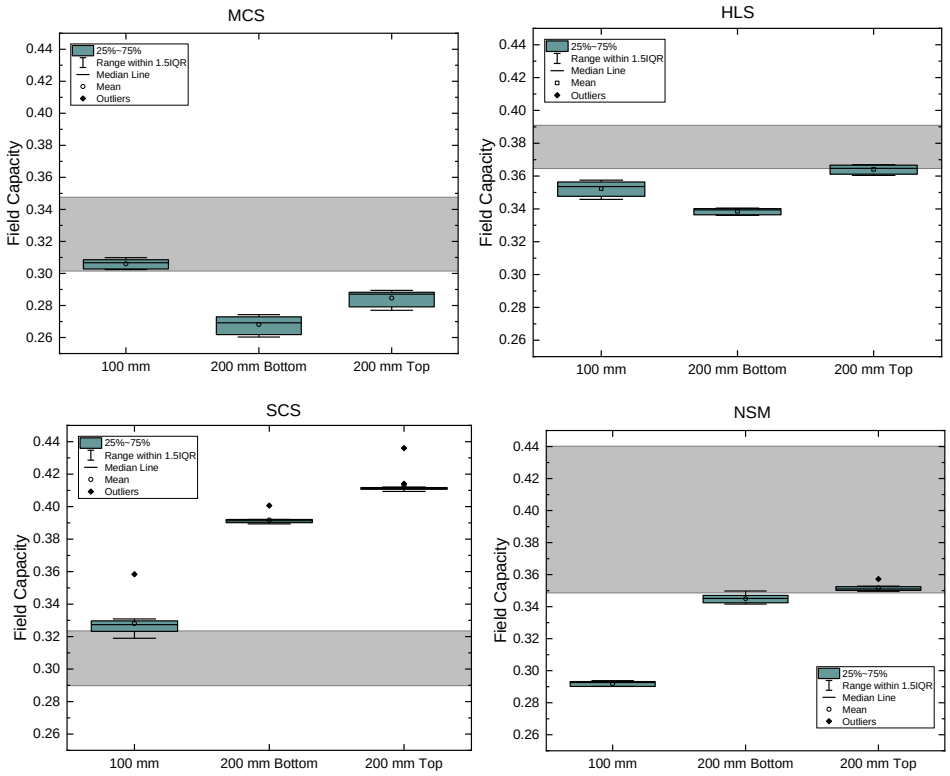

Figure 10.2. Substrate moisture content measured by the moisture probe 2 hours after storm events for the substrate detetnion tests in Section 3.5.1 (the shaded area indicates the range of FLL field capacity).

10.3 Pore size distribution

Based on the fitted SWRC (Durner model, presented in **Table 5.2**), the pore size distribution of the four substrates can be derived using the capillary law theory (Equations 2.2 and 2.3), and **Figure 10.3** presents the derived pore size distribution. The frequency of an equivalent radius is proportional to the numbers of capillaries that have the same radius.

As the Durner equation is a model for a dual-pore system, the derived pore size distribution should show two peaks. However, influenced by the weighting factor and the properties of the pore systems, the second peak (corresponding to small pore sizes) can be less significant than the first peak (corresponding to large pore sizes). For example, the two peaks for MCS and SCS are apparent, while the second peak for HLS and NSM is less significant.

The prose size distribution in a substrate relates to its water-conducting and storage capacities. Continuous capillary paths form between micropores, so these pores dominate the water retention capacity of the substrate. On the other hand, macropores do not form capillary menisci, and water cannot be retained in these pores (Kutílek, 2004). As Water movement in macropores, dominated by gravity forces, is rapid, macropores determine the water flow properties of the

substrate (Conn et al., 2020; Germann and Beven, 1985; Menon et al., 2015). The equivalent pore radius that separates micropores and macropores varies in the literature. For example, Kutílek (2004) and Liu and Fassman-Beck (2017) used a pore radius of 1 to 1.5 mm as the boundary between micropores and macropores; Conn et al. (2020) and Menon et al. (2015) suggested a pore radius of 50 µm as the threshold of micropores and macropores. However, macropores generally refer to the pores with large pore sizes, and micropores are the pores with small pore sizes. For the four green roof substrate, a high proportion of large pore sizes was estimated for MCS and SCS. This is consistent with the results of FLL permeability tests (**Table 5.1**), where MCS and SCS showed a higher value of water permeability than the other two substrates. If a pore radius of 50 µm is used as the boundary of micropores and macropores, HLS shows a higher proportion of pore sizes in the micro-scale than the other substrates. Therefore, a higher water holding capacity is expected in HLS. This is also consistent with the results of FLL MWHC tests (**Table 5.1**), where HLS showed the highest MWHC.

The same exercise was also conducted in Liu (2016), where the pore size distribution of seven green roof substrates was derived from the fitted SWRCs. Comparing the substrates investigated in both studies, the dominant pore size of the substrates (the first peak in the pore size distribution) in both studies is similar (between 0.03 cm to 0.05 cm). However, the substrates in this study contain a broader pore size. This may indicate that the substrates in this study are more heterogeneous than the substrates in Liu (2016).

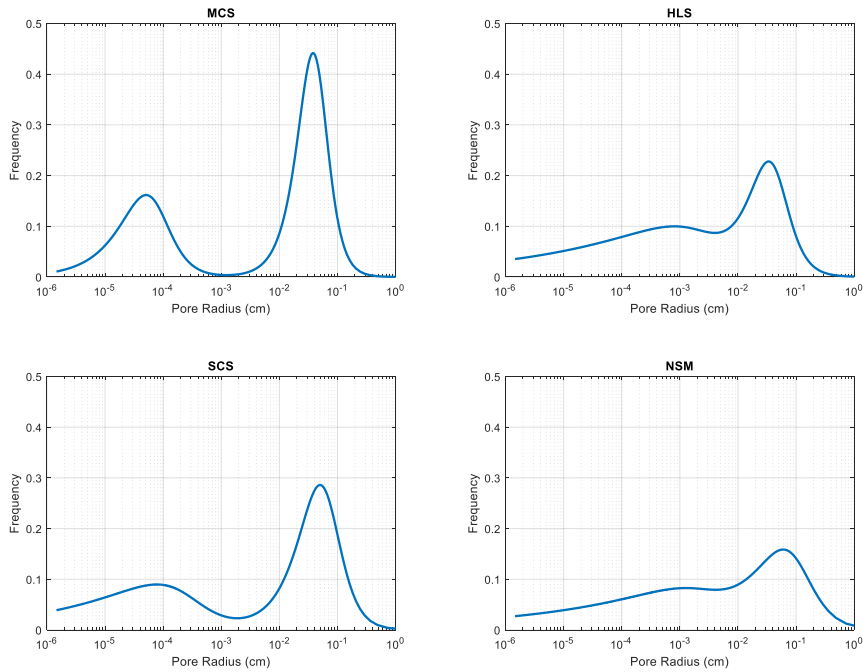

Figure 10.3. Pore size distribution for the four green roof substrates derived from the fitted Durner equation presented in **Table 5.2**.

10.4 Influence of compaction

In the FLL method for determining the substrate's maximum water holding capacity and permeability, six compactions of a 45 kg proctor hammer from 450 mm drop height were applied to the substrate samples. This practice replicates the expected consolidation of the substrate in the field. However, due to the limitation of the experimental apparatus (i.e. risk of shattering the perspex column and ceramic plate), no compaction was applied to the substrate samples for the SWRC and HCF characterisation tests and the substrate detention tests. This section investigates the influence of compaction on the measurements of maximum water holding capacity and permeability using the FLL method.

The maximum water holding capacity and the permeability of the four representative green roof substrates (Marie Curie Substrate (MCS), Heather with Lavender Substrate (HLS), Sedum Carpet Substrate (SCS) and New Substrate Mix (NSM)) were determined based on the FLL method with and without compaction. Compaction refers to the six compactions of a 45 kg proctor hammer from 450 mm drop height, and without compaction refers to the method that the substrate sample was poured in the measurement vessel and levelled in place.

Figure 10.4 shows the results of the measured Maximum Water Holding Capacity (MWHC) and permeability. The maximum water holding capacity of NSM increased after compaction. However, there is no significant difference in MWHC for the rest of the substrates due to compaction. As the water held in micropore spaces (usually <50 µm) does not drain under gravity, the volume of micropores determines the substrate's MWHC (Burés et al., 1991). Compaction has the potential to decrease the total pore volume and increase the MWHC. However, the decrease in pore volume also depends on the particle size distribution (Menon et al., 2015). MSC, HLS and SCS contain a high proportion of large particles and a low percentage of fine particles. The volume of micropore space in these substrates is low, so compaction did not significantly increase these micropore space volume. Whilst for NSM, as it contains more fines than MSC, HLS and SCS, compaction increased the total volume of micropores.

In terms of permeability, except for HLS (the permeability almost stayed the same after compaction), all the substrates showed a decreasing trend in permeability after compaction (**Figure 10.4**). The flow rate and moisture detention through a substrate tend to be controlled by the volume of macropores (>50 µm) (Conn et al., 2020; Menon et al., 2015). Compaction decreased the macropore volume in substrates, leading to a reduction in pore space connection and flow paths that decreased permeability (Conn et al., 2020; Menon et al., 2015).

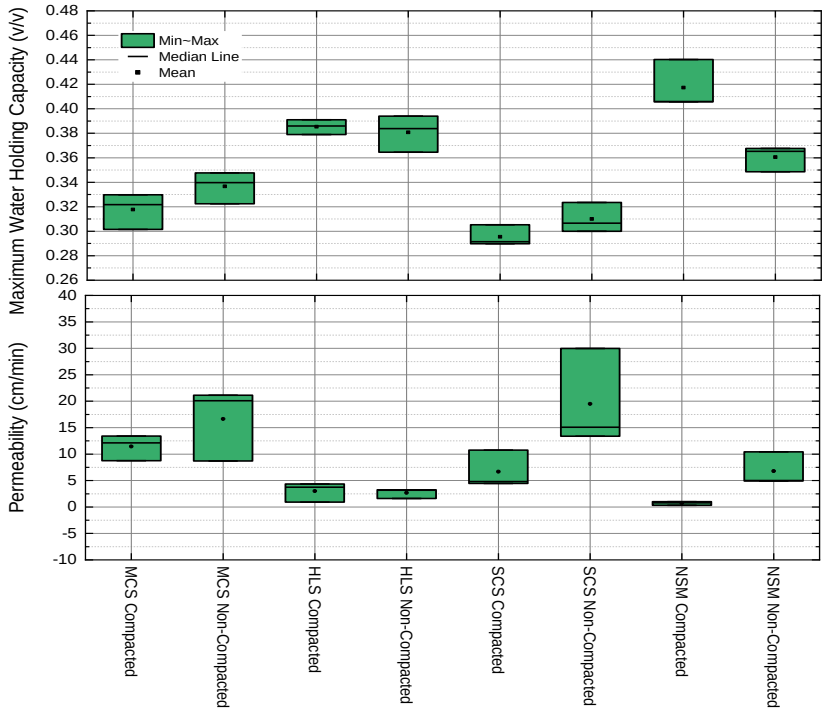

Figure 10.4. The maximum water holding capacity and permeability (FLL method) for four green roof substrates with and without compaction.

The investigation above shows that compaction can alter the substrates' total pore volume and the substrates' hydrological behaviour. This finding here also has implications on the applications of the measured SWRC and HCF reported in this study. It is likely that compaction will not significantly influence the measured SWRC, as micropores are unlikely to be affected by compaction. It is very likely that the HCF will be influenced by the compaction, as the macropores dominate the flux process in the substrate, and those pores are very likely to be affected by compaction. The characterised SWRC and HCF in this study are for non-compacted substrates. These characteristics may not represent the substrates in field green roof test beds where consolidation is expected in the substrates. However, further study is needed to get a better understanding of the difference that compaction makes to the results of SWRC and HCF measurements. This may require further modifications to the experimental apparatus so that compactions can be applied to the substrate samples.

10.5 Instrument accuracy and limitations

Measuring the moisture content in heterogeneous green roof substrates is an acknowledged challenge. In this study, the accuracy of the measured hydraulic conductivity functions depends on an accurate measurement of the substrate’s moisture content. In addition, the moisture content data measured in the detention tests were used to validate the modelled vertical

moisture content profile, and the moisture content here could also influence the assessment of the model performance. The moisture probes used in this study have been calibrated with each specific substrate prior to the HCF characterisation. However, due to the green roof substrate's heterogeneous nature, the raw readings from the moisture probes showed a high variation (especially in the range from field capacity to saturation, which is the region that this study is most interested in). The variations in moisture probes can lead to different substrate moisture content estimations and influence the measured HCF and moisture content profiles. This section discusses the potential influence of moisture probe calibration equations on the measured moisture content.

The raw dielectric permittivity data collected from the ECH2O 5TM moisture probes during calibration (**Figure A.3**) are considered in this section. Five readings from the five moisture probes for the same bulk sample of the substrate at each moisture content were used for analysis in this section. Calibration equations for the four green roof substrates were derived based on the measured data points (**Figure 10.5**). The two horizontal lines (0.3 to 0.5 v/v moisture content) in **Figure 10.5** indicate the typical values for field capacity and saturation in green roof substrates. The variation in moisture probe readings is most significant in the SCS substrate (where a wide range of dielectric permittivity was obtained for the same moisture content), and it is less significant in HLS and NSM. As variation between moisture probes is minor, the variation showed here is believed to be caused by the texture of the substrates. The high variation observed in SCS may indicate that it would be more heterogeneous than HLS and NSM.

The calibration equations used to interpret the moisture content data in Chapter 5 were derived using all the measured data points. In this section, new calibration equations were obtained by fitting to the right and left boundaries of the measured data points. As suggested by the moisture probe manufacturer, a 3rd order polynomial equation was used to fit the measured data. **Figure 10.5** also shows the fitted curves. The moisture probe provides more accurate measurement at the low moisture content (i.e. moisture content <0.3 v/v) than at the high moisture content. The accuracy of the moisture probes also depends on the type of green roof substrate. In MCS, the left calibration curve shows a 'flat' region at moisture content around 0.3, and the same region is witnessed in SCS for the right calibration curve. This indicates that the moisture probe may fail to provide meaningful moisture content measurement in this region if the relevant calibration equation is used. For HLS and NSM, the moisture probe readings are consistent over the calibration moisture contents, and the fitted curves are consistent. As no 'flat' region was observed in the fitted curves for HLS and NSM, the moisture content measurement for these two substrates is believed to be more accurate than MCS and SCS.

The moisture content measurement using the moisture probes relies on a good hydraulic connection between the probe rods and substrate particles. For the substrates containing a high percentage of large particles (MCS and SCS), the connection is poor, so the readings are highly varied. Most green roof substrates are engineered and highly heterogeneous media, and when the moisture content exceeds its field capacity, a saturated zone generates at the bottom of the substrate. This also increases the difficulty of obtaining reliable readings from the probes and subsequently introduces uncertainties to the moisture probe calibration.

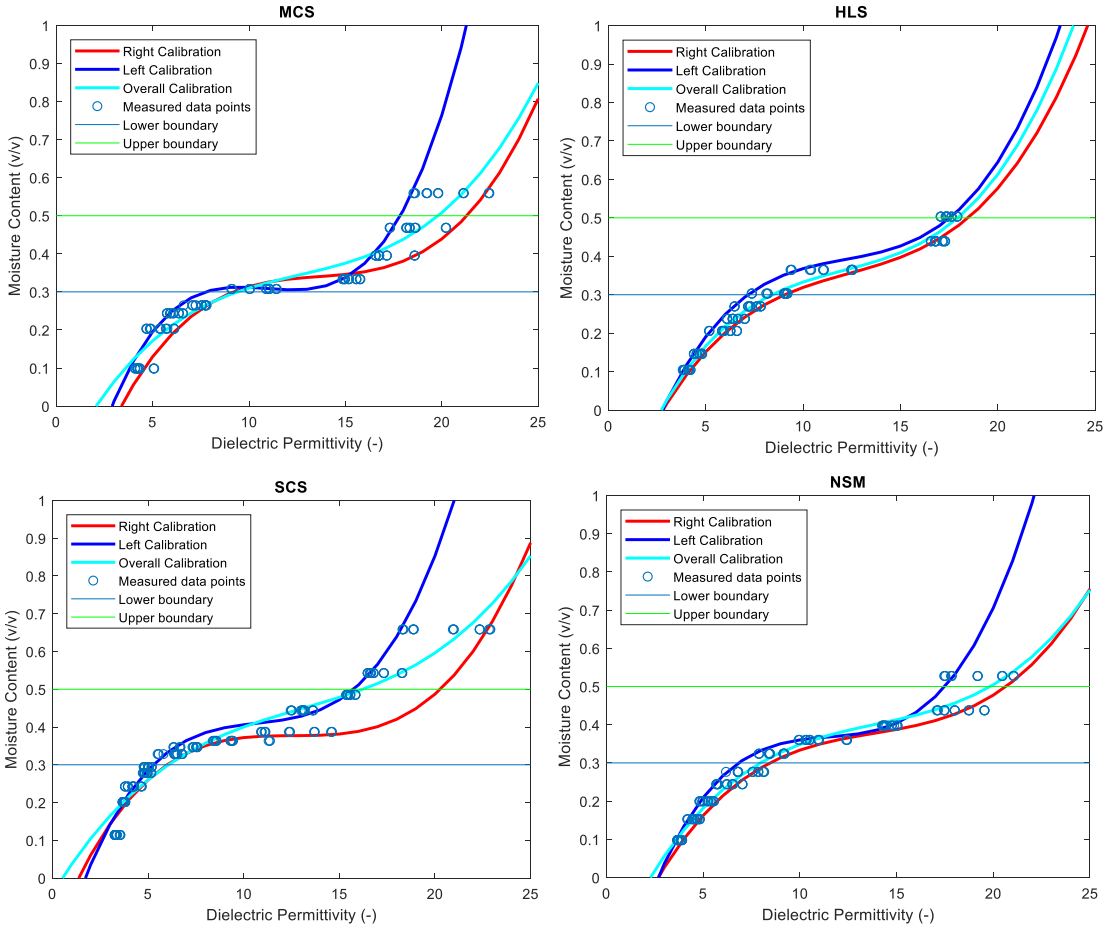

Figure 10.5. Calibration equations determined for the moisture probes using different dataset (the horizontal lines indicate typical lower and upper boundaries for the moisture content measured in the detention tests).

Further investigation was conducted with the measured moisture content profiles during the detention tests (Chapter 5). The left and right moisture probe calibration equations (presented in **Figure 10.5**) were used to determine the moisture content for the 200 mm substrates in response to the design storm 3 (0.5 mm/min for 30 minutes). This design storm was selected as the moisture content change in the substrates in response to this storm is more dynamic than in the other design storms.

Figure 10.6 shows the moisture content profiles measured in the detention tests using the left and right moisture probe calibration equations. It is not surprising that different values of moisture content were obtained when different calibration equations were used. The left calibration equation generally provides higher moisture content values than the right calibration equation. In the HLS and NSM, the calibration equation does not influence the observation that the moisture content at the top part of the substrate changes more rapidly than at the bottom. However, neither the top nor the bottom part of MCS and SCS showed any significant change in response to the rainfall when the left (MSC) or the right (SCS) calibration equation was used. This is caused by the 'flat' regions in the calibration curves (**Figure 10.5**). The moisture content data showed that the initial moisture content at the bottom part of the substrate is drier than the top. However, the actual possible moisture content in the substrate can lie in the region between the right and left calibration curves. There is a possibility that the bottom moisture content is slightly higher than the top moisture content in MCS, HLS and NSM.

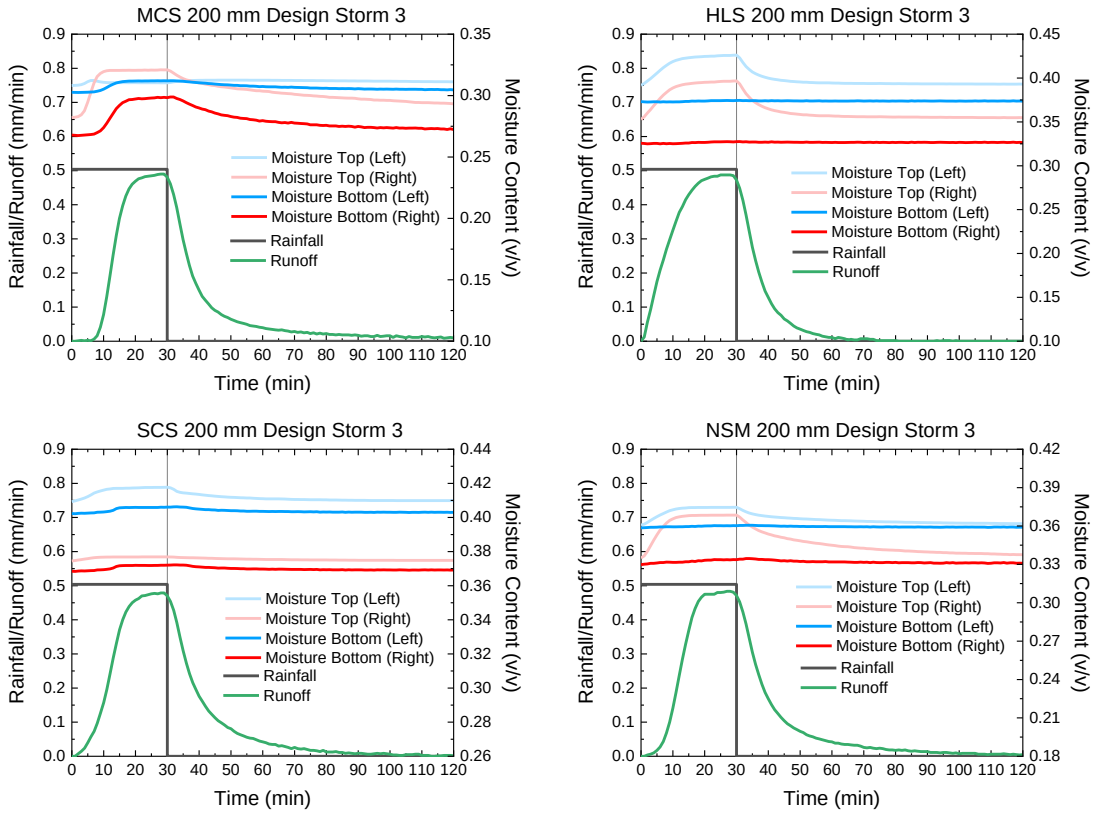

Figure 10.6. The measured moisture content in the substrate in response to the design storms using the calibration equations in **Figure 10.5**.

Overall, it is evident that the moisture probe calibration equations influence the measurement of moisture content. The moisture content data obtained during the infiltration tests can also be altered if a different calibration equation is used. Consequently, a different HCF equation for the

substrate will be obtained, ultimately influencing the modelled runoff profiles. However, further study is needed to investigate the impact of the calibration equations on the HCF and to determine how sensitive the model results are to the calibration equations.

The above investigation revealed that the uncertainties associated with the moisture probe calibration could influence the results of the measured vertical moisture content profiles and may also potentially influence the measured HCF in this study. However, the uncertainties associated with the moisture probe calibration cannot be totally erased when they are used with the highly heterogeneous green roof substrates. It is suggested that it is reliable to utilise moisture content data to understand the dynamic change in green roof substrates, but extra caution should be given to the use of absolute values.

In addition to the moisture probe, the influence of the tensiometers on the measured HCF presented in this study should also be noted. First, it requires a hydraulic contact between the substrate water and tensiometer water to measure the substrate suction head. However, due to the heterogeneous nature of the green roof substrate and the small active area of the tensiometer ceramic tip (i.e. 0.5 cm^2), the measurement from the tensiometer may only represent the value of a small local area of the substrate. Moreover, the tensiometers used in this study were not calibrated due to the lack of a benchmark SWRC for green roof substrates; therefore, although the manufacturer reported accuracy of ± 0.5 kpa, the exact accuracy of the tensiometers measuring the suction head of green roof substrates is unknown. This introduces uncertainties to the measured values of the suction head and, consequently, the HCF.

Throughout this study, the model results were compared with the measured runoff to evaluate the performance of the models. However, it should be noted that limitations with the runoff measurement instruments also result in the difference between the modelled and measured runoff profiles. For example, the pressure transducer used in the substrate and the conventional green roof system detention is not capable of measuring low flow rates (it is designed to measure the pressure in the range of 0.75 m and 1.5 m of water head). The background noise of the pressure transducer tends to mask the small change in water level, resulting in a long failing tail in measured runoff profiles. The approach of using a scale to measure the runoff from the innovative green roof system may not be an ideal method for this type of measurement. The 0.2 kg sensitivity of the scale means fluctuation can occur in measured runoff data at low flow rates. Besides, as a scale may take time to provide a stable reading of the weight placed upon the pan, the scale may not be appropriate to be used to monitor the change of weight that changes rapidly with time (i.e. runoff). The limitation of the scale could result in an inaccurate measurement of

the runoff profiles, and when the measured runoff data was used to assess models, less satisfactory performance was obtained.

It is acknowledged that limitations with the instruments can influence the measured results and the assessment of the model performance. There are instances where the model's less-than-perfect fit to observed data (i.e. with the innovative green roof system) could be due to the accuracy of measured data. However, it should be noted that substrate heterogeneity also always limits the accuracy of the model result.

10.6 SWRC and HCF measurements

The SWRCs measured for the green roof substrates in this study are compiled from non-overlapping data from two different methods (hanging column and pressure extractor), potentially using different batches of the substrate. Therefore, there are some risks and uncertainties associated with using the characterised SWRC data here. The pressure extractor samples were sieved to exclude particles larger than 2 mm, and the sample sizes were very small. The reason for sieving out large particles is that only small pores can hold water against high suctions, and the large particles do not contribute to small pore spaces. Smaller samples were used in the extractor method because the water release process from micropores is slow, and using a small sample reduces the test time. Large samples without sieving were used in the hanging column method to preserve the original substrates' particle size distribution. The uncertainties associated with subsampling were minimised by taking three samples from the same substrate batch. The uncertainties of using two different methods were not addressed in this study. However, this study focuses on the substrate detention behaviour; the SWRC at low suction heads (i.e. data points measured by the hanging column method) alone is more relevant to this study. Therefore, it is believed that the SWRC data measured by the pressure extractor method do not significantly influence the main findings of this study.

Uncertainties associated with altering methods also exist in the HCF measurement. Similar to the SWRC, three different methods (FLL permeability, steady-state infiltration column and transient infiltration column) were applied to characterise substrate HCF without any overlapping data. The FLL method was used to determine the saturated hydraulic conductivity, as it is a widely used method in practice to determine this property for green roof substrates. Some standard methods (i.e. falling head and constant head methods) for determining the saturated hydraulic conductivity of natural soil also exist. However, as those tests use high water heads to generate the head difference, substantial percentages of small particles in the substrate will be flushed away in the tests. This will lead to an overestimate of the substrate's saturated hydraulic

conductivity. The constant head method was also used to measure the substrate's saturated hydraulic conductivity in this study (not shown). Results showed that the constant head method provided a value of saturated hydraulic conductivity 50 times higher than the FLL measurement. It is acknowledged that substrate particles are also lost in the FLL tests. However, under low water pressure, the losses are not significant.

As the substrate saturated hydraulic conductivity is usually high (e.g. 10 cm/min), a very high flow rate is required to saturate the substrate during the infiltration test. The rainfall simulator (**Figure 3.2**) in the infiltration test apparatus was designed to provide evenly distributed rainfall onto the substrate surface, and it is not capable of providing such a high flow rate to the substrate. Therefore, the saturation condition has never been achieved in the infiltration tests, and no such measurement can be made in the test. The steady-state method was used to measure the HCF at high moisture content. As the infiltration apparatus cannot apply a very low flowrate to the substrate, the transient method was used to determine the HCF at low moisture content. Due to limitations with the tensiometers, the suction head data a few hours after inflow stopped cannot be fully captured by the tensiometers. The tensiometers started to work when the moisture content in the substrate has dropped to a certain level. This resulted in a gap in the measured data points between the steady-state and the transient method. Using the determined SWRC to estimate the substrates suction head corresponding to the measured moisture content at the initial drainage process has the potential to solve the problem with the tensiometers. However, this approach will introduce other uncertainties associated with sample size.

Hysteresis is the phenomenon in which soil shows different SWRCs for the drying and wetting processes. The moisture content of the drying phase is typically higher than the moisture content of the wetting curve at the same suction head. The SWRC measured for the green roof substrates in this study is the drying curve (Chapter 5). However, in response to the rainfall event, wetting and drying processes can happen simultaneously in the substrate. The influence of the wetting-drying processes on the model results was briefly discussed in Chapter 7. The hysteresis effect was found to have some impacts on the modelled runoff profiles. However, the wetting curve used in Chapter 7 is a constructed curve without the support of actual experimental data. To fully explore the influence of the hysteresis, additional experiments to characterise the substrate wetting curve are needed. This would involve using the Hanging Colum apparatus (**Figure 3.1**) but starting the test with initially dry samples. The new measured SWRCs would then be used to regenerate the runoff profiles for the detention tests to assess their influence on the model results.

The hysteresis effect could also influence the HCF measurement. In the steady-state method, water was flowing into initially dry substrates, so the water was wetting the substrates. In the transient state method, the water released from initially wet substrates, so it was a drying process. Due to the difference in the wetting and drying processes in the substrate, the actual substrate wetting curve or drying curve may be different from what was measured in this study. The drying process in the steady-state method and the wetting process in the transient state method can be characterised using the apparatus in **Figure 3.2**. This will be achieved by starting the infiltration test with initially dry substrate samples and decreasing the flow rate applied to the substrate to obtain a steady-state condition. The transient technique can be used to interpret the data collected from the initial state to the first steady-state condition corresponding to the highest flow rate.

Two infiltration tests were conducted with the same substrate sample from different batches, and the results of the two tests were averaged to derive the HCF for the substates. This practice is to minimise the uncertainties associate with subsampling. The variation between tests is evident in the measured HCF (**Figure 5.4**). However, as the infiltration test is exceptionally time-consuming, it is impossible to obtain all the possible HCFs for the substrate. There is a possibility that a green roof substrate with the same recipe would show an HCF that is different from the HCF determined in this study. A systematic sensitivity study and uncertainty analysis may be needed to investigate how sensitive the model results are to the HCF. This will need to generate a series of arbitrary HCFs and regenerate the runoff profiles for the detention tests using the Richards Equation. The goodness of fit parameters (i.e. R_t^2) can be used to evaluate the model results and assess the influence of HCF on the model results.

10.7 Model initial and boundary conditions

The lower boundary condition set to the Richards Equation to model the runoff from the green roof substrate has been discussed in Chapter 4. It has been found that a constant head lower boundary condition represents the measured moisture content data better than the seepage and free drainage boundary conditions. This section discusses the initial condition set to the Richards Equation. The measured moisture content data in a field green roof test bed (TB1, Chapter 4) and in the substrate columns in the detention test (Chapter 5) will be used to understand the initial vertical moisture content distribution in the green roof substrate.

For modelling purpose, the initial condition assigned to the substrate is a constant head condition. This condition is to represent a condition of no water flow in the substrate at the beginning of the storms. However, due to the effect of consolidation and the influence of vegetation, the initial

moisture content over the substrate depth does not necessarily need to be at a constant hydraulic head to achieve no flow from the bottom of the substrate. This condition can be exhibited in a system in which low hydraulic conductivity fine media are settled at the bottom, and coarse high hydraulic conductivity media are layered at the top (**Figure 10.7**). In this stratified system, the high moisture content will be expected at the bottom part of the substrate, and low moisture content will be expected at the top part of the substrate at field capacity.

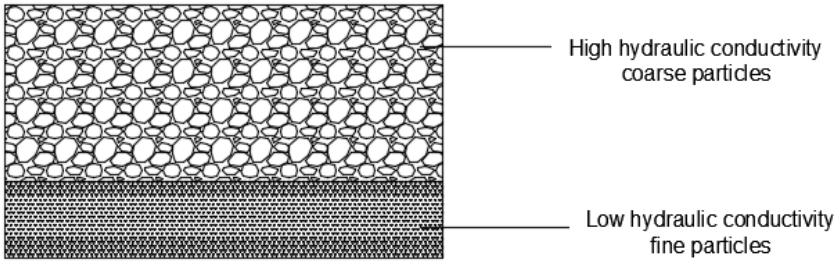

Figure 10.7. A conceptual representation of the stratification effect in green roof substrates.

For preliminary investigation, the moisture content data collected from the field green roof test bed (TB1) at the beginning of five real rainfall events are used (**Table 4.3**). **Figure 10.8** shows the measured and modelled moisture content in TB1 at the beginning of the storms. The modelled moisture content at the middle of the substrate (i.e. 4 cm) is the average moisture content of the three measured moisture content. The moisture content at other depths was calculated based on the measured SWRC and the constant hydraulic head assumption. Both the van-Genuchten and Durner models provide a very similar distribution of the moisture content over the substrate depth at the initial stage. However, compared with the measured moisture content data, the model underestimated the substate vertical moisture content gradient. The difference between modelled and measured vertical moisture content gradient can be attributed to the stratification effect in the substrate over time.

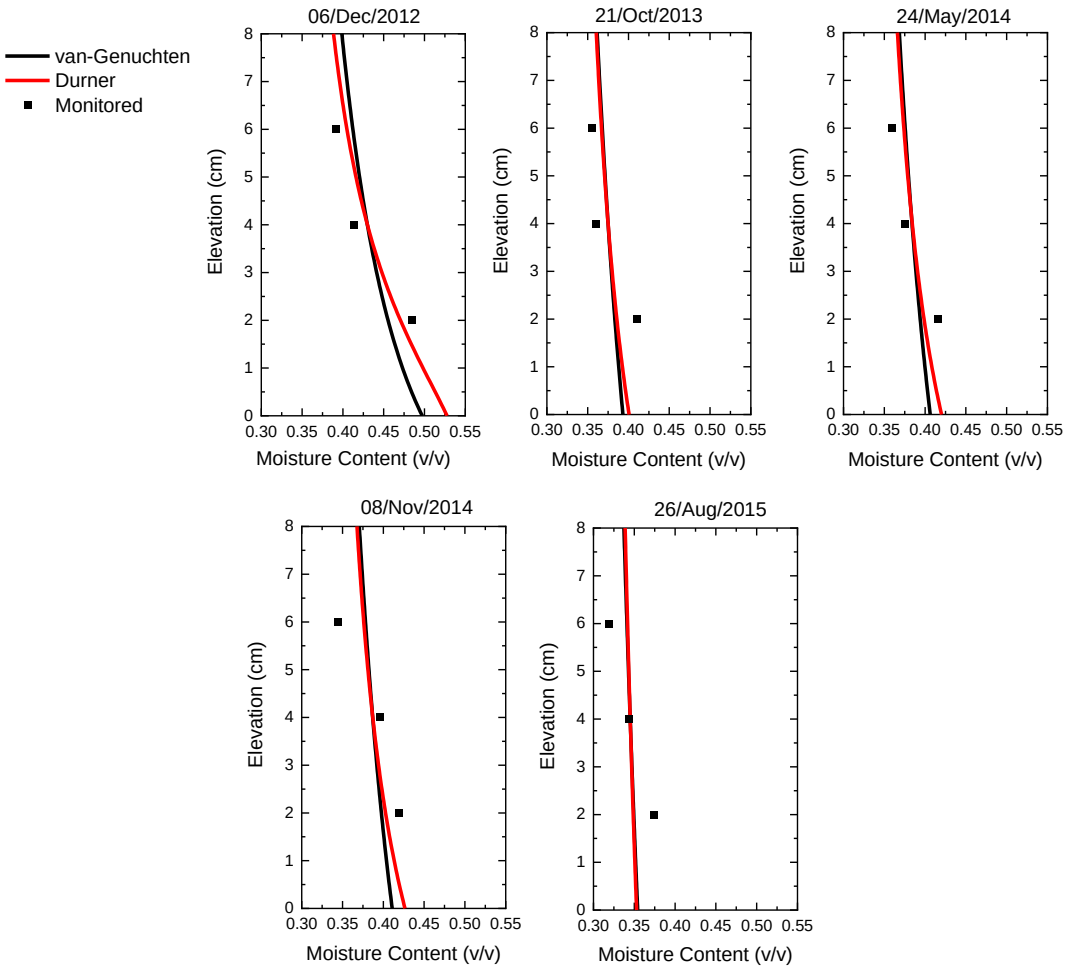

Figure 10.8. Moisture content distribution with the depth of the substrate at initial conditions for a field green roof test bed (TB1).

The moisture content data collected in the detention tests for the 200 mm substrates prior to the design storms (the measured moisture content data can be found in Appendix C) are used for further investigation. **Figure 10.9** shows the modelled moisture content at the 200 mm substrates at the beginning of the storms. The vertical gradient in the bare substrate is significantly lower than in the vegetated substrate in the field. **Figure 10.9** also shows the modelled vertical moisture content distribution at the initial condition. Instead of using the averaged moisture content, the moisture content at the bottom of the substrate (i.e. 4 cm above the base) was set to be the same as the measured moisture content at the same location. This practice here is to keep consistent with the modelling approach with the 100 mm substrate, where only the bottom moisture probe was buried in the substrate for the measurement. The moisture content at other depths was calculated using the Durner model and the constant hydraulic head assumption. For these cases, the model overestimated the vertical moisture content for the substrate at the initial conditions. As they are unvegetated substrates, consolidation is unlikely to happen in the substrate during

the detention tests. The observation here is more likely to be caused by the uncertainties associated with the moisture probe calibration. However, again, it is sensible to utilise the measured moisture content data to measure the dynamic change.

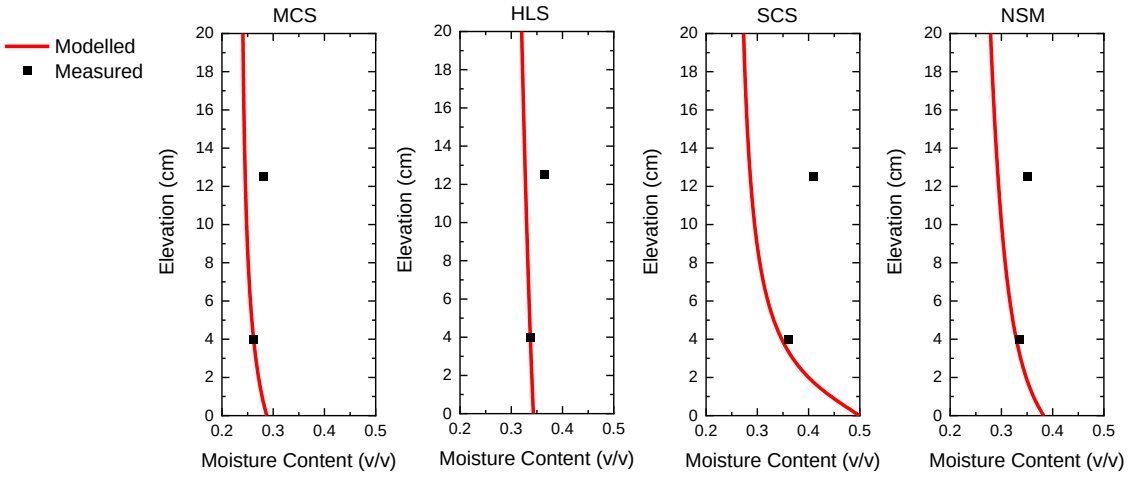

Figure 10.9. Moisture content distribution with the depth of the substrate at initial conditions (substrate columns for the detention tests described in Section 3.5.1).

Overall, based on the field and laboratory moisture content data, differences exist between the measured and modelled vertical initial moisture content. However, given the model results showed good consistency with the measured runoff and moisture content profiles during storms (Chapters 4 and 6), the difference between modelled and measured initial conditions is not considered to be substantial to the model results.

10.8 Model accuracy and substrate heterogeneity

When parameterised from independent physical analyses of each layer's components, the two-stage physically-based model was shown to generate reasonably good estimates of the runoff profile associated with a conventional green roof system (**Figure 7.14**). Nonetheless, it was acknowledged that the simulations tended to underestimate the observed detention effects, particularly on the rising limb of the runoff hydrograph at lower rainfall intensities.

There are a number of considerations relating to the substrate layer model that contribute to further uncertainties. The model assumes 1D – purely vertical – flow in the substrate, and the model is sensitive to the correct characterisation of substrate SWRC and HCF. The characteristics observed in independent media tests may not be representative of the specific sub-sample and compaction levels utilised in the detention experiments or field installations. Indeed, the heterogeneity of substrates will, unfortunately, always limit simulation accuracy for green roof systems. Therefore, whilst further refinements to the two-stage physically-based model may

improve its accuracy in theory, in practice, the proposed model probably represents an appropriate balance between model complexity and the uncertainties inherent in this type of system.

11 Conclusions and Future Work

11.1 Chapter overview

This chapter summarises the conclusions, findings and discussion of the thesis. Recommended further work that has arisen during this study is aslo presented. The key findings relating to the original study objectives and aim are summarised along with some important points are presented at the end.

11.2 Summary of findings

Monitored data and experimental characterisations

1) The basic physical properties of four representative green roof substrates were characterised based on the FLL method; the Soil Water Release Curve (SWRC) of the substrates was measured by the hanging column method; new Hydraulic Conductivity Function (HCF) data for the substrates was measured through infiltration tests using steady-state and transient techniques, and new detention tests were conducted with the green roof substrates using five design storms.
2) The SWRC data for four representative green roof substrates shows that the Durner model correctly represents the water release characteristics of the green roof substrates.
3) Moisture content measured at 6-10 cm suction head may provide a better practical estimate of field capacity in the brick-based green roof substrates than the 100 cm value typically assumed for natural soils.
4) The change in moisture content in response to a storm is more rapid at the top of the substrate than at the bottom.
5) The conventional approach for estimating hydraulic conductivity (Durner-Mualem) failed to represent the hydraulic conductivity function (HCF) for green roof substrates accurately.

The Richards Equation for modelling green roof substrate detention effects

1) The approach of using the Richards Equation to represent the temporary (detention) moisture storage between field capacity and saturation is proved to be capable of regenerating observed runoff profiles.
2) The lower boundary condition of the Richards Equation has a significant impact on predictions of both runoff and vertical water content profile in the substrate, and the constant suction head boundary condition represents the observed behaviour better than the seepage and free drainage boundary conditions.

3) HCF curves derived from measured HCF data points result in better performance than the conventional Durner-Mualem approach in modelling the moisture content and runoff profiles for the green roof substrates.
4) A simplified HCF that uses saturated hydraulic conductivity and the moisture content at 0.1 cm/min provides reasonable estimations of runoff profiles.

Two-stage physically-based green roof detention model

The physically-based drainage layer model

1) A new physically-based green roof drainage layer model based on the Saint Venant equation showed a good ability to regenerate the runoff profiles from plastic-based conventional green roof drainage layers.
2) The model results are sensitive to Manning's n, which is material-specific and can be identified from component isolated detention tests.

Modelling of a conventional green roof system

3) The substrate Richards Equation and the physically-based drainage layer model were combined to form a two-stage physically-based green roof detention model. This model provides good predictions of the runoff profiles from a conventional laboratory green roof test bed.
4) Further calibration of the drainage layer parameters is needed if the two-stage model is going to model an aged field green roof system.

Modelling of an innovative green roof system

5) The physically-based drainage layer model could provide reasonable predictions of the runoff profiles from the detention layer (an innovative configuration used for an innovative green roof system). However, it tends to overestimate the peak runoff in high rainfall intensities.
6) The two-stage physically-based green roof detention model is capable of modelling the runoff from the complete innovative green roof system. However, the model results are less satisfactory than for the conventional green roof system.
7) The unsatisfactory model results are believed to be caused by turbulent flow in the detention layer at high rainfall intensity that the current model is not capable of representing.

The SWMM green roof model for detention modelling

1) Neither the two-stage physically-based drainage layer model nor the SWMM drainage layer model is capable of modelling turbulent flow in the detention layer of the innovative green roof system.
2) The SWMM green roof control model provides better predictions of the runoff profiles from the convention green roof system than the innovative green roof system.
3) The substrate detention model in SWMM green roof LID control does not work well; an improved, simplified modelling approach, that better accounts for the hydraulic conductivity at moisture contents close to field capacity, is required.

11.3 Future work

In addition to the further work discussed in Chapter 10, the questions that emerged during the research of this study and how they may be addressed are considered in this section.

1) Horizontal flow in the substrate

This study assumes that the flow direction in the green roof substrate is vertical, and the flow in the drainage layer is horizontal. The hydraulic conductivity measured for the substrate is the vertical hydraulic conductivity. However, in a real green roof system/set-up, horizontal flow could also occur in the green roof substrate, especially for a system with a steep slope or long drainage length. The effect of substrate horizontal flow could result in a later time to start of runoff as rainfall travels a longer distance horizontally. If a full-scale green roof is intended to be modelled, the horizontal hydraulic conductivity of the substrate will need to be characterised and considered in the model framework.

2) Integrate retention models into the current model framework

This study focused on the detention process in green roof systems. The physically-based model developed in this study is capable of modelling the detention effect in the system. However, for long-term, continuous modelling, the retention model is also needed to be added to the model framework. A good understanding of the evapotranspiration process in green roof systems has been built from previous studies. Retention models capable of representing the system's moisture losses during dry weather period have been well-developed. Follow on research could be to add an appropriate green roof ET model to the current model framework.

3) A robust model accounting for the turbulent flow in the detention layer for the innovative green roof system

It has been found in this study that neither the physically-based drainage layer model nor the SWMM drainage layer model is capable of modelling the runoff profiles from the detention layer in the innovative green roof system very accurately. This is believed to be due to the limitation that the model is not capable of representing the flow conditions in the innovative green roof system's detention layer. Further experimental characterisations are needed to understand the performance of this detention layer, and a suitable model (e.g. porous flow modelling concepts) is also needed for a better representation of this layer.

4) A trade-off model for green roof substrates

It has been found that the Richards Equation provides a better representation of the detention effect in the green roof substrate than the SWMM percolation model. However, the Richards Equation is significantly computationally expensive, and from a stormwater management perspective, the runoff from the bottom of the substrate, rather than the moisture content, is more relevant. A trade-off model that balances the accuracy of model results with model complexity is needed for green roof substrates for practical engineering application. This could start with a detailed investigation into the relationship between hydraulic conductivity and/or other dominant physical properties and the parameters in empirical models. Further modifications may also be needed with model equations.

5) Interactions between green roof layers

The two-stage physically-based green roof detention model developed in this study does not consider the water interactions between green roof layers. For example, the phenomenon that the water in the drainage layer backfills to the substrate cannot be modelled using the current model. Although this phenomenon is rare in a conventional green roof system (as the drainage layer's function is to convey the water effectively), this is more relevant to the innovative green roof system, in which the detention layer has low permeability. If water cannot be drained effectively in the detention layer of the innovative green roof system during extreme rainfall events, the water will backfill to the substrate and influence substrate behaviour.

6) Transfer findings to other SuDS

Whilst the green roof system studied in this research is a typical type of SuDS, compared with other SuDS devices, a green roof system is relatively simple. For example, a complicated vertical moisture content distribution can be found in a deeper substrate layer. Also, the outflow control measures at the bottom of a bio-retention system could increase the model complexity. Moreover, allowing ponding on the surface of a bio-retention system means a different upper

boundary condition is needed for the Richards Equation. Application of the methodology and modelling approaches presented here to other SuDS devices will generate additional knowledge of the transferability of this study's findings.

11.4 Key findings

The important findings of this thesis are presented below.

- New laboratory characterisations of SWRC and HCF on four green roof substrates have been undertaken. This component of the work built on the foundational work of Liu (2016) by specifically focusing on moisture content conditions between the limits of 'field capacity' and saturation, which are particularly relevant to the control of green roof detention processes.
- New laboratory detention tests, in which both runoff and internal moisture content fluctuations have been monitored, have been completed.
- The work has demonstrated that the Mualem equation, used in traditional soil science to estimate an HCF from an SWRC, does not apply to coarse-grained engineered green roof substrates.
- The author has proposed new functional forms for the HCF to characterise the laboratory data, including a simplified version that could be determined from a single laboratory measurement of substrate moisture content at an unsaturated hydraulic conductivity of 0.1 cm/min.
- The author has addressed the limitations of HYDRUS-1D, by implementing a fully-functioning Richards Equation model capable of taking an arbitrary HCF function as input, and used this to confirm that the physically-based model is capable of modelling the detention processes associated with a green roof substrate layer.
- A novel drainage layer detention model based on the Saint Venant equation has been proposed and evaluated. Combined with the substrate layer model, this two-stage model provides a complete physically-based model of a typical green roof system.
- Green roof substrates are heterogeneous in nature; this introduces a number of uncertainties and also implies that the use of these sophisticated physically-based models may be inappropriate for practical engineering applications.
- The author has provided a critical review of the industry-standard SWMM model's green roof LID control. Whilst it is acknowledged that comprehensive physically-based modelling approaches are not appropriate for implementation with this type of drainage network modelling tool, some of the understanding derived from this thesis had led to a number of enhancements to SWMM being recommended. These are briefly summarised below.

- The representation of ET would benefit from the inclusion of factors to account for the fact that actual ET is reduced compared with potential ET when substrate moisture content is restricted (From earlier work, Peng and Stovin, 2017).
- Users should be able to define the initial moisture content in the substrate layer and the drainage layer independently; as the drainage layer will typically be empty prior to the start of a storm event (From earlier work, Peng and Stovin, 2017).
- The substrate detention model in SWMM does not work well; an improved, simplified modelling approach, that better accounts for the hydraulic conductivity at moisture contents close to field capacity, is required.

References

Abdef, E.B., 2012. Analysis of the retention capacity of green roofs 16. https://doi.org/10.2478/v10025-012-0018-8

Assouline, S., Or, D., 2014. The concept of field capacity revisited: Defining intrinsic static and dynamic criteria for soil internal drainage dynamics. Water Resour. Res. 50, 4787–4802. https://doi.org/10.1002/2014WR015475

ASTM, 2010. Standard test methods for measurement of hydraulic conductivity of unsaturated soils, ASTM D7664-10. West Conshohocken. https://doi.org/10.1520/D7664

Berretta, C., Poë, S., Stovin, V., 2014. Reprint of "Moisture content behaviour in extensive green roofs during dry periods: The influence of vegetation and substrate characteristics." J. Hydrol. 516, 37–49. https://doi.org/10.1016/j.jhydrol.2014.04.001

Bouzouidja, R., Rousseau, G., Galzin, V., Claverie, R., Lacroix, D., Séré, G., 2018. Green roof ageing or Isolatic Technosol's pedogenesis? J. Soils Sediments 18, 418–425. https://doi.org/10.1007/s11368-016-1513-3

Brooks, R.H., Corey, A.T., 1964. Hydraulic properties of porous media. Hydrology Papers, Colorado State University, Fort Collins, Colorado.

Brunetti, G., Šimůnek, J., Piro, P., 2016. A Comprehensive Analysis of the Variably Saturated Hydraulic Behavior of a Green Roof in a Mediterranean Climate. Vadose Zo. J. 15, 0. https://doi.org/10.2136/vzj2016.04.0032

Burés, S., Martinez, F.X., Perez, N., 1991. PHYSICAL PROPERTIES OF SUBSTRATE MIXTURES ACCORDING TO THE CHARACTERISTICS OF THE ORIGINAL MATERIALS. Acta Hortic. 207–214. https://doi.org/10.17660/ActaHortic.1991.294.22

Burszta-Adamiak, E., Mrowiec, M., 2013. Modelling of green roofs' hydrologic performance using EPA's SWMM. Water Sci. Technol. 68, 36. https://doi.org/10.2166/wst.2013.219

Carbone, M., Garofalo, G., Nigro, G., Piro, P., 2014. A conceptual model for predicting hydraulic behaviour of a green roof. Procedia Eng. 70, 2013. https://doi.org/10.1016/j.proeng.2014.02.030

Carter, M.R., Gregorich, E.G., 2007. Soil Sampling and Methods of Analysis, Second Edition, 2nd Editio. ed. CRC Press, Boca Raton. https://doi.org/10.1201/9781420005271

Castiglia Feitosa, R., Wilkinson, S., 2016. Modelling green roof stormwater response for different soil depths. Landsc. Urban Plan. 153, 170–179. https://doi.org/10.1016/J.LANDURBPLAN.2016.05.007

Chow, V. Te, 1959. Open-channel hydraulics. McGraw-Hill, New York.

Chow, V. Te, Maidment, D.R., Mays, L.W., 1988. Applied Hydrology, 1st ed. McGraw-Hill, Inc.

Cipolla, S.S., Maglionico, M., Stojkov, I., 2016. A long-term hydrological modelling of an extensive green roof by means of SWMM. Ecol. Eng. 95, 876–887. https://doi.org/10.1016/J.ECOLENG.2016.07.009

Conn, R., Werdin, J., Rayner, J.P., Farrell, C., 2020. Green roof substrate physical properties differ between standard laboratory tests due to differences in compaction. J. Environ. Manage. 261, 110206. https://doi.org/10.1016/j.jenvman.2020.110206

Czemiel Berndtsson, J., 2010. Green roof performance towards management of runoff water quantity and quality: A review. Ecol. Eng. https://doi.org/10.1016/j.ecoleng.2009.12.014

De-Ville, S., 2017. Hydrological Performance Evolution of Extensive Green Roof Systems. The University of Sheffield.

De-Ville, S., Menon, M., Jia, X., Reed, G., Stovin, V., 2017. The impact of green roof ageing on substrate characteristics and hydrological performance. J. Hydrol. 547, 332–344. https://doi.org/10.1016/j.jhydrol.2017.02.006

De-Ville, S., Menon, M., Stovin, V., 2018. Temporal variations in the potential hydrological performance of extensive green roof systems. J. Hydrol. 558, 564–578. https://doi.org/10.1016/j.jhydrol.2018.01.055

de Oliveira, R.A., Ramos, M.M., de Aquino, L.A., 2015. Irrigation Management. Sugarcane 161–183. https://doi.org/10.1016/B978-0-12-802239-9.00008-6

Digman, C., Ashley, M.R., Mwh, D.B., Balmforth, D., Stovin, V., Ciria, J.G., 2012. C713 Retrofitting to manage surface water. CIRIA, London.

Dohnal, M., Dusek, J., Vogel, T., 2010. Improving Hydraulic Conductivity Estimates from Minidisk Infiltrometer Measurements for Soils with Wide Pore-Size Distributions. Soil Sci. Soc. Am. J. 74, 804. https://doi.org/10.2136/sssaj2009.0099

Durner, W., 1994. Hydraulic conductivity estimation for soils with heterogeneous pore structure. Water Resour. Res. 30, 211–223. https://doi.org/10.1029/93WR02676

Dvorak, B.D., Volder, A., 2010. Green roof vegetation for North American ecoregions : A literature review. https://doi.org/10.1016/j.landurbplan.2010.04.009

Fassman-Beck, E., Voyde, E., Simcock, R., Hong, Y.S., 2013. 4 Living roofs in 3 locations: Does configuration affect runoff mitigation? J. Hydrol. 490, 11–20. https://doi.org/10.1016/J.JHYDROL.2013.03.004

Fassman, E., Simcock, R., 2012. Moisture Measurements as Performance Criteria for Extensive Living Roof Substrates. J. Environ. Eng. 138, 841–851. https://doi.org/10.1061/(ASCE)EE.1943-7870.0000532

Fassman, E., Simcock, R., Voyde, E., 2010. Extensive Green (Living) Roofs for Stormwater Mitigation Part 1 : Design and Construction, Environmental Engineering.

Fletcher, T.D., Shuster, W., Hunt, W.F., Ashley, R., Butler, D., Arthur, S., Trowsdale, S., Barraud, S., Semadeni-Davies, A., Bertrand-Krajewski, J.L., Mikkelsen, P.S., Rivard, G., Uhl, M., Dagenais, D., Viklander, M., 2015. SUDS, LID, BMPs, WSUD and more – The evolution and application of terminology surrounding urban drainage. Urban Water J. 12, 525–542. https://doi.org/10.1080/1573062X.2014.916314

FLL, 2008. Guidelines for the Planning, Construction and Maintenance of Green Roofing. hungsgesellschaft Landschaftsentwicklung Landschaftsbau e.V., Bonn, Germany.

Germann, P.F., Beven, K., 1985. Kinematic Wave Approximation to Infiltration Into Soils With Sorbing Macropores. Water Resour. Res. 21, 990–996. https://doi.org/10.1029/WR021i007p00990

Hakimdavar, R., Culligan, P.J., Finazzi, M., Barontini, S., Ranzi, R., 2014. Scale dynamics of extensive green roofs: Quantifying the effect of drainage area and rainfall characteristics on observed and modeled green roof hydrologic performance. Ecol. Eng. 73, 494–508. https://doi.org/10.1016/J.ECOLENG.2014.09.080

Hillel, D., Warrick, A.W., Baker, R.S., Rosenzweig, C., 1998. Environmental soil physics. Academic Press.

Hilten, R.N., Lawrence, T.M., Tollner, E.W., 2008. Modeling stormwater runoff from green roofs with HYDRUS-1D. J. Hydrol. 358, 288–293. https://doi.org/10.1016/j.jhydrol.2008.06.010

Johannessen, B.G., Hamouz, V., Gragne, A.S., Muthanna, T.M., 2019. The transferability of SWMM model parameters between green roofs with similar build-up. J. Hydrol. 569. https://doi.org/10.1016/j.jhydrol.2019.01.004

Kasmin, H., Stovin, V.R., Hathway, E.A., 2010. Towards a generic rainfall-runoff model for green roofs. Water Sci. Technol. 62, 898. https://doi.org/10.2166/wst.2010.352

Kutílek, M., 2004. Soil hydraulic properties as related to soil structure, in: Soil and Tillage Research. Elsevier B.V., pp. 175–184. https://doi.org/10.1016/j.still.2004.07.006

Li, Y., Babcock, R.W., 2014. Green roof hydrologic performance and modeling: A review. Water Sci. Technol. https://doi.org/10.2166/wst.2013.770

Liu, R., 2016. Infiltration Models for Engineered Media in Living Roofs and Bioretention. The University of Auckland.

Liu, R., Fassman-Beck, E., 2018. Pore Structure and Unsaturated Hydraulic Conductivity of Engineered Media for Living Roofs and Bioretention Based on Water Retention Data. J. Hydrol. Eng. 23, 04017065. https://doi.org/10.1061/(ASCE)HE.1943-5584.0001621

Liu, R., Fassman-Beck, E., 2017. Hydrologic response of engineered media in living roofs and bioretention to large rainfalls: experiments and modeling. Hydrol. Process. 31, 556–572. https://doi.org/10.1002/hyp.11044

Liu, R., Fassman-Beck, E., 2016. Effect of Composition on Basic Properties of Engineered Media for Living Roofs and Bioretention. J. Hydrol. Eng. 21, 06016002. https://doi.org/10.1061/(asce)he.1943-5584.0001373

Marsh, T., Hannaford, J., 2007. The summer 2007 floods in England & Wales – a hydrological appraisal. Centre for Ecology & Hydrology.

Marshall, T.J., Holmes, J.W., Rose, C.W., 1996. Soil Physics. Cambridge University Press. https://doi.org/10.1017/CBO9781139170673

Masch, F.D., Denny, K.J., 1966. Grain size distribution and its effect on the permeability of unconsolidated sands. Water Resour. Res. 2, 665–677. https://doi.org/10.1029/WR002i004p00665

Menon, M., Jia, X., Lair, G.J., Faraj, P.H., Blaud, A., 2015. Analysing the impact of compaction of soil aggregates using X-ray microtomography and water flow simulations. Soil Tillage Res. 150, 147–157. https://doi.org/10.1016/j.still.2015.02.004

Meyer, P.D., Gee, G.W., 1999. Flux-Based Estimation of Field Capacity. J. Geotech. Geoenvironmental Eng. 125, 595–599. https://doi.org/10.1061/(ASCE)1090-0241(1999)125:7(595)

Mualem, Y., 1976. A new model for predicting the hydraulic conductivity of unsaturated porous media. Water Resour. Res. 12, 513–522. https://doi.org/10.1029/WR012i003p00513

Murphy, J.M., Brown, S.J., Harris, G.R., 2020. UKCP Additional Land Products: Probabilistic Projections of Climate Extremes.

Nachabe, M.H., 1998. Refining the Definition of Field Capacity in the Literature. J. Irrig. Drain. Eng. 124, 230–232. https://doi.org/10.1061/(ASCE)0733-9437(1998)124:4(230)

NERC, 1999. Flood Estimation Handbook (CD).

NERC, 1975. Flood Studies Report. London, UK.

ONS, 2013. 2011 Census Analysis-Comparing Rural and Urban Areas of England and Wales Summary-Comparing rural and urban areas of England and Wales.

Palla, A., Gnecco, I., 2015. Hydrologic modeling of Low Impact Development systems at the urban catchment scale. J. Hydrol. 528, 361–368. https://doi.org/10.1016/J.JHYDROL.2015.06.050

Palla, A., Gnecco, I., Lanza, L.G., 2012. Compared performance of a conceptual and a mechanistic hydrologic models of a green roof. Hydrol. Process. 26, 73–84. https://doi.org/10.1002/hyp.8112

Palla, A., Gnecco, I., Lanza, L.G., 2009. Unsaturated 2D modelling of subsurface water flow in the coarse-grained porous matrix of a green roof. J. Hydrol. 379, 193–204. https://doi.org/10.1016/j.jhydrol.2009.10.008

Peng, Z., Smith, C., Stovin, V., 2019. Internal fluctuations in green roof substrate moisture content during storm events: Monitored data and model simulations. J. Hydrol. 573, 872–884. https://doi.org/10.1016/j.jhydrol.2019.04.008

Peng, Z., Stovin, V., 2017. Independent Validation of the SWMM Green Roof Module. J. Hydrol. Eng. 22, 04017037. https://doi.org/10.1061/(asce)he.1943-5584.0001558

Poë, S., Stovin, V., Berretta, C., 2015. Parameters influencing the regeneration of a green roof's retention capacity via evapotranspiration. J. Hydrol. 523, 356–367. https://doi.org/10.1016/J.JHYDROL.2015.02.002

Poulsen, T.G., Moldrup, P., Iversen, B. V., Jacobsen, O.H., 2002. Three-region Campbell Model for Unsaturated Hydraulic Conductivity in Undisturbed Soils. Soil Sci. Soc. Am. J. 66, 744–752. https://doi.org/10.2136/sssaj2002.7440

Razzaghmanesh, M., Beecham, S., 2014. The hydrological behaviour of extensive and intensive green roofs in a dry climate. Sci. Total Environ. 499, 284–296. https://doi.org/10.1016/j.scitotenv.2014.08.046

Richards, L.A., 1931. Capillary conduction of liquids through porous mediums. J. Appl. Phys. 1, 318–333. https://doi.org/10.1063/1.1745010

Rosas, J., Lopez, O., Missimer, T.M., Coulibaly, K.M., Dehwah, A.H.A., Sesler, K., Lujan, L.R., Mantilla, D., 2014. Determination of Hydraulic Conductivity from Grain-Size Distribution for Different Depositional Environments. Groundwater 52, 399–413. https://doi.org/10.1111/gwat.12078

Rossman, L.A., Huber, W.C., 2016. Storm Water Management Model Reference Manual Volume III – Water Quality. United States Environ. Prot. Agency III, 235. https://doi.org/EPA/600/R-15/162 |

Rudiyanto, Toride, N., Sakai, M., Šimůnek, J., 2013. A Hysteretic Model of Hydraulic Properties for Dual-Porosity Soils. Soil Sci. Soc. Am. J. 77, 1182–1188. https://doi.org/10.2136/sssaj2012.0339n

Saxton, K.E., Rawls, W.J., 2006. Soil Water Characteristic Estimates by Texture and Organic Matter for Hydrologic Solutions. Soil Sci. Soc. Am. J. 70, 1569–1578. https://doi.org/10.2136/sssaj2005.0117

Seki, K., 2010. SWRC fit: a nonlinear fitting program with a water retention curve for soils having unimodal and bimodal pore structure. Hydrol. Earth Syst. Sci. Discuss. 4, 407–437. https://doi.org/10.5194/hessd-4-407-2007

She, N., Pang, J., 2009. Physically Based Green Roof Model. J. Hydrol. Eng. 15, 458–464. https://doi.org/10.1061/(asce)he.1943-5584.0000138

Šimůnek, J., 2015. Implementation of Overland Flow into HYDRUS-1D, HYDRUS Software Series 6a. Department of Environmental Sciences, University of California Riverside, Riverside, CA.

Šimůnek, J., Šejna, M., Saito, H., Sakai, M., Genuchten, M.T. Van, 2013. The HYDRUS-1D Software Package for Simulating the Movement of Water, Heat, and Multiple Solutes in Variably Saturated Media, Version 4.17,HYDRUS Softerware Series 3, Department of Environmental Sciences, University of California Riverside, Riverside, Cali 343.

Sonnenwald, F., Stovin, V., Guymer, I., 2014. Configuring maximum entropy deconvolution for the identification of residence time distributions in solute transport applications. J. Hydrol. Eng.

19, 1413–1421. https://doi.org/10.1061/(ASCE)HE.1943-5584.0000929

Soulis, K.X., Valiantzas, J.D., Ntoulas, N., Kargas, G., Nektarios, P.A., 2017. Simulation of green roof runoff under different substrate depths and vegetation covers by coupling a simple conceptual and a physically based hydrological model. J. Environ. Manage. 200, 434–445. https://doi.org/10.1016/j.jenvman.2017.06.012

Stovin, V., 2010. The potential of green roofs to manage urban stormwater. Water Environ. J. 24, 192–199. https://doi.org/10.1111/j.1747-6593.2009.00174.x

Stovin, V., Poë, S., Berretta, C., 2013. A modelling study of long term green roof retention performance. J. Environ. Manage. 131, 206–215. https://doi.org/10.1016/j.jenvman.2013.09.026

Stovin, V., Poë, S., De-Ville, S., Berretta, C., 2015. The influence of substrate and vegetation configuration on green roof hydrological performance. Ecol. Eng. 85, 159–172. https://doi.org/10.1016/j.ecoleng.2015.09.076

Stovin, V., Vesuviano, G., De-Ville, S., 2017. Defining green roof detention performance. Urban Water J. 14, 574–588. https://doi.org/10.1080/1573062X.2015.1049279

Stovin, V., Vesuviano, G., Kasmin, H., 2012. The hydrological performance of a green roof test bed under UK climatic conditions. J. Hydrol. 414–415, 148–161. https://doi.org/10.1016/J.JHYDROL.2011.10.022

Twarakavi, N.K.C., Sakai, M., Šimůnek, J., 2009. An objective analysis of the dynamic nature of field capacity. Water Resour. Res. 45, 1–9. https://doi.org/10.1029/2009WR007944

van Genuchten, M.T., 1980. A Closed-form Equation for Predicting the Hydraulic Conductivity of Unsaturated Soils. Soil Sci. Soc. Am. J. 44, 892–898. https://doi.org/10.2136/sssaj1980.03615995004400050002x

VanWoert, N.D., Rowe, D.B., Andresen, J.A., Rugh, C.L., Xiao, L., 2005. Watering regime and green roof substrate design affect Sedum plant growth. HortScience 40, 659–664. https://doi.org/10.2134/jeq2004.0364

Veihmeyer, F., Hendrickson, A., 1931. The moisture equivalent as a measure of the field capacity of soils. Soil Sci. 32, 181–194. https://doi.org/10.1097/00010694-193109000-00003

Vesuviano, G., Sonnenwald, F., Stovin, V., 2014. A two-stage storage routing model for green roof runoff detention. Water Sci. Technol. 69, 1191. https://doi.org/10.2166/wst.2013.808

Vesuviano, G., Stovin, V., 2013. A generic hydrological model for a green roof drainage layer. Water Sci. Technol. 68, 769. https://doi.org/10.2166/wst.2013.294

Vesuviano, G.M., 2014. A Two-Stage Runoff Detention Model for a Green Roof. The University of Sheffield.

Voyde, E., Fassman, E., Simcock, R., 2010. Hydrology of an extensive living roof under sub-tropical climate conditions in Auckland, New Zealand. J. Hydrol. 394, 384–395. https://doi.org/10.1016/j.jhydrol.2010.09.013

Woods Ballard, B., Wilson, S., Udale-Clarke, H., Illman, S., Scott, T., Ashely, R., Kellagher, R., 2015. The SUDS manual, ciria. https://doi.org/London C697

Yio, M.H.N., Stovin, V., Werdin, J., Vesuviano, G., 2013. Experimental analysis of green roof substrate detention characteristics. Water Sci. Technol. 68, 1477–1486. https://doi.org/10.2166/wst.2013.381

Young, P., Jakeman, A., McMurtrie, R., 1980. An instrumental variable method for model order identification. Automatica 16, 281–294. https://doi.org/10.1016/0005-1098(80)90037-0

Appendix A. Instrument Calibration

A.1 Instrument calibration

The measurement of green roof substrate unsaturated hydraulic conductivity involves few electronic instruments. These instruments output electronic signals, calibration was conducted to interoperate the measured signals to meaningful properties.

A.1.1 Moisture probes

The moisture probes used throughout the study are the ECH2O 5TM moisture probes manufactured by Meter Environment LTD (**Figure A.1**). Dielectric permittivity represents the ability of a material to store charge. The dielectric permittivity of air is 1, and it is 80 in the water. In soil, the dielectric permittivity is a value between 1 and 80, depending on the volume of water contained. The ECH2O 5TM moisture probe uses the FDR (Frequency Domain Reflector) technique to measure the dielectric permittivity of the surrounding medium. A 70 MHZ oscillating wave was supplied to the probe prong to charge the material. The stored charge is proportional to soil dielectric and soil moisture content. The raw output of the moisture probe from the data logger is 50 times the dielectric permittivity. The relationship between moisture content and dielectric permittivity, as suggested in the manufactory manual, is a 3rd order polynomial equation. Although reference values for the equation parameters were given by the manufacturer, independent calibration was conducted to increase the accuracy of the measurement. An Em50 data logger (manufactured by Meter Environment LTD.) was connected to the moisture probes to collect, record and read out the measurement from the moisture probe. As a data logger can be connected to up to five moisture probes, the calibration was conducted with five identical probes.

In the calibration, the green roof substrates were dried in the oven for 24 hours at 105 °C and cooled down to air temperature (20 °C) before putting into a 165 mm (height)×150 mm (diameter) transparent cylinder. The cylinder was filled up to 10 cm, and the dry bulk density of the substrates was calculated accordingly. Five moisture probes were then buried into the substrate cylinder, and the reading from the data logger at the total dry condition was recorded. Then the moisture probes were taken out from the cylinder, and a graduated volume of water was added to the dry substrate to increase the moisture content of the substrate to the desire moisture content. After 5 minutes, when the water and the substrate were well-mixed, the five moisture probes were inserted into the substrate again (**Figure A.1**), and the measurement from the moisture probes was recorded when there was no significant change in the reading for 10

seconds. The procedures were then repeated for the substrates and desired moisture contents. Nine to eleven desire water contents were calibrated for each substrate.

Figure A.1 shows the photos of the moisture probes inserted into the substrates during the measurements. A 3rd order polynomial equation was then fitted to the measured data points of the five moisture probes for each type of substrate.

Figure A.1. The moisture probe and the moisture probes inserted into the substrates for calibration.

A.1.2 Pressure transducers

A pressure transducer converts pressure into an analogue electrical signal, and the physical deformation of strain gages achieves the conversion. When the pressure was applied to the strain gages, it will produce an electrical resistance change, which is proportional to the pressure. In this study, the pressure is provided by the static water pressure in the collecting barrel. Two pressure transducers (PDCR 1830 manufactured by Druck Inc.) were used to measure the water level in two collecting barrels in two set-ups during the experiment. The two pressure transducers were calibrated independently. Considering a high rainfall rate will be used in the experiment, two sizes of collecting barrels were used to measure the outflow from the substrate at low rainfall rates and high rainfall rates. The small diameter collecting barrel has an inner diameter of 74 mm and a depth of 500 mm, and the large collecting barrel has an inner diameter of 140 mm and a depth of 500 mm (**Figure A.2**). The two pressure transducers were calibrated with the two sizes of collecting barrels.

The pressure transducer was connected to a Campbell Scientific data logger (CR1000), and a laptop was connected to the data logger to read out the measurement. The calibration started from empty barrels, and a graduated volume of water was added to the barrel each time until the maximum capacity was reached. The stabilised corresponding output voltage from the pressure transducer was recorded with the total volume of water added. The procedures were repeated three times for each pressure transducer and each size of the barrel. A linear relationship was fitted to the measured data points for each pressure transducer and each size of barrels.

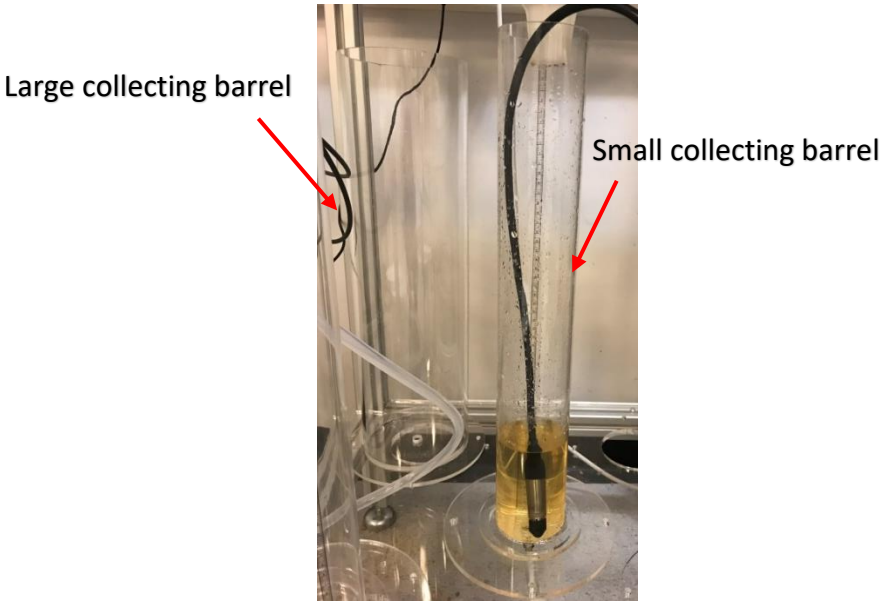

Figure A.2. The pressure transducer and the two sizes of collecting barrel.

A.2 Characterisation of the relationship between pumping rate and rainfall rate

Before the detention test, the relationship between pumping rate and rainfall rate was characterised for the two set-ups using the calibrated pressure transducers and collecting barrels. The apparatus without substrate in **Figure 3.2** was used to determine the relationship. Two pump heads were connected to one peristaltic pump to provide the rainfall for the two set-ups at the same time. The 26G hypodermic needles were used to distribute the inflow, a mesh and a filter sheet were placed at the bottom of the column, and the small 74 mm (diameter) collecting barrels with the pressure transducers were used to collect the outflow. One of the nine pumping rates, ranging from 2 RPM to 28 RPM, was set for 5 minutes before the measurement started. Due to the collecting barrels' capacity, the runoff was measured for 15 minutes to 120 minutes, depending on the pumping rate. The pressure transducers were connected to a data logger for continuous recording at a 1-second interval, and the corresponding rainfall intensities were calculated from the recorded data. A linear equation was fitted to the pumping rate and measured flowrate for each set-up.

A.3 Results

A.3.1 Moisture probes

Figure A.3 shows the measured dielectric permeability corresponding to the desire moisture contents for the four green roof substrates. It can be seen that variations exist between the moisture probes at high moisture content in all the substrates. This is because a saturated zone was developed at the bottom part of the substrate when the moisture content was above the

field capacity. Depending on the depth of the moisture probe was inserted, a variation was witnessed between the probes. The degree of variation also relates to the characteristics of the substrates. For example, HLS and NSM are more homogenous than MCS and SCS as they contain high percentages of fine particles, the moisture probe variation in these substrates is not significant, whilst in the MCS and SCS, the variation is more noticeable. There is no strong evidence showing that the single moisture probe systematically providing a higher value of dielectric permittivity than the others. The variation between the probes is believed to be caused by the characteristics of the substrates rather than the difference between the probes. Therefore, a single equation was calibrated for each type of substrates using all the measured data by the five moisture probes. **Figure A.3** also shows the fitted curves and the statistics of the fitted curves. With R^2 is higher than 0.9 in all the cases, the equation calibrated is capable of describing the relationship between measured dielectric permittivity and moisture content for the green roof substrates. Equations A.1 to A.4 give the equations for the relationship.

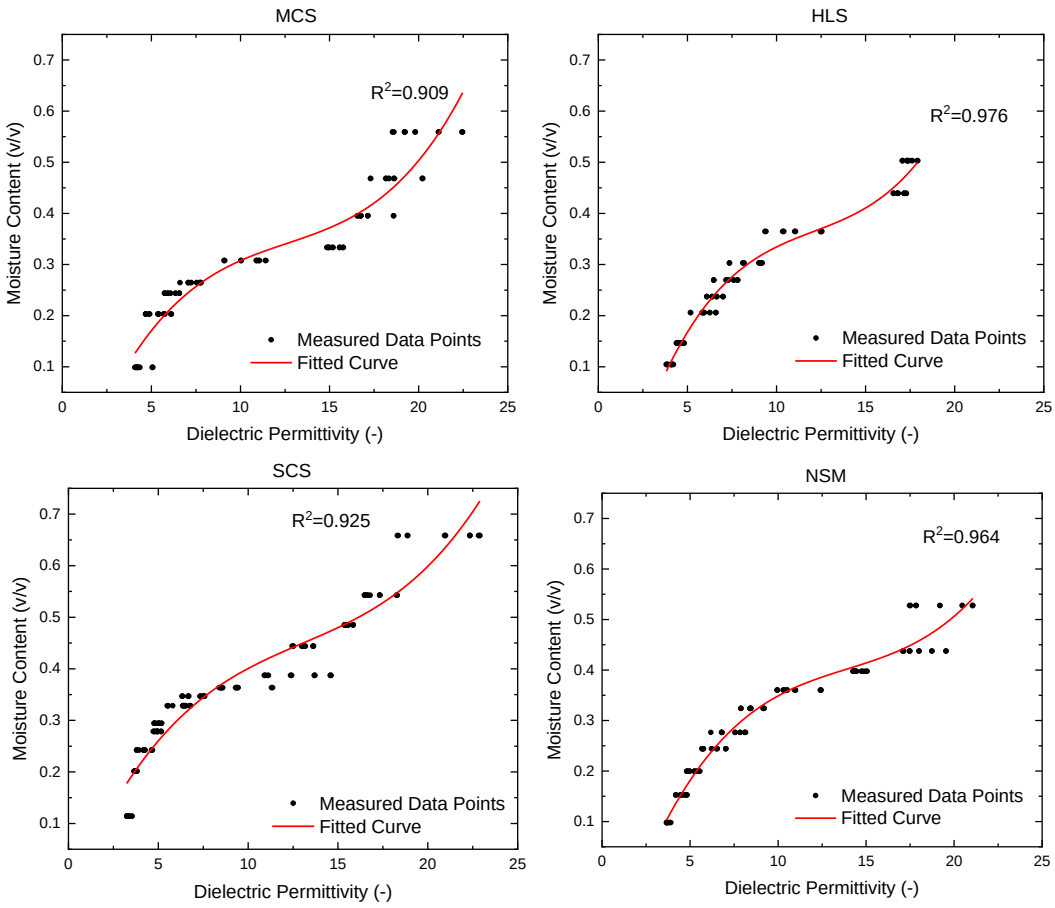

Figure A.3. Measured data points and the fitted curves for the relationship between moisture probe dielectric permittivity and substrates moisture content.

$$\text{moisture content (MCS)} = -0.18 + 0.101 \times \text{dielectric permittivity} - 0.007 \times \text{dielectric permittivity}^2 + 1.871 \times 10^{-4} \times \text{dielectric permittivity}^3 \quad \text{Equation A.1}$$

$$\text{moisture content (HLS)} = -0.307 + 0.14 \times \text{dielectric permittivity} - 0.011 \times \text{dielectric permittivity}^2 + 2.898 \times 10^{-4} \times \text{dielectric permittivity}^3 \quad \text{Equation A.2}$$

$$\text{moisture content (SCS)} = -0.042 + 0.083 \times \text{dielectric permittivity} - 0.005 \times \text{dielectric permittivity}^2 + 1.342 \times 10^{-4} \times \text{dielectric permittivity}^3 \quad \text{Equation A.3}$$

$$\text{moisture content (NSM)} = -0.217 + 0.112 \times \text{dielectric permittivity} - 0.007 \times \text{dielectric permittivity}^2 + 1.724 \times 10^{-4} \times \text{dielectric permittivity}^3 \quad \text{Equation A.4}$$

A.3.3 Pressure transducer

Figure A.4 shows the relationship between the volume of water in the collection barrel and the output voltage. The two pressure transducers were calibrated against the two sizes of the collecting barrel. A good linear relationship presented in the measured data points, and a line was calibrated for the relationship for each pressure transducer and collecting barrel. The R^2 for the fitted lines is almost 1, which indicates a good fit of the calibrated lines to the measured data points. The equations for the relationship are given in Equations A.5 to A.8. It can be seen that even the intercepts of the lines for the two pressure transducers are different, the slopes of the calibrated lines are very close. The initial few readings from the pressure transducer relate to the positions of the pressure transducer was inserted (e.g. the degree to the base of the collecting tube). The slope of the lines is more important to the determination of the runoff rate, as the change of water volume in the collecting barrel was used to calculate the runoff rate.

Pressure transducer 1:

$$\text{volume of water (small collecting barrel)} = \frac{\text{Voltage} - 0.128}{7.382} \times 10^{-4} \quad \text{Equation A.5}$$

$$\text{volume of water (large collecting barrel)} = \frac{\text{Voltage} - 0.119}{2.064} \times 10^{-4} \quad \text{Equation A.6}$$

Pressure transducer 2:

$$\text{volume of water (small collecting barrel)} = \frac{\text{Voltage} - 0.083}{7.605} \times 10^{-4} \quad \text{Equation A.7}$$

$$\text{volume of water (large collecting barrel)} = \frac{\text{Voltage} - 0.065}{2.138} \times 10^{-4} \quad \text{Equation A.8}$$

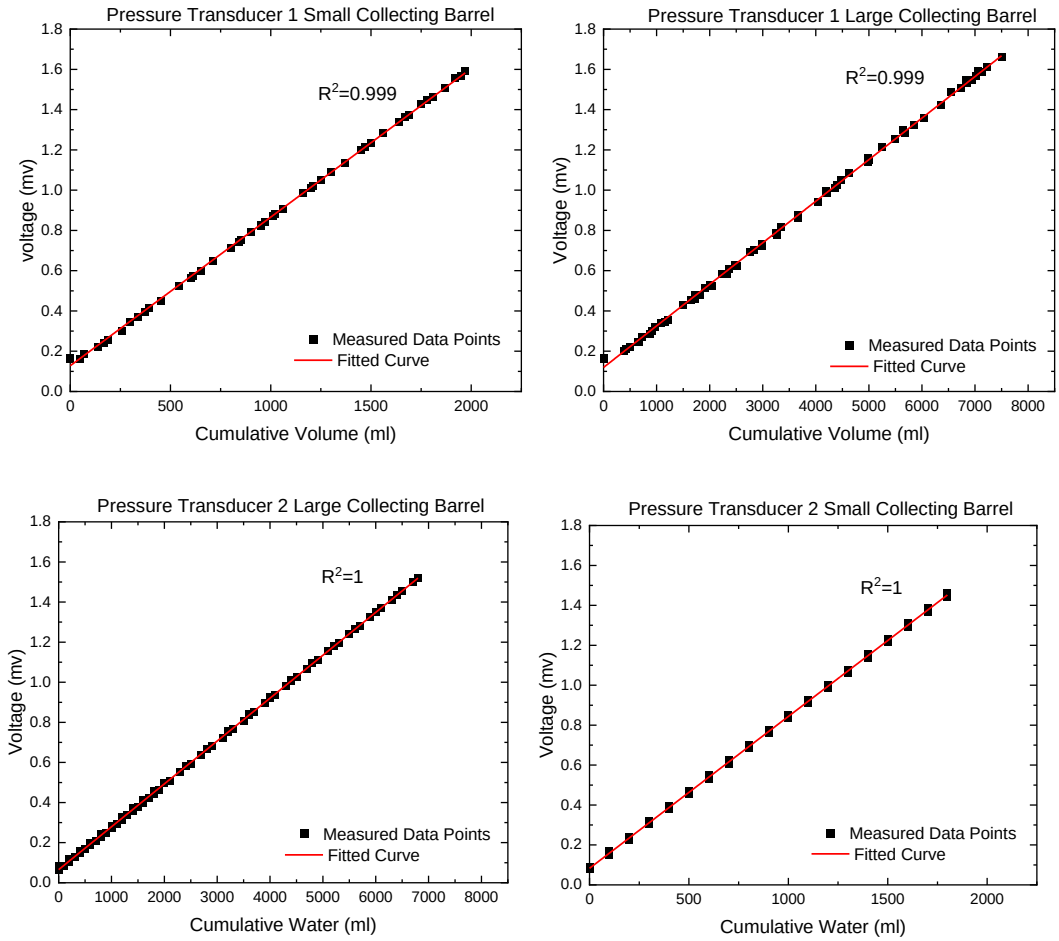

Figure A.4. Measured data points and the fitted curves for the relationship between the cumulative water volume and output voltage.

A.3.4 Pumping rate versus rainfall intensity

Figure A.5 shows the determined flowrate corresponding to the nine desire pumping rates for the two set-ups. A good consistency has been achieved between the two set-ups that the determined flowrates of the two set-ups are very close at the same pumping rate. **Figure A.5** also shows the fitted curves for the relationship between the pumping rate and the flowrate. With R^2=1 for both set-ups, a perfect linear relationship was obtained for the relationship. Equations A.9 and A.10 provide the equations for the relationship of the two set-ups.

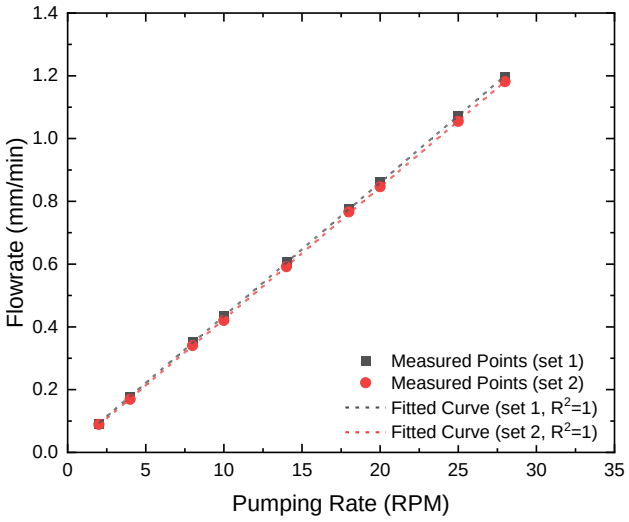

Figure A.5. The determined relationship between the pumping rate and the flowrate.

$$\text{flowrate}_{(\text{set 1})} = 0.042 \times \text{pumping rate} + 0.009 \qquad \text{Equation A.9}$$

$$\text{flowrate}_{(\text{set 2})} = 0.042 \times \text{pumping rate} + 0.003 \qquad \text{Equation A.10}$$

Table A.1 lists the pumping rates calculated from the two calibrated equations (Equations A.9 and A.10) for the two set-ups corresponding to the design storms for the substrate detention tests. The averaged pumping rate of the two set-ups was set as the pumping rate for the peristaltic pump in the detention test to achieve the design storms. As the precision of the peristaltic pump is 0.1 RPM, the decimal of the averaged value in **Table A.1** was set to be 1.

Table A.1. Corresponding pumping rate to the design storms.

Target Flowrate (mm/min)	Pumping Rate (RPM) Set 1	Pumping Rate (RPM) Set 2	Pumping Rate (RPM) Average
0.1	2.14	2.31	2.2
0.37	8.48	8.72	8.6
0.504	11.63	11.91	11.8
0.0509	0.99	1.14	1.1
0.1715	3.82	4.01	3.9
1.076	25.05	25.49	25.3

Appendix B. Solving the Richards Equation in MATLAB: Model Development and Validation

B.1 Introduction

The Richards Equation, in which the change of moisture content is a function of hydraulic head and hydraulic conductivity, has been frequently used in groundwater flow modelling. As the hydraulic conductivity varies with moisture content, the Richards Equation is a second-order partial differential equation. Mathematically, due to the highly nonlinear nature of the Richards Equation, there is no closed-form analytical solution for it, and the only way to solve such equations is to use numerical solutions. HYDRUS-1D is commercial software that was developed to solve the Richards Equation numerically in the vertical direction (Šimůnek et al., 2013). HYDRUS-1D is widely accepted for solving the Richards Equation, and it has been used to model the runoff from green roof systems in many previous studies. The Hydraulic Conductivity Functions (HCF) built into HYDRUS-1D are the two conventional natural soil-based van Genuchten-Mualem and Durner-Mualem models. However, due to the fact that the green roof substrates are slightly different from natural soil, a new HCF, not available within HYDRUS-1D, may need to be derived for green roof substrates. Therefore, a new code to solve the Richards Equation has been produced in MATLAB. The code makes it possible for the user to define any form of the equation for the HCF. To validate the code written in MATLAB, the runoff, suction head and moisture content in response to a design storm were modelled using the code with van Genuchten-Mualem and Durner-Mualem models. The model results were then compared with the results of HYDRUS-1D using the same inputs.

B.2 Method

The Richards Equation can be written in the suction head form as:

$$\frac{\partial h}{\partial t}\frac{\partial \theta}{\partial h} = \frac{\partial}{\partial z}\left[K(h)\left(\frac{\partial h}{\partial z} - 1\right)\right] \qquad \text{Equation B.1}$$

where θ is the moisture content, t is time, z is the spatial variable and $K(h)$ is the unsaturated hydraulic conductivity at suction head h.

To solve the Richards equation, the Soil Water Release Curve (SWRC, the relationship between water content and suction head) and the Hydraulic Conductivity Function (HCF, the relationship between unsaturated hydraulic conductivity and suction head) are needed.

The SWRC can be described by the van Genuchten model (Equation A.2), and the HCF can be described by the van Genuchten-Mualem equation (Equation A.3).

$$S_e = \frac{\theta-\theta_r}{\theta_s-\theta_r} = [1+(\alpha h)^n]^{-m} \quad \text{Equation B.2}$$

$$K(S_e) = K_s S_e^{0.5}\left[1-(1-S_e^{1/m})^m\right]^2 \quad \text{Equation B.3}$$

where S_e is the relative saturation, $S_e = 1$ represents full saturation and $S_e = 0$ represents residual moisture content, θ_r is the residual moisture content θ_s is saturated moisture content, θ is moisture content, h is suction head, α, n are empirical parameters, α is the inverse of air-entry value, n is a pore size distribution index, $m = 1-\frac{1}{n}$, K_S is saturated hydraulic conductivity, and $K(S_e)$ is the unsaturated hydraulic conductivity at S_e.

Alternatively, the SWRC can be described by the dual-porosity Durner model (Equation B.4), and the HCF can be described by the Durner-Mualem equations (Equations B.5 to B.7).

$$S_e = \frac{\theta-\theta_r}{\theta_s-\theta_r} = w[1+(\alpha_1 h)^{n_1}]^{-m_1} + (1-w)[1+(\alpha_2 h)^{n_2}]^{-m_2} \quad \text{Equation B.4}$$

$$S_{e_1} = [1+(\alpha_1 h)^{n_1}]^{-m_1} \quad \text{Equation B.5}$$

$$S_{e_2} = [1+(\alpha_2 h)^{n_2}]^{-m_2} \quad \text{Equation B.6}$$

$$K(S_e) = K_s(wS_{e_1}+(1-w)S_{e_2})^{0.5}\frac{\left\{w\alpha_1\left[1-\left(1-S_{e_1}^{1/m_1}\right)^{m_1}\right]+(1-w)\alpha_2\left[1-\left(1-S_{e_2}^{1/m_2}\right)^{m_2}\right]\right\}^2}{(w\alpha_1+(1-w)\alpha_2)^2} \quad \text{Equation B.7}$$

B.3 Model implementation

The *pdepe* function in MATLAB uses the finite element method to solve initial boundary problems for systems of parabolic and elliptic partial differential equations in space z and time t. The ordinary differential equation resulting from discretisation in space are integrated to obtain approximate solutions at each discretised time. The *pdepe* solves the partial differential equations of the following form:

$$c\left(z,t,h,\frac{\partial h}{\partial z}\right)\frac{\partial h}{\partial t} = z^{-m}\frac{\partial}{\partial z}\left(z^m f\left(z,t,h,\frac{\partial h}{\partial z}\right)\right) + s\left(z,t,h,\frac{\partial h}{\partial z}\right) \quad \text{Equation B.8}$$

With boundary conditions that satisfy the following form:

$$p(z,t,h) + q(z,t)f\left(z,t,u,\frac{\partial h}{\partial z}\right) = 0 \quad \text{Equation B.9}$$

And initial conditions that satisfy the following form:

$$h(z, t_0) = h_0(z) \qquad \text{Equation B.10}$$

h, z and t are as defined for Equation A.1. The length of the spatial matrix z determines the number of vertical cells used for calculations. $c\left(z, t, h, \frac{\partial h}{\partial z}\right)$ is a multiplication matrix, when integrated with the Richards Equation, the multiplication matrix is $\frac{\partial \theta}{\partial h}$, and depending on the SWRC, the exact form of it differs. m relates to the symmetry of the function and it was set to 0 represent the slab symmetry of the Richards Equation. $f\left(z, t, h, \frac{\partial h}{\partial z}\right)$ is a flux term and it is given by $K(h)\left(\frac{\partial h}{\partial Z} - 1\right)$. The source term $s(z, t, h, \frac{\partial h}{\partial z})$ is 0 in this case. The $p(z, t, h)$ and $q(z, t)$ terms in Equation B.9 were set to be the $-R$ (Rainfall) and 1 respectively to represent the upper boundary defined in Equation B.11. The $p(z, t, h)$ and $q(z, t)$ terms were set to be $h(z, t_0) - h_{z=D}$ and 0 to represent the lower boundary defined in Equation B.12.

The upper boundary was set as a Neumann condition in which the surface flux equals the rainfall R (Equation B.11). The rainfall applied was a constant rainfall of 0.569 mm/min, which is equivalent to a 30-minute 1 in 10 year rainfall in Sheffield.

$$K(h)\left(\frac{\partial h}{\partial Z} - 1\right) = R \qquad \text{Equation B.11}$$

The lower boundary was set to be a constant suction head (equal to field capacity) (Equation B.12).

$$h(z = D, t) = h(z = D, t_0) \qquad \text{Equation B.12}$$

The initial condition was set to be a constant hydraulic head; the suction head for the bottom point (z = the depth of the substrate, D) at time t_0 ($h(z = D, t_0)$) was set to the suction head equivalent to field capacity, and the suction heads assigned to the rest of the points were calculated from Equation B.11.

$$h(z, t_0) = h_{z=D} + Z - D \qquad \text{Equation B.13}$$

Table B.1 lists the parameters of the van Genuchten-Mualem model. The parameters of the Durner-Mualem model are in **Table B.2**. The van Genuchten parameters were calibrated from the SWRC for the Heather and Lavender Substrate (HLS) (Werdin, 2011) and the Durner-Mualem model parameters were adopted from Peng et al. (2019) for the same substrate. The field capacity was determined by the FLL method (Peng et al., 2019). It should be noted that the field capacity equivalent suction head is different for each of the SWRC models.

To represent the typical depth of substrate used in green roofs, 100 mm was selected. The simulations were performed with 1 mm spatial-step (i.e. 100 vertical cells) and a 0.1-minute time-step for 100 minutes. Simulations were built in HYDRUS-1D and MATLAB with the same inputs (value of parameters and spatial, time steps). The modelled runoff, suction head, and moisture content at the surface of the substrate using the van Genuchten-Mualem and Durner-Mualem models were compared. A longer time-step (1 minute) and a smaller spatial step (0.1 mm) were also used for the model built in MATLAB, and the influence of them will be discussed in Sections B.4.3 and B.4.4.

Table B.1. Values of van Genuchten-Mualem model parameters

Parameter	Description	Value
Θs	Saturated water content	0.556
Θr	Residual water content	0
α	van Genuchten parameter (1/cm)	0.0347
n	van Genuchten parameter	1.329
ks	Saturated hydraulic conductivity (cm/min)	2.679
D	Substrate depth (cm)	10
$h_{initial}$	Initial suction head at the bottom of the substrate (cm) (equivalent to field capacity)	75.763
R	Rainfall (cm/min) (equivalent to a 30-minute 1 in 10 year rainfall in Sheffield)	0.0569

Table B.2. Values of Durner-Mualem model parameters

Parameter	Description	Value
Θ_s	Saturated water content	0.556
Θ_r	Residual water content	0
α_1	Durner parameter (1/cm)	0.306
n_1	Durner parameter	2.255
α_2	Durner parameter (1/cm)	0.02
n_2	Durner parameter	1.194
w_1	Durner parameter	0.378
k_s	Saturated hydraulic conductivity (cm/min)	2.679
D	Substrate depth (cm)	10
$h_{initial}$	Initial suction head at the bottom of the substrate (cm) (equivalent to field capacity)	11.18
R	Rainfall (cm/min) (equivalent to a 30-minute 1 in 10 year rainfall in Sheffield)	0.0569

B.4 Model validation

Validation of the present model built in MATLAB against HYDRUS-1D will be discussed here. Validation of the basic modelling approach versus real monitored data using the present model can be found in Peng et al. (2019).

B.4.1 van Genuchten-Mualem model

Figure B.1 compares the model results of HYDRUS-1D and the model built in MATLAB (present model) using the van Genuchten -Mualem model. The results of the two approaches are almost identical. The two models give the same predictions of runoff. Minor differences were observed in the modelled surface suction head and moisture content. The differences between the two approaches are considered to be caused by the difference in numerical solution schemes.

(a) (b)

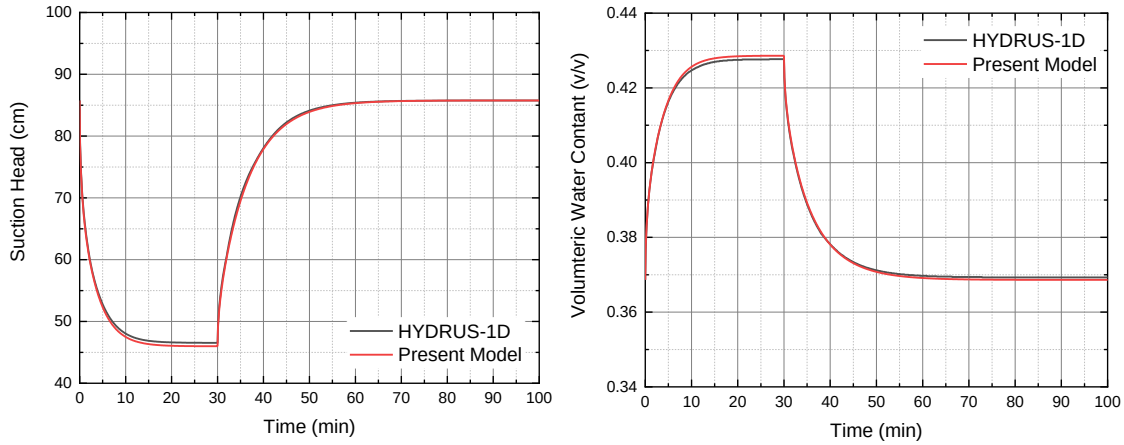

(c)

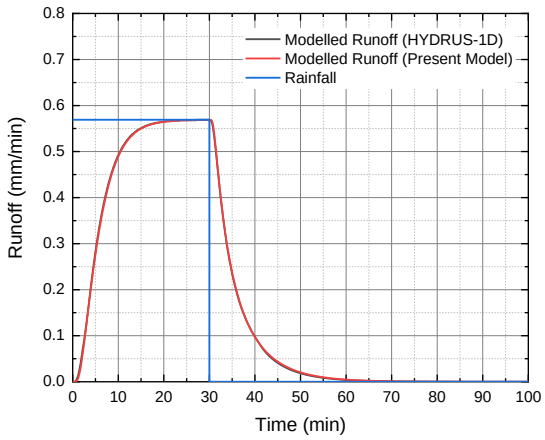

Figure B.1. Comparisons of the model results of HYDRUS-1D and present model using van Genuchten-Mualem model; (a) modelled surface suction head; (b) modelled surface water content; (c) modelled runoff.

B.4.2 Durner-Mualem model

Figure B.2 shows comparisons of the model results using HYDRUS-1D and the model built in MATLAB (present model). The Durner-Mualem model was used within the model. Consistent with the results of the van Genuchten model. The results of the two approaches are almost identical.

The two models give the same predictions of runoff. Only minor differences were observed in the modelled surface suction head and moisture content. Again, the differences between the two approaches are considered to be caused by the difference in numerical solution schemes.

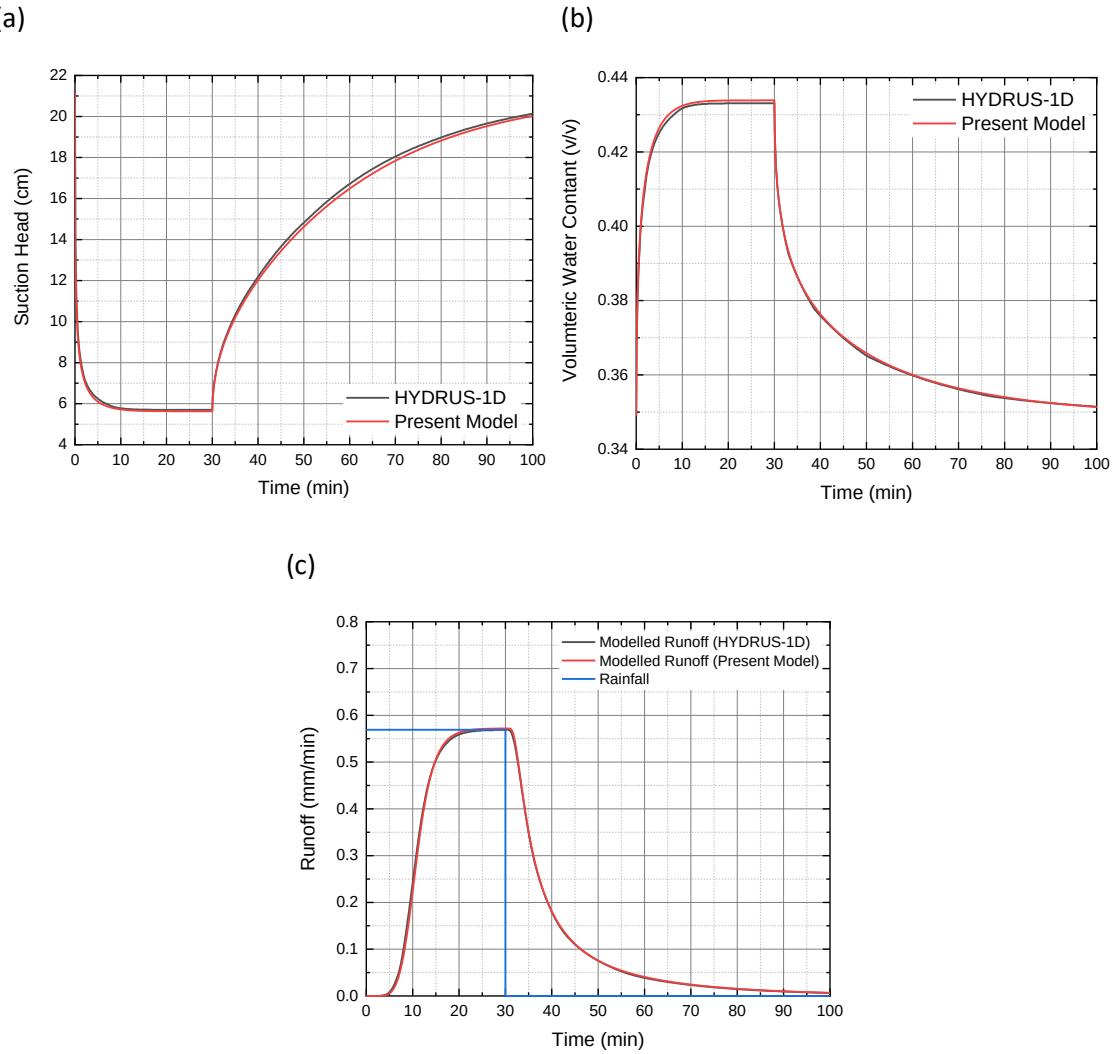

Figure B.2. Comparisons of the model results of HYDRUS-1D and present model using Durner-Mualem model; (a) modelled surface suction head; (b) modelled surface water content; (c) modelled runoff.

B.4.3 Sensitivity analysis

The time step used for simulations in Sections B.4.1 and B.4.2 was 0.1-minute. However, using short time steps is computationally expensive. Therefore, a longer time step (1-minute) was adopted, and the influence of the time step on the model results was investigated. The Durner-Mualem model was used here, and **Figure B.3** shows the model results using the short and the long time-steps. The present model gives the same model results when using short and long time steps. Therefore, it can be concluded that the time step has no influence on the model results

and, considering the expense of computation, a longer time step (1 minute) is therefore suggested to be used for simulations.

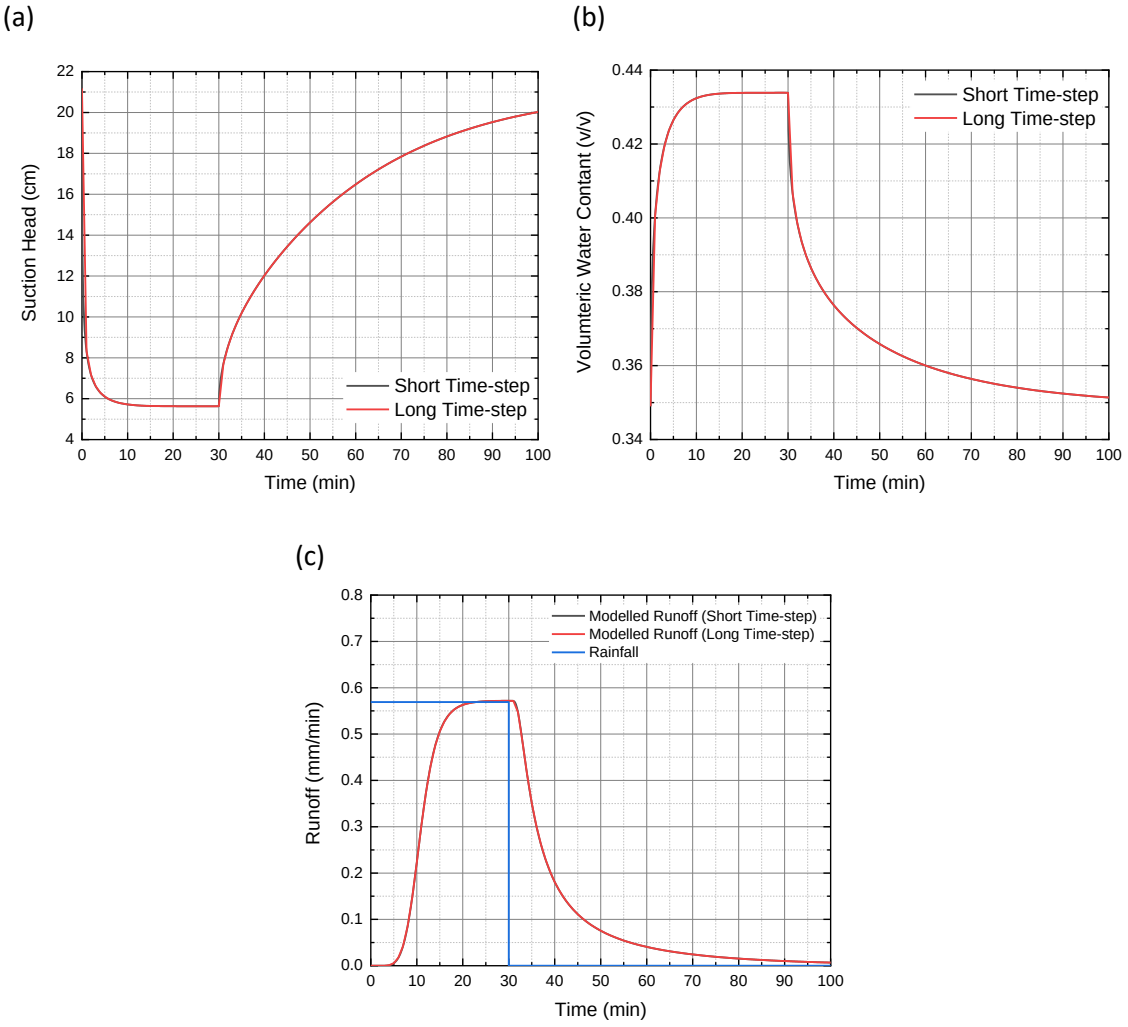

Figure B.3. Comparisons of the model results of using Durner-Mualem model with short and long time-steps; (a) modelled surface suction head; (b) modelled surface water content; (c) modelled runoff.

B.4.4 Spatial discretisation sensitivity analysis

The spatial step used in previous sections (Sections B.4.1 to B.4.3) was 1 mm. In this section, the influence of the spatial step on the results of the present model is investigated. The Durner-Mualem model was adopted. The time-step used for the simulation is 0.1 minute, and the spatial step was decreased to 0.1 mm. **Figure B.4** compares the model results using 0.1 mm spatial-step (small spatial-step) and the model results of using 1 mm spatial-step (large spatial-step). The present model gives the same results regardless of spatial steps. Therefore, a large spatial step (1 mm) is suggested for simulations to save the computational expense.

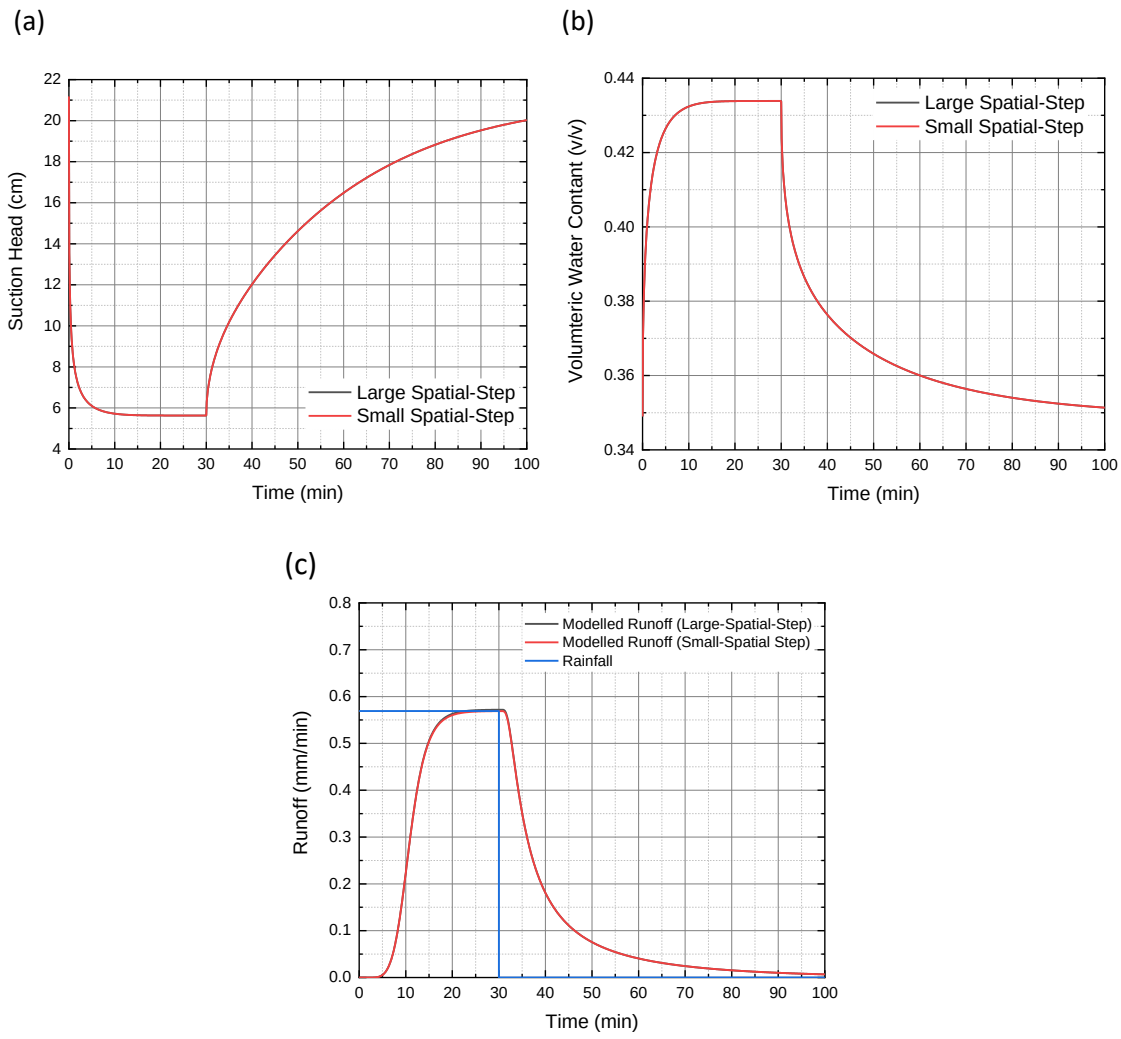

Figure B.4. Comparisons of the model results of using Durner-Mualem model with small and large spatial-steps; (a) modelled surface suction head; (b) modelled surface water content; (c) modelled runoff.

B.5 Conclusions

A high level of consistency has been achieved between the model results of HYDRUS-1D and the present model built in MATLAB. It has been confirmed that the present model can provide a correct solution to the Richards Equation independently of the SWRC models and the spatial/time steps. It may, therefore, be concluded that the present model could be used for simulations with new HCFs.

References

Peng, Z., Smith, C., Stovin, V., 2019. Internal fluctuations in green roof substrate moisture content during storm events: Monitored data and model simulations. J. Hydrol. 573, 872–884. https://doi.org/10.1016/j.jhydrol.2019.04.008

Šimůnek, J., Šejna, M., Saito, H., Sakai, M., Genuchten, M.T. Van, 2013. The HYDRUS-1D Software Package for Simulating the Movement of Water, Heat, and Multiple Solutes in Variably Saturated Media, Version 4.17, HYDRUS Software Series 3, Department of Environmental Sciences, University of California Riverside, Riverside, California, USA, 343.

Werdin, J. (2011). Determination of moisture retention curves for a variety of green roof substrates by using the Pressure Plate Method. In: 1st National Green Roof Student Conference. Sheffield, UK, 2011.

Appendix C. Supplementary Materials for Green Roof Substrate Detention Tests (Chapter 5 and Chapter 6).

Table C.1. Mean standard deviations of runoff and moisture content profiles for the three replication tests in the detention tests.

substrate	Depth	Design Storm	Runoff (mm/min)	Moisture Content Bottom (v/v)	Moisture Content Top (v/v)
MCS	100 mm	1	0.0008	0.0002	
		2	0.0010	0.0011	
		3	0.0007	0.0008	
		4	0.0085	0.0006	
MCS	200 mm	1	0.0031	0.0008	0.0016
		2	0.0017	0.0012	0.0014
		3	0.0021	0.0011	0.0007
		4	0.0037	0.0009	0.0009
HLS	100 mm	1	0.0011	0.0007	
		2	0.0011	0.0014	
		3	0.0005	0.0234	
		4	0.0018	0.0005	
HLS	200 mm	1	0.0013	0.0005	0.0004
		2	0.0019	0.0005	0.0006
		3	0.0004	0.0220	0.0239
		4	0.0021	0.0003	0.0003
SCS	100 mm	1	0.0013	0.0089	
		2	0.0020	0.0013	
		3	0.0014	0.0006	
		4	0.0026	0.0010	
SCS	200 mm	1	0.0016	0.0002	0.0004
		2	0.0022	0.0004	0.0003
		3	0.0021	0.0004	0.0004
		4	0.0027	0.0003	0.0002
NSM	100 mm	1	0.0009	0.0002	
		2	0.0017	0.0003	
		3	0.0016	0.0004	
		4	0.0014	0.0004	
NSM	200 mm	1	0.0012	0.0002	0.0001
		2	0.0022	0.0004	0.0003
		3	0.0024	0.0012	0.0003
		4	0.0024	0.0003	0.0003

Table C.2. Initial moisture content measured by the bottom probe and the corresponding suction head (calculated from the Durner model) for the detention tests.

Substrate	Substrate Depth	Design Storm	Moisture Content	Corresponding Suction Head
-	mm	-	v/v	cm
MCS	100	1	0.302	7.410
		2	0.304	7.295
		3	0.307	7.161
		4	0.308	7.073
MCS	200	1	0.260	12.863
		2	0.265	11.890
		3	0.269	10.910
		4	0.272	10.423
HLS	100	1	0.346	22.723
		2	0.350	20.439
		3	0.353	19.199
		4	0.355	18.122
HLS	200	1	0.335	29.916
		2	0.337	27.935
		3	0.339	26.758
		4	0.340	26.195
SCS	100	1	0.320	7.400
		2	0.320	7.385
		3	0.323	7.083
		4	0.327	6.733
SCS	200	1	0.390	3.608
		2	0.389	3.632
		3	0.390	3.621
		4	0.391	3.592
NSM	100	1	0.293	15.420
		2	0.292	16.086
		3	0.290	16.794
		4	0.290	16.695
NSM	200	1	0.342	5.406
		2	0.342	5.373
		3	0.344	5.151
		4	0.347	5.003

Appendix D. Example of MATLAB Code

This section provides the MATLAB code used in this study. The code includes the Transient method of calculating the unsaturated hydraulic conductivity using the measured moisture content and suction data (Chapter 3); the Durner-Mualem and the Durner Three-Segment HCF curve of modelling the runoff from the substrate in response to design storms (Chapter 4, Chapter 6 and Appendix B); and the Saint-Venant model integrating with Manning's equation (Chapter 7). The example code is identical to the code actually used. However, the variables in the example code were given more logical names and explanations for better readability.

D.1. Unsaturated hydraulic conductivity calculation using the transient method

D.2. Substrate runoff modelling using Durner-Mualem approach

D.3. Substrate runoff modelling using Durner and Three-segment HCF curve approach

D.4. Drainage layer runoff modelling using the Saint Venant equation (integrated with manning's equation)

D.1. Unsaturated hydraulic conductivity calculation (Transient Method). m

```
clear
clc
load NSM_Test1%load measured data (New Substrate Mix)
tension2=-test_tension3; % tension of upper tensiometer (test_tension3, lower) (cm)
tension3=-test_tension2; % tension of lower tensiometer (test_tension2, upper) (cm)
moisture2=test_moisture2; % moisture of lower probe
moisture3=test_moisture3; % moisture of upper probe

dt1=10;%time-step for internal drainage method (min)
dt2=180;%time-step for ET method (min)

deltah1=17.5;%distance between the base of the substrate and the lowest tensiometer
deltah2=12;%distance between the middle tensiometer and the lowest tensiometer
deltah3=12; %distance between the upper tensiometer and the middle tensiometer



% find direction of flow, find the interception point where the flow
% direction is upwards
for i=2:length(tension2)
gradient_find(i-1,1)=-1+(-tension2(i-1)+tension3(i-1))/deltah2;
end
index=find(gradient_find(:,1)<=-2,1, 'first')+1;

% internal drainage method data
 tension2_drainage=tension2(1:index); %tensiometer data
 tension3_drainage=tension3(1:index); %tensiometer data
 moisture2_drainage=moisture2(1:index); %moisture probe data
 moisture3_drainage=moisture3(1:index); %moisture probe data
```

```
 %select data at each 10 minutes
for i=2:length(tension2_drainage)/dt1
    tension2_5(1,1)=tension2_drainage(1,1);
    tension3_5(1,1)=tension3_drainage(1,1);
    moisture2_5(1,1)=moisture2_drainage(1,1);
    moisture3_5(1,1)=moisture3_drainage(1,1);
    tension2_5(i,1)=tension2_drainage((i-1)*dt1);
    tension3_5(i,1)=tension3_drainage((i-1)*dt1);
    moisture2_5(i,1)=moisture2_drainage((i-1)*dt1);
    moisture3_5(i,1)=moisture3_drainage((i-1)*dt1);
end

% unsaturated hydraulic conductivity calculations using internal drainage
% method
for i=2:length( tension2_5)
    q(i-1,1)=deltah2*(moisture2_5(i-1)-moisture2_5(i))+deltah1*(moisture3_5(i-1)-
moisture3_5(i));
    gradient(i-1,1)=-1+(-tension2_5(i-1)+tension3_5(i-1))/deltah2;
    k_drainage(i-1,1)=-q(i-1)./gradient(i-1)/dt1; %cm/min
    wc_drainage(i-1,1)=0.5*(moisture2_5(i)+moisture3_5(i));
end


% ET method data
 tension2_ET=tension2(index:end);%tensiometer data
 tension3_ET=tension3(index:end);%tensiometer data
 moisture2_ET=moisture2(index:end);%moisture probe data
 moisture3_ET=moisture3(index:end);%moisture probe data

 %select data at each 180 minutes
for i=2:length(tension2_ET)/dt2
    tension2_5_ET(1,1)=tension2_ET(1,1);
```

```
    tension3_5_ET(1,1)=tension3_ET(1,1);
    moisture2_5_ET(1,1)=moisture2_ET(1,1);
    moisture3_5_ET(1,1)=moisture3_ET(1,1);

    tension2_5_ET(i,1)=tension2_ET((i-1)*dt2);
    tension3_5_ET(i,1)=tension3_ET((i-1)*dt2);
    moisture2_5_ET(i,1)=moisture2_ET((i-1)*dt2);
    moisture3_5_ET(i,1)=moisture3_ET((i-1)*dt2);
end

% unsaturated hydraulic conductivity calculations using ET method
for i=2:length(tension2_5_ET)
    q_ET(i-1,1)=deltah3*(moisture2_5_ET(i-1)-
moisture2_5_ET(i))+deltah2*(moisture3_5_ET(i-1)-moisture3_5_ET(i));
    gradient_ET(i-1,1)=-1+(-tension2_5_ET(i-1)+tension3_5_ET(i-1))/deltah2;
    k_ET(i-1,1)=-q_ET(i-1)./gradient_ET(i-1)/dt2; %cm/min
    kwc_ET(i-1,1)=0.5*(moisture2_5_ET(i)+moisture3_5_ET(i));
end

%plot results
scatter (wc_drainage, k_drainage) %internal drainage method
hold on
scatter (kwc_ET,k_ET)%ET method
set(gca,'yscale','log')
xlabel('Time (min)')
ylabel('Hydraulic Conductivity (cm/min)')
```

D.2. Durner-Mualem runoff modelling. m

```
function pdex1
close all
clc
m = 0;
options=odeset('Maxstep',0.01)
depth=20; %substrate depth cm
nodes=201;
dx=depth/(nodes-1); %spatial-step
x = linspace(0,depth,nodes);
time=100; %simulation time-length min
elements=time;
dt=time/elements; %time-step
t = linspace(0,time,elements);

sol = pdepe(m,@pdex1pde,@pdex1ic,@pdex1bc,x,t,options); %call the pdepe function

u = sol(:,:,1);%solved results for suction head distribution

% parameters of Duner-Mualem model (NSM)
F=0.486;
r=0;
w1=0.462;
w2=1-w1;
a1=0.707;
n1=1.708;
a2=0.021;
n2=1.184;
m1=1-1/n1;
m2=1-1/n2;
ks=6.7829; % saturated hydraulic conductivity cm/min
```

```
t1=0.5;

WC=r+(F-r).*(w1.*(1+(a1.*(-u)).^n1).^-m1+w2.*(1+(a2.*(-u)).^n2).^-m2); %convert solved suction head to moisture content

se1=(1+(a1.*-u(:,end)).^n1).^-m1;
se2=(1+(a2.*-u(:,end)).^n2).^-m2;
p1=1-(1-se1.^(1/m1)).^m1;
p2=1-(1-se2.^(1/m2)).^m2;
k1=ks.*(w1.*se1+w2.*se2).^t1.*(w1.*a1.*p1+w2.*a2.*p2).^2./(w1.*a1+w2.*a2).^2; %hydraulic conductivity at node 201 (cm/min, estimated by the Durner-Mualem method)

se3=(1+(a1.*-u(:,end-1)).^n1).^-m1;
se4=(1+(a2.*-u(:,end-1)).^n2).^-m2;
p3=1-(1-se3.^(1/m1)).^m1;
p4=1-(1-se4.^(1/m2)).^m2;
k2=ks.*(w1.*se3+w2.*se4).^t1.*(w1.*a1.*p3+w2.*a2.*p4).^2./(w1.*a1+w2.*a2).^2;%hydraulic conductivity at node 200 (cm/min, estimated by the Durner-Mualem method)

Q=-0.5*(k1+k2).*(u(:,end)-dx-u(:,end-1))./dx; %bottom runoff cm/min
save Q200_3
plot (t,Q)
ylabel('Flow Rate cm/min')
xlabel('Time min');

% ---------------------------------------------------------------
function [c,f,s] = pdex1pde(x,t,u,DuDx) %define the Richards Equation to the standard form
% parameters of Duner-Mualem model (NSM)
F=0.486;
r=0;
```

```
w1=0.462;
w2=1-w1;
a1=0.707;
n1=1.708;
a2=0.021;
n2=1.184;
m1=1-1/n1;
m2=1-1/n2;
ks=6.7829; % saturated hydraulic conductivity cm/min
t1=0.5;
%k=saturated hydraulic conductivity when saturated
if u>=0
    c=0;
    k=ks;
    s=0;
f = k.*DuDx-k;
else
% define parameters in the standard function
se1=(1+(a1.*-u).^n1).^-m1;
se2=(1+(a2.*-u).^n2).^-m2;
p1=1-(1-se1.^(1/m1)).^m1;
p2=1-(1-se2.^(1/m2)).^m2;
k=ks.*(w1.*se1+w2.*se2).^t1.*(w1.*a1.*p1+w2.*a2.*p2).^2./(w1.*a1+w2.*a2).^2;
f = k*DuDx-k;
d1=n1*m1*a1*(-a1*u)^(n1-1)/(1+(-a1*u)^n1)^(m1+1);
d2=n2*m2*a2*(-a2*u)^(n2-1)/(1+(-a2*u)^n2)^(m2+1);
c=(F-r)*(w1*d1+w2*d2);
s = 0;
end
% --------------------------------------------------------------
function u0 = pdex1ic(x) %initial condition (constant hydraulic head)
```

```
o=-5.151003047; %suction head corresponding to the measured moisture content
(measured by the lower moisture probe)
u0=o+x-16;%suction head for the rest of the nodes


 % --------------------------------------------------------------
function [pl,ql,pr,qr] = pdex1bc(xl,ul,xr,ur,t,x) %boundary conditions
load Rainfall_200 %rainfall input mm/min
load Time %time min
index=find(t<=Time,1,'first')
R=Rainfall_200 (index,3)/10;
o=-5.151003047; %suction head corresponding to the measured moisture content
(measured by the lower moisture probe)
pl=R; %upper boundary condition (rainfall input)
ql = 1;
pr =ur-o-4; %lower boundary condition (constant head)
qr = 0;
```

D.3. Durner Three-Segment HCF curve runoff modelling. m

```
function pdex1
close all
clc
m = 0;
options=odeset('Maxstep',0.01)
depth=10; %depth of the substrate cm
nodes=101;
dx=depth/(nodes-1); %spatial-step
x = linspace(0,depth,nodes);
time=100; %simulation time min
elements=time;
dt=time/elements; %time-step
t = linspace(0,time,elements);

sol = pdepe(m,@pdex1pde,@pdex1ic,@pdex1bc,x,t,options);

u = sol(:,:,1); %solved suction head distribution

% parameters of Duner-Mualem model (NSM)
F=0.486;
r=0;
w1=0.462;
w2=1-w1;
a1=0.707;
n1=1.708;
a2=0.021;
n2=1.184;
m1=1-1/n1;
m2=1-1/n2;
```

```
WC=r+(F-r).*(w1.*(1+(a1.*(-u)).^n1).^-m1+w2.*(1+(a2.*(-u)).^n2).^-m2); %convert
solved suction head distribution to moisture content using Durner model

se1=(1+(a1.*-u(:,end-1)).^n1).^-m1;
se2=(1+(a2.*-u(:,end-1)).^n2).^-m2;
se3=(1+(a1.*-u(:,end)).^n1).^-m1;
se4=(1+(a2.*-u(:,end)).^n2).^-m2;

% parameters for the three-segment curve
para1=9.3369;
para2=22.05;
para3=49.678;
para4=-3.7075;
para5=-7.9664;
para6=-14.266;
 %the two interception points
xc1=0.228;
xc2=0.335;

%moisture content at node 101 and 100
thelta1=(w1.*se1+w2.*se2).*(F-r)+r;
thelta2=(w1.*se3+w2.*se4).*(F-r)+r;

%the three-segment curve equation
for i=1:length(thelta1);
 if xc2<=thelta1(i)
            HCl1(i,1)=para1*thelta1(i)+para4;
      elseif thelta1(i,1)>=xc1 && thelta1(i)<=xc2
            HCl1(i,1)=para2*thelta1(i)+para5;
      else
            HCl1(i,1)=para3*thelta1(i)+para6;
 end
```

```
end

for j=1:length(thelta2);
if xc2<thelta2(j);
            HCl2(j,1)=para1*thelta2(j)+para4;
      elseif xc1<=thelta2(j) && thelta2(j)<=xc2
            HCl2(j,1)=para2*thelta2(j)+para5;
      else
            HCl2(j,1)=para3*thelta2(j)+para6;
end
end
 k1=10.^HCl1;
 k2=10.^HCl2;

 Q=-0.5*(k1+k2).*(u(:,end)-dx-u(:,end-1))./dx;

save Q100_4_1
plot (t,Q)
ylabel('Flow Rate cm/min')
xlabel('Time min');

% ---------------------------------------------------------------
function [c,f,s] = pdex1pde(x,t,u,DuDx) %define the Richards Equation to the standard
form
% parameters of Duner-Mualem model (NSM)
F=0.486;
r=0;
w1=0.462;
w2=1-w1;
a1=0.707;
n1=1.708;
a2=0.021;
```

```
n2=1.184;
m1=1-1/n1;
m2=1-1/n2;
ks=6.7829;
t1=-0.5;

if u>=0
    c=0;
    k=ks;
    s=0;
f = k.*DuDx-k;
else

se1=(1+(a1.*-u).^n1).^-m1;
se2=(1+(a2.*-u).^n2).^-m2;

% parameters for the three-segment curve
para1=9.3369;
para2=22.05;
para3=49.678;
para4=-3.7075;
para5=-7.9664;
para6=-14.266;

%the two interception points
xc1=0.228;
xc2=0.335;

%convert suction head to moisture content
thelta=(w1.*se1+w2.*se2).*(F-r)+r;

%the three-segment curve equation
```

```
if xc2<thelta;
            HCl=para1*thelta+para4;
        elseif xc1<=thelta && thelta<=xc2;
            HCl=para2*thelta+para5;
        else
            HCl=para3*thelta+para6;
end

k=10.^HCl;

f = k*DuDx-k;
d1=n1*m1*a1*(-a1*u)^(n1-1)/(1+(-a1*u)^n1)^(m1+1);
d2=n2*m2*a2*(-a2*u)^(n2-1)/(1+(-a2*u)^n2)^(m2+1);
c=(F-r)*(w1*d1+w2*d2);
s = 0;
end


% ------------------------------------------------------------
function u0 = pdex1ic(x) %initial condition (constant hydraulic head)
o=-15.42016303; %suction head corresponding to the measured moisture content
(lowest moisture probe)
u0=o+x-6; %suction head for the rest of the nodes at t=0.

% ------------------------------------------------------------
function [pl,ql,pr,qr] = pdex1bc(xl,ul,xr,ur,t,x)
load Rainfall_100 %rainfall input mm/min
load Time %time min
index=find(t<=Time,1,'first')
R=Rainfall_100 (index,1)/10;
o=-15.42016303; %suction head corresponding to the measured moisture content
(measured by the lower moisture probe)
```

```
pl=R; %upper boundary condition (rainfall input)
ql = 1;
pr =ur-o-4; %lower boundary condition (constant head)
qr = 0;
```

D.4. Drainage layer Saint-Venant (Manning's equation) modelling. m

```
%define model parameters
global time Rainfall Time dx x_end sl n t_duration
dx=0.01; %spatial-step (m)
time=120; %simulation time (min)
t_duration=30; % duration of the rainfall (min)
Rainfall=1.5; % rainfall intensity (mm/min), constant rainfall input for 30 min
x_end=5; %length of the detention layer (m)
sl=2/100; %slope
n=0.06; % Manning's n
Time=[1:1:time]; %time series (min)
Manning %run manuscript named manning
Flow %run manuscript named flow

%%%%%%%%%%%%%%%%%%%%%%%%%%%%%%%%%%%%%%%%%%
%Manning. m, this is the manuscript to calculate water level distribution (m)
function pdex1
global x_end dx time
%defining mesh
m = 0;
x = 0:dx:x_end;
elements=time;
t = linspace(1,time,elements);

%call the function
sol = pdepe(m,@pdex1pde,@pdex1ic,@pdex1bc,x,t);
%extract results
u = sol(:,:,1);
save Test
```

```
% --------------------------------------------------------------
function [c,f,s] = pdex1pde(x,t,u,DuDx) %defining the equation
global t_duration Rainfall sl n Time
c =1; %specific yield.
f =1/(n*sqrt(sl))*u^(5/3)*(DuDx-sl); %manning's equation
%define upper boundary as inflow
if t<=t_duration
  R1=Rainfall/1000;
else
  R1=0;
end
s=R1;

% --------------------------------------------------------------
function u0 = pdex1ic(x) %initial water level 0 m
u0 =0.000;

% --------------------------------------------------------------
function [pl,ql,pr,qr] = pdex1bc(xl,ul,xr,ur,t) %boundary conditions
global n sl
pl=ul; %upstream, 0 water level
ql =0;
pr =1/(n*sqrt(sl))*ur^(5/3)*sl; %downstream, free drainage
qr =1;

%%%%%%%%%%%%%%%%%%%%%%%%%%%%%%%%%%%%%%%%%%%%%%%%%%%%%%%%%%%%
%Flow. m, this is the manuscript to calculate the runoff per unit length and width
(mm/min)
load Test
data1=u; %load the solved water level distribution
s=size(u);
```

```
summ=zeros(s);
%calculate the change in water level at each time-step
for i=2:s(1)
    for j=1:s(2)
    summ(1,1)=0;
    summ(i,j)=u(i,j)-u(i-1,j);
    end
end

% rainfall input at each spatial and time-step in m
global t_duration Rainfall
rainfall_input=zeros(s(1),s(2));
rainfall_input(1,1)=0;
rainfall_input(2:t_duration,:)=Rainfall/1000;

% runoff=inflow-storage m
flow1=rainfall_input-summ;

% runoff per unit length mm/min
global x_end dx
qout=zeros(s(1),1);
for i=1:s(1)
    qout(i,1)=sum(flow1(i,:))/((x_end)/dx+1)*1000;
end
```